Universitat Autònoma de Barcelona

THE ROLE OF THE PDK1 PIF-POCKET-DEPENDENT CASCADE IN EMBRYONIC CORTICOGENESIS

Sònia Pascual-Guiral

The role of the PDK1 PIF-pocket dependent cascade in embryonic corticogenesis

Sònia Pascual-Guiral

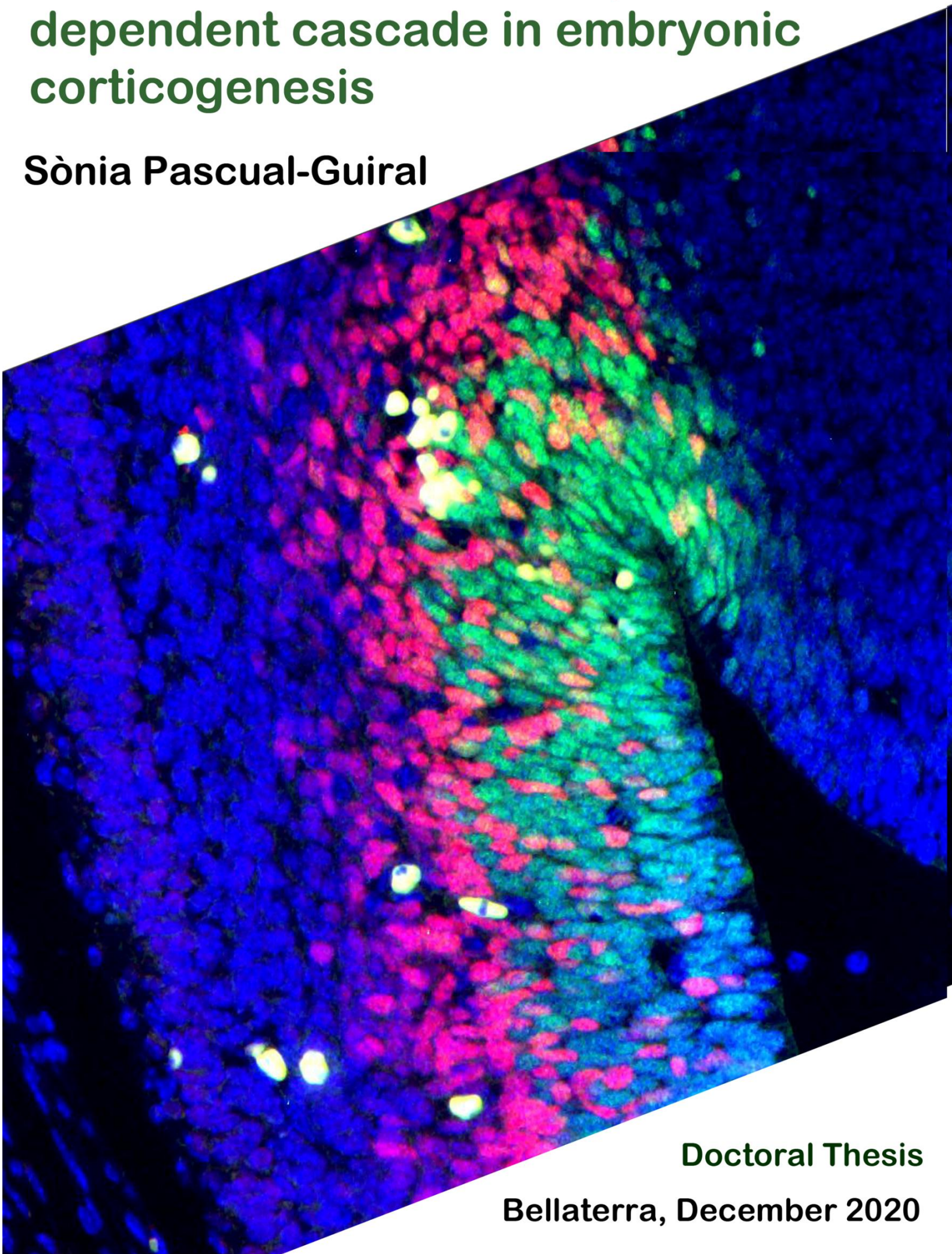

Doctoral Thesis

Bellaterra, December 2020

Universitat Autònoma de Barcelona

Departament de Bioquímica i Biologia Molecular & Institut de Neurociències

Unitat de Bioquímica, Facultat de Medicina

THE ROLE OF THE PDK1 PIF-POCKET-DEPENDENT CASCADE IN EMBRYONIC CORTICOGENESIS

Sònia Pascual-Guiral

Director: Dr José Ramón Bayascas Ramírez

DOCTORAL THESIS

PhD degree in Neurosciences

Bellaterra, December 2020

Universitat Autònoma de Barcelona

Departament de Bioquímica i Biologia Molecular & Institut de Neurociències

Unitat de Bioquímica, Facultat de Medicina

The role of the PDK1 PIF-POCKET-dependent cascade in embryonic corticogenesis

Doctoral thesis report presented by Sònia Pascual-Guiral in candidance for the PhD degree in Neurosciences from Universitat Autònoma de Barcelona.

This work was done at the Departament de Bioquímica i Biologia Molecular, Unitat de Bioquímica of the Facultat de Medicina and Institut de Neurociències de la Universitat Autònoma de Barcelona, under the supervision of Dr. José Ramón Bayascas Ramírez.

Thesis director — Dr José Ramón Bayascas Ramírez

Candidate — Sònia Pascual-Guiral

DOCTORAL THESIS

Bellaterra, December 2020

INDEX

ACRONYMS

ACRONYMS

ACRONYM	MEANING
ºC	Degree Celsius
4E-BP1	Eukaryotic translation initiation factor 4E -binding protein 1
5'-UTR	5'-untranslated region
µl	microliter
µm	micrometers
µM	micromolar
Acryl	Acrylamide
ADP	Adenosine diphosphate
AGRE	Autism Genetic Resource Exchange
Akt	AKR mouse strain that develops thymomas
AMPA	α-amino-3- hydroxy-5-methyl-4-isoxazolepropionic acid
AMPK	5' adenosine monophosphate-activated kinase
ANOVA	Analysis of Variance
AP	Apical Progenitors
aPKCs	Atypical PKCs
APS	Ammonium persulfate
Arf1	ADP-ribosylation factor 1
ATF1	Activating Transcription Factor-1
ATP	Adenosine triphosphate
Asp	Aspartic acid
Aspm	Abnormal spindle-like microcephaly-associated
A.U.	Arbitrary Units
BAD	Bcl-2-associated death promoter
Bcl2A1	Bcl-2-related protein A1
BDNF	Brain-derived neurotrophic factor
bp	Base pair
bHLH	Basic helix-loop-helix
BRAP	BRCA1 associated protein
BSA	Bovine serum albumin
CAD	Carbamoyl-phosphate synthetase 2, aspartate transcarbamylase, and dihydroorotase synthesis
CAMK	Calcium/calmodulin-dependent protein kinase
cAMP	3',5'-cyclic adenosine monophosphate
CASTOR1	Cellular arginine sensor for mTORC1
cc	Corpus callosum
CDK	Cyclin-dependent kinase
CDK2	Cyclin-dependent kinase 2
CGE	Caudal Ganglionic Eminence
CH	Cortical Hem
ChIP	Chromatin immunoprecipitation
cm	Centimetre
CMV	Cytomegalovirus
CNS	Central Nervous System
CP	Cortical Plate
CPN	Callosal projection neurons

CR	Calretinin
CREB	cAMP-response-element-binding protein
CThPN	Corticothalamic projections neurons
Ctip2	COUP-TF-interacting protein 2
CTKD	C-terminal catalytic domain
Cys	Cysteine
Cxcl12	C-X-C motif chemokine 12
Cxcr	C-X-C chemokine receptor
Da	Dalton
DAG	Diacylglycerol
***dam*$^-$ / *dcm*$^-$**	DNA adenine methyltransferase $^-$ / DNA cytosine methyltransferase $^-$
DSHB	Developmental Studies Hybridoma Bank
DCX	Doublecortin
DEPTOR	DEP- domain-containing mTOR- interacting protein
DISC1	Disrupted in Schizophrenia 1
DIV	Day In Vitro
DMEM	Dulbecco's modified Eagle's medium
DMSO	Dimethyl sulfoxide
DNA	Deoxyribonucleic acid
dNTPs	Deoxynucleotide triphosphates
E. coli	*Escherichia coli*
ECL	Enhanced Chemiluminescence
EDTA	Ethylenediaminetetraacetic acid
EGTA	Ethylene glycol-bis(β-aminoethyl ether)-N,N,N',N'-tetraacetic acid
EdU	5-ethynyl-2'-deoxyuridine
Emx2	Empty spiracles homeobox 2
ER	Endoplasmatic Reticulum
ERK	Extracellular signal-regulated kinase
FBS	Fetal bovine serum
Fezf2	Family zinc finger 2
Foxg1	Forkhead transcription factor
FOXO	Forkhead box O
g	Gram
GABA	Gamma-Aminobutyric acid
GAD67	Glutamate decarboxylase 67 KDa
GAP	GTPase activating protein
GAT-1	GABA membrane transporter
GATOR1	GAP activity toward Rags
GEF	Guanine nucleotide exchange factors
GFP	Green Fluorescent Protein
Glu	Glutamic Acid
GP	Globus Pallidus
GPCR	G protein-coupled receptor
GTP	Guanosine triphosphate
GSK3	Glycogen synthase kinase 3
h	Hour
HA	Hemagglutinin
HBSS	Hank's Balanced Salt Solution
HEPES	4-(2-hydroxyethyl)-1-piperazineethanesulfonic acid

HIF	Hypoxia Inducible Factors
His	Histidine
HM	Hydrophobic motif
HRP	Horseradish peroxidase
Htr3a	Serotonin receptor 3A
IGF-1	Insulin-like growth factor 1
IN	Interneurons
INTDEN	Intensity of staining
IP	Intermediate Progenitor
IPN	Neurogenic IP
IRES	Internal ribosome entry site
IRS-1	Insulin Receptor Substrate 1
IUE	*In utero* electroporation
JIP1	c-Jun N-terminal kinase interacting protein-1
JNK1	c-Jun N-terminal kinase 1
Kb	Kilobases
KD	Kinase Domain
KDa	kiloDaltons
KN	Kinase-inactive
KRB	Krebs-Ringer Buffer
LB	Luria Broth
LGE	Lateral Ganglionic Eminence
linkB	Linker B
LTD	Long term Depression
MEM	Eagle's minimal essential medium
ml	milliliter
mLST8	Mammalian lethal with SEC13 protein 8
mm	milimeters
mM	milimolar
M	Molar
MRI	Magnetic Resonance Imaging
mRNA	messenger RNA
miRNA	microRNA
mSIN1	Sty1/SAPK interacting protein
mTOR	mammalian Target of Rapamycin
mTORC	mTOR Complex
MAP2	Microtubule-associated protein 2
MAPK	Mitogen-activated protein kinase
MAPKAPK	MAPK-activated protein kinase
MEF	Mouse embryonic fibroblasts
mg	miligram
MGE	Medial Ganglionic Eminence
min	minutes
ml	mililiters
mm	milimeters
mM	milimolar
MSK	Mitogen- and stress- activated kinase
MZ	Marginal Zone
n.a.	non added

N2a	Neuro2a
Ncx	Neocortex
Neurog2	Neurogenin2
ng	nanogram
NGF	Nerve growth factor
NLS	Nuclear localization signals
nM	nanomolar
NMDA	N-methyl- D-aspartate
NPCs	Neural progenitor cells
Nrg	Neuregulin
NSCs	Neural stem cells
NT	Neurotrophin
NTKD	N-terminal kinase domain
ON	Overnight
OSVZ	Outer SubVentricular Zone
OTV	Orthovanadate
P	Phosphate
p75NTR	p75 neurotrophin receptor
Pax5	Paired box protein-5
Pax6	Paired box protein-6
P/S	Penicillin / Streptomycin
PBS	Phosphate Buffered Saline
PBS^{a}	PBS supplemented
PCNA	Proliferating Cell Nuclear Antigen
PCR	Polymerase chain reaction
PCx	Piriform cortex
PDCD4	Programmed Cell Death Protein 4
PDK1	3-phosphoinositide-dependent protein kinase-1
PDK1$_i$	PDK1 inhibitor GSK2334470
PEI	Polyethyleminine
PH	Plekstrin Homology
pH3	Phospho-Histone 3
Phe	Phenylalanine
PHLPP2	PH domain leucine-rich repeat-containing protein phosphatase 2
PI-3-P	phosphatidylinositol 3-phosphate
PI3K	phosphoinositide 3-kinase
PIF	PDK1-interacting fragment
PKB	Protein kinase B
PKCs	Protein Kinase C
PN	Projection neurons
POA	Preoptic area
PP	Preplate
PLC	phospholipase C
PP2A	protein phosphatase 2A
PRAS40	40k Da Proline-rich Akt substrate
PROTOR1/2	protein associated with rictor 1 or 2
PtdIns(4,5)P_2	Phosphatidylinositol 4,5-bisphosphate
PtdIns(3,4,5)P_3	Phosphatidylinositol (3,4,5)-trisphosphate
PTEN	Phosphatase and tensin homolog

PV	Parvalbumin
PX	Phox homology
raptor	regulatory-associated protein of mTOR
RBD	RAS-Binding Domain
rDNA	Ribosomal DNA
REDD1	Regulated in development and DNA damage responses 1
RFP	Red Fluorescent Protein
RG	Radial Glia
RGC	Radial Glia Cells
RheB	Ras Homologue enriched in Brain
RiBi	ribosome biogenesis
rictor	rapamycin-insensitive companion of mTOR
RLPK	RSK-like protein kinase
RNA	Ribonucleic acid
rpS6	Ribosomal protein S6
rRNA	Ribosomal RNA
RSK	p90 ribosomal S6 Kinase
RTK	Receptor Tyrosine Kinase
S6K	Ribosomal S6 kinase
Satb2	Special AT-rich sequence-binding protein-2
SCPN	Subcerebral projection neurons
SDS	Sodium dodecyl sulfate
Sema	Semaphorin
Ser	Serine
SGK	serum- and glucocorticoid-inducible kinase
SH2	Src-homology 2
Smad2/3	Mothers against decapentaplegic homolog 2/3
SP	Subplate
Sox2	SRY-box containing gene 2
Sox5	Sex determining region Y-box 5
SST	Somatostatin
Str	Striatum
SVZ	SubVentricular Zone
TAE	Tris-Acetate-EDTA
Tbr1	T-domain transcription factor T-box 1
Tbr2	T-domain transcription factor 2
TBS	Tris Buffered Saline
TBST	Tris Buffered Saline with Tween
TD	Trophic Deprivation
TE	Tris EDTA
TEMED	N, N, N', N'-tetramethylethylenediamine
TGF-β	Transforming Growth Factor beta
TOP	5' terminal oligopyrimidine
Thr	Threonine
TK	thymidine kinase
T_m	Melting temperature
Trk	Tropomyosin receptor kinase
tRNA	Transfer RNA
TSC	Tuberous sclerosis complex

Tuj1	Neuron-specific Class III β-tubulin
UPR	Unfolded Protein Response
UT	Untreated
UTR	Untranslated region
UV	Ultraviolet
V	Volt
VIP	Vasoactive intestinal peptide
VZ	Ventricular Zone
WB	Western Blot
Wm	White matter

SUMMARY

Summary

The 3-Phosphoinositide-dependent protein kinase 1 (PDK1) is the master kinase that coordinates the PI3K signalling pathway by activating 23 kinases of the AGC family, including PKB. PDK1 acts after recognizing a conserved docking site on its substrates, once it has been previously phosphorylated by a different kinase. PKB is the only exception that does not require this interaction to be fully activated by PDK1. A mutant form of PDK1, leucine at position 155 to glutamic acid (L155E), in which the pocket recognizing the substrate-docking site was disrupted, was created and expressed in neuron-specific conditional knock-in mice. This mutation disrupted all PI3K-dependent signalling but PKB, which was activated normally. Previous results showed that the resulting adult mutant miceexhibited reduced neuronal polarization and differentiation *in vitro*, as well as abnormal neuronal positioning and diminished neuronal connectivity in the cortex and hippocampus *in vivo*. Here it is demonstrated that the PDK1 L155E mutation causes microcephaly. Intermediate progenitors (IPs) are reduced in number by the expression of the PDK1 L155E mutation during neurodevelopment, and mitosis is reduced in their predecessors, the apical progenitors (APs). However, the generation of deep layers immature Tbr1-positive neurons is increased, which do not translate into an increased pool of their derived Ctip2-positive specified neurons, that are actually diminished. Surprisingly, layering is maintained correctly. To elucidate in the future the possible specific role of ribosomal protein S6 kinase (S6K) in neurodevelopment as the key PDK1 efector, a novel double phosphomimetic construct, $S6K^{T229D/T389D}$, was created, which confirmed to work independently of both PDK1 and mTORC1 in a constitutively active manner.

Resum

La proteïna quinasa depenent de 3-fosfoinositidis (PDK1) és la quinasa mestra que coordina la via de senyalització de la fosfoinositol 3-quinasa (PI3K) ja que activa fins a 23 quinases de la família AGC, inclosa la PKB. PDK1 actua després de reconèixer un lloc d'acoblament conservat en els seus substrats, un cop aquest ha estat fosforilat prèviament per una altra quinasa diferent. PKB és la única excepció, ja que no requereix d'aquesta interacció per a que PDK1 l'activi eficientment. Una forma mutant de PDK1 on la leucina a la posició 155 va ser mutada a àcid glutàmic (L155E), malmetent així la butxaca que reconeix el lloc d'acoblament dels substrats, va ser creada i expressada en ratolins de forma condicional específicament en neurones. Aquesta mutació blocà la senyalització dependent de PI3K excepte per PKB, que s'activà de forma normal. Resultats anteriors havien demostrat que aquests ratolins mutants tenen una polarització i diferenciació neuronal reduïda *in vitro*, així com una col·locació neuronal anòmala i una connectivitat neuronal disminuïda a l'escorça i l'hipocamp *in vivo* en l'edat adulta. Aquí es demostra que la mutació PDK1 L155E causa microcefàlia. Els progenitors intermedis (IP) estan reduïts en nombre quan s'expressa la proteïna PDK1 L155E durant el neurodesenvolupament, i la mitosi dels seus predecessors, els progenitors apicals (AP), és menor a E15.5. Tanmateix, la generació de neurones immadures de capes profundes Tbr1-positives augmenta, però això no es tradueixen en un augment de la subpoblació neuronal Ctip2-positives derivada d'elles, que en realitat es veu disminuïda. L'estratificació de les capes, però, es manté correctament. Per dilucidar en un futur el possible paper específic de la quinasa de la proteïna ribosomal S6 (S6K) com a efector clau de PDK1 en el neurodesenvolupament, es va crear una nova proteïna doble fosfomimètica, $S6K^{T229D/T389D}$, que va confirmar de funcionar independentment tant de PDK1 com de mTORC1 d'una manera constitutivament activa.

Resumen

La proteína quinasa dependiente de 3-fosfoinosítidos (PDK1) es la quinasa maestra que coordina la vía de señalización de la fosfoinositol 3-quinasa (PI3K), ya que activa hasta 23 quinasas de la familia AGC, incluida PKB. PDK1 actúa tras reconocer un sitio de acoplamiento conservado de sus sustratos una vez éste ha sido fosforilado previamente por otra quinasa diferente. PKB es la única excepción, ya que no requiere de esta interacción para que PDK1 la active eficazmente. Una forma mutante de PDK1 donde la leucina de la posición 155 fue mutada a ácido glutámico (L155E), dañando así el bolsillo que reconoce el lugar de acoplamiento de los sustratos, fue creada y expresada en ratones de forma condicional específicamente en neuronas. Esta mutación bloqueó la señalización dependiente de PI3K excepto por PKB, que se activó de forma normal. Resultados anteriores habían demostrado que estos ratones mutantes tienen una polarización y diferenciación neuronal reducida *in vitro*, así como un posicionamiento neuronal anómalo y una conectividad neuronal disminuida en la corteza y el hipocampo *in vivo* en la edad adulta. Aquí se demuestra que la mutación PDK1 L155E causa microcefalia. Los progenitores intermedios (IP) están reducidos en número cuando se expresa la proteína PDK1 L155E durante el neurodesarrollo, y la mitosis de sus predecesores, los progenitores apicales (AP), es menor a E15.5. Sin embargo, la generación de neuronas inmaduras de capas profundas Tbr1-positivas aumenta, pero esto no se traduce en un aumento de la subpoblación neuronal Ctip2-positivas derivada de ellas, que en realidad se ve disminuida. La estratificación de las capas, sin embargo, se mantiene correctamente. Para dilucidar en un futuro el posible papel específico de la quinasa de la proteína ribosomal S6 (S6K) como efector clave de PDK1 en el neurodesarrollo, se creó una nueva proteína doble fosfomimètica, $S6K^{T229D/T389D}$, que confirmó funcionar independientemente tanto de PDK1 como de mTORC1 de una forma constitutivamente activa.

INTRODUCTION

Cortical development

The neocortex is the brain region that controls the higher-brain executive tasks involved in the cognitive control of behaviour and language functions, such as executive attention, working memory and decision-making. These orders are processed through synaptic plasticity, this is, the ability to change synapse connectivity depending on experience.

The transmission of the information by the cortex needs the presence of both glutamatergic excitatory neurons and GABAergic inhibitory interneurons, but also a correct connectivity amongst them. Glutamate is the major excitatory neurotransmitter in the nervous system, while γ-Aminobutyric acid (GABA) is the principal inhibitory one. Receptors and transporters for both molecules are found in the post-synaptic neurons. Glutamatergic and GABAergic neurons are originated from different progenitor pools that are located in different areas of the brain. Their range of connectivity is also different (Anderson *et al.*, 1997; Tamamaki, Fujimori and Takauji, 1997; Malatesta, Hartfuss and Götz, 2000).

Neocortex is mainly formed by excitatory glutamatergic neurons. They are born in the dorsal telencephalon, where a pool of pluripotent neural progenitors exists in the walls of the lateral ventricles. The adult cortex resolves into a laminar structure formed by 6 layers, each characterized by its specific composition of excitatory and inhibitory neurons. (Figure 2B, 2C). Corticodevelopment program includes instructions for their correct neurogenesis, radial migration and wiring. Through embryonic neurodevelopment, neurons differentiate into a vast variety of subtypes and reach their expected final-position layer thanks to the expression of their specific pattern of genes, which change dynamically as neurons undergo lineage bifurcation and maturation. Once positioned, they launch their axonal projections to different regions of the brain that can be intracortical, subcortical or subcerebral (Figure 2A) (Molyneaux *et al.*, 2007; Lodato and Arlotta, 2015).

Many efforts have been done in the last decades to define makers expressed specifically by each subpopulation of neurons. Recent evidences suggest that area specification of the distinct projection neurons subclasses could be regulated by postnatal epigenetic modification together with some genetic programs specific for each neuronal subtype (Harb *et al.*, 2015).

GLUTAMATERGIC NEURONS

After the closure of the neural tube, neuroepithelial cells convert to Radial Glia Cells (RGC), the neural stem cells of the cortex, also called Apical Progenitors. RGC are progenitors for both neuronal and glial lineages with their soma located at the ventricular zone (VZ) (Malatesta, Hartfuss and Götz, 2000; Miyata *et al.*, 2001; Noctor SC, Flint AC, Weissman TA, Dammerman RS, 2001; Heins *et al.*, 2002). During embryonic days E10.5 and E11.5, they undergo symmetric divisions, where daughter cells still maintain their pluripotent character, or differentiative divisions that set the fate of the daughter cell to one or another lineage. The symmetrical multiplication is called neural expansion (Figure 1).

The first differentiative division that commits with the neuronal lineage generates the Intermediate Progenitors (IP), a pool of cells that can still undergo one or two proliferative divisions but cannot change their fate (Haubensak *et al.*, 2004; Miyata *et al.*, 2004; Noctor *et al.*, 2004). These cells are found in the subventricular zone (SVZ). On the next division they undergo, IPs decide the subpopulation of projection neurons that they are specifying to and start expressing subpopulation-specific marker. Neurons are characterized for being terminally-differentiated undividing cells, so after this last division, post-mitotic neurons lose their ability to re-enter the cell cycle (Englund, 2005).

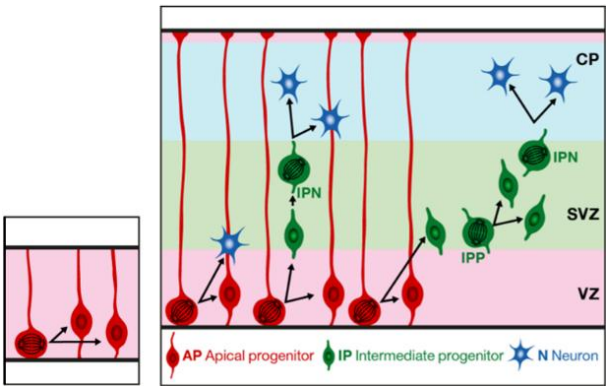

Figure 1: Schematic representation of cortical development of glutamatergic neurons: Apical Progenitors (AP, red) resident in the ventricular zone (VZ) undergo symmetric divisions from embryonic days E10.5 to E11.5 (left). At E12.5 divisions become neurogenic, producing Intermediate Progenitors (IP, green) and / or inmature postmitotic neurons (N, blue), dictated by a change in spindle orientation (from planar to oblique). IP are created in the subventricular zone (SVZ), where they can duplicate symmetrically for one or two times (IPP = Proliferative IP) or prepare to give birth to postmitotic neurons (IPN = Neurogenic IP), that will populate the Cortical Plate (CP) [modified from (Postel *et al.*, 2019)].

As the proliferative area is found in the ventricular and subventricular zones of the neocortex, newly-born neurons must migrate radially towards the meninges in an inside-out fashion that pushes the more recently born neurons up to the pial zone,

the region most separated from the ventricle (Figure 2B) (He *et al.*, 2015). Radial migration is supported by a scaffolding formed by the radial glia itself. These cells extend long processes from their nucleus, that is attached to the ventricular wall, to the most pial surface (Rakic, 2003). Migrating neurons assume a bipolar morphology and attach / detach to these appendices to translocate their somas towards their leading processes while reorganizing their cytoskeleton. Microtubule dynamics is key in this step, and both excessive stability and instability interfere with nuclear migration (Marín *et al.*, 2010). Interestingly, radial migration is not straight forward and includes multiple readaptations of the cell's morphology. Indeed, IPs and neurons generated from APs stop for 24 hours when they arrive to the SVZ, where they assume a multipolar morphology. The majority of them then launch a bipolar leading process back retrogradely to the ventricle and only after this extension contacts the ventricle, neurons reverse migration again towards the cortical plate and go back to their bipolar morphology (Kriegstein and Noctor, 2004; Noctor *et al.*, 2004).

Post-mitotic neurons, which in mice are originated from E12.5 onwards, are functionally classified according to the destination that their mature axonal projections reach. Importantly, their specialization depends on the neocortical layer they reach during neurodevelopment. Subcerebral projection neurons (SCPN) are always located in layer V and send axons to the optic tectum, brainstem and spinal cord. Layer VI is populated with corticothalamic projections neurons (CThPN) that send axons to the thalamus. Finally, callosal projection neurons (CPN) can be found in all layers except for IV (II/III, V and VI) and send axons to the contralateral cortex [reviewed in (Woodworth *et al.*, 2012)] (Figure 2A).

Glutamatergic ontogeny needs of stepped overlapping waves of expression and repression of specific transcription factors that progressively restrict the potential cell fate of each neuron. The different neuronal subpopulations can be nowadays labelled experimentally by detecting those molecular biomarkers that are key determinant elements for neuronal specification. Noteworthy, some of them are initially coexpressed but refined later on during neuronal differentiation (Figure 2C, P3) (Toma *et al.*, 2014).

Specific markers for RGC are the paired box protein Pax6, but also empty spiracles homeobox 2 (Emx2) and SRY-box containing gene 2 (Sox2) (Muzio and Mallamaci, 2003; Englund, 2005; Azim *et al.*, 2009). Pax6 participates in cell decision of the apical progenitors, and Pax6 mutants show an increased self-renewing tax because they fail to stop cell-cycling (Sansom *et al.*, 2009).

As they commit with the neuronal lineage, Pax6 is downregulated and IPs express

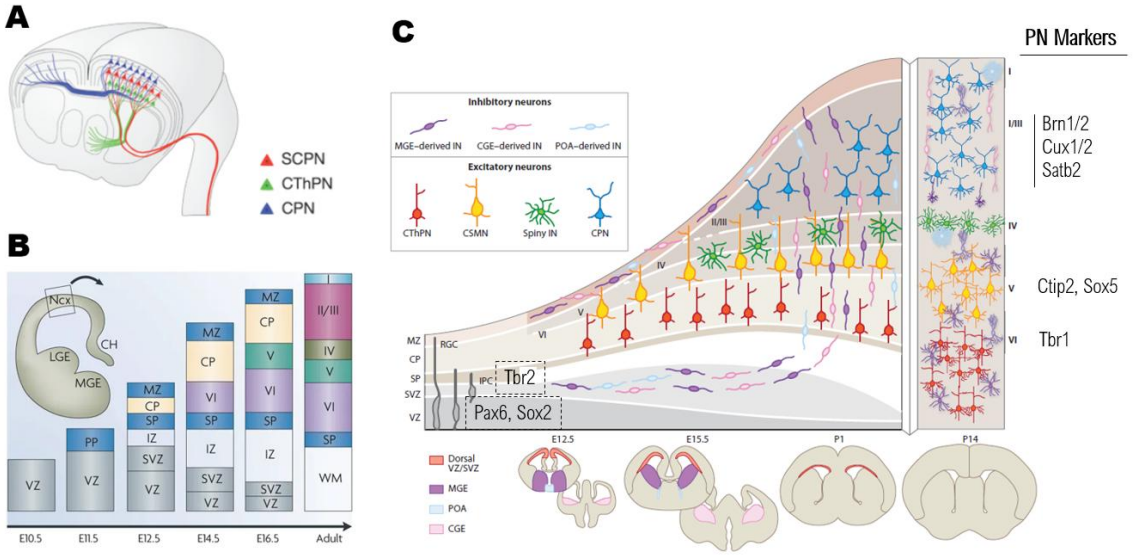

Figure 2: Final positioning and cortical developing of the projection neurons of the neocortex: (A) Major subtypes of projection neurons according to their hodology. Subcerebral Projection Neurons (SCPN, red) connect layer V of the cortex to structures outside the cerebrum including the pons, spinal cord and striatum; Corticothalamic Projection Neurons (CThPN, green) connect layer VI to the Thalamus and Callosal Projection Neurons (CPN, blue) are located in all layers except for layer IV and maintain single projections to the contralateral cortex. **(B)** Schematic representation of the formation of the Neocortex (Ncx) during different developing stages (embryonic day E10.5 to Adult). Progenitors of the ventricular zone (VZ) duplicate and create the subventricular zone (SVZ). The progeny of both layers expands in between the preplate (PP). The cortical plate (CP) starts forming and gradually developing into 6 different layers (in roman numerals) thanks to temporally overlapping neurogenic waves. The deepest VI layer is the first to be formed at E14.5, proving the inside-out fashion of stratification of the Ncx, where that later born neurons arriving from the VZ migrate across earlier born neurons. The initial Marginal Zone (MZ) at the pial surface ends up being populated by migrating Cajal-Retzius cells and becoming Layer I. SP = subplate; LGE = Lateral Ganglionic Eminence; MGE = Medial Ganglionic Eminence; CH = Cortical Hem. **(C)** Final composition of the 6 layers of the neocortex depicting both the excitatory neurons and interneurons (IN) in the adult brain (P14 right column) and during its development (E12.5 to postnatal P1). Projection neurons (PN) (red, yellow, dark blue) originate from the VZ as explained above. Selected biomarkers specific for PN are noted in the right column for fully developed layers and in dashed boxes for VZ and SVZ populations. Inhibitory and granular interneurons (purple, pink, clear blue, green) are expanded in the ventral telencephalon, that includes the Medial Ganglionic Eminence (MGE), Caudal Ganglionic Eminence (CGE) and the preoptic area (POA). They reach the neocortex following migratory streams that run tangentially to the radial glia scaffold in the MZ and the SVZ, and then switch to radial migration to position themselves. The represented areas are located for each stage of brain developmental (inferior raw). RGC = Radial Glial cells; IPC = Intermediate Progenitors Cells [modified from (Molyneaux *et al.*, 2007; Greig *et al.*, 2013; Lodato and Arlotta, 2015)].

Tbr2, a T-domain transcription factor, also called Eomes (Englund, 2005), or Btg antiproliferation factor 2 (also called Tis21) (Iacopetti *et al.*, 1999), which are specific markers for IP (Sessa *et al.*, 2008). However, IPs can also express at lower levels factors that will become exclusive for specific subpopulation of projection neurons (Zimmer *et al.*, 2004). When IPs become postmitotic projection neurons, Tbr2 is silenced and the immature post-mitotic neurons express other transcription factors depending on their time of birth.

Neurons that form the preplate express the T-domain transcription factor T-box, brain, 1 (Tbr1). When time progresses, Tbr1 ends up marking layer VI neurons and thus is a specific marker for corticothalamic projection neurons (Englund, 2005). This matches nicely with Tbr1 positive-cells being the earliest born neurons (created at E12.5 in mice) and occupying the deeper layer following the explained inside-out fashion of migration. Subcortical projection neurons (SCPN) that populate layer V appear just later. They are labelled by COUP-TF-interacting protein 2 (Ctip2) and sex determining region Y-box 5 (Sox5). Ctip2 functions downstream of another transcription factor, the family zinc finger 2 (Fezf2) and is necessary for correct pathfinding of SCPN axons (Arlotta *et al.*, 2005; McKenna *et al.*, 2011; Guo *et al.*, 2013).

Late-born neurons begin to emerge at E13.5. They express Special AT-rich sequence-binding protein-2 (Satb2), migrate to the upper layers (II/III) and become callosal projection neurons (Britanova *et al.*, 2005). Satb2 is an active transcriptional modulator that regulates the expression of a diversity of other upper-layer specific markers, such as Cux2, Brn-1 and -2 (also called Pou3f2 and Pouf2 respectively) (Dominguez, Ayoub and Rakic, 2013; Toma and Hanashima, 2015) (Figure 3). Finally, layer IV is not composed by projection neurons (PN) but by granule cells that are recipient for inputs from the thalamus and act as a gateway for processing information from peripheral sensory organs. Parvalbumin - expressing basket cells have a major role in this layer (Chittajallu and Isaac, 2010).

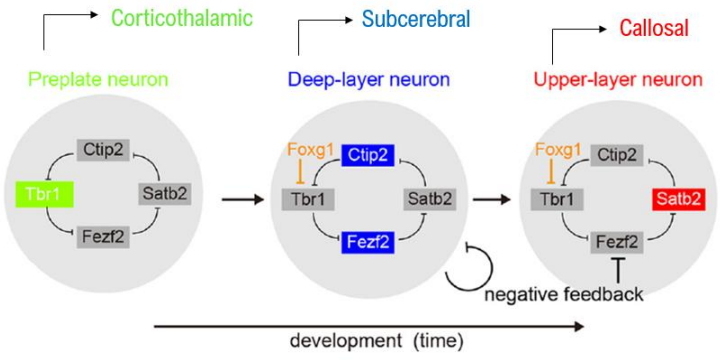

Figure 3: Transcriptional cascade for glutamatergic neuronal subpopulation specification. Forkhead transcription factor (Foxg1) activation downregulates the biomarker of layer VI corticothalamic and preplate neurons Tbox, brain, 1 (Tbr1). Tbr1 was directly repressing family zinc finger 2 (Fezf2), which once unleashed induces COUP-TF-interacting protein 2 (Ctip2) expression, responsible for layer V subcerebral specification. The accumulation of these type of neurons represses their own inducing transcription factors, which enables the expression of Special AT-rich sequence-binding protein-2 (Satb2) and the differentiation to upper II/III layer callosal neurons. Satb2 expression has been repressed by Fezf2, which is now inhibited by the negative feedback, but now can repress Ctip2 [modified from (Toma and Hanashima, 2015)].

These transcription factors activate and repress each other in time starting with the forkhead transcription factor (Foxg1). Foxg1 starts the expression program of general PN competences and suppresses the one of early progenitors by directly downregulating Tbr1 expression (Kumamoto *et al.*, 2013). Tbr1 stops repressing Fezf2, which once unleashed represses Satb2, thereby releasing Ctip2 from Satb2 inhibition. Later on, the expression of both SCPN biomarkers is repressed by the same post-mitotic neurons they are generating. Then, Satb2 is expressed downstream of Foxg1 to generate upper layer neurons, and represses Ctip2 and Tbr1 (Britanova *et al.*, 2008; Chen *et al.*, 2008; Han *et al.*, 2011; McKenna *et al.*, 2011; Toma *et al.*, 2014; Toma and Hanashima, 2015) (Figure 3).

Additionally, recent studies show that neuronal specification is not only controlled by transcriptional factors, but also by epigenetic mechanisms such as DNA methylations and histone modifications. Indeed, some of the factors above mentioned, like Tbr2, have shown to directly induce chromatin remodelling to specific gene loci (Sessa *et al.*, 2017).

However, (Franco *et al.*, 2012) results challenged this theory by revealing the existence of 2 possible distinct subpopulations of RGC already specialized into upper- and lower-layers -generating progenitors as early as the onset of cortical development. The authors state the coexistence of multiple RGC pools, a theory that had been previously stated (Beck and Burns, 1959) and cannot be discarded.

SWITCH FROM SYMMETRIC TO ASYMMETRIC DIVISIONS

The mechanisms that determine the fate of daughter cells after the mitosis of the apical and basal progenitors are not still completely understood. However, two major processes have shown to play a role in the switch from proliferative to neurogenic divisions.

- **Cell cycle length**

Cell cycle is regulated differently depending whether the division is symmetrical or asymmetrical. The time they spend in some critical steps affect the rate of neuron generation. Specifically, longer G_1 marks divisions that will be neurogenic, while longer S-phase (where DNA in the nucleus is replicated) is related to renewing divisions. Indeed, elongated S-phase or G_2 correlating with enhanced pluripotency are observed in mouse embryonic stem cells (Lukaszewicz *et al.*, 2002; Calegari and Huttner, 2003; Calegari *et al.*, 2005; Arai *et al.*, 2011; Gonzales *et al.*, 2015).

G_1 is a gap phase where cells control the stability of their genomic material before starting DNA replication. In this stage, cells show an increased responsiveness to extracellular cues that force differentiation and thus exit from the cell cycle. Therefore, shortening it is supposed to shield cells against responding to neurogenic signals by restricting their window of opportunity. Oppositely, its lengthening could facilitate the integration of the external differentiative indications and allow sufficient time for unequal distribution of heritage. G_1 induces changes in chromatin structure that promote the binding of transcription factors associated with differentiation. Also, cell cycle progression mark specific times (such as late G_1) where pro-differentiation transcription factors are phosphorylated and translocated into the nucleus through cyclin-dependent activation of protein kinases controlling cell division (CDK) (Ali *et al.*, 2011; Coronado *et al.*, 2013; Pauklin and Vallier, 2013; Dekker, 2014).

The duration of the overall neuronal population's cell cycle extends as corticogenesis advances, while the fraction of cells that exit cell cycle via differentiation increases. This is explained by this non-homogenic duration of the cell cycle for the two different types of divisions. By mid-corticogenesis, neurogenic division become the largest fraction and progenitor pool gets exhausted, which increases the mean cell cycle duration in the whole cortex (Polleux *et al.*, 1997). However, the shortened G_1 role in differentiation was challenged recently, and more studies are needed (Huurne *et al.*, 2017).

- **Mitotic spindle orientation**

The mitotic spindle is formed by centrosomes, microtubules and proteins associated to them such as kinesin and dynein. Progenitors that divide symmetrically to generate 2 daughters that retain the stem cell potential maintain a spindle orientation perpendicular to the lamina, as shown by the orientation of the sister chromatins. Instead, cells dividing asymmetrically change their cleavage from a plane to an oblique angle. This can have an effect on the way that the apical plasma membrane gets distributed in the 2 resulting cells. Even if this part represents only the 1-2% of the total cell surface, it contains all the adherent junctional complexes that link (or not) daughters to the most apical part of the VZ. Being so small, if the cleavage plane is not perfectly perpendicular, cleavage furrow does not bisect but bypasses it and one of the daughters does not inherit any part of the apical plasma membrane ((Kosodo *et al.*, 2004; Fish *et al.*, 2006), reviewed in (Lancaster and Knoblich, 2012)).

Mutations found in patients have confirmed the relevance of spindle orientation in a correct progenitor proliferation. The most common cause of primary microcephaly

in humans is mutation in ASPM, which encodes the abnormal spindle-like microcephaly-associated (Aspm) protein that functions (redundantly with another protein) by orientating the spindle poles (Bond *et al.*, 2002; Tungadi *et al.*, 2017). Also, CPAP mutation that encode incorrect versions of the *Cenpj* protein lead to microcephaly. The progenitors expressing this mutated protein are unable to form the spindle correctly and end up generating fewer progenitors. Interestingly, this aberrant cleavage planes change the fate of progenitors from apical to basal, but it does not increase neuronal production (Garcez *et al.*, 2015).

Defects on spindle orientation also affect neuron migration. Lissencephaly (smooth brain) is considered a neuronal migration disease, and can be caused by mutations in LIS1, a gene that regulates microtubule function and dynein motor activity, or DCX, encoding for doublecortin, a microtubule-associated protein expressed exclusively in neuronal tissue necessary for neuronal migration (Tanaka *et al.*, 2004).

- **Extrinsic factors**

Evidences support that both a cell-intrinsic program and extrinsic factors cooperate to determine the fate of daughter cells. Correct corticogenesis progression acts as an external cue itself, generating a signalling loop. The glutamate and GABA released by PN and interneurons respectively when they settle into the cortical plate stimulates the proliferation of precursors. As explained before (Figure 3), deep layer neurons signal back to cease its own generation and promote the upper layers production, and they do so by forcing VZ precursors to a SVZ identity. Axons established by deeper layer neurons release mitogenic factors that shorten G_1 phase and promote proliferation. Cajal-Retzius cells that arrive at the marginal zone (MZ) (that will later transform into layer I) secrete a glycoprotein called reelin responsible for a correct neuronal migration that also accelerates the proliferation in both VZ and SV [reviewed (Dehay and Kennedy, 2007; Lakomá, Garcia-Alonso and Luque, 2011; Bartolini *et al.*, 2017; Silva *et al.*, 2018)].

GABAergic INTERNEURONS

Interneurons are GABAergic inhibitory neurons that stablish local connections and are divided in different groups according to their spiking profiles (Figure 4B, 4C). They are born in the subpallium structures called medial ganglionic eminence (MGE), caudal ganglionic eminence (CGE) and preoptical area (POA). Each area generates different types of interneurons, that are differentiated by the expression of parvalbumin (PV), somatostatin (SST) or the serotonin receptor 3A (Htr3a),

among others that allows distinguising them even more [reviewed in (Lim *et al.*, 2018)].

From these areas to their final positions, interneurons follow a migration composed by 3 phases: tangential migration to and into the pallium, cortical plate dispersion and layering. All these steps are guided by chemorepulsive and chemoattractive cues produced by different cell types that promote the motogenic movement of the interneurons [reviewed in (Marín, 2013)]. Interneurons are expelled from MGE by chemorepulsive cues and lead towards the cortex by gradients of chemoattractive factors that are produced by pallium's cells and diffuse at a long range in the tissue, such as neuregulin-1 (Nrg1) (Marín *et al.*, 2003; Wichterle *et al.*, 2003). Other factors, such as brain-derived neurotrophic factor (BDNF), neurotrophin-4 (NT4), GABA and glutamate, have proven *in vitro* to induce motogenic movement of interneurons (Figure 4A) (Polleux *et al.*, 2002; Bortone and Polleux, 2009; Inada *et al.*, 2011).

When entering the pallium, interneurons follow two specific migratory streams: a superficial path that runs through the MZ, and a deep path that runs exactly over the SVZ (Figure 4A). Remarkably, interneurons dispersion is avoided: they do not penetrate the CP during the tangential migration step, where pyramidal cells are still forming cortical layers at that time (Lavdas *et al.*, 1999; Wichterle *et al.*, 2001). There is an active exclusion of interneurons from the CP by chemorepulsive signaling but the main mechanism of control is that migration paths are composed of specific cells (leptomeninges and IP) who express C-X-C motif chemokine 12 (Cxcl12, also called stromal-derived factor 1 or SDF-1), a chemokine that induces interneurons migration. Cxcl12 has a strong affinity for the heparan sulfates proteoglycans of the extracellular matrix, so it does not diffuse into the CP and allows the exact framing of these migration routes. Receptors C-X-C chemokine receptor type 4 (Cxcr4) and Cxcr7 are necessary for responsiveness to Cxcl12. Loss of responsiveness to Cxcl12 is the trigger used by interneurons to switch from tangential to radial movement and start invading the CP. This is a progressive event where early-born interneurons start infiltrating to the CP first, while late-born interneurons are still migrating tangentially from the subpallium. Mutant mice lacking Cxcr4 or Cxcr7 receptors prematurely accumulate interneurons in the CP by infiltrating them as soon as they reach this area. Thus, CP contains indeed a chemoattractive activity towards interneurons, but it is not strong enough to act until interneurons lose their receptiveness to the Cxcl12 arising from the lamina. Additionaly, semaphorins (semas) mark repelling zones that prevent interneurons to enter the CP prematurely (Stumm *et al.*, 2003; Tamamaki *et al.*, 2003; Tiveron *et al.*, 2006; Li *et al.*, 2008; López-Bendito *et al.*, 2008; Rueda *et al.*, 2008; Tanaka *et al.*, 2010; Sánchez-Alcañiz *et al.*, 2011; Wang *et al.*, 2011).

Finally, interneurons must localize their specific layer into the cortex to finally develop their specific morphology and electrophysiological profile. Chemoattractive signals expressed by the specific pyramidal cells of every cortical layer dictate the final position of their paired interneurons, whose identity is likely specified at their birth. This idea was proved experimentally by manipulating ectopically the identity but not the localization of pyramidal cells during neurodevelopment. Changing subcerebral projection neurons to callosal projection neurons without moving them from layer V in mice resulted in disrupted layering of interneurons and reduced presence of somatostatin and parvoalbumin-positive interneurons, which were ectopically located in upper layers II-IV (Lodato *et al.*, 2011). The final positioning of interneurons is completed in postnatal days and includes a round of programmed cell death that eliminates more than 30% of the interneurons generated embryonically, specifically the ones that are not functionally integrated and present no activity. This apoptotic program is mediated by an increase in the levels of phosphatase and tensin homolog (PTEN) (Pla *et al.*, 2006; Lodato *et al.*, 2011; Southwell *et al.*, 2012; Bartolini *et al.*, 2017; Wong *et al.*, 2018).

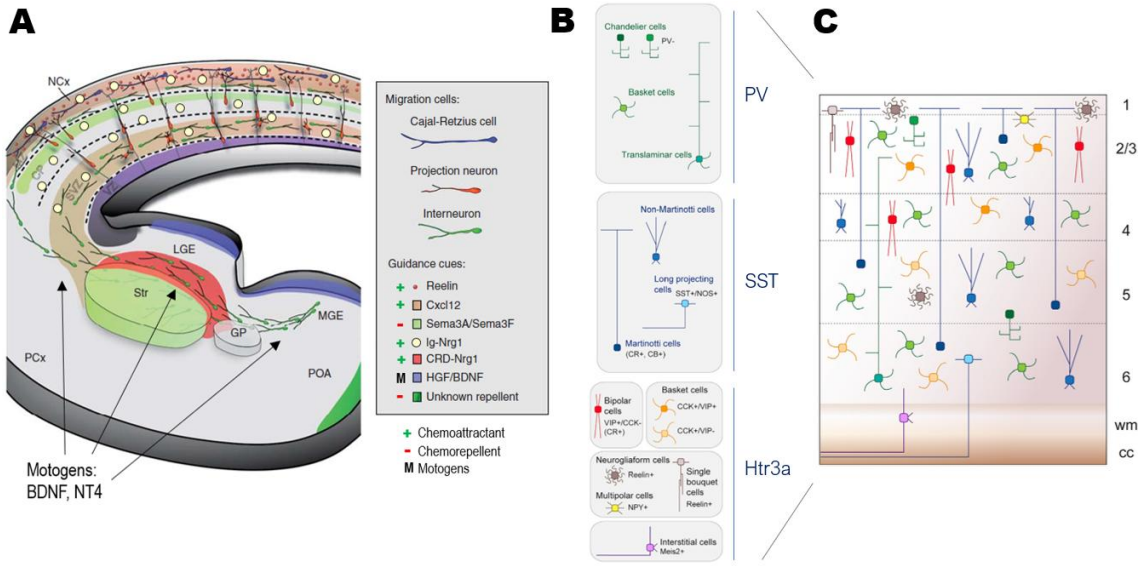

Figure 4: Diversity, positioning and migration pathways of the GABAergic interneurons in the mouse cortex: (A) Migration streams (in mauve and beige) that run through the marginal zone (MZ) and the subventricular zone (SVZ), and guidance cues that lead the interneurons (green) born in the subpallium to the neocortex (Ncx). Nrg = Neuregulin; Sema = Semaphorins; BDNF = brain-derived neurotrophic factor; Cxcl12 = C-X-C motif chemokine 12; CP = Cortical plate; VZ = Ventricular Zone; LGE = Lateral Ganglionic Eminence; MGE = Medial Ganglionic Eminence; Str = Striatum; POA = Preoptical area; GP = Globus Pallidus; PCx = piriform cortex **(B)** Schema depicting the main classes of cortical interneurons, their morphology and expressed markers: parvoalbumin (PV), somatostatin (SST), and the serotonin receptor 3A (Htr3a), which includes calretinin- (CR) and vasoactive intestinal peptide (VIP)-expressing subtypes. **(C)** Laminar distribution of the different subtypes of interneurons in the different layers of adult cortex of mice. Some of them are found in many while others have a much more restricted laminar distribution. Wm = white matter; cc = corpus callosum [modified from (Marín *et al.*, 2010; Lim *et al.*, 2018)].

Signalling in the Developing Neocortex

NEUROTROPHINS

The survival, fate, axonal outgrowth and synaptic plasticity of neurons are controlled, among others, by secreted proteins called neurotrophins, which are expressed during development but also in adulthood. Four neurotrophins constitute the "classic" neurotrophin family in mammals: Nerve growth factor (NGF), Brain-derived neurotrophic factor (BDNF), Neurotrophin (NT)-3 and NT-4/5. Each of them signals through a specific transmembrane receptor of the tropomyosin receptor kinase (Trk) family: TrkA for NGF, TrkB for both BDNF and NT-4/5, and TrkC for NT-3. All neurotrophins can also bind with low affinity to a shared receptor named p75 neurotrophin receptor (p75NTR). The non-mature proforms of the neurotrophins (previous to their maturating cleavage) also bind p75NTR with high affinity. Noteworthy, p75NTR is the only neurotrophic receptor that can transmit both pro-survival and apoptotic signals.

Neurotrophin binding triggers Trk dimerization and autophosphorylation of different tyrosine residues at their intracellular domains. This event activates three main signalling cascades: phosphoinositide phospholipase C (PLCγ), mitogen-activated protein kinase (MAPK) / extracellular signal-regulated kinase (ERK) and phosphatidylinositol 3-kinase (PI3K). Overall, MAPK/ERK and PI3K pathways promote neuronal differentiation and survival, while PLCγ activates calcium dependent proteins and promotes the expression of ion channels. Due to these relevant roles, alterations in neurotrophin transmission could translate into neural dysfunction [reviewed in (Reichardt, 2006; Nieto, Kukuljan and Silva, 2013; Numakawa *et al.*, 2013)].

PI3K REGULATED SIGNALING PATHWAY

Phosphatidylinositol-3-kinases (PI3Ks) are a family of kinases that act on different intracellular inositol lipids that reside in the membranes. The generated phosphoinositides act as secondary messengers to activate signaling pathways that regulate important physiological functions such as cell proliferation, size, survival, motility or glucose homeostasis (Engelman, 2009; Vanhaesebroeck *et al.*, 2010; Thorpe, Yuzugullu and Zhao, 2015).

3 classes of PI3 kinases (class I to III) exist according to their substrate specificity. The most studied one is class-I, whose activity is triggered by extracellular signals such as growth factors, hormones or cytokines. They couple intracellularly to tyrosine kinase receptors (class-Ia PI3K) or G protein-coupled receptors (GPCRs) (class-Ib). These two subclasses use different regulatory subunits to activate different isoforms of the PI3K p110 catalytic subunit, which transform phosphatidylinositol 4,5-bisphosphate (PtdIns(4,5)P_2) into phosphatidylinositol (3,4,5)-trisphosphate (**PtdIns(3,4,5)P_3**). Instead, class-II and Class-III PI3Ks reaction product is phosphatidylinositol 3-phosphate (PI-3-P). They are not receptor-regulated, but have instead a role in controlling endosomal, lysosomal and phagosomal trafficking systems by participating in vesicle tethering, protein sorting and trafficking steps (Vanhaesebroeck, Stephens and Hawkins, 2012).

When Class-Ia PI3Ks are activated, their p85 regulatory subunit binds to previously activated RTKs (Receptor Tyrosine Kinases). This binding allows the recruitment of cytosolic p85-p110 heterodimers to the membrane. In the dimer, p85 is both stabilizing and at the same time inhibiting p110. When dimers translocate, the catalytic subunit gets spatially in contact with its membrane-lipid substrate, PtdIns(4,5)P_2, enabling the reaction to take place and producing PtdIns(3,4,5)P_3 in the membrane (Figure 5) (Jiménez *et al.*, 2002).

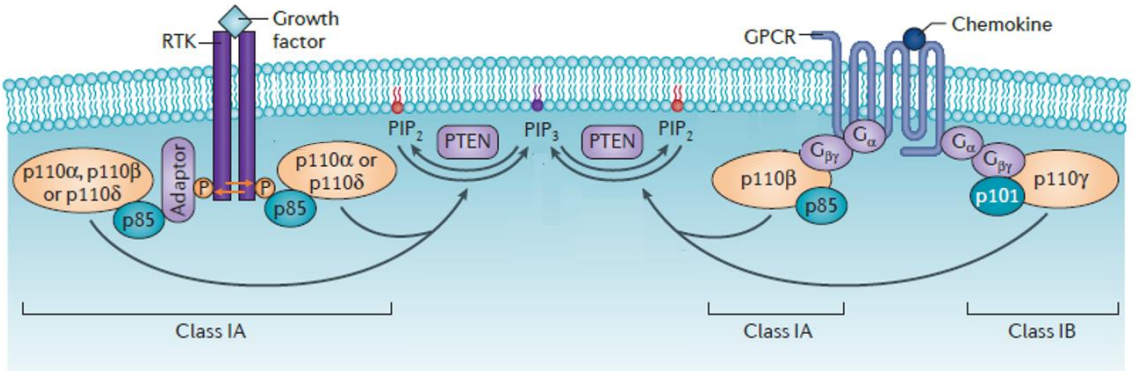

Figure 5: Signalling by class I phosphatidylinositol-3-kinases (PI3K). Extracellular stimuli bind its transmembrane receptors, which can be receptor tyrosine kinases (RTK) for class-IA, or G-protein coupled receptors (GPCR) for class-IB. RTKs activation induces their dimerization and transautophosphorylation in Tyrosine residues, whilst GPCRs activation leads to the activation of their cognate trimeric G proteins. Either the phosphorylated Tyr residues of RTKs or the heterodimer Gβγ subunit released from the GPCRs can recruit the regulatory subunits p85 (or p101 for GPCRs) of PI3K, that translocate from the cytoplasm in form of heterodimers containing the catalytic subunit of PI3K, p110. Once in the membrane, p110 phosphorylates phosphatidylinositol 4,5-bisphosphate (PIP_2) into phosphatidylinositol (3,4,5)-trisphosphate (PIP_3), who also remains in the lipidic bilayer. Phosphatase and tensin homolog (PTEN) is the phosphatase that converts PIP_3 back to PIP_2 [modified from (Thorpe, Yuzugullu and Zhao, 2015)].

Phosphatase and tensin homolog (PTEN) is the enzyme responsible for terminating the stimuli once the signal is transmitted. It is a lipid and protein phosphatase that removes the 3' phosphate from PtdIns(3,4,5)P_3 to produce PtdIns(4,5)P_2. By doing so, it inactivates PI3K signaling. Accordingly, PTEN is a tumor suppressor gene whose loss of function is present in a wide spectrum of PI3K-driven cancers (Vanhaesebroeck *et al.*, 2010). PTEN regulation is not completely understood, but a recent study discovered a feedforward loop acting while the PI3K / Forkhead box O (FOXO) pathway remains active, which increases PTEN protein levels through the FOXO-induced expression of a PTEN-stabilizing deubiquitinase (Park *et al.*, 2019).

Although 50–100 estimated downstream effectors of PI3K exist in every cell (Vanhaesebroeck, Stephens and Hawkins, 2012), studies have focused in a small number of them, and specifically in the PI3K / phosphoinositide-dependent kinase-1 (PDK1) / Protein kinase B (PKB) axis. This is because this pathway was found to be incorrectly activated in many cancers, and both PI3K and PKB proteins showed oncogenic properties (Staal, Hartley and Rowe, 1977; Chang *et al.*, 1997). PKB (also known as Akt) is a serine-threonine kinase activated in response to PI3K and is its major effector in cancers.

PDK1 AND THE AGC KINASE FAMILY

The PtdIns(3,4,5)P_3 triggered signalling pathway mostly relays on the phosphoinositide-dependent kinase-1 (PDK1) kinase. PDK1 is a widely expressed, constitutively active enzyme that responds to rises in the levels of this second messenger. This kinase is meant to elicit many of the cellular responses to PI3K activation by activating in turn as much as twenty-three protein kinase isoforms of the AGC family, of which PDK1 is also a member of.

As PDK1 is constitutively active, regulating the capacity to interact with its substrates plays a key role in this pathway. This is dictated by dynamic, structurally-based modifications of both PDK1 and its substrates, which can change their cellular localization or their ability and affinity to interact each other. Because of that, the structural and biochemical discoveries of the pathway governed by PDK1 have advanced hand by hand during the last two decades, by meant of structural, biochemical, cellular and genetic approaches, to finally place PDK1 as the first example of a so-called master kinase controlling a complex network rather than a linear signalling cascade. Unravelling the structural details of PDK1 and the AGC kinase family substrates was key to understand the mechanisms of regulation of this intrincate signalling cascade (Figure 7), which are depicted in the next section.

Structural motifs of PDK1

- **The Hydrofobic Motif (HM)**

All eukaryotic protein kinases exhibit similar catalytic domains. The active site lies in a cleft formed by two different lobes: the predominantly β-sheet conformed small N-terminal lobe and the α-helical enriched C-terminal lobe (Hanks and Hunter, 1995). Besides that, a number of kinases of the AGC family present a C-terminal conserved hydrophobic motif (**HM**) that includes the FXXF(S/T)F signature (Figure 6) (Rettenmaier *et al.*, 2014). PDK1 lacks any HM and is therefore the most remarkable exception to this rule. The Ser/Thr residue laying in this hydrophobic motif was found to be phosphorylated in many AGC family members by different upstream protein kinases, which served to trigger the binding of PDK1 to these substrates in order to phosphorylate and activate them. For this reason, the hydrophobic motif was called the PDK1 – Interacting Fragment (PIF) (Balendran *et al.*, 1999).

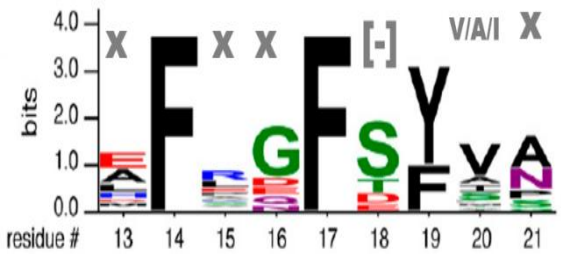

Figure 6: Diagram showing the consensus sequence within the hydrophobic motif (HM) of 28 PDK1-interacting AGC kinases. Sites with high variability are shown in grey letters. [-] indicates the presence of a negatively charged amino acid that can either be Asp, Glu, or a phosphorylated Ser/Thr. x = any amino acid [modified from Retternmaier *et al.*, 2014]

- **The PIF pocket**

The region in the PDK1 protein responsible for the interaction with its phosphorylated substrates was found to be a hydrophobic pocket located in the small lobe of the catalytic domain, which was called the **PIF-pocket**. This binding site is also present in the different AGC family members, and serves an important intramolecular role in maintaining the activated conformation of the kinase. The most essential amino acid in establishing interactions with the HM was found to be Leucine 155, located in the core of the PDK1 hydrophobic PIF-pocket. When mutated to Glutamic Acid, the interaction with and activation of most PDK1 substrates is reduced or even abolished. Notably, the ability of PDK1 to phosphorylate and activate PKB, however, was not affected (Biondi *et al.*, 2000; Collins *et al.*, 2003). Supporting the necessity of a previous phosphorylation in the HM, a different regulatory phosphate-binding site was found close to the PIF pocket. In this region, Arginine 133 was predicted to accommodate the negative charges of a phosphate group. Mutation of this residue to alanine confirmed its role in activating correctly PDK1 substrates such as Ribosomal protein S6 kinase (S6K),

p90 ribosomal S6 kinase (RSK) or Serum and glucocorticoid-regulated kinase (SGK), while PKB was again normally activated (Biondi *et al.*, 2002; Collins *et al.*, 2005).

- **The T-loop**

Binding of PDK1 to the HM leads to the phosphorylation of the substrates in the activation loop, also called **T-loop** (Mora *et al.*, 2004). This T-loop is present in any eukaryotic kinase, and it is essential in regulating the catalytic kinase activity by promoting the structural transition to the active conformation. The T-loop is found in the catalytic domain but connects both N- and C- terminal lobes through an αC-helix (Biondi *et al.*, 2002). The phosphorylation of the T-loop transmits conformational changes through the relocation of this αC-helix, which coordinates the creation of a network of hydrogen bonds in the cleft of both lobes between a Glutamic Acid of the αC-helix, a Lysine of the N-lobe and the phosphates of the ATP, which stabilizes the active conformation of the enzyme (Komander *et al.*, 2005).

- **The Pleckstrin Homology (PH) domain**

Apart from the kinase domain, the C-terminal end of PDK1 contains a modular structure called Plekstrin Homology (**PH domain**). This domain interacts with high affinity with PtdIns(3,4,5)P_3 and with lower to PtdIns(3,4)P_2 (Alessi *et al.*, 1997). The presence of this domain is not shared as a common trait of the AGC kinase family. Apart from PDK1, the only AGC kinases possessing this domain are PKB isoforms, where it is located at their N-terminus and can only and specifically interact with PtdIns(3,4,5)P_3.

PI3K pathway activation induces the recruitment of both PDK1 and PKB to the plasma membrane through the binding of their PH domains to the newly generated the PtdIns(3,4,5)P_3 second messenger. There, their colocalization facilitates the rate at which PDK1 can phosphorylate and activate PKB (Currie *et al.*, 1999). However, if this colocalization cannot occur (e.g. in PDK1 PH-domain mutants) PKB is still activated, but at reduced levels (Bayascas *et al.*, 2008).

Amongst the amino acids that conformed the phosphoinositide binding site of PDK1, Lysine 465 was predicted to stablish fundamental interactions with phosphates at position 3' and 5' of the inositol ring. Mutating this residue to a Glutamic Acid abolished phosphoinositide binding (Komander *et al.*, 2004). Cells expressing this PDK1 mutant were unable to activate PKB efficiently, while the rest of PDK1 substrate were unaffected (Bayascas *et al.*, 2008).

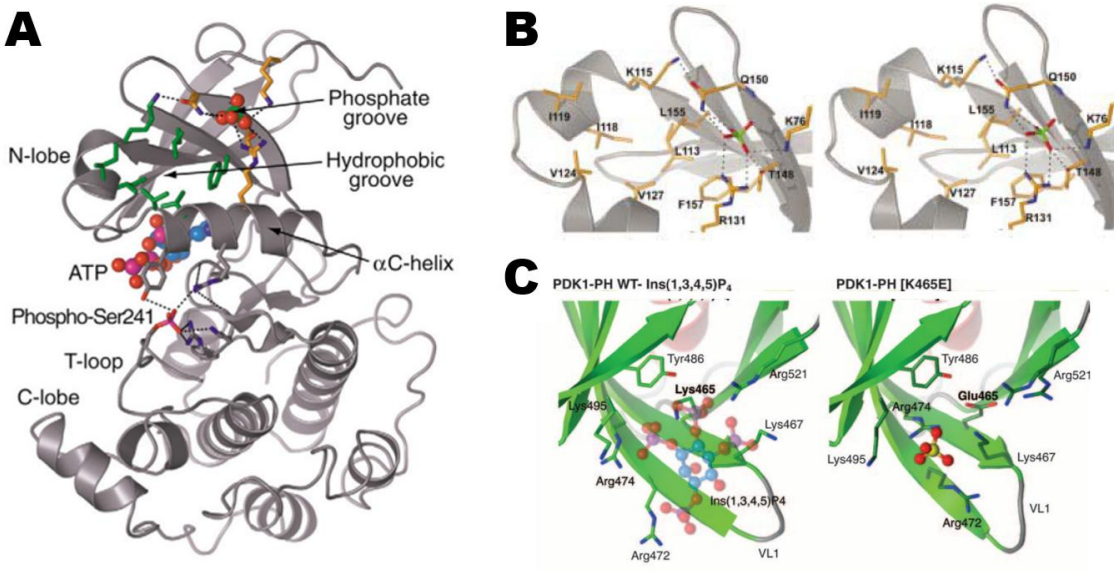

Figure 7: **Tertiary structure of PDK1**. **(A) Representation of the kinase domain of PDK1.** Color code: green = residues forming the hydrophobic motif (HM); orange = residues forming the phosphate pocket. ATP and a sulfate molecule are depicted as colored spheres, where purple = phosphate ions; red = oxygen atoms. Sulphate is coming from the crystallization preparation and occupies the pocket destined to the phosphate of the phosphorylated HM, acting as an alternative tetrahedral oxy-anion **(B) A stereo image of the residues forming the PIF- and the phosphate – pockets**. PDK1 backbone is shown as a grey ribbon. Color code: orange = carbon atoms; black dotted lines = hydrogen bonds **(C) Structure of the isolated PDK1 PH domain**, both the wild type (left, amino acid 465 = Lysine) and K465E (right, amino acid 465 = Glutamic Acid) versions. PtdIns(1,3,4,5)P_4 is represented as a ball-and-sticks model (color code: blue = inositol ring; purple/red = phosphate groups). Green ribbon represents PH domain β-sheets and some of its relevant residues are depicted. The introduction of the K654E mutation does not affect overall PH domain structure but blocks interaction with PtdIns(1,3,4,5)P_4, reason why a sulphate (yellow and red spheres) appears bound to the pocket in substitution of the phospholipid [modified from (Biondi *et al.*, 2002; Collins *et al.*, 2005; Bayascas *et al.*, 2008)].

- **Other motifs**

Other members of the AGC kinase family can present an additional structure called turn or zipper motif, which is not present in PDK1. It is located between the catalytic domain and the HM and contains a conserved phosphorylation site (Ser/Thr followed by a Proline). Turn motifs are in some cases indispensable for maintaining the stability of the whole enzyme. They are also involved in shielding the HM against dephosphorylation by guiding it into their own PIF-pocket where it interacts intramolecularly (Frödin *et al.*, 2002; Hauge *et al.*, 2007).

Activation of PDK1

PDK1 is considered a constitutively active enzyme due to the ability to autophosphorylate on its activation loop at Serine 241 (Ser241) and on its PH domain residue Threonine 513 (Thr513). The fact than bacterially expressed PDK1 exhibited intrinsic activity confirmed this notion. Autophosphorylation is helped by the formation of PDK1 homodimers, which is triggered after PtdIns(3,4,5)P_3 binding. While Ser241 phosphorylation is required for PDK1 activation and stability, preventing Thr513 phosphorylation in the otherwise activated PDK1 leads to loss of affinity to the membrane (Casamayor, Morrice and Alessi, 1999; Komander *et al.*, 2005; Masters *et al.*, 2010). Despite being constitutively active, PDK1 activity can be further stimulated by extracellular signals *in vivo*. This can be explained through dynamic changes in the conformational status of the kinase that fine tune its activation. For instance, interactions with different species of anionic phospholipids that are antagonistic amongst them; or the creation and disruption of different homodimeric states, that can be inhibitors or enhancers of its activity. Indeed, recent structural analysis showed that the PH domain of PDK1 (specifically, its basic residues Arginine 466 and Lysine 467) can bind anionic phospholipids other than PtdIns(3,4,5)P_3 such as phosphatidylserine (PtdSer) with lower affinity. This interaction, that happens when PtdIns(3,4,5)P_3 is not present in the membrane, restructures homodimers in a way that the two kinase domains are too proximal, which could block the access of the substrates to the active site (Figure 8) (Heras-Martínez *et al.*, 2019).

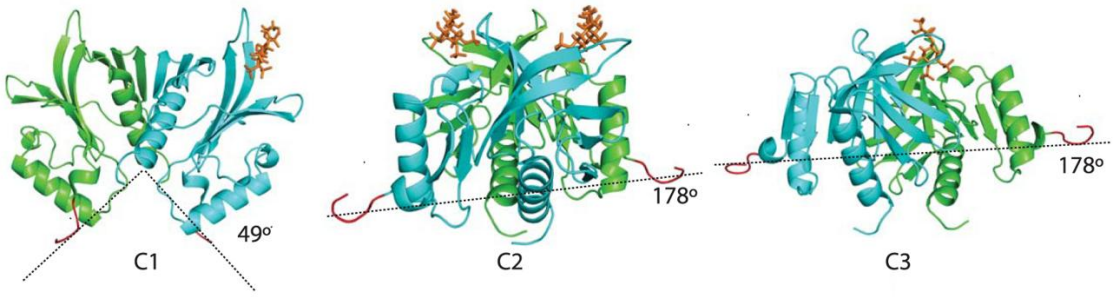

Figure 8: **Three possible homodimeric conformers** (Cn) **of the PH domain of PDK1.** Homodimerized PDK1 PH domains conformations when binding phosphatidylserine (C1) vs PtdIns(3,4,5)P_3 (C2: 2 molecule bound to the 2 PH domains of the dimer; C3: 1 molecule bound to only 1 PH domain of the homodimer). Color code: PDK1 PH domains = green and blue (1 molecule of PDK1 / each); orange stick model = phospholipids; Purple segments: unstructured N-terminal linkers that mediate association to the kinase domains. Angles quantify the aperture given to the substrates of PDK1 to access the kinase active site [modified from (Heras-Martínez *et al.*, 2019)].

Mechanism of activation of the AGC kinases

The growth factor stimulated AGC kinase family members share a common mechanism of activation where two phosphorylations need to occur in two different but highly conserved motifs: the HM and the T-loop. PDK1 is responsible for the final phosphorylation in the T-loop of its substrates. However, to be able to interact with most substrates but PKB, they must first receive a previous phosphorylation in their HM (Figure 10A, C). This phosphorylation is catalyzed by a variety of kinases acting on the PDK1 substrates (Figure 9) and binding to the phosphorylated HM has allosteric effects on PDK1 catalytic site that increase its activity (Biondi *et al.*, 2001, 2002). Phosphorylations on the activation loop and the HM synergize in stabilizing the αC-helix of the AGC kinases, binding to one side of it each.

Most of the phosphorylations on the PDK1 substrates that are agonist-dependent are performed by one or another of the mammalian target of rapamycin (mTOR) complexes, mTORC1 or mTORC2. This makes this phosphorylation event sensible to extracellular signals, such as insulin or growth factors, or internal, such as energy levels or amino acids existence. However, exceptions such as PKCs exist [reviewed in (Bayascas, 2010)].

Importantly, for none of the PDK1 substrates, HM phosphorylation alone is enough for their activation. However, it is necessary for their own stabilization. Indeed, AGC kinases bind intramolecularly their own phosphorylated HM by means of their own PIF-pockets. This stabilizes allosterically their active conformation by affecting the αC-helix structure and the conformation of their ATP-binding site, decreasing the K_m for ATP binding (Frödin *et al.*, 2002; Leroux, Schulze and Biondi, 2018).

The hydrophobic motif kinases: mTOR complexes

- **mTORC1**

  Composition of the complex

mTORC1 complex is formed by mTOR, regulatory-associated protein of mTOR (raptor) and mammalian lethal with SEC13 protein 8 (mLST8), which is dispensable for the function of the complex (Figure 11). Its activation is regulated by Ras Homologue enriched in Brain (Rheb) and the tuberous sclerosis complex (TSC) complex, which includes TSC2 and TSC1. Rheb G-protein is a guanosine triphosphate (GTP)ase that is normally inhibited because TSC complex selectively activates Rheb's owns GTPase activity, acting as a GAP (GTPase activating

protein). Only when TSC complex is inactive, Rheb is derepressed, which allows the formation of the complex mTORC1 [reviewed in (Liu and Sabatini, 2020)].

A

Kinase	Regulatory Mechanisms
	Phosphorylation
AKT	PDK1, mTORC2, DNA-PK
CRIK	Autophosphorylation?
DMPK	Raf-1
GRK	PKC (GRK2), autophosphorylation (GRK5)
LATS	MST1/2
MAST	?
MRCK	Transautophosphorylation
MSK	ERK1/2, p38, autophosphorylation
NDR	Autophosphorylation, MST3
PDK1	Transautophosphorylation
PKA	PDK1/autophosphorylation?
PKC	PDK1, mTORC2
PKG	Autophosphorylation
PKN	PDK1
PRK*	?
ROCK	Autophosphorylation?
RSK	PDK1, ERK, autophosphorylation
RSKL	-
S6K	PDK1, mTORC1
SGK	PDK1, mTORC2
SGK494	?

B

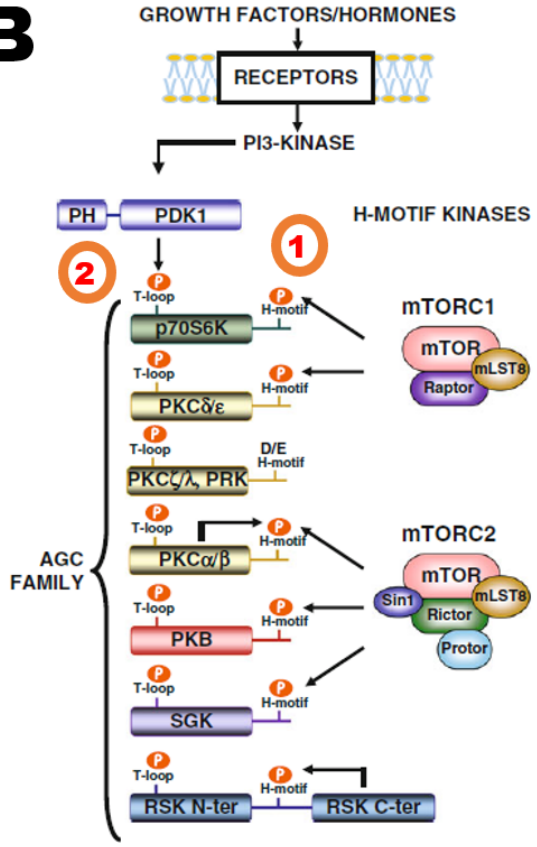

Figure 9: **Cascades regulating the activation of the AGC kinase family members. (A) Upstream kinases that activate the AGC kinases.** mTOR complexes together with PDK1 are predominant. - = no evidences; ? = still not determined; CRIK: citron rho-interacting kinase; DMPK: dystrophia myotonica-protein kinase; DNA-PK: DNA-dependent protein kinase; ERK: extracellular signal-regulated kinase; GRK: G protein-coupled receptor kinase; LATS: large tumour suppressor; MAST: microtubule-associated Ser/Thr kinase; MRCK: myotonic dystrophy kinase-related; MSK: mitogen- and stress-activated protein kinase; MST: mammalian sterile 20-like; mTORC: mTOR complex; NDR: nuclear Dbf2-related kinase; PDK1: 3-phosphoinositide dependent kinase; PI3K: phosphoinositide 3-kinase; PKA: cAMP-dependent protein kinase; PKC: protein kinase C; PKG: cGMP-dependent protein kinase; PKN: PKC-related protein kinase; PRK: Protein kinase; RSK: ribosomal S6 kinase; RSKL: RSK-like kinase; S6K: p70 ribosomal S6 kinase; S100B; SGK: serum- and glucocorticoid-induced protein kinase; SGK494: Sugen kinase 494. **(B) Mechanism of activation of the agonist-stimulated AGC kinases.** Dual phosphorylation of the AGC family members in the T-loop and hydrophobic motif (H-motif) is shown. Growth factors, hormones and cytokines activate PI3K, whose product promotes the phosphorylation and activation by PDK1. mTOR complexes (mTORC1 and mTORC2) are formed after activation by both extracellular and intracellular signals. A first phosphorylation by mTOR complexes in the Hydrophobic motif (H-motif) of the PDK1 substrates takes place (encircled 1). This allows the interaction between PDK1 and its substrates by the coupling of their phosphorylated H-motif into the PDK1 PIF-pocket. Only then, the second phosphorylation in the activation loop (T-loop) by PDK1 happens (encircled 2), and substrate kinases become fully activated [modified from (Bayascas, 2010; Pearce, Komander and Alessi, 2010)].

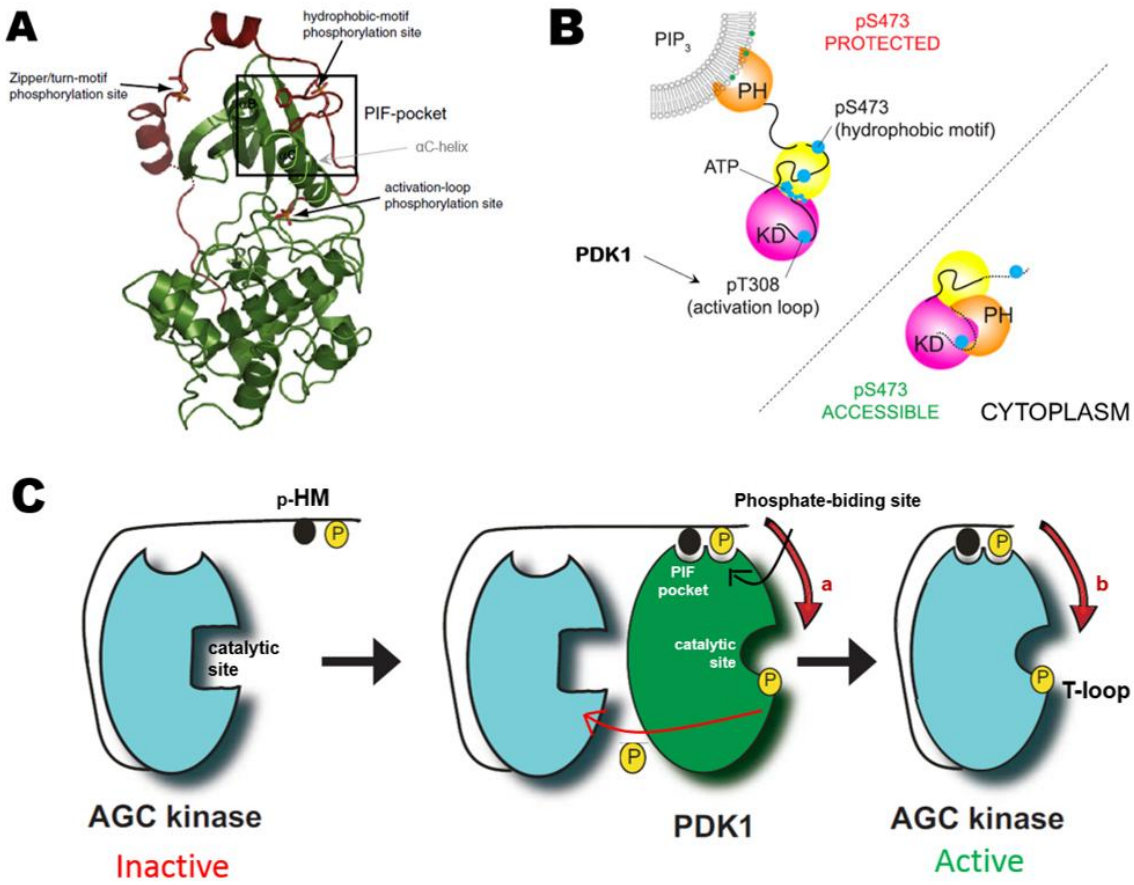

Figure 10: **Structural interactions regulating the activation of agonist-dependent AGC kinases. (A) The three most shared phosphorylation motifs necessaries for the activation of the AGC kinases.** Positioning of the relevant activating motifs to be phosphorylated inside the structure of the AGC kinases: the hydrophobic motif (HM), the activation loop (also called T-loop), and the optional turn/zipper -motif. The PIF-pocket is also shown (squared). The T- loop and the HM get phosphorylated one in each side of the αC-helix (highlighted in light green) and stabilize it and the whole AGC kinase into the active conformation. The specific structure depicted as an example here corresponds to PKCβ II. **(B) PIF-pocket-independent activation of PKB.** The Plekstrin Homology (PH)-domain of PKB is recruited to the plasma membrane by the phosphatidylinositol (3,4,5)-trisphosphate (PIP_3) generated by PI3K. This association reshapes PKB in a way that deprotects its activation loop to make it accessible for PDK1, which in turns phosphorylates the Threonine 308 (pT308). The other activating site, pS473, is phosphorylated by mTORC2 complex after stimulation by growth factors and hormones and gets structurally protected when PKB is bound to the membrane. Instead, the cytoplasmatic conformation of PKB allows its free PH domain to intramolecularly bind its own kinase domain (KD), auto-inhibiting the activation by PDK1 and leaving pS473 spatially accessible to phosphatases. Because of that, membrane-dissociated PKB is deactivated in a short time. **(C) PIF-pocket-dependent PDK1 activation of the AGC kinases.** A phosphorylation in the HM of the inactive AGC kinases is necessary to interact with the PDK1 interacting (PIF)-pocket of PDK1 and annexed phosphate-binding pocket. This selective docking triggers the second activating phosphorylation in the T-loop of the substrates by PDK1. Red arrows indicate allosteric effects, where (a) the binding of their substrates into the PIF-pocket promotes the active conformation of the catalytic site of PDK1, and (b) the intramolecular interaction of the phosphorylated HM with their own PIF-pocket stabilizes the active conformation of the AGC kinases [modified from (Arencibia *et al.*, 2013; Lučic *et al.*, 2018; Leroux *et al.*, 2019)].

TSC2 is regulated by both inhibitory and activatory phosphorylations acting at different sites. Cascades triggered by PI3K and Ras inactivate TSC2 through its downstream effectors PKB, RSKs and ERK. Instead, in response to hypoxia or in conditions of low intracellular energy, REDD1 (regulated in development and DNA damage response 1) or 5' adenosine monophosphate-activated kinase (AMPK), respectively, activate TSC2 to indirectly maintain mTORC1 inactive (Inoki, Zhu and Guan, 2003; Roux *et al.*, 2004; Ma *et al.*, 2005; Deyoung *et al.*, 2008).

40 kDa Proline-rich Akt substrate (PRAS40) is another endogenous inhibitor of the mTORC1 complex that binds to Raptor. When phosphorylated by PKB at Threonine 246, it dissociates from the complex and facilitates its access to its substrates (Sancak *et al.*, 2007; Wang *et al.*, 2007).

Activation of mTORC1 complex

mTORC1 is a master regulator that triggers the growth response to amino acids and nutrients availability. Oppositely, increases in AMP levels actively block mTORC1 complex, and so does hypoxia. Growth signals induce mTORC2-mediated PKB activation, who then phosphorylates its substrates TSC2 and PRAS40. These phosphorylations create binding sites for the adaptor proteins 14-3-3, which send the mTORC1 inhibitors to proteasomal degradation, allowing the activation of the complex. Contrarily, in a situation of lack of oxygen, Hypoxia Inducible Factors (HIF) promote the expression of REDD1, who has a high affinity for 14-3-3 proteins and hijacks them. As these adaptors are not available to bind TSC2 or PRAS40, even if they are phosphorylated, mTORC1 formation remains blocked yet in presence of trophic stimulation. Low energy levels, for example in a glucose deprivation scenario, activate AMPK, which phosphorylate TSC2 in a site that enhances its activity.

Amino acids are critical regulators of mTORC1, and above all of them, leucine and arginine. Their levels are detected by sensors that directly bind these two amino acids or their co-substrates (like the methyl donator s-adenosyl methionine) (Gu *et al.*, 2017). These sensors activate different downstream cascades depending on whether they are free in starvation conditions or sequestered by abundance of nutrients. Specific sensors and their downstream signalling are different depending on the two possible sources of amino acids: cytoplasmatic or lysosomal, who elicits the amino acid recovery by the induction of autophagy.

Actually, lysosomes are necessary for both responses, as the specific activators of mTORC1 are embedded into its membrane. For example, the above mentioned Rheb can only maintain its active, GTP-bound conformation when it is bound to the lysosomal membrane (Inoki, Zhu and Guan, 2003). The recruitment of the

mTORC1 complex to the lysosome membrane is regulated by the Rag GTPases, who already reside there (Sancak *et al.*, 2008). Rags are a family of 4 small GTPases that pair themselves as obligated heterodimers where a subunit of RagA or RagB binds to another of RagC or RagD. These heterodimers interact directly with the Raptor adaptor of the mTORC1 complex but only if the combination between Rags and the nucleotide they are loaded with is as follows: $RagA/B^{GTP}$ - $RagC/D^{GDP}$. The reverse loading status makes Rags unable to bind mTORC1 (Rogala *et al.*, 2019). In turn, Rags nucleotide-bound status is regulated by guanine nucleotide exchange factors (GEFs) or GTPase activator proteins (GAP) that act on them. GEFs load GTP into Rags in exchange of GDP to create active or inactive $heterodimer^{nucleotide}$ combinations, while GAPs stimulate the hydrolysis of its GTPs. GAP activity toward Rags (GATOR1) is a relevant GAP complex. One of its subunits has direct GAP activity towards GTP bound to RagA/B and thus acts as an inhibitor of mTORC1 (Shen, Choe and Sabatini, 2017). GATOR1 is not directly regulated by amino acids and it needs to be recruited itself to the lysosome (Wolfson and Sabatini, 2017). On the opposite hand, another complex, called GATOR2, antagonizes GATOR1 and thus potentiates mTORC1 activation (Wolfson *et al.*, 2016).

Leucine levels in the cytoplasm are sensed by mTORC1 thanks to the cytosolic Sestrin proteins. Indeed, leucine molecules can directly bind a pocket of Sestrin2. In starvation conditions, Sestrin2 is free and directly binds and inhibits GATOR2, which now cannot prime mTORC1 translocation to the lysosome. Arginine cytoplasmatic levels instead are sensed by the cellular arginine sensor for mTORC1 (CASTOR1). This protein works also by inhibiting GATOR2 when arginine is missing, and dissociating when there is abundance, allowing GATOR2 to act.

Lysosomal detection of the amino acid level depends on arginine. This residue regulates the export of essential amino acids out of the lysosome by the arginine - dependent SLC38A9 transporter, which is anchored in the lysosomal membrane. In this way, the autophagic products can be recovered into the cytoplasm and sensed by Sestrin2 and CASTOR1. Moreover, this channel also loads Rag heterodimers in the active GTP-bound combination (Wyant *et al.*, 2017).

Interestingly, while 8 amino acids (Ala, Arg, His, Leu, Met, Ser, Thr, and Val) signal through Rags, two of them, namely glutamine and asparagine, have proven to activate mTORC1 independently of the GTPases. They act through ADP-ribosylation factor 1 (Arf1) through a mechanism that is still unknown. As a clue, asparagine has already demonstrated to regulate mTORC1 activity by acting as an exchange factor in the uptake of extracellular amino acids, action that requires of a concomitant exportation of a molecule of arginine (Krall *et al.*, 2016; Meng *et al.*,

2020). Finally, recent studies have found that leucine can activate mTORC1 independently of the lysosomal localization of mTOR in a mechanism that depends on sensing the increased levels of uncharged tRNAs (Averous *et al.*, 2014, 2016).

Apart from amino acids, growth factors also activate mTORC1. The most studied effector is insulin, which signals through the PI3K / PKB / TSC2 axis as explained above. Instead, various cellular stresses inhibit mTORC1 activation to block proliferation. An increase in Endoplasmatic Reticulum Unfolded Protein Response (UPR) increases the levels of Sestrin proteins, whose only overexpression is enough to suppress mTORC1 signalling *in vitro* independently of leucine levels. Both ATP depletion marking a glucose deprivation and DNA damage induce AMPK activity to activate TSC2 and block mTORC1 (Liu and Sabatini, 2020).

Effects of mTORC1 activation

mTORC1 activation triggers the cascade for cell proliferation and cell size growth. Through transcriptional, translational, and posttranslational mechanisms, it stimulates the biosynthesis of proteins, lipids, nucleic acids, ribosomal RNA, ATP and reduced cofactors. At the same time, it blocks catabolic autophagy and β-oxidation of lipids. It even redirects the expression of cell cycle regulators.

Very importantly, mTORC1 activation redirects the cellular priorities for glucose usage towards an accumulation of ATP and carbon atoms. Cells increase the expression of glycolytic enzymes to promote glycolysis over oxidation; they strengthen the pentose phosphate pathway to reduce NADPH that will feed the

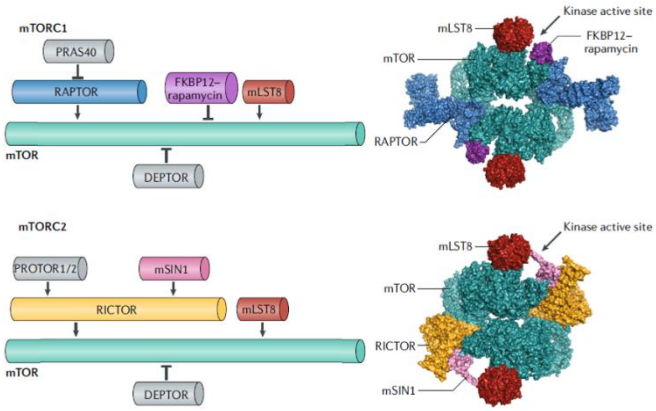

Figure 11: **Components of the two complexes formed by the mammalian target of rapamycin (mTOR), mTORC1 and mTORC2.** Composition of mTORC1 (up) and mTORC2 (down) complexes, with their structural representation. mTOR kinase (green) is the shared kinase domain, while other components are regulatory. mammalian lethal with SEC13 protein 8 (mLST8, burgundy) is shared but the rest are complex-specific. The binding site of rapamycin to mTOR when forming mTORC1 (FKBP12–rapamycin, purple) is depicted; in mTORC2, rapamycin-insensitive companion of mTOR (Rictor, yellow) regulator hides that domain, turning mTORC2 complex into insensitive to rapamycin. Proline- rich AKT substrate 40 kDa (PRAS40, grey) is an endogenous inhibitory component of the mTORC1 complex recruited by the Regulatory- associated protein of mTOR (Raptor, blue) adaptor. DEPTOR: DEP- domain-containing mTOR- interacting protein; PROTOR1/2: protein associated with rictor 1 or 2; mSIN1: MAPK- interacting protein [modified from (Liu and Sabatini, 2020)].

lipids and nucleotides production; and they increase mitochondrial biogenesis [reviewed in (Dibble and Cantley, 2015; Liu and Sabatini, 2020)].

- **mTORC2**

Composition of the complex

mTORC2 complex is formed by mTOR, mLST8 and rapamycin-insensitive companion of mTOR (rictor). Rictor binds MAPK- interacting protein 1 (mSIN1), protein associated with rictor 1 or 2 (PROTOR1/2) and also Deptor, which is shared by the 2 complexes. Interestingly, mSIN1 contains a PH domain which guides mTORC2 into the plasma membrane (Figure 11) (Yuan and Guan, 2015).

Activation of mTORC2 complex

mTORC2 is regulated by growth factors, specifically by insulin or serum through the PI3K pathway and the subsequent generation of PtdIns(3,4,5)P_3. mTORC2 is endogenously found in membranous compartments such as plasma membrane, the outer mitochondrial membrane and a subpopulation of early and late endosomes. Even if the apparition of the phospholipid enriches the presence of the complex in the cell membrane through the PH domain of mSIN1, the mTORC2 activity specific from this cell fraction is independent on PI3K (as happens in the mitochondria). Curiously, the only PI3K-regulated mTORC2 activity is the one present on early and late endosomes, suggesting the existence of different subpopulations of mTORC2 with distinct sensibility to PI3K signaling (Ebner *et al.*, 2017). Recent studies point at the small GTPases of the Ras family as the responsible proteins regulating the location of mTORC2 complex instead of external cues, by binding the mTOR kinase and MAPKAP1 directly (Kovalski *et al.*, 2019). The PH domain encoded by mSIN1 also autoinhibits the mTORC2 complex by interacting with the mTOR kinase when PtdIns(3,4,5)P_3 is not being generated (Liu *et al.*, 2015).

Effects of mTORC2 activation

Importantly, mTORC2 is the kinase necessary for phosphorylation of some of the PDK1 substrates, such as PKB, several PKCs and SGK1. However, it's notable to say that phosphorylation of certain PKB substrates can happen without mTORC2-mediated PKB phosphorylation (e.g. TSC2 and glycogen synthase kinase 3 (GSK3)) but it remains indispensable for others (e.g. FOXO1/3a) [reviewed in (Liu and Sabatini, 2020)]. Also, blocking the formation of mTORC2, specifically by knocking rictor down, impairs the regulation of the cytoskeleton through PKCα and affects chemotaxis in migration, which is very relevant for metastasis (Ikenoue *et al.*, 2008).

- **Crosstalk between mTORC1- and mTORC2- regulated pathways**

Insulin -activated pathway controls the termination of its own signal by a negative feedback where p70-S6K1, a downstream effector of the pathway, phosphorylates and inactivates Insulin Receptor Substrate 1 (IRS-1) (Shah, Wang and Hunter, 2004; Um, Frigerio and Watanabe, 2004). This downregulation dampers mTORC2-mediated response as well, which is also PtdIns(3,4,5)P_3-dependent.

PKB stands out the most relevant protein intertwining the effects of both pathways. Indeed, it is responsible and necessary for phosphorylating and thus inactivating two of the inhibitors of the mTORC1 complex: PRAS40 and TSC2. However, this can only happen if PKB has been previously phosphorylated by mTORC2 at its residue Serine 473, followed by a second phosphorylation done by PDK1 at residue Threonine 308 to complete the optimal activation of PKB.

PDK1 substrates

Amongst PDK1 substrates, I will do a brief close-up on the most studied and relevant ones: Ribosomal protein S6 kinase (S6K), Protein kinase B (PKB), Protein Kinase C (PKCs), serum and glucocorticoid-regulated kinase (SGK) and Glycogen synthase kinase 3 (GSK3).

- **Ribosomal protein S6 kinase (S6K)**

Two different members of the S6K family exist that are coded by two different genes: S6K1 and S6K2. They are 83% homologous on their kinase domains but differ in their C- and N-terminal domains. Both of them generate different isoforms. S6K1 is the most studied protein, as it is the only S6K protein activated in conditions of nutrient deprivation, and p70-S6K1 its most studied isoform. p85-S6K1 is a different isoform that contains 23 additional amino acids in the N-terminal. S6K2 also expresses different isoforms, being the predominant p54-S6K2, but also existing p56-S6K2, with additional 13 amino acids in the N-terminal. Finally, shorter versions of S6K1 generated by alternative splicing have been found in mice (p31-S6K1) and humans (h6A and h6C) which are oncogenic, while long variants also generated by alternative splicing have the opposite effect and act as tumour-suppressors. The additional sequences of the largest isoforms encode for nuclear localization signals (NLS). However, the subcellular location of p85-S6K1 and p56-S6K2 was found to be predominantly cytoplasmatic, and what is more, the shorter p70-S6K1 version, that does not encode any NSL, can also be found in the nucleus. Its location is however regulated by the cell cycle, only appearing in the nucleoplasm during mid G_1 phase. This translocation is dependent on mTOR

phosphorylation (Grove *et al.*, 1991; Rosner and Hengstschla, 2011; Ben-Hur *et al.*, 2013; Pardo and Seckl, 2013).

S6Ks are activated following the dual phosphorylation mechanism explained above, where the first one is catalyzed by mTORC1 in the HM, followed by PDK1 in the T-loop. For p70-S6K1, the phosphorylated residues are Threonine 389 within the HM and Threonine 229 at the T-loop. S6K1 has also an auto-inhibitory domain at the C-terminus that interacts with its own N-terminus and hides the phosphorylation residues to its upstream kinases. This inhibitory domain has to be phosphorylated as the first step towards the activation, specifically at Serines Ser411, Ser418, Ser421 and Ser424, which opens the inhibitory domain and the dual activating phosphorylation can happen. These phosphorylations are made by c-Jun N-terminal kinase 1 (JNK1) and can lead to S6K degradation if mTORC1 is not activated jointly (Zhang, Gao and Ye, 2013). Inactivating post-traductional modifications have also been reported, such as S6K acetylation in the C-terminal. *In vivo*, this is prevented by sirtuins, a family of deacetylases with are relevant for controlling cell cycle, mitochondrial metabolism and aging. On the other hand, S6K2 has been less studied. It contains almost the same phosphorylation sites than S6K1, only lacking one of the serines in the inhibitory domain, which is phosphorylated downstream of MEK/ERK. Then, it is activated by mTOR phosphorylation at Threonine 388 and PDK1 at Threonine 228. Finally, S6Ks activity is regulated by phosphatases. p70-S6K1 is specifically dephosphorylated by protein phosphatase (PP2A) at Thr229 and PH domain leucine-rich repeat-containing protein phosphatase 2 (PHLPP2) at Thr389 (Price, Mukhopadhyay and Avruch, 1991; Alessi *et al.*, 1998; Burnett *et al.*, 1998; Pullen *et al.*, 1998; Banerjee *et al.*, 2006; Pardo and Seckl, 2013; Zhang, Gao and Ye, 2013; Hong *et al.*, 2014; Tavares *et al.*, 2015).

S6K participates in the control of cell signalling, cell cycle, transcription, protein synthesis, cell proliferation, apoptosis and cytoskeleton rearrangement. The best-known target of S6Ks is ribosomal S6 protein (rpS6), a component of the 40S ribosome subunit. Both the S6K1 and S6K2 are required for the complete phosphorylation of the ribosomal S6 protein, although S6K2 has a more important contribution (Pende *et al.*, 2004). However, the role of rpS6 phosphorylations is uncertain, as mice expressing a mutated version of rpS6 that cannot be phosphorylated are viable and have an unaffected translation of 5' terminal oligopyrimidine (TOP) mRNAs (the ones encoding for components of the translational machinery). Surprisingly, the protein synthesis and cell division of their embryonic fibroblasts (MEF) are accelerated, resulting in these cells being smaller than the control MEFs (Ruvinsky *et al.*, 2005). Recent evidences suggest that phosphorylation is needed for the transcription of genes involved in ribosomal biogenesis. Indeed, S6K is a major regulator of the ribosome biogenesis (RiBi), and

mice lacking S6K1 and S6K2 display defects on this transcriptional program. Over 75% of ribosomal of RiBi factors are controlled by S6K, together with another substrate of mTORC1, eukaryotic translation initiation factor 4E -binding protein 1 (4E-BP1). Specifically, their combined action stimulates RNA polymerase I and III machinery to transcript ribosomal RNA (rRNA), needed for *de novo* assembly of ribosomes (Mitchell *et al.*, 2015; Filer *et al.*, 2017). This effect can be attributed to S6Ks substrate rpS6, as the same RiBi-reduced transcriptional activation is observed in mice lacking S6K1 and S6K2 (Chauvin *et al.*, 2014).

p70-S6K1 also promotes protein synthesis because some of its substrates regulate the interaction of the RNA helicase eukaryotic initiation factor-4A (eIF4A) with the 40S ribosomal subunit during cap-dependent translation. This helicase is necessary to scan the mRNA 5'-untranslated region (5'-UTR) in search of the AUG start codon. Specifically, p70-S6K1 phosphorylates Programmed Cell Death Protein 4 (PDCD4), a hijacker of eIF4A when unphosphorylated, and eIF4B, a stabilizer of the interaction of eIF4A with other ribosomal subunits. Interestingly, mRNAs with more stable secondary structures are more affected by the lack of helicase inside the translational complex. Thus, p70K-S6K inhibition could not only affect the global rates of protein synthesis but also profile the pattern of which ones are expressed (Yang *et al.*, 2003; Holz *et al.*, 2005; Dennis, Jefferson and Kimball, 2012).

S6K is a key element in the negative feedback loop that terminates the signalling started by insulin trough PI3K. In particular, it phosphorylates and inactivates Insulin Receptor -1 (IRS-1). This leads to a contradictory situation when mTOR is inhibited chemically. Then, the insulin signal is amplified instead of stopped, because S6K is unable to repress IRS-1 (Um, Frigerio and Watanabe, 2004; Depeursinge *et al.*, 2010).

Both S6K1 and S6K2 have shown to regulate transcriptional factors, with S6K2 being especially relevant in $CD4^+$ T helper cells, as they need this kinase to differentiate into Th17 subclass (Kurebayashi *et al.*, 2012). S6K1 also regulates apoptosis by phosphorylating proteins that participate in the programmed cell death such as GSK3 protein (Zhang, Gao and Ye, 2013) and the pro-apoptotic protein Bcl-2-associated death promoter (BAD) (Harada *et al.*, 2001). Finally, S6K is the upstream activator kinase for activating carbamoyl-phosphate synthetase 2, aspartate transcarbamylase, and dihydroorotase (CAD), the enzyme that catalyses the first three steps of the *de novo* synthesis of pyrimidine synthesis (Benjamin *et al.*, 2011; Ben-Sahra *et al.*, 2013).

Interestingly, recent studies showed that S6K could have a tissue-specific regulation that changes completely its substratome, based on distinct phosphorylations on its C-terminal auto-inhibitory domain. In adypocites stimulated

with insulin, S6K1 is phosphorylated in Ser424 and Ser429, which, united to the canonical activating phosphorylations, changed S6K1 structure and substrate specificity, loosing affinity for the classical substrates, such as rpS6, and gaining instead affinity to novel substrates related to lipid metabolism (Arif *et al.*, 2019).

- **PKB**

PKB is a central effector of the PI3K pathway induced by insulin, as it is the kinase responsible for phosphorylating and inactivating two mTORC1 inhibitors, TSC2 and PRAS40. It was discovered as the protein encoded by the Akt oncogene, and indeed many human cancers display recurrent activation of PKB (Noorolyai *et al.*, 2019).

PKB is activated by dual phosphorylation of PDK1 in Threonine 308 at the T-loop and mTORC2 at Serine 473 within the HM. PKB contains a PH domain that promotes the translocation of the kinase to the plasma membrane and colocalization with its activator PDK1, increasing the efficiency of PKB activation (Lizcano and Alessi, 2002) (Figure 12). However, without translocation, PKB activation can happen anyway, but at a slower rate (Zurashvili *et al.*, 2013). This correlates with the fact that PKB orthologs lacking any PH domain have been found in ancestral eukaryotes, in which even reduced levels of PKB activity play essential roles for cell survival. Later on in evolution, the appearance of the PH domain in metazoans created an additional, highly efficient mechanism of PKB activation which attributed new substrates to the kinase that participate in more complex, sofisticated processes such as neuronal differentiation (Zhou *et al.*, 2014). Recent studies propose an active role of PKB bond to the membrane in its activation. Indeed, PKB bound to PtdIns(3,4,5)P_3 (or even PtdIns(4,5)P_2) assumes a conformation that protects it from dephosphorylation. Instead, it is robustly

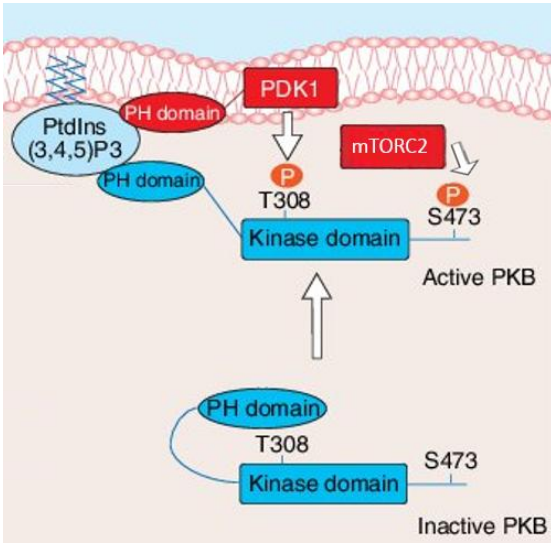

Figure 12: **Mechanism of activation of PKB, based on its cellular location.** The PH domain promotes the interaction of both PKB and PDK1 with the PtdIns(3,4,5)P_3 generated at the plasma membrane by PI3K after stimulation with extracellular signals. This colocalization converts PKB into a substrate for PDK1, who phosphorylates its Threonine 308 (T308) at its T-loop. PKB needs a second activating phosphorylation on its hydrophobic motif at Serine 473 (S473), which is performed by the mTORC2 complex activated after extracellular stimulation by growth factors and hormones. Activation of PKB by PDK1 only based on the interaction with its phosphorylated HM, without PtdIns(3,4,5)P_3 binding, can also happen but at inefficient rates [modified from Lizcano *et al.*, 2002].

autoinhibited due to intramolecular interactions between its own free PH and kinase domain when dissociated from the membrane, since this soluble conformation is easily accessible by phosphatases (Ebner *et al.*, 2017; Lučic *et al.*, 2018).

PKB has three isoforms (called PKBα/Akt1, PKBβ/Akt2 and PKBγ/Akt3), that are encoded by different genes but share 85 % of their sequence and structure. PKBα is expressed ubiquitously, but PKBβ and PKBγ are overrepresented in insulin-responsive tissues (such as liver, skeletal muscle and adipocytes) and brain and testis, respectively. Consequently, single-isoform knockout mice suffer from different phenotypes: growth retardation and increased neonatal death for PKBα, type II diabetes-like syndrome for PKBβ and decreased brain size for PKBγ (Tokuda *et al.*, 2011). However, all three isoforms are present in the brain but expressed with area- and cell-type- specificity and having isoform-specific functions. In relation to this findings, isoform-specific mutations appear preferentially in patients with schizophrenia (PKBα), gliomas (PKBβ) or brain growth (PKBγ) (Levenga *et al.*, 2017).

PBK is necessary for neuronal survival as it acts directly on elements that will otherwise activate the apoptotic program. PKB phosphorylates Bcl2 associated agonist of cell death (Bad), an inhibitor of the Bcl-2 - mediated apoptosis, and FoxO3, a transcription factor that induces the expression of pro-apoptotic genes. Finally, PKB also targets GSK3 and suppresses its downstream apoptotic program (Cross *et al.*, 1995; Brunet *et al.*, 1999; Orike *et al.*, 2001). However, the relevance of PKB specifically in neurotrophin-induced neuronal survival is starting to be challenged, as Bad knockout mouse neurons do not show alterations in apoptosis (Jiao and Li, 2011; Rai *et al.*, 2019).

- **p90 ribosomal S6 kinase (RSK) and mitogen- and stress-activated kinase (MSK)**

RSKs, also known as MAPKAP-K1, are a family of four (*RSK1-4*) 80% homologous serine–threonine protein kinases. All of them are detected in all human tissues although their relative levels vary between tissues: *RSK1* is expressed preferentially in lung, bone marrow and T-cells; *RSK2* in T-cells, lymph nodes and prostate; and *RSK3* in lung, brain, spinal cord and retina. Instead, *RSK4* is expressed homogeneously but its mRNA is less abundant than the other three isoforms. In the brain, the *RSK3* gene was predominantly expressed in the developing neural and sensory tissues, while *RSK2* could be detected in regions with high synaptic activity, including the neocortex, hippocampus and Purkinje cells, but only in adult samples. RSKs regulate several cellular processes including cell proliferation, survival, transcription and translation and have been broadly studied because more than 30% of all human cancers harbour mutations on them

[reviewed in (Anjum and Blenis, 2008; Romeo, Zhang and Roux, 2012; Lara, Seckl and Pardo, 2013)].

RSK proteins are characterized by having two functional catalytic domains in the same polypeptide belonging to different families and separated by a linker region. The N-terminal kinase domain (NTKD) belongs to the AGC family while the C-terminal catalytic domain (CTKD) is homologous to the calcium/calmodulin-dependent protein kinase (CAMK) family ones (Jones *et al.*, 1988; Bjørbaek, Zhao and Moller, 1995; Fisher and Blenis, 1996). They also contain a docking site known as D-domain at their C-terminal, which recruits ERK1/2 when RSK is still inactive (Smith *et al.*, 1999). Indeed, activation of the Ras/MAPK pathway by extracellular signals involved in cell growth and proliferation results in RSK phosphorylation by ERK at three different sites. The first phosphate is placed on the CTKD of RSK and serves to activate this domain (Zhao, Bjørbæk and Moller, 1996), which now can autophosphorylate the HM of its own molecule, situated in the linker region (Dalby *et al.*, 1998). ERK1/2 additionally phosphorylates 2 residues in the turn motif of the linker of RSK, necessaries to allow the interaction of PDK1 with the phosphorylated HM. PDK1 then phosphorylates Serine 221 in the NTKD, leading to a fully active RSK (Jensen *et al.*, 1999; Frödin *et al.*, 2000).

RSK1-3 are cytoplasmatic proteins that transit momentarily to the membrane before translocating to the nucleus once activated, together with its activator ERK. Instead, RSK4 stays in the cytoplasm even after stimulation (Chen, Sarnecki and Blenis, 1992; Richards *et al.*, 2001; Dümmler *et al.*, 2005).
RSKs have plenty of substrates, including the 40S ribosomal subunit protein S6 (rpS6), the one that allowed its original identification because of its *in vitro* activity (Erikson and Maller, 1985). Later studies demonstrated that S6Ks, whose specificity was elucidated later, were the major phosphorylators of rpS6 inside somatic cells (Chung *et al.*, 1992). This was confirmed by specific chemical inhibition of mTORC1 using Rapamycin (that does not affect RSKs activation), or with the *S6K1*$^{-/-}$ *S6K2*$^{-/-}$ double *knockout* mice. Both experiments rendered an almost completely abolished phosphorylation of rpS6 (Pende *et al.*, 2004; Roux *et al.*, 2007). However, these same mice allowed the discovery that RSKs have distinct, non-redundant roles in phosphorylating rpS6 in response to agonists or oncogenes that activate the MAPK pathway. Interestingly, RSKs have a more restricted pattern of rpS6 phosphorylation, as they can only phosphorylate 2 (Ser235 and Ser236) out of the 4 serines that are bulkily phosphorylated by S6Ks (Roux *et al.*, 2007). Another essential role of RSKs was also observed during *Xenopus laevis* oocyte maturation, where they are responsible for rpS6 phosphorylation before germinal vesicle breakdown during a period where S6Ks are still inactive (Schwab *et al.*, 1999). Importantly, all this demonstrated that rpS6 phosphorylation can occur in an mTOR-independent manner.

All the substrates of RSKs are phosphorylated by their N-terminal kinase domain of the AGC family, since the CTKD plays only an intramolecular regulatory role. Indeed, RSKs share the consensus target sequence for their substrates with other AGC kinases, suggesting a potential degree of redundancy between these proteins (Bjørbaek, Zhao and Moller, 1995).

Later on, most of the roles firstly attributed to RSKs turned out to be actually performed by a family of kinases that are structurally homologs to RSKs, the mitogen- and stress-activated kinases (MSK): MSK1 (also known as RLPK (RSK-like protein kinase)) and MSK2 (also known as RSK-B (RSK-like B) (Wiggin *et al.*, 2002). They are members of the AGC kinase family but are also included in the functional subgroup of CAMKs termed the MAPKAPK (MAPK-activated protein kinase) family, a group characterized by the fact that they are activated by different MAPKs (Roux *et al.*, 2004). They share the same 2 catalytic domain structure and mechanism of activation with the RSKs, but MSKs have an additional upstream activator. Indeed, MSKs integrate both the ERK1/2 and p38 pathways, as both kinases can directly phosphorylate and activate their CTKD. In their case, a second activating phosphorylation by PDK1 is not necessary for their full activation (Deak *et al.*, 1998; Williams *et al.*, 2000; McCoy *et al.*, 2005; Hauge and Frödin, 2006).

MSKs are present in multiple tissues, but immune and neuronal cells exhibit the higher expression. In brain, MSK1 is the major isoform, but both can be detected. MSK1/2 *knockout* mice were viable and did not exhibit gross defects in CNS neurodevelopment. In adulthood, however, *knockouts* recovered worse from ischemic or seizure episodes because their adult neuronal proliferation and arborization in the dentate gyrus neurons were reduced [reviewed in (Reyskens and Arthur, 2016)].

MSK have a myriad of substrates. The best characterized are Histone H3 and the transcription factors cAMP-response-element-binding protein (CREB) and activating transcription factor-1 (ATF1) [reviewed in (Arthur, 2008)]. CREB is a transcription factor that regulates the expression of hundreds of genes that have cAMP-responsive elements in their promoters. It is especially relevant in memory formation after fear conditioning and circadian rhythms. RSKs also phosphorylate CREB (De Cesare *et al.*, 1998), but the fact that the majority of the genes regulated by MSKs are also targets of CREB suggests a bigger relevance of MSK compared to RSK in controlling this pathway. Another AGC kinase that phosphorylates CREB in the same residue than MSKs is PKA, but their role seems to differ. ChIP experiments suggest a very efficient role of PKA's action in recruiting the necessary transcription coactivators to all CREB-dependent promoters, while MSK has to be the one mediating CREB phosphorylation to induce the genes triggered downstream of MAPK signalling (Naqvi, Martin and Arthur, 2014). CREB allows

MSK to regulate neuronal proliferation, synaptic plasticity and memory (Reyskens and Arthur, 2016). Nevertheless, RSKs activation has also been involved in promoting neuronal survival (Anglada-Huguet *et al.*, 2016).

- **Protein Kinase C (PKC)**

PKCs are divided in three subfamilies: conventional (α, βI/βII and γ), activated by calcium and diacylglycerol (DAG) together; novels (δ, ε, η and θ), that do not require calcium but still need DAG; and atypical aPKCs (ζ and ι), activated by stimuli other than these. To remain structurally stable, they need to be phosphorylated by PDK1 in their activation loop as soon as they are synthesized, or they will be degraded (Balendran *et al.*, 2000). However, phosphorylation of their HM is not necessary for PDK1-mediated action (Gao, Toker and Newton, 2001). Instead, they rely on an intramolecular mechanism of regulation where a pseudosubstrate domain, the αC-helix and the PIF-pocket communicate allosterically with the catalytic site. This inhibits the activity of the kinase before contacting the second messengers that stimulate them (Lopez-Garcia *et al.*, 2011).

PKCα and PKCβI/βII are expressed in cells of various tissues including the brain, whereas PKCγ is specifically expressed in neurons. They phosphorylate and induce internalization of the α-amino-3- hydroxy-5-methyl-4-isoxazolepropionic acid (AMPA) receptor, thus participating in the formation of new memory by Long Term Depression (LTD) processes [reviewed in (Hirai, 2018)].
Nestin-Cre-dependent aPKCs ablated mice and avian suffered from disorganized cortical layering due to the loss of the apical junctions of the radial glia. However, their neurogenic rates were unaffected (Imai *et al.*, 2006; Ghosh *et al.*, 2008).

aPKCs play an important role in axon specification, specifically in the step where a single neurite amongst the many equivalent ones extended by the developing neurons is selected to become an axon, while the rest are devoted to arborizing into dendrites. aPKCs assemble in complexes together with polarization proteins Par3 and Par6 localized in the growth cone of the axon-to-be, while they are excluded from the neurites destined to form dendrites. Par3 is the subunit of the complex subcellularly regulated by kinesins, but whether aPKCι or aPKCζ is the catalytical one is still unclear (Shi, Jan and Jan, 2003; Hapak, Rothlin and Ghosh, 2018). PKB was also found enriched in the growth cone, being recruited by the c-Jun N-terminal kinase interacting protein-1 (JIP1), whereas the presence of both proteins is reduced by glutamate (Dajas-Bailador *et al.*, 2014).

- **Serum and glucocorticoid-regulated kinase (SGK)**

SGK is an mTORC2-activated group of kinases containing three isoforms (1 to 3) with different variants each. All of them are expressed in the brain. They show a high homology except for their N-terminals, where SGK1 express a hydrophobic motif that promotes its binding to the endoplasmatic reticulum while SGK3 has a Phox homology (PX) domain that binds to PI-3-P. Their expression is rapidly induced by the presence of serum and glucocorticoid (García-Martínez and Alessi, 2008; Basnet *et al.*, 2018).

SGKs regulate cell proliferation, apoptosis and neurotransmission. They have been broadly studied because they are dysregulated in a variety of tumours, but more specifically because they are structurally very similar to PKB, except for the fact that they do not contain any PH domain. More importantly, SGK1 and PKB have the same consensus phosphorylation motif for their substrates and thus share functions and effectors. The most relevant ones are the activation of the proapoptotic functions of FoxO3 and the inhibition by phosphorylation of GSK3 (Brunet *et al.*, 2001; Sakoda *et al.*, 2003; Lang *et al.*, 2010).

SGKs have also been studied in depression, since this pathology results in the production of high levels of the stress hormone cortisol, a major regulator of SGKs. Indeed, anxiety/depression mouse models are achieved through chronic exposure to corticosterone, which increase the activation of SGK1, whereas antidepressants re-normalize this situation. Importantly, this reduction allows the recovery of adult hippocampal neurogenesis. SGK also contributes to the cell protection against oxidative insults. Accordingly, its activity is increased in Alzheimer's cortex, but this can worsen the pathology, as it has been reported that SGK can phosphorylate tau (Chun *et al.*, 2004) [reviewed in (Lang *et al.*, 2010; Iqbal, Howard and LoGrasso, 2015; Zhang *et al.*, 2016; Meng *et al.*, 2019)].

- **Glycogen synthase kinase 3**

GSK3 is not an AGC kinase nor a direct substrate of PDK1, but some of them, including PKB, p70-S6K1, SGK1, aPKCs or PKAs, convey in phosphorylating and regulating GSK3. GSK3s is a family of two proteins (GSK3α and GSK3β) expressed ubiquitously. Only GSK3β is required for development; its deletion results in postnatal death and thus is the most studied one. More than 100 substrates have been proposed for GSK3β, including transcription factors, although not all of them have been *boda fide* confirmed. What's more, some of the substrates engage in positive feedback loops avoiding GSK3 inactivation, making difficult to distinguish amongst substrates and regulators.

GSK3β is constitutively active and becomes inhibited by phosphorylations. Many signalling pathways regulate its activity, including PI3K, WNT and elevated 3',5'-cyclic adenosine monophosphate (cAMP) levels, which inhibit GSK3β; or the MAPK/ERK cascade, that leads to its activation. GSK3 participates in apoptosis, cell proliferation, cell differentiation, control of microtubule structure, cell cycle progression and management of cellular stress. GSK3 activation can produce a wide range of effects on its targets, including altering enzymatic activity, protein localization or stability by targeting its substrates for proteasomal degradation. However, previous phosphorylation of the target by another kinase is required for GSK3β activity. This phenomenon is called priming [reviewed in (Duda *et al.*, 2018; Hapak, Rothlin and Ghosh, 2018; Robertson, Hayes and Sutherland, 2018)].

GSK3β has shown to have a role in neurodegenerative and psychiatric disorders. It regulates the inhibitory GABAergic neurotransmission and is the principal target of the classical lithium-derived antipsychotics, because the dopaminergic receptors transduce through GSK3β. Indeed, chemical inhibition of GSK3 alone can recover the effects of mutation-induced schizophrenic behaviours in mice (Beaulieu *et al.*, 2004; Mao *et al.*, 2009; Tyagarajan *et al.*, 2011).

PDK1 mice genetic models

A number of mice mutant models of PDK1 were created in order to elucidate the role of this kinase. Not surprisingly, the first attempts to abolish the function of this protein resulted in not viable or unable to develop organisms. For example, knockout of PDK1 in yeasts (*Saccharomyces cerevisiae*), nematodes (*Caenorhabditis elegants*), *Drosophila* or *Mus musculus* resulted in lethality (Casamayor, Morrice and Alessi, 1999; Paradis *et al.*, 1999; Williams *et al.*, 2000). While mice lacking the catalytical domain of PDK1 were embryonically lethal, PDK1 hypomorphic mice which only expressed 10 - 20% of the total amount of PDK1 were viable and fertile, but 40 – 50% smaller in size (Lawlor *et al.*, 2002).

After the PIF-pocket and the PH domain were discovered and characterized, knockin models expressing punctual disruptive mutations of each of these domains were also enginered. Yet, they also showed embryonic lethal phenotypes (Collins *et al.*, 2003; McManus *et al.*, 2004). This pointed out at the essential role of the PDK1 signalling pathway in embryonic development. ES cells derived from these mice, however, were key to elucidate the real PDK1 substrates in physiological conditions and to faithfully describe their mechanisms of regulation by PDK1. In the PIF-pocket-mutated ES cells, a change of Leucine 155 to a Glutamic acid (L155E) resulted in loss of the activity of the downstream kinases PKC, SGK, S6K and RSK,

but not PKB. Meanwhile, selective inactivation of the PH-domain by three amino acid mutations (Arginine 472 to 474 to Leucine) abolished exclusively PKB activity.

Thus, conditional knockin and knockout models were necessary to study the role of the PDK1-mediated signalling *in vivo* [reviewed in (Bayascas, 2010)]. When PDK1 was conditionally eliminated by knockout-targeted Cre-Lox approaches in muscle and liver, the resulting mice died after a few weeks of age (Mora *et al.*, 2003, 2005). Likewise, targeting the pancreas generated viable individuals who however suffer from diabetes; impaired T-cell differentiation was observed when these cells were targeted, and microcephaly appeared in the nervous system conditional knockout (Hinton, Alessi and Cantrell, 2004; Hashimoto *et al.*, 2006; Chalhoub *et al.*, 2009).

Also, knockin animals that can selectively abolish the PKB-dependent or the PKB-independent PDK1-mediated signalling pathways were created. These animals expressed versions of PDK1 where specifically the docking-sites of PDK1 (but not its catalytical activity) were altered. PKB activation by PDK1 was compromised, but not abolished, by mutating the Lysine 465 within the PH domain to Glutamic Acid, which disrupted the interaction of PDK1 with the PtdIns(3,4,5)P_3 second messenger (Zurashvili *et al.*, 2013). PDK1 K465E mice, in which the PDK1 mutation is expressed in the whole organism, are viable but smaller than wild type. Surprisingly, these animals are protected against diabetes (Bayascas *et al.*, 2008), PTEN-induced tumorigenesis (Wullschleger *et al.*, 2011) and amyloid-β toxicity (Yang *et al.*, 2018). On the other hand, the study of the PKB -independent PDK1-regulated pathway employed the PIF-pocket L155E mutation. Apart from the whole organism model, this modification has been targeted to muscle (Bayascas *et al.*, 2006), T-cells (Kelly *et al.*, 2007) and central nervous system (Cordón-Barris *et al.*, 2016).

- **The PDK1 L155E CNS-specific mutant mice**

Tissue-specific mutants expressing the L155E version of PDK1 were efficiently achieved thanks to the minigene strategy (Bayascas *et al.*, 2006). This method uses the Cre-Lox recombination system. Cre is a recombinase that targets specific 34-base pair DNA sequences called LoxP (Nagy, 2000). Both the enzyme and the target sequences are derived from bacteriophage P1 but have been widely implemented in mammals. The specific targeting of the desired tissue is done by forcing the expression of the recombinase under a tissue-specific promoter, or even subpopulation-specific promoter.

In the PDK1 L155E minigene strategy (Figure 13A), PDK1 expression starts normally from the endogenous locus through the two first exons. However, the rest of the exons of the wild type protein are encoded from a LoxP-flanked sequence

called minigene. This cassette contains exons 3 to 14 of the wild type PDK1 sequence, followed by a transcription termination and three polyadenylation signals. After the cassette, exon 3, the mutant L155E version of the exon 4, and the rest of the exons 5 to 14 of the endogenous locus will follow.

In the absence of Cre recombinase, the wild type PDK1 included in the minigene is used and transcription is meant to stop at the termination signals of the end of the minigene, thereby preventing the incorporation of the mutant exons. Only when Cre is expressed under the control of the targeted tissue-specific promoter, the wild-type minigene is eliminated and the only expressed version of PDK1 must be the mutated one. Thus, the PDK1 L155E protein is expressed when the minigene is deleted. The animals carrying the conditional mutation were called PDK1$^{floxed/floxed}$ (PDK1$^{fl/fl}$), which in turn can also be either Cre^{-} or Cre^{+}.

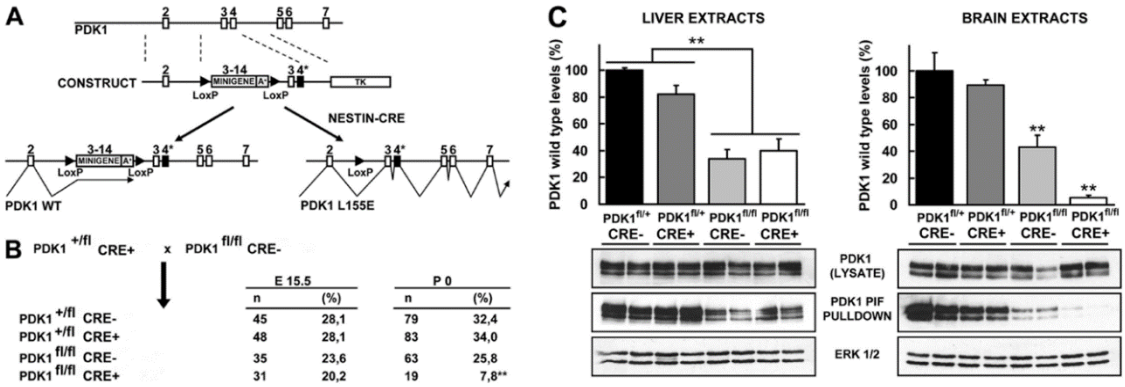

Figure 13: **Generation of the Central Nervous System - specific PDK1 L155E mice (A) Diagram** depicting exons 2 to 7 from the wild type PDK1 gene (PDK1) and the full construct (CONSTRUCT) that includes the minigene and a thymidine kinase (TK) negative selectable marker. Minigene is double flanked by LoxP sites and includes the open reading frame of exons 3 to end at exon 14 of wild type PDK1 gene and three polyadenylation sites (A+). Exon 3 and mutated Leu155Glu exon 4 continue after the minigene sequence (represented by the black box labelled with an asterisk). White boxes represent exons and triangles represent LoxP sites. **(B) Breeding strategy** used to generate PDK1$^{fl/fl}$ Cre^{+}, including obtained number (n) and proportion (%) of mice of each genotype. While prenatal E15.5 litters are fecundated under Mendelian proportions, PDK1$^{fl/fl}$ Cre^{+} offspring that carry pregnancy to their birth (P0) is lower-than-expected (**, $P < 0.005$ by χ^2 test). **(C)** PDK1 contained in brain and liver extracts of animals of the three genotypes was pulled-down with antibodies sequestrating all versions of the protein (LYSATE) or the ones capable to interact with PIF synthetic fragments (PIF PULLDOWN), corresponding exclusively to the wild type version. Protein obtained was immunoblotted and quantified after correction by the total amount. The mean result from two animals per genotype and their standard error were expressed as percentage of the PDK1$^{+/fl}$ Cre^{-} (top). ERK1/2 is shown as loading control [modified from (Cordón-Barris *et al*., 2016)].

To target specifically the Central Nervous System, Cre recombinase was expressed under the control of the Nestin gene. These recombinant mice have been broadly used to direct recombination to the neuroepithelium stem cells from embryonic day

E7.75 to early postnatal development (Dahlstrand, Lardelli and Lendahl, 1995; Gavériaux-Ruff and Kieffer, 2007; Bernal and Arranz, 2018). However, the minigene strategy reported to not be able to stop efficiently the transcription of the engineered PDK1 allele beyond the minigene termination sequences (Bayascas *et al.*, 2006). This leaking allows the expression of the mutant PDK1 even in absence of Cre recombinase. This leads to the PDK1 L155E mutant protein representing up to the 60% of total PDK1 expressed by the $PDK1^{fl/fl}$ mice in non Cre-targeted tissues like liver (Figure 13C), and this same percentage was found in the CNS in the absence of Cre recombinase (Figure 13D). PDK1 total levels, however, remains unchanged in any genotype (Cordón-Barris *et al.*, 2016). Instead of being a problem, this situation showed to be useful. The exacerbation of the symptoms showed by the adult $PDK1^{fl/fl}$ Cre^{-} and Cre^{+} mice, respectively, when compared to the control $PDK1^{fl/-}$ Cre^{-} mice, correlated to their levels of mutant protein (Cordón-Barris *et al.*, 2016). Indeed, the more abundant the mutant protein expressed was, the more aberrant the phenotypes observed were. Adult $PDK1^{fl/fl}$ Cre^{+} mice presented exacerbated disruptive behaviours and abnormal brain morphology (Cordón-Barris *et al.*, 2016), briefly showcased in Figure 14 and listed below.

These phenotypes included:

-Reduced axonogenesis and polarization in neurons cultured *ex vivo*: Axon lengths were reduced around 40% when compared to the control. Moreover, the percentage of neurons that still did not show any axon by day *in vitro* (DIV) 4 was increased (Figure 14A, B).

-Reduced connectivity in the adult mice brain: decreased density of the axonic and dendritic network in the cortex (Figure 14C) and the hippocampus.

-Abnormalities in cortical layering: subpopulations dispositions were altered in the $PDK1^{fl/fl}$ Cre^{-} and furthermore in the Cre^{+} adult mice. Neurons were compacted specifically in the layer IV of the cortex in the $PDK1^{fl/fl}$ Cre^{-} mice (Figure 14D, Cux1), and this was accentuated in the $PDK1^{fl/fl}$ Cre^{+} animals. Glutamatergic interneurons were responsible of this increment in the density with no change in the total number of neurons. Also, a specific subpopulation of interneurons (the parvalbumin-expressing ones) were excluded specifically from this layer (Figure 14D, Parv). Finally, GABAergic marker glutamate decarboxylase 67 KDa (GAD67) expression was reduced in the cortex in a dose-dependent manner.

-Disruptive behaviour: The $PDK1^{fl/fl}$ Cre^{+} mice displayed multiple behavioural disturbances, both cognitive and noncognitive. Mice were hypersensitive to stressful situations but at the same time less active and motivated to reconduct them (including freezing, reduced exploration and impaired short-term working

memory). Cognitively, learning and memory were affected, but also attention and executive functions. All these symptoms could be compatible with clinical features of the schizophrenic spectrum.

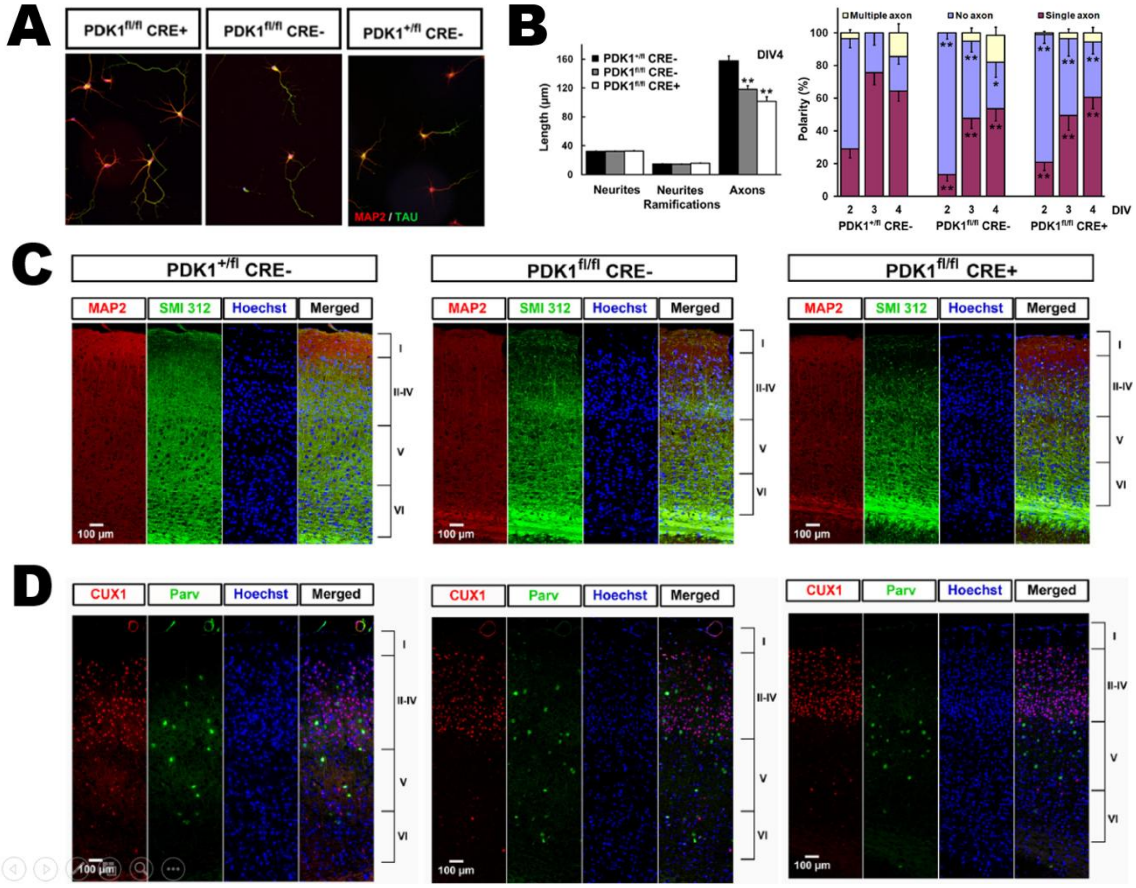

Figure 14: Alterations provoked by the L155E PDK1$^{fl/fl}$ mutation in the adult cortex and the *ex vivo* cultured hippocampal neurons. (A, B) Deficient axonal outgrowth and polarization of PDK1$^{fl/fl}$ Cre^{-} and PDK1$^{fl/fl}$ Cre^{+} hippocampal neurons cultured *ex vivo*, as observed in the (A) micrographs of day *in vitro* DIV4 neurons stained with the dendrite-specific marker MAP2 (red) and the specific axonal marker Tau-1 (green) and confirmed by the (B) quantification of the polarization (expressed as percentage of the total) and the µm length of neurites, neurite ramifications and axons. Each bar represents the means and their standard errors from a 100 neurons sample from three different embryos per condition. * $P < 0.05$ and ** $P < 0.005$, compared to controls. **(C)** Reduced connectivity in the PDK1$^{fl/fl}$ Cre^{-} and the PDK1$^{fl/fl}$ Cre^{+} adult mice cortex, as shown by the decreased coverage of the axonal (stained by the SMI312 marker) and neuritic (MAP2) patterning. **(D)** Compaction of cortical layer IV with no change in the total number of neurons, as revealed by the layer II- to IV-specific marker CUX1. Also, interneurons expressing parvalbumin got excluded from layer IV in the PDK1$^{fl/fl}$ Cre^{+} mice. (C, D) Pictures correspond to epifluorescence micrographs of coronal sections of the somatosensory cortex of the specified genotypes. Hoechst stains nucleus. Cortical layers are indicated on the right in roman numerals [modified from (Cordón-Barris *et al.*, 2016)].

Schizophrenia

Schizophrenia is a psychiatric disorder that affects 0'7% of the population and shows a strong genetic predisposition. Behavioural evidences of the disease appear in the early twenties in men and four years later in women and consist in positive symptoms that include psychotic episodes such as delusions and hallucinations, and negative symptoms such as social and motivational deficits. In childhood, patients show cognitive deficits such as memory and attention shortfalls. However, the insults (both genetic and environmental) leading to these phenotypes can act from embryonic to early adolescence stages (Saha *et al.*, 2005).

The exact molecule/-s disfunction causing this disease remains unclear. However, different theories, based on indirect evidences, try to explain the etiology of this pathology.

The "Dopamine hypothesis" states that schizophrenia is caused by a presynaptic hyperdopaminergic accumulation. It was formulated after some pharmacological treatments that either increased or depleted dopamine levels turned out to mimic psychotic schizophrenia symptoms or have an antipsychotic effect, respectively. Indeed, first- and second-generation antipsychotic drugs block the dopamine D_2 receptors present in the post-synapses, hindering its transmission in the brain. However, negative symptoms are not restored with these treatments [reviewed in (Howes, McCutcheon and Stone, 2015)].

The "Glutamate" or "NMDA receptor hypofunction hypothesis" postulates that there is a deficit in glutamatergic neurotransmission in schizophrenia. Glutamatergic neurotransmission is the mayor kind of excitatory signalling, with glutamatergic neurons accounting for 60 to 80 percent of total brain's metabolic activity (Shen *et al.*, 1999). Among all the glutamate receptors present in the brain, schizophrenia has been related with a dysfunction of the N-methyl- D-aspartate (NMDA) receptor, a presynaptic protein that modulates neurotransmitter release. Again, this theory arose after schizophrenic symptoms were relieved after treating patients with glutamic acid. However, no glutamatergic drugs are available in the market (Stone, Morrison and Pilowsky, 2007; Gibert-Rahola and Villena-Rodriguez, 2014).

More recently, the "GABA hypothesis" was formulated to explain the cognitive deficits observed in schizophrenia. This hypothesis integrates the previous ones and is based on the knowledge that dopaminergic neurons are regulated by glutamatergic projections. Then, a reduction on NMDA receptors availability or functioning in the GABAergic interneurons leading to a disinhibition of the glutamatergic projections would increase the glutamate release on them and provoke the activation of the dopaminergic neurons. Thus, the dopamine role in

schizophrenia could be a secondary consequence of the altered glutamatergic function (McGuire *et al.*, 2008; Stone *et al.*, 2010).

When moving from the "who" to the "how" this pathology appears, schizophrenia, together with other behavioural psychiatric diseases such as autism, is nowadays considered to be caused by an anomalous cortical circuitry establishment during cortical development, with a "two-hit component". This model includes a genetic predisposition (first hit) that creates a susceptibility due to abnormally developed brain connections, and a second hit that can be postnatal and triggers the neurological response (Bayer, Falkai and Maier, 1999). In schizophrenia, a dysfunctional inhibitory cortical circuitry is recognized as the core clinical feature of the disorder. Accordingly, patients have reduced gamma frequency oscillations, a physical phenomenon required to synchronize the inhibition of pyramidal neurons by their neighbour GABAergic interneurons. Specifically, a subclass of interneurons expressing the calcium binding protein parvalbumin (PV), are responsible for coordinating this event. *Post-mortem* samples of schizophrenia patients showed no change in the number of PV^+ interneurons, but these showed alterations on proteins relevant for neurotransmission, including reduced mRNA and protein levels of PV and the 67-kDa isoform of glutamic acid decarboxylase (GAD67, the enzyme responsible for GABA production), reduced GABA membrane transporter (GAT-1) in axonal terminals and increased $GABA_A$ receptor in the post synapsis of their adjoining pyramidal neurons (Lewis, 2014; del Pino, Rico and Marín, 2018).

Finally, schizophrenia being a "neurodegenerative disorder" is a theory that has still not been rejected. Lifetime studies of white and grey matter of adult patients revealed that white matter suffers a reduction before the onset of the symptoms, and an accelerated decline on its chronic stages (Kochunov and Hong, 2014).

OBJECTIVES

Main objective: To determine the role of the PDK1 PIF-pocket-dependent cascade in embryonic corticogenesis by characterizing the PDK1 L155E neuron-specific conditional *knockin* mice.

Objective 1: To experimentally assess whether the embryos and adults $PDK1^{fl/fl}$ CRE^{-} and $PDK1^{fl/fl}$ CRE^{+} mice are microcephalic.

Objective 2: To characterize the neocortex morphology of the PDK1 L155E neuron-specific conditional *knockin* mice at different stages of neurodevelopment.

Objective 3: To assess whether proliferation and apoptosis are affected by the PDK1 L155E mutation during embryonic neurodevelopment in the mice neocortex.

Objective 4: To characterize the specification of neuronal subpopulations in the neocortex of the PDK1 L155E neuron-specific conditional *knockin* mice.

Objective 5: To explore a possible dysregulation in the length of different phases of the cell cycle during the embryonic corticogenesis of the PDK1 L155E neuron-specific conditional *knockin* mice.

Objective 6: To create a mutant form of p70-S6K able to phosphorylate its substrate rpS6 in the absence of PDK1- and mTORC1- activating phosphorylations.

MATERIALS & METHODS

Mice

The Nestin-Cre transgenic mice were kindly provided by Ulrich Mueller at the Scripps Research Institute (Tronche *et al.*, 1999). The PDK1 L155E conditional knock-in mice were previously described (Bayascas *et al.*, 2006). Breeding strategy was planned as explained in Figure 13. Animals housing and experimentation were according to the 2010/63/UE regulation. Specifically, food and water were available *ad libitum*; temperature was kept between 19 – 22 ºC; humidity was between 40 – 60%; mice were maintained on a 12h/12h light / dark cycle. The study complied with the ARRIVE guidelines developed by the NC3Rs (Kilkenny *et al.*, 2010).

GENOTYPING: DNA EXTRACTION AND PCR ANALYSIS

Genotyping was performed by PCR using genomic DNA isolated from tails. The presence of both the *Cre* recombinase and the wild type or L155E conditional allele of PDK1 was checked for each individual in two different reactions.

DNA extraction from the tails was done following standard procedures. Briefly, tails were digested in 500 µl of Digestion Buffer (100 mM EDTA pH 8,0, 100 mM NaCl, 50 mM Tris pH 8,0, 1 % sodium dodecyl sulphate (SDS), plus 1 mg / mL of freshly added proteinase K. Tubes were incubated overnight at 56 ºC if tails came from adult mice, or 4 hours at 65 ºC with 800 rpm shacking for embryo tails. DNA extraction was next performed at room temperature. First, 167 µL of 5 M NaCl were added into each tube, samples were mixed by inverting the tubes vigorously several times and centrifuged at 14.800 rpm for 5 minutes. The supernatants were transferred by decantation to a new tube, mixed with 465 µL of isopropanol (0'8 V:V) by repeated vigorous inversion of the tubes, centrifuged for 10 (adult tails) or 5 (embryo tails) minutes at 14.800 rpm, and the pellets washed with 1 mL room temperature 70% ethanol and centrifuged again at 14.800 rpm for 5 minutes. Supernatants were then removed, samples centrifuged once more for 1 minute at 14.800 rpm, remaining ethanol removed with a pipette, pellets air dried for 10 minutes and then dissolved in 150 µL (adult tails) or 300 µL (embryo tails) of Buffer TE (1 mM Tris-HCl, 10 mM EDTA pH 7,5) overnight at 4 ºC. DNA was stored at this temperature ready for PCR analysis.

The detection of the mutant PDK1 alleles was done using the following primers (Bayascas *et al.*, 2006):
F 5'- GGAACTTACTCTGTAGACCAGGCTG / **R** 5'- GACGTGTCCTAATACTACCACAAGTGGC.

The PCR yields a product of 171 base pairs (bp) for the wild type allele and a 212 bp product for the 155E allele, in which the presence of the floxed minigene cassette incorporate some additional nucleotides corresponding to the 5' LoxP site.

For the detection of Cre transgene the following primers were employed: Cre1 (5'-AAATGGTTTCCCGCAGAACC-3') and Cre10 (5' TAGCTGGCTGGTGGCAGATG-3'), which retrieve a band of 585 bp.

L155E and Cre PCRs were run as follows: 94 ºC for 5 minutes, followed by 35 cycles of (denaturalization 1 minute at 94 ºC; annealing 2 minutes at 63 ºC; elongation 3 minutes at 72 ºC), then 7 minutes of a final extension at 72 ºC. The amplified products were separated in 3% agarose gel electrophoresis

AGAROSE GELS

The percentage (w/v) used ranged from 0'8 % to 3 % (small products of PCR, e.g. genotyping procedures), being 1% the most used. 100 ml of gel were prepared by weighting the necessary agarose powder and boiling it in the microwave with Tris-Acetate-EDTA (TAE) 1X inside an Erlenmeyer. Excessive boiling was avoided. Then, 5 µl of RedSafe dye were added, warm liquid was poured in a sealed tray with a comb in it and allowed to solidify for 20 minutes. Samples were then loaded with Orange G Loading Buffer (Table 1) in the negative electrode side and then run

Tris – Acetate - EDTA (TAE)

COMPONENTS	50X	1X	For 1 L of 50X
Tris	2 M	40 mM	242 g Tris-HCl
Glacial acetic acid	1 M	20 mM	57,1 ml stock
EDTA	50 mM	1 mM	18,61 g EDTA
ORANGE G LOADING BUFFER			
COMPONENTS	**10X**	**1X**	**For 100 mL of 10X**
Tris pH 8,0	10 mM	1 mM	1 ml Tris 1M pH 8,0
EDTA pH 8,0	100 mM	10 mM	20 ml EDTA 0,5 M pH 8,0
ORANGE G	25% (w/v)	2,5% (w/v)	25 mg
Glycerol	60% (v/v)	6% (v/v)	60 ml

Table 1. Solutions for loading and running an agarose gel. EDTA = ethylenediaminetetraacetic acid; TAE = Tris – acetate – EDTA.

at constant 100 V current until the front overcame 2/3 of the length of the gel. Then, images were taken with a GeneGenius machine (Syngene).

Materials and antibodies

MATERIALS AND CONSTRUCTS

All reagents were from Sigma-Aldrich, Merck, unless otherwise stated. Primers for genotyping and directed mutagenesis were also purchased from Sigma. pCAGS-linkB-IRES-RFP plasmid was kindly provided by Dr Lluís Cordón-Barris at the Dr Laurent Nguyen lab. DH5α *Escherichia coli* (*E. coli*) competent cells were kindly provided by Dr José Manuel López Blanco.

Dulbecco's modified Eagle's medium (DMEM), Hank's Balanced Salt Solution (HBSS), MEM (Eagle's minimal essential medium), OptiMEM, Neurobasal medium, B27 supplement, MEM vitamins and trypsin inhibitor were purchased from Gibco, ThermoFisher. *DpnI*, Penicillin / Streptomycin, fetal bovine serum (FBS), L-Glutamine, Comassie Protein Assay Kit, Lipofectamine 2000, Luria Broth (LB), LB-agar, Alexa-associated secondary antibodies, and peroxidase-associated secondary antibodies (Pierce) were from Fisher Scientific. Acetic acid, 2-propanol, absolute ethanol and 96% ethanol were purchased from Scharlab. Gel Extraction and PCR Cleanup Kit (#28704) and HiSpeed Plasmid Midi Kit (#12643) were from Qiagen. Multiwell plates, T25 flasks, cryogenic vials and plaques for bacterial were from Falcon, Fisher Scientific. Protan 0,45 µm nitrocellulose membranes were purchased from GE Healthcare. Precision Plus protein molecular weight markers were obtained from Bio-Rad. Super RX-N Fujifilms were purchased from MTB. The plasmid expressing GFP was purchased from Invitrogen. RedSafe dye for agarose gels came from iNtRON Biotechnologies. Hyperladder 1 kba DNA marker was from Biolane. Paraformaldehyde was purchased from Electron Microscopy Science. Polyethyleminine (PEI) was from PolyScience. Acrylamide was from Merck. *Pfu* polymerase was from Agilent. Tubes with loose cap for pre-culture were bought to VWR. Fluoromount-G was purchased from Southern Biotech. Methanol was from J.T. Baker. Human recombinant BDNF was obtained from Alomone, and the Calbiochem inhibitor rapamycin (#553210) was purchased from Merck - Millipore. Hoechst 33342 was from ThermoFisher (#H1399). Ligase (#M0202S) and restriction enzymes *ClaI* (#R0197S), *EcoRI* (#R0101S), *EcoRV* (#R0195S), *NheI* (#R0131S), *SacI* (#R0156S) and *XbaI* (#R0145S) and methylase deficient *dam-/dcm- E. coli* competents were obtained from New England Biolabs (NEB). Calcium phosphate transfection kit CalPhos Mammalian Transfection Kit was purchased from Clontech Laboratories # 631312 (Takara Bio Company).

ANTIBODIES

The total PKBα antibody was kindly provided by Dr Dario Alessi from the University of Dundee. It was raised in sheep against the sequence RPHFPQFSYSASGTA, corresponding to residues 466 to 480 of rat PKBα, and affinity purified on the appropriate antigen. The following antibodies were purchased from Cell Signalling: phospho-S6K Thr389 (#9205), total S6K (#9202), phospho-S6 ribosomal protein Ser235/236 (#2211), total S6 ribosomal protein (#2217), phospho-PRAS40 Thr246 (#2997), phospho-pan-PDK1 site PKCγ Thr514-P (pan) antibody (#9379) that recognizes the phosphorylated Thr229 on the T-loop of S6K as demonstrated in (Cordón-Barris *et al.*, 2016), and phospho-S6K Thr389-P (#9234). Total PRAS40 (238-256) (#S115B, 2nd bleed) was purchased to the MRC PPU Reagents service of the University of Dundee. The SGK1 antibody (#S5188) was obtained from Sigma and the PKCα antibody (#P16520) from Transduction Laboratories. Appropriate secondary antibodies coupled to horseradish peroxidase were obtained from Pierce, Fisher Scientific.

For the immunofluorescence experiments, the anti-phospho-histone 3 (#06-570), was purchased from Millipore; the anti-Tbr2 (rabbit) (#ab23345), anti-Ki67 (#ab156956), anti-doublecortin (#ab18723), anti-Tbr1 (#ab31940) and anti-Ctip2 (#ab18465) antibodies were obtained from Abcam; the anti-cleaved caspase 3 (#9661) antibody was from Cell Signalling Technology; anti-Pax6 (#PAX6) was purchased from Developmental Studies Hybridoma Bank; finally, anti-calbindin (#CB38) was from Swant. The appropriated Alexa Fluor 594-conjugated goat anti-rabbit (#A11072), Alexa Fluor 488-conjugated goat anti-rabbit (#A11070), Alexa Fluor 488-conjugated goat anti-mouse (#A11017), Alexa Fluor 594-conjugated goat anti-mouse (#A11020) and Alexa Fluor 488-conjugated rabbit anti-rat (#A21210) fluorescent secondary antibodies were obtained from Invitrogen, ThermoFisher.

Generation of the S6K$^{T229[D/E]/T389D}$ constructs

DIRECTED MUTAGENESIS

"pCMV5 HA p70 S6 kinase M1-S421 T412E" plasmid, here called **S6K^{T389D}**, was acquired from Protein Phosphorylation and Ubiquitylation Unit (MRC) repository of the University of Dundee (#DU 53345). This plasmid contains a 1'8 kilobases (kba) insert encompasing nucleotides 22 to 1599 (out of a total of 2287) of the rat p70-S6K1 mRNA sequence (GenBank NM_031985.1). This encodes amino acids 1 to 424 of the rat p70-S6K1 protein with an added N-terminus hemagglutinin (HA) tag.

The coding sequence of the autoinhibitory loop located at the C-terminus of the kinase (nucleotides 1291 to 1596), although retained within the insert, is not translated onto protein since two STOP codons were introduced at positions 1229 and 1230, avoiding the expression of this motif. Thus, the activity of S6K^{T389D} and its derivates becomes independent of the stimuli needed to phosphorylate and release this autoinhibitory motif (Alessi *et al.*, 1998).

"pCMV5 HA PKB alpha T308D S473D" plasmid, from now on **PKB$^{T308D/S473D}$**, was also acquired from MRC repository (#DU 2004). This plasmid contains a 1520 bp insert corresponding to nucleotides 555 to 1997 (out of a total of 3008) of the human PKBα mRNA sequence (GenBank NM_005163.2) encoding the whole protein with an added N-terminus hemagglutinin (HA) tag. Threonine 308 and Serine 473 had both been mutated to aspartic acids, turning this PKB into constitutively active independently on its upstream effectors PDK1 and mTORC2 (Alessi *et al.*, 1996).

pCMV5-S6K^{T389D} plasmid contained a directed mutation on Threonine 412 (equivalent to Thr 389 in the human sequence) in the hydrophobic motif, which had been mutated to an aspartic acid. This cassette was used as a template to create two new versions that included an additional second directed mutation in the Thr229: Thr229-to-Glu (T229E, called S6K$^{T229E/T389D}$) and Thr229-to-Asp (T229D, S6K$^{T229D/T389D}$). The mutations were introduced by site-directed mutagenesis using 2 pairs of overlapping primers encompassing the desired mutation position. The S6K$^{T229D/T389D}$ primer pair (**F** 5'- TGGAACAGTCACGCAC**GAC**TTCTGTGGAACAATA / **R** 5-' TATTGTTCCACAGAAGTCGTGCGTGACTGTTCCA), T_m 79'4ºC; and S6K$^{T229E/T389D}$ (with a 5' *EcoRI* site incorporated) (**F** 5'- TGGAACAGTCACGCAC**GAA**TTCTGTGGAACAATA / **R** 5-' TATTGTTCCACAGAATTCGTGCGTGACTGTTCCA), T_m 79 ºC, were used. The protocol used for mutagenic PCRs is described Table 2.

template DNA (5-50 ng) *(MidiPrep Grade)*	1 µl
primer Forward, at 1 µM	1'25 µl
primer Reverse, at 1 µM	1'25 µl
10 mM dNTPs mixture *(containing 10 mM for each nucleotide)*	1 µl
Reaction buffer 10X	5 µl
high fidelity *Pfu* polymerase	1 µl
autoclaved H_2O	40'5 µl
TOTAL VOLUME	50 µl

Table 2: **Solutions used for a mutagenic PCR experiment.** dNTPs = deoxyribonucleotide triphosphate; PCR = Polymerase Chain Reaction

Then, the Polymerase chain reaction (PCR) consisted on: 95'5 ºC for 30 seconds, then 18 cycles of (denaturalization 30 seconds at 95 ºC; annealing 1 minute at 53 ºC; elongation 7 minutes at 68 ºC).

The product of the PCR was digested with *DpnI* for 1 hour at 37 ºC (Table 3). This enzyme cleaved DNA when methylated, a modification that only can be acquired in a cellular context but not in the chemically controlled PCR tube. With this step, unmutated template DNA (which had been amplified in an *E. coli* culture) is eliminated and only newly created DNA including the mutation remained.

DNA (coming from mutagenic PCR)	49 µl
DpnI	1 µl
TOTAL VOLUME	50 µl

Table 3: **Solutions used for a *DpnI* digestion experiment.** PCR = Polymerase Chain Reaction.

The product of this reaction was transformed into *E. coli* competent cells (protocol explained afterwards) and the incorporation of the mutation was checked by sequencing.

DNA SEQUENCING

The incorporation of the mutation was confirmed by Sanger sequencing analysis done at the Servei de Genòmica i Proteòmica of the Universitat Autònoma de Barcelona with an Applied Biosystems ABI3130XL sequencer.

DNA was diluted in autoclaved water to a concentration of 10 ng / µl and a minimum amount of 15 µl (enough for sequencing with the forward and also the reverse primers). 2 µl of primer per reaction diluted in autoclaved water at 5 µM were used. Results were checked with the Chromas v2.6.6. program (Technelysium Pty Ltd, Tewantin, Old, AU).

SUBCLONING

The *in utero electroporation* (IUE) experiments required subcloning the constitutively active constructs into plasmids driven by a CAG-type promoter, which reaches high levels of expression in mammals due to their fused chicken β-actin

promoter plus cytomegalovirus (CMV) early enhancer element and an splice acceptor from the rabbit β-globin gene (Niwa, Yamamura and Miyazaki, 1991).

Dr Lluís Cordón-Barris kindly provided a the pCAGGS-linkB-IRES-RFP plasmid (from now on, **pCAG-RFP**), a bicistronic pCAG plasmid encoding for red fluorescence protein (RFP) and a cloning site separated by an internal ribosome entry site (IRES). The enzymatic targets available in the linker region were (in the following order): *SacI* + *NheI* + *NruI* + *SmaI*/*XmaI* + *EcoRV* + *ClaI* + *XhoI*. The empty vector weights 6'2 kba.

The S6K$^{T229D/T389D}$ construct was subcloned by linearizing pCAG and by liberating the insert from pCMV5-S6K$^{T229D/T389D}$ using *SacI* + *ClaI* on both (Figure R15A). Since *ClaI* is sensitive to methylation, DNA was obtained in a *dam*$^{-}$*/dcm*$^{-}$ *E. coli* methyltransferases deficient strain, which allows the purification of unmethylated plasmidic DNA and therefore sensitive to *ClaI* digestion.

Unfortunately, PKB$^{T308D/S473D}$ construct presented an internal *SacI* target inside its sequence and could not be subcloned using the same strategy. For that purpose, I took advantage that *XbaI* and *NheI* generated cohesive ends (even if they targeted different sequences). Indeed, the cloning site of pCAG-RFP contained a *NheI* site that could linearize it. PKB$^{T308D/S473D}$ presented a single *XbaI* sequence after its STOP codon, but any before the start one. A previous PCR using pCMV5-PKB$^{T308D/S473D}$ as a template was performed to add a *XbaI* target to the 5' of the insert (Figure 15B). The construct was amplified with a forward primer that hybridized to the cloning site previous to the start of PKB$^{T308D/S473D}$ and contained an additional hanging sequence before that encoding the *XbaI* target sequence T[↓*]CTAGA (TCTAGA). The reverse primer instead, was designed to amplify from the end of the insert with no modifications. From the first round of polymerase activity, an insert with its additional *XbaI* target in its 5' was amplified. The sequence of the designed primers were:
F 5'- GG**TCTAGA**GAGCTCGTTTAGTGACCGTCA / **R** 5'-CCTCTAGAGCTCGAATTCATCAGGCCGTG

PCR reaction was as follows: 95 ºC for 2 minutes, then 30 cycles of (denaturalization 30 seconds at 95 ºC; annealing 30 seconds at 51'5 ºC; elongation 3 minutes at 72 ºC), then a final extension of 5 minutes at 72 ºC.

After PCR and *DpnI* digestion, the product and the pCAG-RFP empty vector were enzymatically restricted with *XbaI* and *NheI* respectively, to generate the necessary complementary sticky ends. Restriction enzymes and buffers were retired by running the samples in 0'8% agarose gel. Special preparative wider wells were prepared by taping together 2 teeth of the comb. Samples were run and the gel was exposed to low energy ultraviolet (UV) light to physically visualize both the linearized plasmid and the insert. The bands in the gel were marked with a clean

scalpel and once the UV light was turned off these slices of gel were fully cut off and recovered into fresh tubes. The exposure time was kept to the minimum to limit the potential mutagenic effect of the UV light. The emptied gel was afterwards photographed in the GeneGenius machine to ensure fully recovery of the material and to keep track of their correct location respect the size markers.

The gel piece recovered for each sample was weighted (and the mass of their tubes, which were tared beforehand, subtracted). For extracting the DNA from the agarose gel, the Gel Extraction and PCR Cleanup Kit from QIAGen was used following the instructions of the manufacturer. Briefly, Buffer QG was added to the gel blocks at a proportion of 3 volumes (µl) of Buffer QG : 1 mg gel. Agarose was melted in this buffer by incubation at 50 ºC for 10 minutes and posteriorly DNA was precipitated by adding 1 gel volume (µl) of isopropanol and mixing. The DNA was then bound to a QIAquick column by eluting the whole volume through it with the help of 1 minute-centrifugations at 12.000 x*g*. The column was then soaked for 1 minute with 500 µl of Buffer QG, which was also removed by centrifugation. 750 µl of Buffer PE were then incubated to wash the resin for 5 minutes and also discarded by centrifugation. An additional 1-minute centrifugation was done to remove all the residual ethanol. In that moment, the column was placed standing straight in a fresh tube, 30 µl or Buffer EB (10 mM Tris-HCl pH 8'5) added in the centre of the membrane and incubated for 4 minutes. After centrifugation, the eluted DNAs were quantified with a Nanodrop™ 2000 spectrophotometer (ThermoScientific). If any volume was spared after ligation, it was stored at -20 ºC.

LIGATION

Purified restricted insert and plasmid were joint by enzymatic ligation made by mixing the receptor plasmid and the insert at a molar ratio of [3 insert : 1 vector] with 100 ng of total DNA (Table 4). The size of both elements had to be considered when calculating the ratio. Finally, the following reaction was prepared and incubated overnight at 16 ºC. The whole volume resultant from ligation was transformed into DH5α *E. coli* competent cells (transformation protocol explained ahead).

The $PKB^{T308D/S473D}$ subcloning strategy into pCAG using the same sticky ends in both sides prevented limiting the right orientation of the insert. To assess it, a diagnostic restriction analysis was conducted. pCAG-RFP empty vector showed to have an internal *SalI* target 1'8 kba upstream from the *EcoRV* target of its cloning site. *EcoRV* in turn, laid downstream from the *NheI* target used to linearized the plasmid. The $PKB^{T308D/S473D}$ insert encoded another *SalI* sequence coming from the remains of its cloning site, which fell near to its AUG start codon.

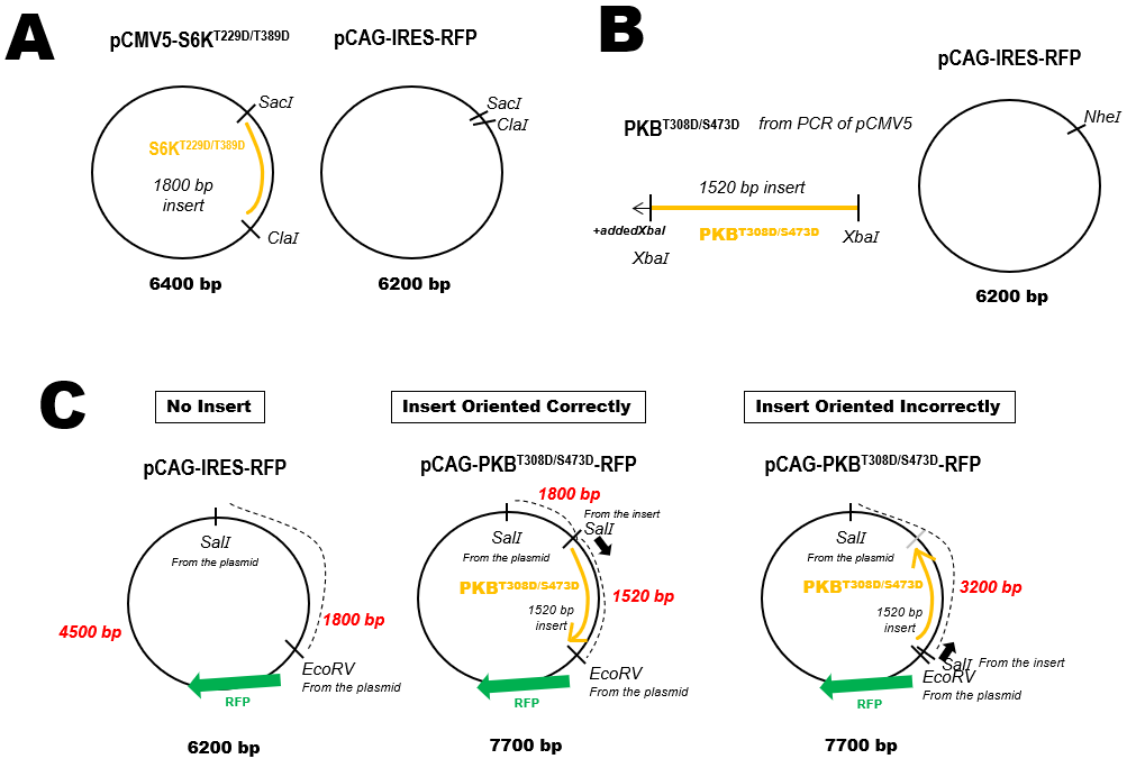

Figure 15. Subcloning strategies and restriction maps of the pCAG-S6K$^{T229D/T389D}$-RFP and the pCAG-PKB$^{T308D/S473D}$-RFP plasmid. (A, B) Cloning strategies. (A) pCAG-S6K$^{T229D/T389D}$-RFP (top left panel) was obtained by linearizing the destination plasmid and liberating the S6K$^{T229D/T389D}$ insert with the oriented combined cuts of *SacI* and *ClaI*. **(B)** pCAG-PKB$^{T308D/S473D}$-RFP (top right panel) instead used the cohesive ends generated by *XbaI* and *NheI* to insert the PKB$^{T308D/S473D}$ construct unorientedly. A targeting sequence for *XbaI* before the start codon of the PKB$^{T308D/S473D}$ insert had to be introduced by PCR with specially designed primers. **(C) Restriction strategy to unravel the orientation of the inserted PKB$^{T308D/S473D}$ construct.** Empty vector (bottom left panel), cassette inserted in the right orientation (bottom middle panel) or incorrect orientation (bottom right panel) are depicted. Whether the restriction sites were encoded by the plasmid (*EcoRV*, *SalI*) or the cloning site of the insert (additional *SalI*) is specified. Grey bar indicates the end of the insert sequence when incorrectly oriented. Dashed lines indicate generated bands that can map the orientation of the insert. RFP = Red Fluorescence Protein; bp = base pairs.

This situation generated different patterns of restriction when pCAG-PKB$^{T308D/S473D}$-RFP was double digested with *EcoRV* + *SalI* that allowed to assess the orientation of the insert. If oriented incorrectly, the *SalI* target of the PKB$^{T308D/S473D}$ and the *EcoRV* of the plasmid laid so close they generated no band. The insert remained instead bound to the 1'8 kba fragment generated by the plasmidic *SalI* and together created a 3'2 kba fragment. In contrast, when oriented correctly, the PKB$^{T308D/S473D}$ insert is liberated by combined cut of *SalI* and *EcoRV* at its two ends, and an additional band of 1'8 kba is generated by plasmidic *SalI* (Figure 15C).

Following these strategies, pCAG-S6K$^{T229D/T389D}$-RFP and pCAG-PKB$^{T308D/S473D}$-RFP were engineered.

vector	X µl	*e.g. 1 µl of the 4 kba vector + 4 µl of the 1'8 kba insert*
insert	X µl	
ligase buffer 10X	1 µl	
T4 ligase	1 µl	
autoclaved H_2O	*up to* 10 µl	
TOTAL VOLUME	10 µl	

Table 4: **Solutions used for a ligation experiment.**

TRANSFORMATION

Routinely, DNA digested with *DpnI* was transformed into DH5α *E. coli* competent cells. Transformation was also used to recover delivered DNAs dotted in paper. When unmethylated DNA was needed, transformation was performed on *dam-/dcm-* methyltransferase deficient competent *E. Coli* cells. Briefly, DNA was mixed with 50 µl of highly competent *E. coli* cells inside the sterile environment surrounding the sterile halo of a flame and incubated in ice for 10 minutes. Then, a thermic shock was performed by immerging the tubes in a water bath set at 42 ºC for 90 seconds, and then on ice for 2 minutes. Bacteria were allowed to growth and express the antibiotic resistance on 200 µl of complete Luria's broth (LB) for 1 hour at 37 ºC and then seeded under a sterile ambient in LB agar plates containing the appropriate antibiotic. Controls were always transformed and plated in parallel, including thermally shocked cells not exposed to DNA and positive controls with the template vectors existing before the PCR, which transfected better due to their supercoiled structure acquired in the prokaryotic cells. Plates rested for 10 minutes at room temperature and then left upside down in the incubator at 37 ºC overnight for a maximum of 16 hours.

Next day, different single colonies were amplified by picking them individually with a sterile tip dropped inside a loose-cap preculture tube containing 3 ml of LB media supplemented with the appropriate antibiotic. Cells were amplified overnight (16 hours) at 37 ºC in a thermal bacterial shacker with 200 rpm orbital agitation. If further amplification was needed for high- volume extractions, next day 100 µl of this pre-culture were seeded in 100 ml of LB + antibiotic and incubated in the same conditions.

GLYCERINATED STOCKS

Precultures were also used to prepare glycerinated stocks of *E. coli* cells expressing the different plasmids. These stocks were kept at -80 ºC and can be revived at any time even years later. 650 µl of preculture were mixed with 650 µl of glycerol 100 % inside cryotubes using cutted-tips for a wider, less aggressive pipetting, and stored at -80 ºC. When the plasmid was needed again, tubes were taken in dry ice to the sterile halo of a flame, then a fire-sterilized Kolle handle was punched inside the frozen mass to collect some glycerinate, being aware to not to burn the stock with an excessively hot wire. Bacteria were streak on LB + agar + antibiotic plates and allowed to soak into the agar for 10 minutes at room temperature. Then, the plates were placed upside down in the incubator at 37 ºC 16 hours. Next day, isolated colonies were used to grow a preculture as explained above, and the plates parafilmed and stored at 4 ºC for not more than a month. The glycerinated stock was kept out of -80 ºC for as little time as possible.

DNA EXTRACTION FROM *E. coli*

Plasmidic DNA was extracted from precultures using the GenElute™ MiniPrep Kit following the instructions of the manufacturer. Briefly, 1500 µl of pre-culture were pelleted for 1 minute at 12.000 x*g* and then resuspended in 200 µl of Resuspension Solution. Cells were lysed by adding 350 µl of Lysis Solution and mixing gently by inversion for 6 – 8 times. Lysis was allowed to progress for less than 5 minutes and neutralized by adding 350 µl of chilled Neutralization Buffer and inverting the tube 4 – 6 times gently. Debris was precipitated by centrifuging at 12.000 x*g* for 10 minutes. The cleared supernatant was transferred to a column that had been previously equilibrated with 500 µl of Column Preparation Solution flushed by a 1-minute centrifugation at 12.000 x*g*. These same conditions were applied to the centrifugations that followed from now on. When the lysate had been centrifuged out of the column, this was washed with 500 µl of Optimal Wash Solution, the flow-through discarded and column washed again with 750 µl of Wash Solution. After discarding this liquid, the column was centrifugated alone for 2 minutes to remove the excess of alcohol. Then, the column was transferred to a fresh collection tube and 50 µl of Elution Buffer were passed through the column to recover the DNA, that was stored at -20 ºC.

Instead, high-volume plasmidic DNA recovery was done using the HiSpeed Plasmid Midi Kit from QIAGen following the instructions provided by the manufacturer. Briefly, cells were pelleted at 4.400 x*g* for 15 minutes and 4 ºC and resuspended with 6 ml of Buffer P1, being very thoughtful not to leave any unsuspended flocks. Then, 6 ml of Buffer P2 were added to lyse the cells for 5

minutes (after mixing by inversion 4-6 times) and lysis was stopped with 6 ml of chilled Buffer P3 (4-6 inversion mixing was repeat). This lysate was immediately poured inside the barrel of a QIAfilter Cartridge where it was incubated for 10 minutes at room temperature. In the meanwhile, a QIATip was equilibrated with 4 ml of Buffer QBT. All liquids were allowed to transit the column by gravity. Once the incubation of the lysate had finished, the cap of the cartridge was removed, the plunger inserted and the cell lysate filtered into the barrel of the equilibrated column, where it passed through by gravity. Then, 20 ml of Buffer QC were added to wash the column, and after that, 5 ml of Buffer QF were added to elute the DNA into a fresh tube. DNA was precipitated by adding 3'5 ml of room temperature isopropanol (0'7 volumes), mixed by vigorous inversion and then incubated for 5 minutes at room temperature. Then, the DNA was recovered from the eluate / isopropanol mixture by passing it through the QIAprecipitator with the help of a syringe. 2 ml of ethanol 70% were afterward flushed to wash the precipitator. Every time a new liquid (or air) had to be added in the syringe, this was first detached from the QIAprecipator and only then the plunger was retracted, syringe reattached, and the new liquid / air added. After washing, the membrane of the QIAPrecipitator was dried by forcing the pass of air multiple times with the help of the attached syringe and wiped with clean absorbent paper. Finally, DNA was eluted into a fresh tube with 780 µl of Buffer TE, which passed through the membrane once and then was recovered from the eppendorf to pass a second time to maximize the recovery yield. For higher concentrations, the procedure was followed until the precipitation step. Then, the use of the Qiaprecipitator was avoided and instead the eluate mixed with isopropanol was centrifugated for 1 hour at 4.400 x*g* at 4 ºC in 15-ml Falcon tubes. The supernatant was carefully removed, pellet allowed to air dry and resuspended in 250 µl of Elution Buffer, PBS or autoclaved water. DNA was stored at -20 ºC. If sterile DNA was needed, air drying and DNA dilution were done inside the halo of a flame.

ENZYMATIC RESTRICTIONS

Enzymatic restrictions were used on the daily bases to confirm the identity of the

DNA (coming from Mini and MidiPreps)	1 µl
BSA 1X *(*diluted stock 10X 1 µl stock + 9 µl autoclaved water)*	1 µl
NEB buffer 10X	1 µl
restriction enzyme	1 µl
autoclaved H_2O	6 µl
TOTAL VOLUME	10 µl

Table 5: **Solutions used for an enzymatic restriction.** BSA = Bovine Serum Albumin.

plasmids obtained in every batch of Mini and MidiPreps. Reaction mix were prepared as detailed in Table 5. The reaction was incubated for 1 hour at 37 ºC. Then 2 µl of Orange G loading buffer (Table 1) were added to each tube and samples were loaded into 1% agarose gels.

Experiments with cell lines and neuronal cultures

PRIMARY NEURONAL CULTURES

Neuronal primary cultures were established from embryonic day 15.5 (E15.5) or E18.5. Embryos were extracted from the uterus of a pregnant female by Caesarea and beheaded. Their craniums were opened and brains and tails for genotyping were obtained, putting attention in maintaining the traceability of each sample to its corresponding embryo. Brains were processed individually, as genotypes could not be known in the moment of the primary cell culture. Cortices or hippocampus were recovered separately in solution 1 (for solutions, see Table 6) after their meninges were removed, and pelleted afterwards at 1500 rpm for 30 seconds. Tissues were then enzymatically digested for 10 minutes at 37 ºC in solution 2 and reaction was stopped by adding solution 4 and centrifuging at 1500 rpm for 10 seconds. Supernatants were discarded and pellets were resuspended in solution 3 and mechanically disaggregated by pumping 10 times through the tip of a Pasteur pipette and 10 additional times through a filter. Filtrates containing the free cells were collected in solution 5, centrifuged 5 minutes at 1000 rpm and resuspended in DMEM supplemented with 30 mM glucose, 2 mM L-Glutamine, 500 U / mL penicillin – 0'5 mg / ml streptomycin and 10% FBS. Cells were counted with the Scepter™ 2.0 Handheld Automated Cell Counter (Millipore) and then diluted to a density of $2 \cdot 10^5$ cells / ml (for cortical cells) or $7'5 \cdot 10^4$ cells / ml (for hippocampal cultures) in supplemented DMEM. Then, cells were seeded in 24-wells plates containing 12-mm diameter coverslips previously coated with 150 µg / mL poly-D-Lysine overnight and then rinsed once with PBS. Cells were allowed to attach to the plates for two hours in supplemented DMEM at 37 ºC and 5% CO_2, and after this time the medium was replaced by fresh Neurobasal medium complemented with 30 mM glucose, 2 mM L-Glutamine, 250 U / ml penicillin – 0'25mg / ml streptomycin and 2% B27 supplement. Cells were incubated at 37 ºC and 5% CO_2 for 1, 2 or 4 days *in vitro* (DIV) before experiments were conducted.

SOLUTION	REAGENTS	Volume or weight
Phosphate Buffered Saline (PBS) (1X)	H_20 PBS 10X Glucose 30% P/S (10000U/ml / 10mg/ml)	427,5 ml 50 ml 10 ml 12'5 ml
Krebs-Ringer Buffer (KRB) 10X	NaCl 120 mM KCl 40'55 mM KH_2PO_4 7'35 mM $NaHCO_3$ 250 mM Glucose 143 mM H_20	70'70 g 3'60 g 1'66 g 21'40 g 25'70 g till 1000 ml
Magnesium Stock 3'8%	$MgSO_4 \cdot 7H_2O$ H_20	19 g to 50 ml
Calcium Stock 1'2%	$CaCl_2 \cdot 2H_2O$ H_20	0'12 g to 10 ml
CELL CULTURE SOLUTIONS, FRESHLY PREPARED		
Solution 1	KRB 1X BSA Fraction V Magnesium Stock 3'8%	50 ml 0'15 g 0'4 ml
Solution 2	Solution 1 Trypsin	10 ml 2'5 mg
Solution 3	Solution 1 DNAase Trypsin inhibitor Magnesium Stock 3'8%	10 ml 0'8 mg 5'2 mg 100 µl
Solution 4	Solution 1 Solution 3	8'4 ml 1'6 ml
Solution 5	Solution 1 Magnesium Stock 3'8% Calcium Stock 1'2%	5 ml 40 µl 6 µl

Table 6. Solutions for a primary neuronal cell culture. Recipes for the preparation of solutions used in the primary neuronal cell cultures are provided. P/S = Penicillin / Streptomycin; BSA = Bovine Serum Albumin

NEURONS TRANSFECTION

Neuronal transfection was attempted by two different methods: lipofectamine and calcium phosphate. Various conditions, including total DNA amount (from 0'5 to 2 µg), DNA proportion between Green Fluorescence Protein (GFP)-encoding plasmid and plasmid of interest (0'5 µg GFP : 0'5 µg plasmid of interest and 0'7 µg GFP: 0'3 µg plasmid of interest); time of transfection (from 45 minutes to 3 hours); DIVs before transfection (DIV1, DIV2, DIV3 and DIV7) and DIVs of culture following the transfection (from 1 to 4 DIVs) were tested. For calcium phosphate, also two transfection mediums (normal supplemented culture medium and MEM supplemented with 2% B27 supplement, 0'2 mg/ml $NaHCO_3$, 20 mM D-glucose, 0'5 mM L-glutamine and 25 U/ml P/E) were tested.

Transfection with Lipofectamine was performed as explained elsewhere (Zurashvili *et al.*, 2013). Briefly, half of the conditioned media (250 µl) from plates with hippocampal cells cultured for DIV1, DIV2 or DIV3 was recovered from the wells and kept in a tube in the bath at 37º C before the experiment started. Then the following mixtures were prepared in Opti-MEM Medium (volumes per well to be transfected):

Tube 1: 0'7 µl Lipofectamine 2000 + 49 µl Opti-MEM.
Tube 2: 1 µg of total DNA (mix of plasmid of interest and GFP reporter plasmid) + 49 µl Opti-MEM.

Tube contents were incubated separately for 5 minutes at room temperature, and then the content of tube 1 was transferred drop wisely into the tube 2 and mixed by tipping. The mixture was incubated together for 20 minutes at room temperature to allow the DNA-liposome complex formation and then 100 µl per well were added drop wisely and a back and forth movement was applied to allow a perfect distribution of the reagents. The cells were transfected with the complexes for 90 minutes at 37 ºC and 5% CO_2 and then the medium containing Lipofectamine was removed and replaced with the stored 250 µl conditioned medium supplemented with additional 250 µl per well of complete fresh Neurobasal medium, topping-up back to 500 µl / well. Transfection was evaluated after 24 and 48 h by assessing the expression of the fluorescent proteins GFP or RFP.

Transfection by calcium phosphate complexes instead was tested as explained elsewhere (Jiang and Chen, 2006). Before starting, the whole medium was replaced by fresh complete Neurobasal or supplemented MEM. The conditioned medium was meanwhile stored at 37 ºC and 5% CO_2 in an empty plate and supplemented with 100 µl / well of fresh complete Neurobasal media to restore the volume lost during the process or by evaporation.

Then, the following mixtures were prepared (volumes per well):

Tube 1: 1 µg of total DNA (*with various ratios of plasmid of interest and GFP reporter plasmid*) + 3'1 µl 2 M $CaCl_2$ + sterile water to top up to 25 µl.
Tube 2: 25 µl Hank's balanced salt solution (HBS) 2X.

Tube contents were incubated separately for 5 minutes at room temperature, and then the content of tube 1 was transferred drop wisely into the tube 2, adding only 1/8 of Tube 1 volume each time and then vortexing gently (maximum 600 rpm) for 2-3 seconds. Attention to this step was essential to create Ca^{2+} - phosphate precipitates small enough that can be easily endocytosed by the neurons and thus transfect them. Instead, continuous vortexing often resulted in large and unevenly distributed precipitates. The mixture was next incubated for 20 minutes at room temperature with no additional vortexing to allow the formation of the complexes, and then 50 µl per well were added drop wisely into the cells and back and forth movement was applied to the plates to allow a perfect distribution of the reagent. The cells were transfected with the complexes for variable times ranging from 45 minutes to 3 hours at 37 ºC and 5% CO_2. During transfection, fresh transfection medium was pre-incubated in an empty plate inside a 10% CO_2-set incubator for 20 minutes to allow its saturation by this gas at this high concentration. When the transfection time ended, the medium containing the calcium phosphate was aspirated and 500 µl / well of CO_2-saturated medium were added. This acidified medium dissolved the precipitates of phosphate calcium, which greatly decreased cell toxicity caused by the transfection. The transfected cells with tamponed medium were incubated for 20 minutes at 37 ºC and 5% CO_2 (important: never incubate cells in the 10% CO_2 incubator). Finally, this medium was replaced by the original conditioned medium.

EVALUATION OF PROLIFERATION AND APOPTOSIS

E15.5 cortical neurons cultured at 7'5 $\cdot 10^4$ cells / well in complete neurobasal medium supplemented with B27 for the indicated number of days *in vitro* were fixed as explained afterwards and processed for immunocytochemistry with antibodies recognizing the ki67 proliferation marker and the active caspase 3 apoptotic marker (explained ahead).

CULTURING OF CELL LINES

HeLa cells were routinely cultured in T25 culture flasks in DMEM with GlutaMax supplemented with 10% of heat-inactivated FBS and penicillin/streptomycin (20

units/ml and 20 µg/ml, respectively). Cells were maintained at 37 °C in a saturating humidity atmosphere containing 5% CO_2. When 80% confluence was reached, cells were rinsed with PBS and detached with a 0'05% trypsin – EDTA solution for 3 minutes at 37 ºC 5% CO_2. Cells were recovered and centrifuged at 1.100 rpm for 5 minutes, pellet resuspended in fresh medium and cells seeded at the adequate cell densities in culture dishes or 6 well-plates using the same culture medium described above. For starvation tests, cells were seeded at $7'5 \cdot 10^5$ cells / ml (2ml / well); for transfection assays, $2'5 \cdot 10^5$ cells / ml (2 ml / well).

TRANSFECTION, STARVATION AND STIMULATION

3 µg / well of the plasmid of interest were mixed with 15 µl / well of polyethylenimine (PEI) in 250 µl / well of serum-free DMEM per well, incubated 20 minutes at room temperature and then added drop wisely in top of a 6-well plate with 30% confluent cells. 48 hours later, 80% confluent cells were starved as indicated in every figure legend, with 2 PBS washes before the addition of the starving medium, and then reincubated the indicated time at 37ºC 5% CO_2. If a treatment with drugs was necessary, compounds were prepared in 1 ml / well of starvation medium, which replaced the original one and then incubated for 45 minutes at 37 ºC 5% CO_2. Cells were stimulated or not with 100 ng/ml of IGF-1 for 30 minutes at 37 ºC 5% CO_2. IGF-1 was prepared at 100 µg/ml in 100 µl / well of starvation medium and added drop wisely to the wells, that were immediately rocked to mix. Protein extracts were then obtained and analysed by Western Blot.

NEURONAL AND CELL LINES FIXATION

Medium was removed and 500 µl / well of 4 % paraformaldehyde (PFA) (diluted in PBS from the 32% stock) were added for 24 wells-plates. Plates were incubated for 20 minutes at room temperature with no agitation, then 2 washes with PBS were made and cells left in fresh 500 µl / well. The borders of the plates were parafilmed to minimize evaporation, plates were sealed in foil if fluorescence proteins had been transfected and stored at 4 ºC for posterior immunofluorescence evaluation.

CELL AND TISSUE EXTRACTS

Cells were scraped from the wells in ice-cold Lysis Buffer (50mM Tris-HCl pH 7'5, 1mM EGTA, 1mM EDTA, 1mM sodium orthovanadate, 50mM sodium fluoride, 5mM sodium pyrophosphate, 10mM sodium-glycerophosphate, 0'27 M sucrose, 1% [v/v] Triton X-100, 0'1% [v/v] 2-mercaptoethanol and a 1:100 dilution of protease

inhibitor cocktail) (Table 7). The resulting extracts were collected in eppendorf tubes and incubated on ice for 30 minutes before centrifugation. Tissue extracts were prepared by homogenizing the frozen tissues on ice in a 10-fold volume excess of ice-cold lysis buffer using a Polytron (Kinematika GmbH). Both lysates were centrifuged at 4°C for 10 minutes at 13.000 rpm, and the supernatants were collected in fresh tubes and preserved at -20°C.

LYSIS BUFFER

	COMPONENT	M.W.	grams/L or	VOLUME FROM STOCK for 1 L
	50 mM Tris-HCl pH 7'5	121'14		50 ml Tris-HCl 1M pH 7'5
	1 mM EGTA	380'35		4 ml EGTA 250 mM pH 7'5
	1 mM EDTA	372'24		2 ml EDTA 500 mM pH 8'0
	1 mM Na-orthovanadate	183'91		10 ml Na-OTV 100 mM*
	50 mM Na-fluoride	41'99	2'1	
	5 mM Na-pyrophosphate	446'06	2'23	
	10 mM Na-B-glycerol-P	216'11	2'16	
	0'27 M sucrose	342'30	92'42	
	1% (v/v) Triton X-100	*n.a.*	*n.a*	10 ml Triton X-100
Freshly added	0'1% 2-mercaptoethanol	*n.a.*	*n.a*	0'01 ml 2-mercapto/10 ml buffer
Freshly added	Protease inhibitor cocktail	*n.a.*	*n.a*	0'1 ml Prot. Inhibit/10 ml buffer

Table 7. Recipe for the Lysis Buffer. Composition and instructions to prepare the lysis buffer and the stock solutions necessary to prepare it. *To prepare Na-OTV 100 mM stock, dissolved powder was brought to pH 7'0, then the solution was microwaved until it achieved a yellow colour, which indicated complete dissolution of the compound. 50 ml aliquots were then prepared and stocked at -20 ºC. n.a. = not applicable; EDTA = ethylenediaminetetraacetic acid; EGTA = ethylene glycol-bis(β-aminoethyl ether)-N,N,N',N'-tetraacetic acid; Na-OTV = Na-orthovanadate.

PROTEIN QUANTIFICATION AND WESTERN BLOTTING

The protein concentration was quantified by a Coomassie assay, using bovine serum albumin as a standard. Previously, cell extracts were diluted 1/5 (5 µl sample + 45 µl H_2O), then 10 µl of this dilution was mixed with 90 µl H_2O and 900 µl of Coomassie reagent, by duplicate. For each experiment, loading samples were prepared with 20 - 30 µg of protein + a fifth of the total volume of loading buffer (Table 8) and distilled water to top up to the total volume. Final volume was decided according to the maximum that a well can hold, the optimal being between 20 and 38 µl. For phospho- and total- S6 detection, 10 µg of protein were loaded.

All the samples were boiled at 95 ºC for 10 minutes immediately before loading them in SDS-polyacrylamide gels. These were prepared with different percentages of acrylamide depending on the weight of the protein to be detected (Table 8). The

running gel was allowed to polymerize for 30 minutes with 2-propanol on top to keep the front straight (which then had to be cleaned), and on top of this the stacking gel with the pint inside was allowed to polymerize for 20 minutes. Electrophoresis was run at 150 V until the dye front has left the gel, or until a selected molecular weight marker hit the bottom of the gel, sunk in running buffer (Table 9).

SOLUTIONS (ml)	**RUNNING GEL**				**STACKING GEL**	
Percentage (%)	**5%**	**7'5%**	**10%**	**15%**	**3'6%**	**5%**
dH_2O	11'6	10	8'3	5	5'8	3'8
30% acryl 0'8 bis	3'4	5	6'7	10	1'3	0'85
1'5 M Tris pH 8'8	5	5	5	5	-	-
0'5 M Tris pH 6'8	-	-	-	-	0'325	0'325
10% SDS	0'25	0'25	0'25	0'25	0'025	0'025
10% APS	0'15	0'15	0'15	0'15	0'05	0'05
TEMED	0'03	0'03	0'03	0'03	0'005	0'005

Table 8: Recipes for the preparation of SDS-PAGE running and stacking gels. Acryl = acrylamide; bis = bisacrylamide; SDS = sodium dodecyl sulphate; TEMED = N, N, N', N'-tetramethylethylenediamine; APS = ammonium persulfate.

The proteins separated in the gel were electrotransferred at 100 V for 1h 15 minutes onto Protran nitrocellulose membranes previously activated for 1 minute with transfer buffer. The transferring sandwich was mounted inside cassettes with differentiated covers. Both lids were protected with 1 sponge and 3 pieces of filter papers each. Then, the gel was placed in the black lid-side, the first one to receive the electric current and covered with the membrane ensuring no air was left in the middle. Transfer was made inside covering Transfer Buffer (Table 10) in a cubette surrounded by ice.

When finished, the total loading was checked visually by staining 20 seconds the membranes with the reversible protein-binding dye Ponceau, which was removed by washes with distilled water. Then, blocking was done with 10% non-fat dry milk in TBS + 0'1% Tween (**TBST**) (Table 10) for 1 hour at room temperature, and membranes were washed 5 minutes with TBST. Afterwards, they were incubated with the appropriate specific primary antibodies overnight at 4 ºC (Table 11). Phospho-antibodies were diluted in TBST + 0'5% BSA, added on top of the membrane, covered with plastic film to avoid dehydration and incubated steadily in the fridge. Instead, total antibodies were diluted in 5 ml of TBST + 5% non-fat milk and incubated inside 50 ml Falcons in a tube roller placed in a cold chamber.

Next day, membranes were washed 3 times 10 minutes with TBST and incubated with the adequate secondary antibodies conjugated with peroxidase for 1 hour at room temperature. Secondary antibodies were diluted in 5% non-fat milk. Membranes were washed again 3 times for 10 minutes with TBST and exposed for 1 minute to homemade enhanced chemiluminescence (ECL) solution, prepared by mixing 1 ECL1 : 1 ECL2 (Table 9). Excess of ECL was removed and membranes were placed in between protecting plastics in dark-sealed cassettes and their emitted light captured by Super RX-N Fujifilms in the dark for the necessary time (depending on the antibody, from 10 seconds to 20 minutes).

SOLUTION	REAGENTS	FOR 50 ml	FOR 10 ml
ECL1	Tris-HCl 1M pH 8'5	5 ml	1 ml
	Luminol 0'5M in DMSO	250 µl	50 µl
	P-Coumaric Acid 79.2 mM in DMSO	250 µl	50 µl
ECL2	Tris-HCl 1M pH 8'5	5 ml	1 ml
	Hydrogen Peroxide 8.8M	32 µl	6'4 µl

Table 9: Recipe of enhanced chemiluminescence (ECL) reagents

Immunofluorescence experiments

IMMUNOHISTOCHEMISTRY

Embryos were obtained from E12.5 to E15.5 plug-tested pregnant females. Mothers were culled by cervical dislocation, embryos recovered and decapitated. The whole heads were fixed for 2 hours in 4% paraformaldehyde at room temperature and then preserved in 70% ethanol at 4°C. The tails of the embryos were recovered separately for genotyping, being thorough that the identity of each sample could be traced back to its corresponding embryo. Heads from three littermates of different genotypes were embedded in the same paraffin block following standard procedures, and then sliced into 5-µm-thick coronal sections with a Leica RM2255 microtome.

LAEMMLI-SDS SAMPLE BUFFER (LOADING BUFFER, STOCK 5X)

COMPONENT	5X	1X	For 100 ml of 5X
Tris-HCl pH 6'8	125 mM	25 mM	25 ml Tris-HCl 0'5 M pH 6'8
Glycerol	50 %	10 %	50 ml
SDS	10 %	2 %	10 g
Bromophenol Blue	0'01 %	0'0025 %	12'5 mg
β-Mercaptoethanol	- *(add fresh)*	1%	Freshly added

RUNNING BUFFER (STOCK 10X)

COMPONENT	1X	10X	For 1 litre of 10X
Tris base	25 mM	250 mM	30'3 g
Glycine	192 mM	1'92 M	144'1 g
SDS	0'1 % (w/v)	1% (w/v)	10g

TRANSFER BUFFER (STOCK 10X)

COMPONENT	1X	10X	For 1 litre of 10X
Tris base	25 mM	250 mM	30'3 g
Glycine	192 mM	1'92 M	144'1 g

TBS BUFFER (STOCK 10X)

COMPONENT	1X	10X	For 1 litre of 10X
NaCl	150 mM	1'5 M	87'6 g
Tris base	25 mM	250 mM	30'3 g

Table 10. **Western Blot Buffers.** Recipes for preparing the western blot stock buffers. SDS = sodium dodecyl sulphate; w/v = weight / volume; TBS = Tris buffered saline

PRIMARY ANTIBODY	HOST	SUPPLIER	REFERENCE	DILUTION
tPKBα	Sheep	Dundee	-	1 µg/ml
pan-pPKCγ (T514-P) / pS6K (T229-P)	Rabbit	CST	#9379	1:1000
pPRAS40 (T246-P)	Rabbit	CST	#2997	1:1000
tPRAS40	Sheep	Dundee	#S115B	1 µg/ml
pS6 (S235-P)	Rabbit	CST	#2211	1:5000
tS6	Rabbit	CST	#2217	1:1000
pS6K (S389-P)	Rabbit	CST	#9205	1:1000
tS6K	Rabbit	CST	#9202	1:1000

SECONDARY ANTIBODY	HOST	SUPPLIER	REFERENCE	DILUTION
Anti-Rabbit HRP-conjugated	Goat	Pierce	#31460	1:5000
Anti-Mouse HRP-conjugated	Goat	Pierce	#31430	1:2500
Anti-Sheep HRP-conjugated	Rabbit	Pierce	#31480	1:2500

Table 11: Primary and secondary antibodies for western blot. A list of primary and secondary antibodies is provided, as well as their source and the working dilution. CST = Cell Signaling Technology

For experimentation, the paraffin was melted with dry heat for 2 hours at 60 °C. Then, tissues were rehydrated by passing through a bank of solutions with decreasing hydrophobicity that included: Xilol (I) 5 minutes → Xilol (II) 5 minutes → Ethanol 100% (I) 3 minutes → Ethanol 100% (II) 3 minutes → Ethanol 96% 3 minutes → Ethanol 70% 3 minutes → Ethanol 50% 3 minutes → H_20 3 minutes. Antigen retrieval was performed after that by boiling the samples for 10 minutes in 10mM sodium citrate adjusted at pH 6. Then, the slides were cooled down inside the boiling solution for 30 minutes on ice and washed with Tris buffered saline (25mM Tris pH 7'5, 150mM NaCl) (TBS) for 10 minutes 3 times. Blocking was done with 5% goat serum in TBS + 0'02% Triton for 30 minutes at room temperature and incubation overnight at 4°C with primary antibodies diluted in the blocking solution (Table 12). 100 µl of primary antibody were dropped onto each slide inside a humidified chamber and covered with shape-matching parafilm sheets, assuring no bubbles were left. Next day, the sections were rinsed three times with TBS buffer, incubated for 1'5 hours at room temperature with the corresponding secondary antibodies diluted 1:400 in TBS (Table 12), counterstained with 1 µg/ml Hoechst 33342 and washed 3 more times with TBS before mounting in Fluoromount-G reagent (15 µl / slide), assuring no bubbles were formed.

PRIMARY ANTIBODY	HOST	SUPPLIER	REFERENCE	DILUTION
Calbindin	Rabbit	Swant	CB38	1/20 - 1/500
Caspase-3 cleaved	Rabbit	CST	9661	1:200
Ctip2	Rat	Abcam	ab18465	1/500
Doublecortin	Rabbit	Abcam	ab18723	1:500
ki67	Rat	Abcam	ab156956	1:50
Pax6	Mouse	DSHB	PAX6	1:5
pH3 (Ser10)	Rabbit	Millipore	06-570	1:500
Tbr1	Rabbit	Abcam	ab31940	1:500
Tbr2	Rabbit	Abcam	ab23345	1:500

SECONDARY ANTIBODY	HOST	SUPPLIER	REFERENCE	DILUTION
Anti-Rabbit Alexa Fluor 488	Goat	Invitrogen	#A11070	1:400
Anti-Rabbit Alexa Fluor 549	Goat	Invitrogen	#A11072	1:400
Anti-Mouse Alexa Fluor 488	Goat	Invitrogen	#A11017	1:400
Anti-Mouse Alexa Fluor 549	Goat	Invitrogen	#A11020	1:400
Anti-Rat Alexa Fluor 488	Rabbit	Invitrogen	#A21210	1:400

Table 12: Primary and secondary antibodies for immunofluorescence analysis. A list of primary and secondary antibodies is provided, as well as their source and the working dilution. pH3 = phospho-Histone 3; CST = Cell Signaling Technology; DSHB = Developmental Studies Hybridoma Bank.

IMMUNOCYTOCHEMISTRY

Fixed cells were rinsed 3 times with PBS for 5 minutes, permeabilized with 0'02% saponin diluted in PBS for 7 minutes at room temperature and then rinsed again with PBS for 5 minutes. Unreacted aldehydes coming from the fixation process were then blocked with glycine at 10 mM + 0'01% saponin in PBS for 15 minutes. This treatment avoided a possible increase in the background fluorescence of the experiment. Samples were then blocked with 5% bovine serum albumin (BSA) + 0'01% saponin + 10 mM glycine in PBS for 1 hour at room temperature. Primary antibodies (Table 12) were prepared in PBS + 0'01% saponin + 1% normal goat serum. 1 drop per sample (15 µl / drop) were layered on a parafilm sheet inside a humidified chamber and then the 2-mm diameter coverslips containing the fixed cells were laid on them upside down, with cells facing the parafilm sheet. Samples were incubated overnight at 4 °C, rinsed 3 times for 5 minutes with PBS and incubated with the appropriate secondary antibodies diluted 1:400 (Table 12) in the same solution used to dilute the primary antibodies for 90 minutes at room temperature, counterstained with 1 µg/ml of Hoechst 33342 and washed 3 more

times with PBS. Then, coverslips were mounted on microscope slides with Fluoromount-G reagent (3 µl / cover). Importantly, if cells had been transfected with GFP or RFP during the experiment, they were kept in dark during the whole process.

Imaging

Immunostained sections were photographed with a Nikon Eclipse 90i epifluorescence microscope, and the captured images were processed and analysed with ImageJ 1.52a v1.8.0_112 (Wayne Rasband, National Institutes of Health, USA) and Fiji (http://pacific.mpi-cbg.de/wiki/index.php/Main_Page) software. Dividing the embryological cortex into equal bins was done with a personalized macro developed by Servei de Microscopia, Universitat Autònoma de Barcelona, that superimposed a n-slots grid over the images opened in the ImageJ. Images had to be previously cropped to contain only sample (ventricle to pia, no remaining black space). The counting of positively-stained and total neurons was done automatically with the CellProfiler software for Windows v3.1.9. (Mcquin *et al.*, 2018).

Magnetic Ressonance

Adult mice were intraperitoneally anesthetized with 0'4 mg/g body weight of pentobarbital, and then an intracardiac injection of 70 heparin units was administered before perfusion with 0'9% NaCl, followed by 4% buffered paraformaldehyde. Brains were extracted and hemispheres dissected, then the right hemispheres were frozen at -80 °C for biochemical analysis and the left hemispheres were fixed for 2 hours at room temperature in 4% paraformaldehyde and then preserved in 70% ethanol solution at 4°C. For the experiment, they were embedded in 1'5% agarose dissolved in phosphate-buffered saline (PBS). For this procedure, agarose was prepared and boiled as explained elsewhere (*Materials and Methods*, *"Agarose Gels"*) then cooled down until warm (to avoid tissue harm) but still liquid and poured in a 15 ml Falcon containing one hemisphere until it was completely covered. The matrices were allowed to solidify overnight, then the tubes were cracked open and discarded before the experiment. 1H magnetic resonance imaging (MRI) studies were performed in a 7T Bruker BioSpec 70/30 USR spectrometer equipped with a mini-imaging gradient set (400 mT/m), a 72-mm inner-diameter circular polarized linear transmitter volume coil, and a received-only

mouse head surface coil. Images were acquired using a multislice fast low-angle shot (FLASH) sequence from the Bruker Paravision 5.1 library (repetition time 450 ms; echo time 5'4 ms; excitation flip angle 40°) in 33 contiguous 0'5 mm thick slices, an acquisition matrix of 256 by 256, and a field of view of 19'2 mm X 19'2 mm, giving a voxel resolution of 0'0028125 mm^3. The imaging data were Fourier transformed in ParaVision and then visualized using ImageJ software.

Organ volume was determined using the Cavalieri method (Gundersen and Jensen, 1987) applied to both MRI data sheets of the adult brain and physical sections of embryonic brain samples. MRI images were displayed in ImageJ, head and brain outlined and their total number of pixels was multiplied by the voxel resolution and doubled to obtain the adult brain volume, assumedly twice the volume of one hemisphere. Embryonic brain paraffin-embedded sections of 5 µm thick that were separated by a constant distance between sections [*k*] of 96 µm were photographed with a digital camera Nikon SMZ800 stereomicroscope at X1 magnification. A square lattice grid of 0'9149 mm^2 (d^2) was then overlaid on the photographs using the program Photoshop vCS5.1, and the number of intersections (*P*) hitting either the whole head or the brain was scored. The volume was estimated by using the formula $\Sigma P \times d^2 \times k$.

Statistical analysis

Student's T test or Two-way analysis of variance (ANOVA) with the Bonferroni post-tests were applied to compare differences among groups, or amongst groups included in related variables, respectively. Data analysis was done using Prism software (Graph-Pad Software, La Jolla, CA).

RESULTS

Microcephaly induced by the PDK1 L155E mutation

PDK1$^{fl/fl}$ CRE^{+} adult brains showed evidences to be smaller in volume than their control counterparts, but also their whole-body size was found to be smaller as well (Cordón-Barris *et al.*, 2016). To explore whether or not the brain size was reduced to scale, left hemispheres of adult mice of the three described genotypes were weighted and also analysed using MRI imaging. Cavalieri method was used to quantify the resultant images as explained in Materials and Methods. Both PDK1$^{fl/fl}$ CRE^{-} and PDK1$^{fl/fl}$ CRE^{+} showed a reduction of the body weight of 25% (Figure

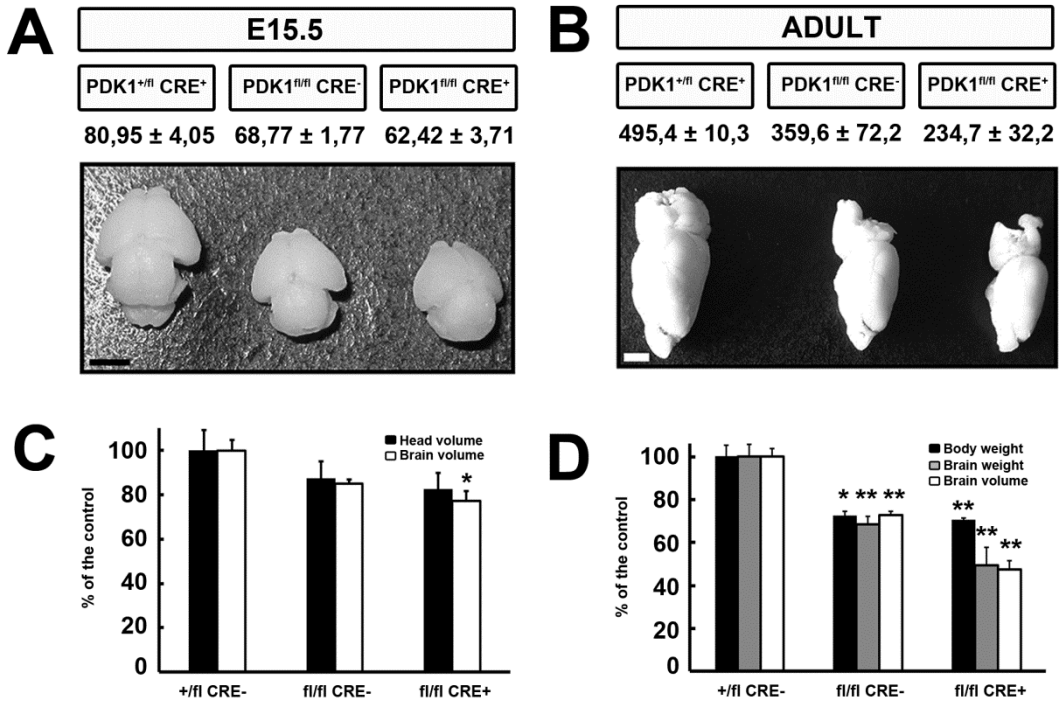

Figure R1: PDK1$^{fl/fl}$ CRE^{+} mice are microcephalic. **(A, B) Total brain volume values** (mm^3) and representative photographs of E15.5 embryonic brains (A) or adult left hemispheres (B). Scale bars correspond to 1 mm and 2 mm, respectively. **(C, D)** Quantification of embryo (C) and adult (D) brain and head volumes and body weight (D) expressed as % of the control. Histological sections of three E15.5 embryo brains inside their heads per genotype (C) were photographed and volume quantified using the Cavalieri method as described in Materials and Methods. Magnetic Resonance Imaging pictures of one of the hemispheres of three adult brains per genotype (D) were also quantified using the Cavalieri method. (A - D) Data are represented as means and standard errors of the mean and are expressed as percentages of the controls. n = 3 mice per genotype for brain and head volumes; for body weight n = 9 (+/- Cre-), n = 4 (-/- Cre-) and n = 13 (-/- Cre+). *, P < 0'05; **, P < 0'005 compared to the controls.

R1D). As to the brain, the PDK1$^{fl/fl}$ CRE^{-} exhibited a 25% reduction in both volume and mass of the brain compared to the PDK1$^{+/fl}$ CRE^{-} controls, which is proportional to the reduction in body weight.

However, the PDK1$^{fl/fl}$ CRE^{+} adult mutant brain was reduced about 50% in volume and mass compared to those from the PDK1$^{+/fl}$ CRE^{-} controls, confirming that these animals exhibited microcephaly (Figure R1B, R1D). Then, stereological methods were conducted on sagittal sections of embryonic whole heads of the indicated genotypes at E15.5. At this developmental stage, PDK1$^{fl/fl}$ CRE^{+} brains were 25% smaller in volume than the PDK1$^{+/fl}$ CRE^{-} controls, beyond the 15% reduction showed by their whole head volume, which was measured in parallel from the same samples (Figure R1A, R1B).

I completed the study of the activation of the downstream pathway controlled by PDK1 in both embryonic *ex vivo* cultured cortical neurons and brain extracts at E15.5 samples (Figure R2A, R2B). Most other substrates had been at the time characterized by former members of the lab. Here, I described that neurons and brain extracts from PDK1$^{fl/fl}$ CRE^{-} and PDK1$^{fl/fl}$ CRE^{+} showed reduced S6K phosphorylation on both the mTORC1-dependent (Thr389) and the PDK1-dependent (Thr229) residues.

This lower phosphorylation of S6K at the two activating residues resulted in reduced activation of this kinase, as demonstrated by the almost abolition of the phosphorylation of its substrate, the S6 ribosomal protein, at the Ser235 site, both in the brain extracts and the BDNF-stimulated *in vitro* cortical neurons of the PDK1$^{fl/fl}$ CRE^{+} mutant mice. Interestingly, the PDK1$^{fl/fl}$ CRE^{-} mice were still able to retain as much as 65% of the BDNF-induced phosphorylation of S6 protein compared to the PDK1$^{+/fl}$ CRE^{-} controls, and 40% in the whole brain extracts. RSK phosphorylation, the other major kinase responsible of phosphorylating rpS6, was also previously shown in the lab to be decreased at both the autophosphorylated residue (Ser380-P) and the PDK1-dependent (Ser229-P) residue (Cordón-Barris *et al.*, 2016).

The study was completed by describing the activation of another set of PDK1 substrates, the PKCs. The PDK1-dependent phosphorylation on this family of proteins is especially important, as it is required both for the stabilization and the activation of the corresponding PKC isoform. When the PDK1-dependent phophorylation of PKCα at the Thr497 residue was monitored alongside to their total protein amounts, Thr497 phosphorylation was found 60% decreased in the PDK1$^{fl/fl}$ CRE^{+} cultured neurons, whereas the total PKCα protein levels were as a consequence 40% reduced. These effects replicated in the PDK1$^{fl/fl}$ CRE^{+} brain extracts. Interestingly, the low levels of PDK1 wild type protein retained in the

PDK1$^{fl/fl}$ CRE^{-} mice were sufficient to promote both PKCα phosphorylation and stabilization, since both the phosphorylation levels and the total protein amounts were not significantly different when compared to the PDK1$^{+/fl}$ CRE^{-} controls.

These results were included in the publication (Cordón-Barris *et al.*, 2016).

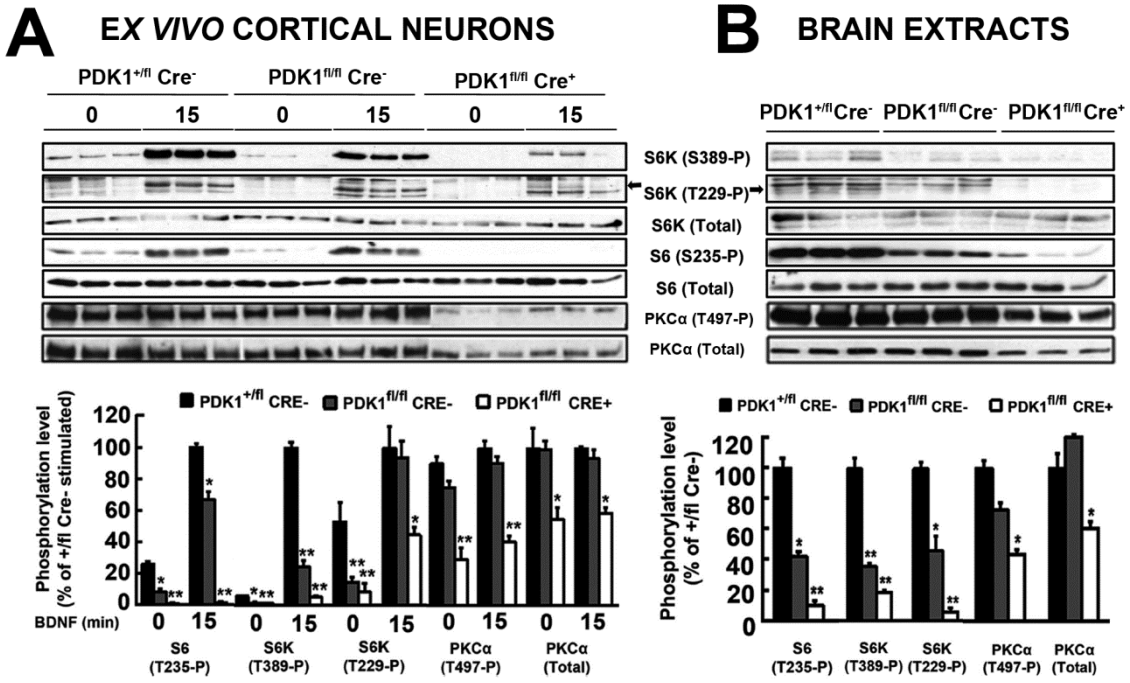

Figure R2: Activation of S6K1, S6 and PKCα is inhibited in PDK1$^{fl/fl}$ CRE^{+} mice brains and *in vitro* cultured neurons. (A) Cortical neurons from three independent embryos of the indicated genotypes were cultured for 6 DIV and then serum starved for 4 hours and either left unstimulated (0) or stimulated with 50 ng/ml of BDNF for 15 minutes (15). **(B)** Whole-brain protein extracts were obtained at E15.5 from three independent embryos of each depicted genotype. Lysates were immunoblotted with the indicated antibodies to monitor the activation of S6K, ribosomal protein S6, and PKCα. Each lane corresponds to a different embryo. In the lower row, band densitometry quantification of the ratio between phosphorylated and total protein levels is shown. Bars represent the means and standard errors of the mean obtained for three different mice per genotype analysed and is expressed as a percentage of the BDNF-stimulated control samples (A) or control brain tissue samples (B). *, P < 0'05; **, P < 0'005 compared to the controls.

Abnormal embryonic neurodevelopmental of the PDK1$^{fl/fl}$ CRE^{+} mice

REDUCED PROLIFERATION WITHOUT INCREASED APOPTOSIS IN THE PDK1$^{fl/fl}$ CRE^{+} CORTICAL NEURONS

This same study demonstrated that the binding of the PDK1 PIF pocket to its substrate-docking site was not essential to support neuronal survival *in vitro*, since the viability of cortical neurons from both PDK1$^{fl/fl}$ CRE^{+} E15.5 mutant embryos and PDK1$^{+/fl}$ CRE^{-} controls cultured *in vitro* showed similar decrease after trophic factor deprivation and recovered to the same levels upon BDNF rescue.

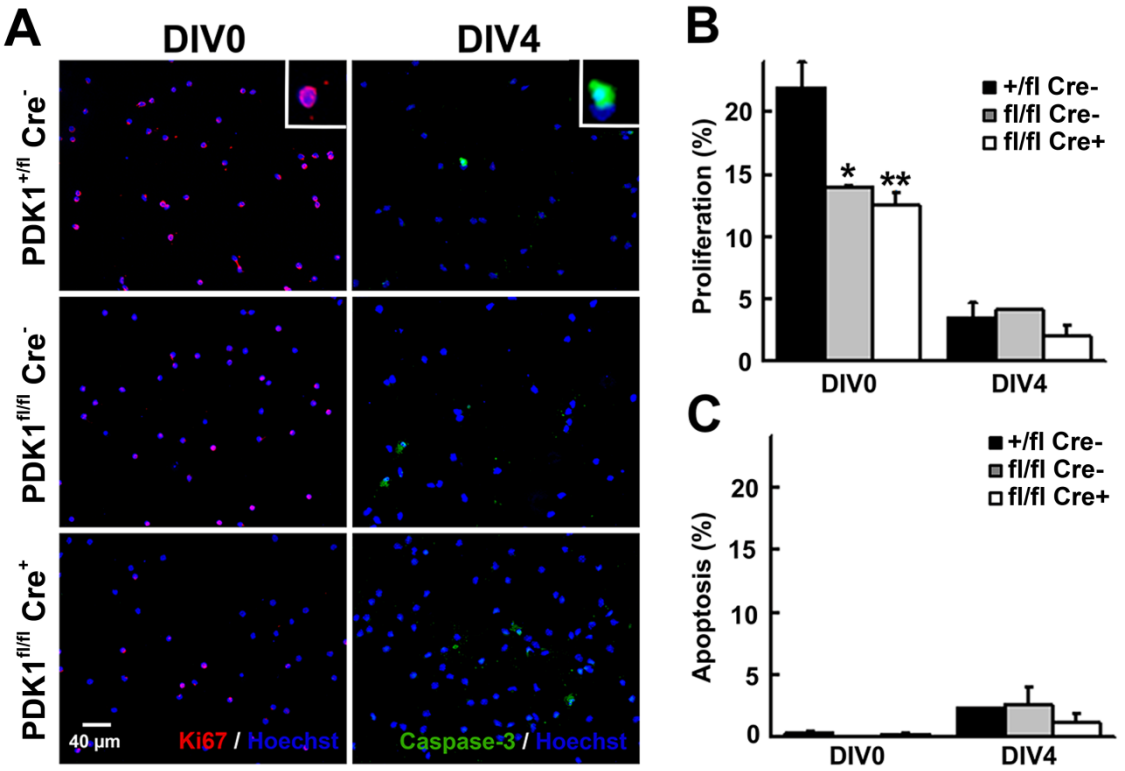

Figure R3: Reduced neuronal proliferation in PDK1$^{fl/fl}$ CRE^{-} and PDK1$^{fl/fl}$ CRE^{+} embryos. (A) Representative micrographs of E15.5 embryonic cortical neurons of the indicated genotypes cultured for the indicated days *in vitro* (DIVs) and immunostained with the described antibodies. Insets show enlarged single-cell representative images of the nuclear staining of Ki67 in red and the cytoplasmic active caspase-3 staining in green. **(B, C)** The percentages of primary cortical neurons expressing the Ki67 proliferation marker (B) or the active caspase 3 apoptotic marker (C) were scored at the indicated time points. The bars correspond to the means and standard errors of the mean from 10 different fields per culture and three independent embryonic cultures per genotype. *, P < 0'05; **, P < 0'005 compared to the controls.

Thus, the dynamics of embryogenesis rather than the viability of the neurons could explain the microcephaly observed in the adult brain. I first looked at the proliferation and cell death rates of E15.5 neurons cultured *in vitro*. Just after seeding, at DIV0, neurons showed the higher rate of proliferation, as judged by the ki67 staining, of above 20% in the $PDK1^{+/fl}$ CRE^{-} controls, which was significantly reduced by 5% in both the $PDK1^{fl/fl}$ CRE^{-} and $PDK1^{fl/fl}$ CRE^{+} cultured cortical neurons (Figure R3A, R3B). As days *in vitro* progressed, proliferation rates dropped, and neurons were no longer proliferating at DIV4 (Figure R3B).

Programmed cell death was monitored with cleaved caspase-3 staining, a marker of active processes of apoptosis (Figure R3A). None of the genotypes displayed any relevant amount of cell death when just seeded at DIV0 (Figure R3C). Occasionally, cell death slightly increased as days *ex vivo* progressed, most likely due to *in vitro* culturing conditions, and reached a peak at DIV4 that represented less than 5% of the scored neurons and was comparable in the three genotypes (Figure R3A, R3C).

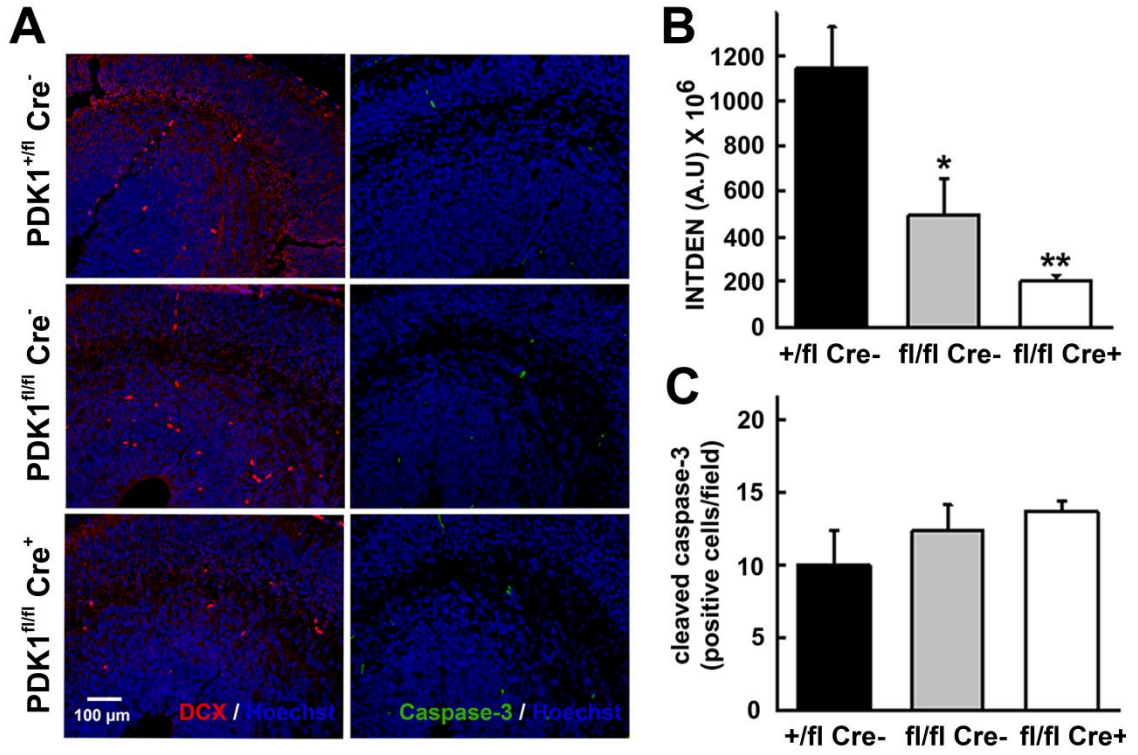

Figure R4: **Reduced immature neurons generation in $PDK1^{fl/fl}$ CRE^{-} and $PDK1^{fl/fl}$ CRE^{+} embryos. (A)** Epifluorescence microscopy images of E15.5 embryonic brain coronal sections of the indicated genotypes immunostained with the described antibodies. DCX, doublecortin, a marker for neurogenesis. Active caspase-3, a marker for apoptosis. **(B, C)** The (B) intensity of doublecortin staining (INTDEN) and (C) the number of caspase 3-positive cells per field were quantified and expressed as the means and standard errors of the mean from three independent sections obtained from three different embryos per genotype. A.U, arbitrary units. *, P < 0'05; **, P < 0'005 compared to controls.

In vivo, in coronal sections of E15.5 embryonic cortical tissue, active apoptosis was also negligible, as judded by the staining with the cleaved caspase-3, which was spurious (Figure R4A, R4C). As a first approach, quantification of proliferation was made by staining coronal neocortical tissue samples of E15.5 embryos with doublecortin (DCX), a marker of immature newly born neurons. Doublecortin is a stabilizer of microtubules, reason why its pattern of staining is cytoplasmatic, and is widely expressed by migrating and differentiating neurons (Francis *et al.*, 1999; Romero-Grimaldi, Moreno-López and Estrada, 2008). We observed a 56'95% reduction in DCX intensity of staining in the $PDK1^{fl/fl}$ CRE^{-} and 81'97% in the $PDK1^{fl/fl}$ CRE^{+} embryos compared to the $PDK1^{+/fl}$ CRE^{-} controls (Figure R4A, R4B).

REDUCED INTERMEDIATE PROGENITORS, BUT NOT APICAL PROGENITORS GENERATION, IN THE $PDK1^{fl/fl}$ CRE^{+} NEOCORTEX

Decreased generation of immature neurons could arise from a reduced pool of intermediate progenitors (IP), a subpopulation that specifically expresses the transcription factor Tbr2 (Sessa *et al.*, 2008). Staining with this marker confirmed that the number of IPs was 40% reduced in the $PDK1^{fl/fl}$ CRE^{+} embryos when compared to the $PDK1^{+/fl}$ CRE^{-} controls (Figure R5A, R5B). Moreover, the proximal border where they started arising located further away from the ventricle in the $PDK1^{fl/fl}$ CRE^{+} samples when compared to the $PDK1^{+/fl}$ CRE^{-} controls (Figure R5C). However, the distal limit of the expression area did not vary in any of the three analysed genotypes (Figure R5E), which resulted in reduced $Tbr2^{+}$ layer thickness in the $PDK1^{fl/fl}$ CRE^{+} mutant embryos (Figure R5D).

In turn, a decreased production of IPs could originate from a reduced proliferation or a reduced number of apical progenitors (AP), a subpopulation that expresses in an exclusive manner the transcription factor Pax6. Although they tended to be reduced in the mutants, staining of E15.5 samples did not show statistical differences in $Pax6^{+}$ cells amongst the three genotypes (Figure R6B, R6H).

In fact, APs were found reduced in the regions more away from the ventricle of the $PDK1^{fl/fl}$ CRE^{+} cortices, where $PDK1^{+/fl}$ CRE^{-} cortex was still populated with $Pax6^{+}$ neurons. When the total thickness of each cortex was divided in 8 equal partitions, called bins, $Pax6^{+}$ population could scarcely be found in the 3^{th} bin of the E15.5 $PDK1^{fl/fl}$ CRE^{+} embryos counting from the ventricle, while $PDK1^{+/fl}$ CRE^{-} controls and $PDK1^{fl/fl}$ CRE^{-} embryos presented them (Figure R6D), and was only detected in the bin 4 of the $PDK1^{+/fl}$ CRE^{-} controls. IPs, stained by Tbr2, were reconfirmed to be present in smaller number in the first bin close from the ventricle in the E15.5 $PDK1^{fl/fl}$ CRE^{+} samples than in the $PDK1^{+/fl}$ CRE^{-} and $PDK1^{fl/fl}$ CRE^{-} ones, but to

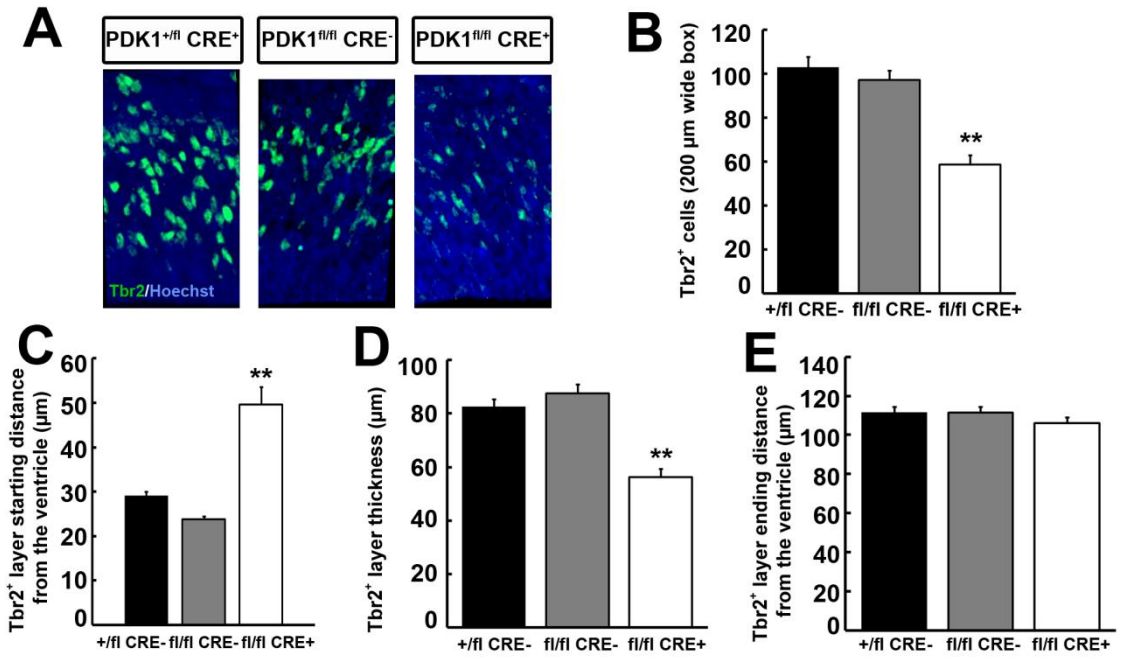

Figure R5: **Reduced intermediate neuronal progenitor number and distancing from the ventricle in the PDK1$^{fl/fl}$ CRE^{+} embryos. (A)** Representative epifluorescence microscopy images of E15.5 embryonic brain coronal sections of the indicated genotypes immunostained with Tbr2, a marker for intermediate progenitors (IP). Hoechst (blue) stains the nucleus. **(B-E)** The total number of Tbr2-positive cells per field in 200 µm-wide boxes (B), their mean proximal (C) and distal (E) distances to the ventricle (in µm), and the thickness of the expressing layer (D) were quantified and expressed as the means and standard errors of the mean from three independent sections obtained from three different embryos per genotype. *, P < 0'05; **, P < 0'005 compared to controls.

end the area of expression at the same bin 5 in all three genotypes (Figure R6F).

When evaluating the situation at E14.5, a time when a peak of neurogenesis is active (Molyneaux *et al.*, 2007), staining revealed that Pax6^{+} population showed no significant differences in total number amongst genotypes at that age (Figures R6A, R6G). APs could be found occupying a greater proportion of the PDK1$^{fl/fl}$ CRE^{+} neocortex (up to bin 6) than in the PDK1$^{fl/fl}$ CRE^{-} and PDK1$^{+/fl}$ CRE^{-} (up to bin 5) (Figure R6C) samples, maybe due a reduced total thickness of the neocortex. However, Tbr2-expressing IPs were at this stage still generated at lower rates in the PDK1$^{fl/fl}$ CRE^{+} embryos (50'3 ± 3'75) than in the PDK1$^{+/fl}$ CRE^{-} controls (109'7 ± 3'55) (Figure R6I). Their binned distribution showed that, at this age, they again appear more distanced from the ventricle (Figure R6E), only reaching more than 10 positive cells per bin from bin 5 onwards, instead of bin 3 as seen in the PDK1$^{+/fl}$ CRE^{-} controls. Also, at E14.5, Tbr2^{+} cells can be found at more pial fractions in the PDK1$^{fl/fl}$ CRE^{+} mice (up to bins 7 and 8) where PDK1$^{fl/fl}$ CRE^{-} or PDK1$^{+/fl}$ CRE^{-} mice presented any. In the PDK1$^{fl/fl}$ CRE^{-} mice, Tbr2^{+} IPs accumulated strongly in the medial bins 3 and 4, and then got exhausted in the pial fractions 7 and 8.

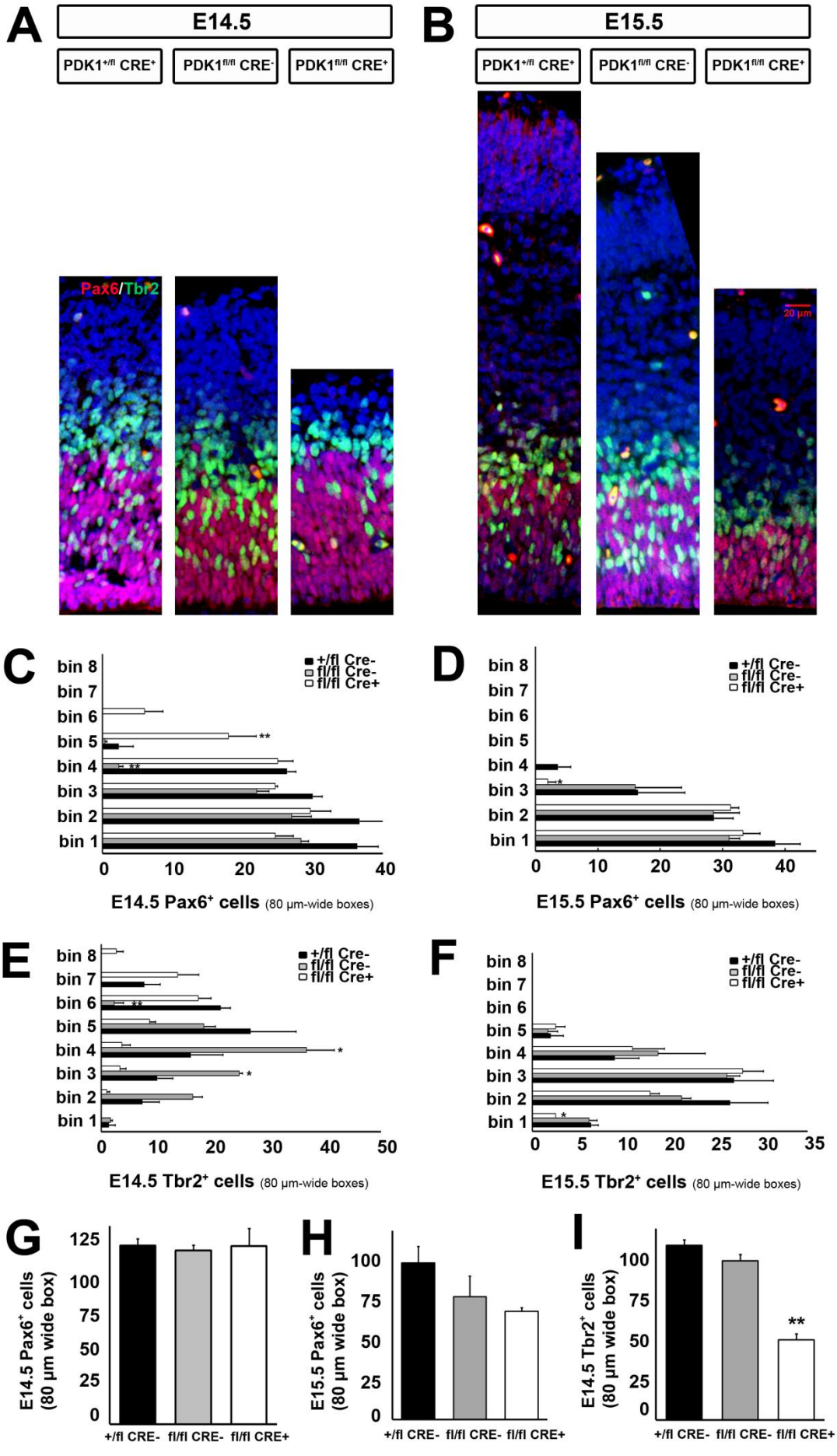
A
E14.5
PDK1+/fl CRE+
PDK1fl/fl CRE-
PDK1fl/fl CRE+
Pax6/Tbr2
B
E15.5
PDK1+/fl CRE+
PDK1fl/fl CRE-
PDK1fl/fl CRE+
20 µm
C
bin 8
bin 7
bin 6
bin 5
bin 4
bin 3
bin 2
bin 1
+/fl Cre-
fl/fl Cre-
fl/fl Cre+
0 10 20 30 40
E14.5 Pax6+ cells (80 µm-wide boxes)
D
E15.5 Pax6+ cells (80 µm-wide boxes)
E
0 10 20 30 40 50
E14.5 Tbr2+ cells (80 µm-wide boxes)
F
0 5 10 20 25 30 35
E15.5 Tbr2+ cells (80 µm-wide boxes)
G
E14.5 Pax6+ cells (80 µm wide box)
0 25 50 75 100 125
+/fl CRE- fl/fl CRE- fl/fl CRE+
H
E15.5 Pax6+ cells (80 µm wide box)
0 25 50 75 100
I
E14.5 Tbr2+ cells (80 µm wide box)
0 25 50 75 100

Figure R6: **Reduced intermediate, but not apical, neuronal progenitor number at E14.5 and E15.5 in the PDK1$^{fl/fl}$ CRE^{+} embryos. (A, B)** Representative epifluorescence microscopy images of (A) E14.5 and (B) E15.5 embryonic brain coronal sections of the indicated genotypes immunostained with Tbr2 (green), marker for intermediate progenitors (IP), and Pax6 (red), marker for apical progenitors (AP). Hoechst (blue) stains the nucleus. **(C-I)** Binned (C, D, E, F) and total (G, H, I) distribution of Pax6- (C, D, G, H) and Tbr2- (E, F, I) expressing neurons in E14.5 (C, E, G, I) and E15.5 (D, F, H) samples. The number of stained neurons in 80 μm-wide boxes were quantified and expressed as the means and standard errors of the mean from three independent sections obtained from three different embryos per genotype. *, P < 0'05; **, P < 0'005 compared to controls.

INCREASED PROLIFERATION AT E14.5 THAT DIMINISHED AT E15.5 WITH REDUCED MITOSIS IN THE PDK1$^{fl/fl}$ CRE^{+} MICE

After the obtained results, the proliferation status of the Pax6-expressing AP seemed an important factor to check, both at E14.5 and E15.5. APs resulted to be proliferative in their totality at both gestation times and for the three genotypes analysed (Figure R7A, R7B).

Differences were observed in the fraction of proliferating cells (ki67^{+}) that are not APs (Pax6^{-}) in the PDK1$^{fl/fl}$ CRE^{+} mice at both E14.5 (Figure R7C) and E15.5 (Figure R7H), with opposite effects at each age. At E14.5, PDK1$^{fl/fl}$ CRE^{+} had more proliferative, non AP cells in 80 μm-wide boxes (76'46 ± 1'42) than the PDK1$^{+/fl}$ CRE^{-} controls (55'77 ± 3'99). However, at E15.5 this fraction was significantly smaller in the PDK1$^{fl/fl}$ CRE^{+} mutant mice (24'18 ± 0'83) than in the controls (31'75 ± 1'77) in the same boxes (Figure R7H). Indeed, the total number of ki67^{+} cells that are also Pax6^{-} at E14.5 was higher in the PDK1$^{fl/fl}$ CRE^{+} mutant mice (46'67 ± 2'36) than in the PDK1$^{+/fl}$ CRE^{-} controls (34'00 ± 1'50) (Figure R7D). At E15.5, puzzingly, the decrease in the percentage translated onto an increased total number of cells, which was however not statistically significant (Figure R7I).

When comparing the percentage of non APs (Pax6^{-}) that were proliferating (ki67^{+}) at E14.5, they represented a greater proportion in the PDK1$^{fl/fl}$ CRE^{+} mice (76'46% ± 1'42) than in the PDK1$^{+/fl}$ CRE^{-} controls (55'77% ± 3'99) (Figure R7F). At E15.5, again, this difference was not statistically significant (Figure R7K).

This translated in a decrease at E15.5 in the μm of thickness of the layer that these ki67^{+} cells occupied in the PDK1$^{fl/fl}$ CRE^{+} mutant mice (130 ± 3'41) versus the PDK1$^{+/fl}$ CRE^{-} controls (185'2 ± 6'42) (Figure R7J). However, when normalizing them with the total width of their respective whole cortices, the difference was buffered (Figure R7L). No significative differences were observed at E14.5 for neither of these parameters (Figure R7E, R7G).

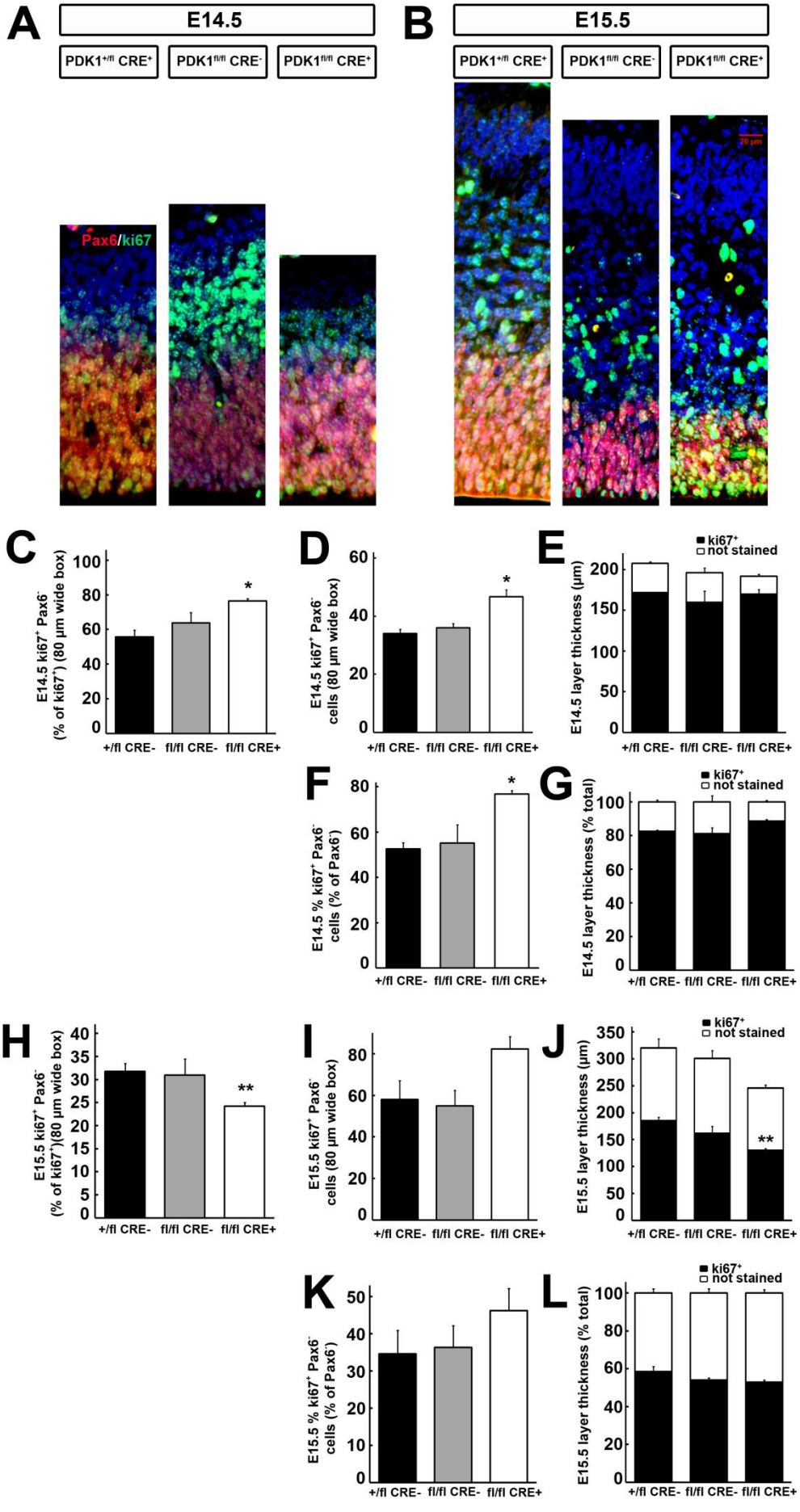
A
E14.5
PDK1+/fl CRE+
PDK1fl/fl CRE-
PDK1fl/fl CRE+
Pax6/ki67
B
E15.5
PDK1+/fl CRE+
PDK1fl/fl CRE-
PDK1fl/fl CRE+
20 µm
C
E14.5 ki67+ Pax6- (% of ki67+) (80 µm wide box)
+/fl CRE- fl/fl CRE- fl/fl CRE+
D
E14.5 ki67+ Pax6- cells (80 µm wide box)
+/fl CRE- fl/fl CRE- fl/fl CRE+
E
ki67+
not stained
E14.5 layer thickness (µm)
+/fl CRE- fl/fl CRE- fl/fl CRE+
F
E14.5 % ki67+ Pax6- cells (% of Pax6-)
+/fl CRE- fl/fl CRE- fl/fl CRE+
G
ki67+
not stained
E14.5 layer thickness (% total)
+/fl CRE- fl/fl CRE- fl/fl CRE+
H
E15.5 ki67+ Pax6- (% of ki67+)(80 µm wide box)
+/fl CRE- fl/fl CRE- fl/fl CRE+
I
E15.5 ki67+ Pax6- cells (80 µm wide box)
+/fl CRE- fl/fl CRE- fl/fl CRE+
J
ki67+
not stained
E15.5 layer thickness (µm)
+/fl CRE- fl/fl CRE- fl/fl CRE+
K
E15.5 % ki67+ Pax6- cells (% of Pax6-)
+/fl CRE- fl/fl CRE- fl/fl CRE+
L
ki67+
not stained
E15.5 layer thickness (% total)
+/fl CRE- fl/fl CRE- fl/fl CRE+

Figure R7: **The whole population of apical progenitors is proliferating in the three genotypes. Non-AP-proliferating cells are increased at E14.5 and later decreased at E15.5 in the PDK1$^{fl/fl}$ CRE^{+} embryos. (A)** Representative epifluorescence microscopy images of (A) E14.5 and (B) E15.5 embryonic brain coronal sections of the indicated genotypes immunostained with Pax6 (red), marker for apical progenitors, and ki67 (green), marker of cellular proliferation. Hoechst (blue) stains the nucleus. **(C, H)** Percentage of proliferating cells (ki67^{+}) that are not apical progenitors (Pax6^{-}) in relation to the total proliferative cells per field in 80 µm-wide boxes. **(D, F, I, K)** Number of proliferating cells (ki67^{+}) that are not apical progenitors (Pax6^{-}) in 80 mm wide box thickness (µm) (D, I) and its percentage respect to the total (F, K) at E14.5 (D, F) and E15.5 (I, K). **(E, G, J, L)** Absolute thickness (µm) (E, J) and its percentage respect to the total (G, L) occupied by the ki67-expressing and not expressing cells at E14.5 (E, G) and E15.5 (J, L). All the values express the means and standard errors of the mean from three independent sections obtained from three different embryos per genotype. *, P < 0'05; **, P < 0'005 compared to controls.

Once assessed that all APs had their proliferating programme on, it was interesting to know how many were actually undergoing mitosis. Phospho-histone-H3 (pH3) is an specific marker for mitosis as it is a histone that is only phosphorylated when mitosis is active since it is involved in regulating mitotic chromosome condensation and decondensation (Wei *et al.*, 1998). APs from PDK1$^{fl/fl}$ CRE^{+} were less active in mitosis (27'87% ± 0'86) than the PDK1$^{fl/fl}$ CRE^{-} (30'14% ± 2'11) and the PDK1$^{+/fl}$ CRE^{-} controls (38'44% ± 1'30) ones (Figure R8A, R8B). However, the numbers of non-APs mitotic populations were low and equivalent in the three genotypes (Figure R8C). Interestingly, if the absolute number of cells undergoing mitosis in 80 µm-wide boxes were scored, no significant difference could be found amongst the three genotypes (Figure R8D), masking the reduction in mitotic APs caused by the L155E mutation.

Additionally, there is a tendency to a shift in the pH3 nuclear pattern of staining amongst the three genotypes, with a predominance in a punctuated pattern in the PDK1$^{fl/fl}$ CRE^{+} mutants (69'42 ± 7'55) and the PDK1$^{fl/fl}$ CRE^{-} semimutants (66'86 ± 2'85) mutants, whereas the PDK1$^{+/fl}$ CRE^{-} controls showed an increase in the whole nuclear stain that balanced the punctuated (54'03 ± 3'72) pattern (Figure R8E).

Another cell cycle phase that can be quantified is S-phase. By exposing neurons to the thymidine analogous 5-ethynyl-2'-deoxyuridine (EdU) after disaggregating them from their cortices and just before seeding them *in vitro* on cell culture plates, the cells undergoing this phase would be the only ones able to incorporate the labelled nucleotide, because they are the only ones sinthesizing DNA. This analogous base is not toxic and does not stop any of the cellular processes in which participates, allowing cells to keep on living even if they incorporated EdU to their genome (Salic and Mitchison, 2008). E15.5 cortical neurons were exposed to EdU for 4 hours

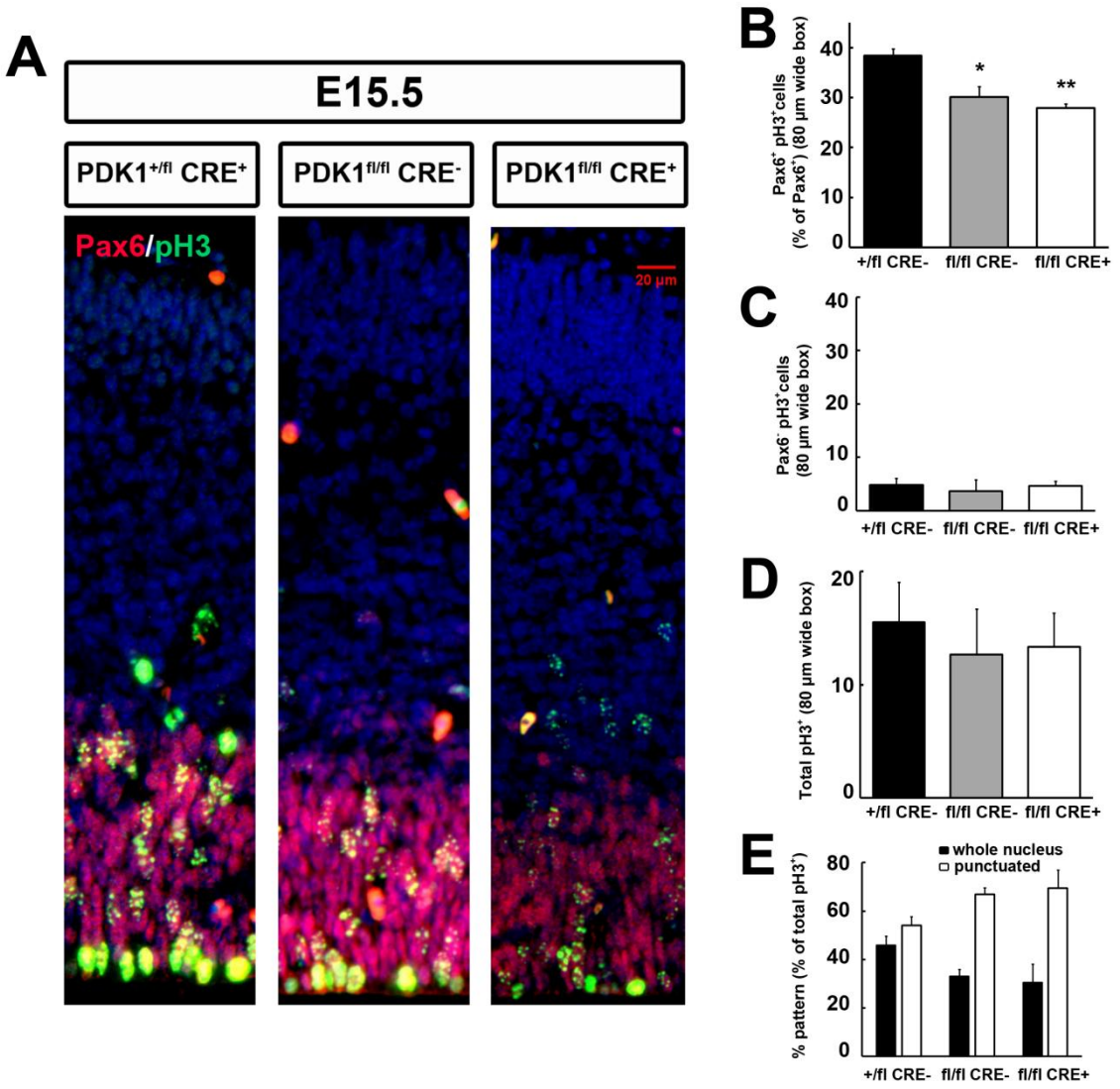

Figure R8: **Reduced apical progenitors mitotic tax in E15.5 PDK1$^{fl/fl}$ CRE^{-} and PDK1$^{fl/fl}$ CRE^{+} embryos. (A)** Representative epifluorescence microscopy images of E15.5 embryonic brain coronal sections of the indicated genotypes immunostained with phospho-Histone 3 (pH3) (green), a marker for dividing cells undergoing mitosis, and Pax6 (red), a marker for apical progenitors. Hoechst (blue) stains the nucleus. **(B)** Percentage of apical progenitors undergoing mitosis respect the total of Pax6^{+} cells counted in 80 µm-wide boxes. **(C)** Total number of cells undergoing mitosis excluding the apical progenitors (Pax6^{-}) counted in 80 µm-wide boxes. **(D)** Total number of cells undergoing mitosis in the whole cortex height of 80 µm-wide boxes. **(E)** Percentage of punctuated or whole nuclear-staining patterns respect the total of pH3^{+} cells. Cells were scored in 80 µm-wide boxes and results expressed as the means and standard errors of the mean from three independent sections from three different embryos per genotype. *, P < 0'05; **, P < 0'005 compared to controls.

when seeded and checked for EdU incorporation after 24 hours (the peak in proliferation observed with ki67 (Figure R3B)) (Figure R9A), but the three genotypes showed no significant differences (Figure R9B).

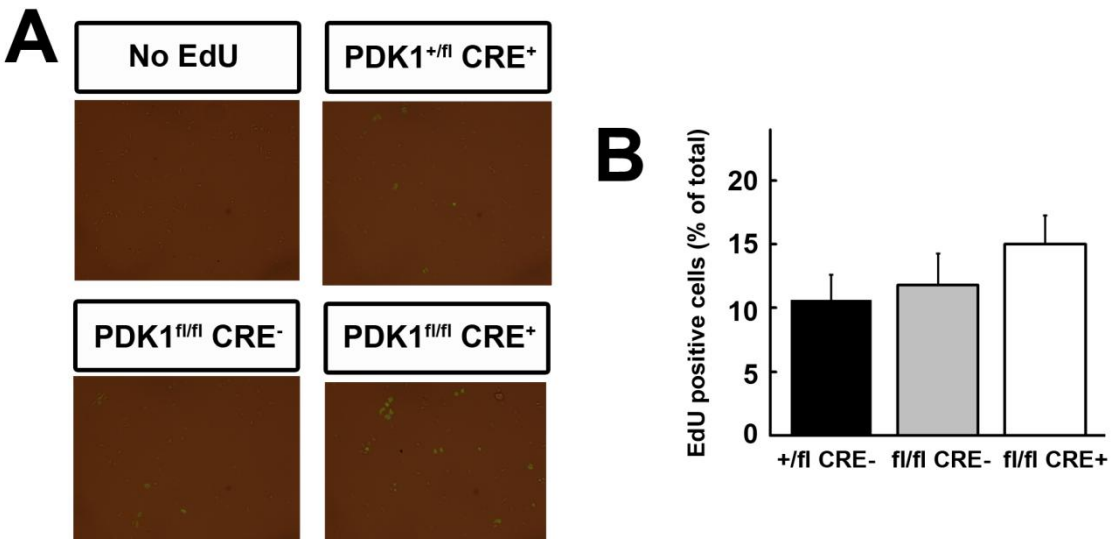

Figure R9. *In vitro* cortical neurons disaggregated from cortices at E15.5 showed no differences in the capacity to incorporate 5-ethynyl-2'-deoxyuridine (EdU) in the three analised genotypes (A) Representative bright-field and epifluorescence microscopy merged images of cortical neurons coming from E15.5 embryonic cortices of the indicated genotypes after being exposed or not (no Edu) for 4 hours to 5-ethynyl-2'-deoxyuridine (EdU) and allowed to attach for 24 hours, then photographed with bright light and green light while still alive. **(B)** The percentage was obtained by scoring the total and the EdU stained nuclei from three different fields per well and three wells per condition divided by the total. *, P < 0'05; **, P < 0'005 compared to controls.

REDUCED GENERATION OF CTIP2+ NEURONAL SUBPOPULATION WITH INCREASED PRODUCTION OF THEIR TBR1+ PROGENITORS IN THE PDK1fl/fl CRE+ MICE AT E15.5

The reduced pool of both APs, IPs and proliferating cells at E15.5 could be due a premature neurogenesis that consumed the progenitors before the adequate time.

Therefore, E14.5 and E15.5 cortices were subjected to Ctip2 staining. Ctip2 is a marker of a specific subpopulation of mature neurons that will occupy layer V in the adult cortex. This subpopulation is formed from Tbr1-expressing cells, a still somehow pluripotent pool of neurons that are destined to occupy deep layers of the cortex. Ctip2 neuronal specification starts at E13.5 (Molyneaux *et al.*, 2007).

The generation of this subpopulation resulted not promoted when the mutant PDK1 L155E protein was expressed. By contrast, the number of Ctip2-positive cells scored in 80 µm-wide boxes was decreased at E14.5 in the PDK1fl/fl CRE+ full mutant mice (34'67 ± 2'36) compared with PDK1+/fl CRE- control (72 ± 3'12) (Figure R10A, R10G). Also, their positioning was displaced to more distal pial bins (7 and

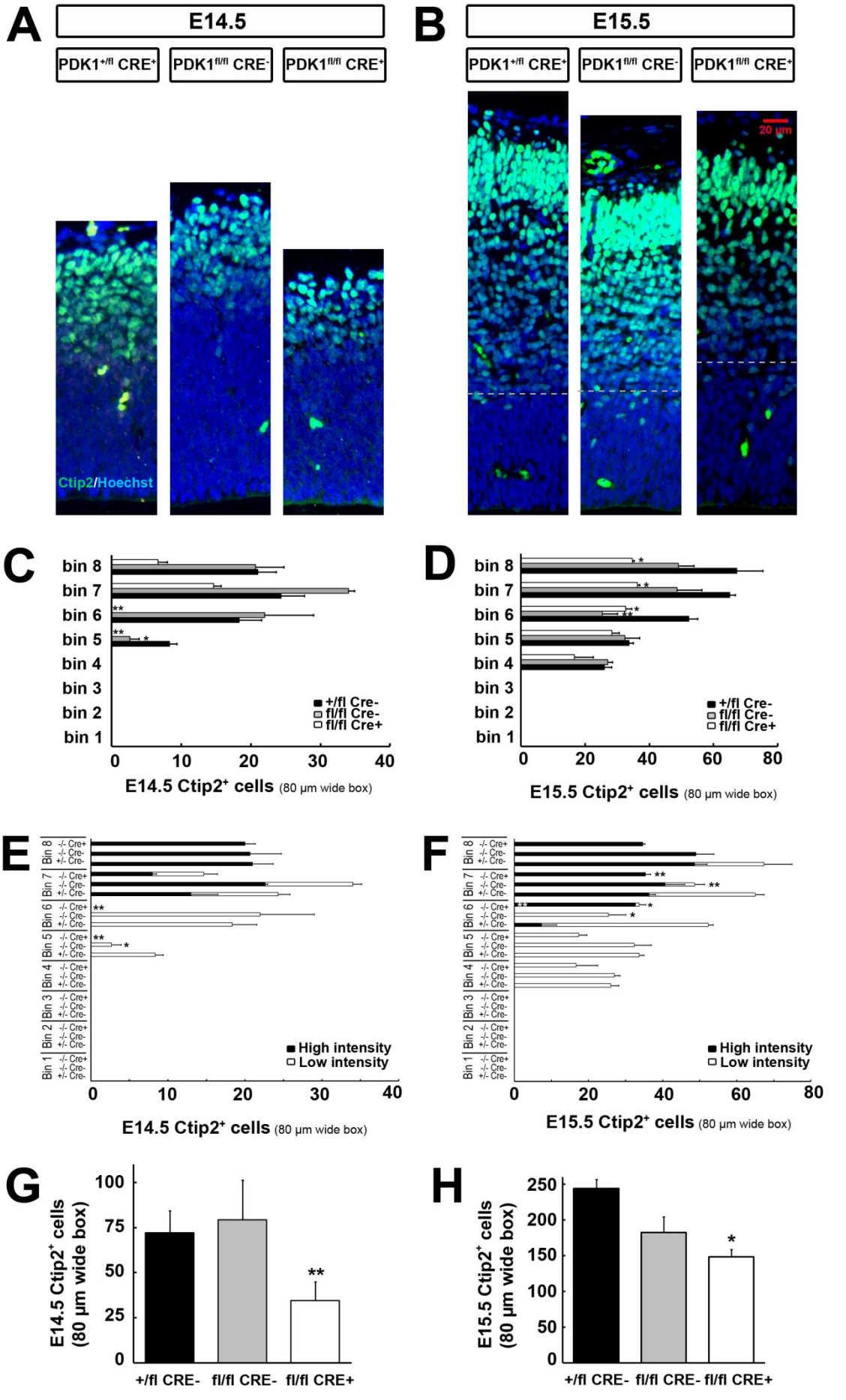
A
E14.5
PDK1+/fl CRE+
PDK1fl/fl CRE-
PDK1fl/fl CRE+
Ctip2/Hoechst
B
E15.5
PDK1+/fl CRE+
PDK1fl/fl CRE-
PDK1fl/fl CRE+
20 µm
C
bin 8
bin 7
bin 6
bin 5
bin 4
bin 3
bin 2
bin 1
+/fl Cre-
fl/fl Cre-
fl/fl Cre+
E14.5 Ctip2+ cells (80 µm wide box)
D
E15.5 Ctip2+ cells (80 µm wide box)
E
High intensity
Low intensity
E14.5 Ctip2+ cells (80 µm wide box)
F
E15.5 Ctip2+ cells (80 µm wide box)
G
E14.5 Ctip2+ cells (80 µm wide box)
+/fl CRE- fl/fl CRE- fl/fl CRE+
H
E15.5 Ctip2+ cells (80 µm wide box)
+/fl CRE- fl/fl CRE- fl/fl CRE+

Figure R10: **Reduced and displaced number of Ctip2- expressing neurons at E14.5 and E15.5 in the PDK1$^{fl/fl}$ CRE^{+} embryos. (A, B)** Representative epifluorescence microscopy images of E14.5 (A) and E15.5 (B) embryonic brain coronal sections of the indicated genotypes immunostained with Ctip2 (green), a marker for the subpopulations of mature neurons that will occupy layer V of the neocortex. Hoechst (blue) stains the nucleus. (B) Grey dashed lines mark the point from where Ctip2 staining is observed. **(C-F)** Binned distribution of the Ctip2-expressing total number of cells (C, D) or stained with high and low intensity patterns (E, F) in 80 µm-wide boxes at E14.5 (C, E) and E15.5 (D, F) cortices. **(G, H)** Total number of the Ctip2-expressing cells in 80 µm-wide boxes at E14.5 (G) and E15.5 (H) cortices. Cells were scored in 80 µm-wide boxes and values expressed as the means and standard errors of the mean from three independent sections obtained from three different embryos per genotype. *, P < 0'05; **, P < 0'005 compared to controls

8), being excluded from bins 5 and 6, where Ctip2 – expressing cells could be found in the PDK1$^{+/fl}$ CRE^{-} mice and, in a reduced number, in the PDK1$^{fl/fl}$ CRE^{-} ones (Figure R10C).

At E15.5, the total Ctip2-positive population, as scored in 80 µm-wide boxes, was 25% decreased in the PDK1$^{fl/fl}$ CRE^{-} semimutant (182'33 ± 22'02) and 39% in the PDK1$^{fl/fl}$ CRE^{+} full mutant (148'67 ± 10'25) when compared to the PDK1$^{+/fl}$ CRE^{-} control (244'33 ± 12'21) (Figure R10H). This came from a reduction in the number of Ctip2^{+} cells in the PDK1$^{fl/fl}$ CRE^{+} when compared to the PDK1$^{+/fl}$ CRE^{-} control in the most pial part of the neocortex (bins 6 to 8), while reductions in PDK1$^{fl/fl}$ CRE^{-} were only significant at bin 6 (Figure R10D). Two different populations were observed according to their staining levels: a high intensity one, positioning most close to the pia, and a second one of lower intensity (Figure R10B). The reduction in the Ctip2^{+} number of cells of the PDK1$^{fl/fl}$ CRE^{+} mice coincided with a specific reduction of the low intensity cells in the PDK1$^{fl/fl}$ CRE^{-}, and an absence in the PDK1$^{fl/fl}$ CRE^{+} mice in bins 6 and 7 (Figure R10F), even if lower intensity Ctip2 – expressing cells could be found for the first time at bin 4 in the three genotypes (Figure R10F). These two patterns of Ctip2-stained cells were already present at E14.5, but there were no differences in their distribution between genotypes in those bins that showed no differences in number of Ctip2^{+} cells. Bins 5 and 6, that lacked Ctip-stained cells in the PDK1$^{fl/fl}$ CRE^{+} samples, presented only weakedly stained cells in the other two genotypes (Figure R10E).

Ctip2 staining in E15.5 samples revealed a non-stained zone close to the ventriculus (grey dashed lines in Figure R10B). To confirm if this band corresponded exclusively to APs, and thus Ctip2+ low-intensity cells were born exactly at this border, a co-staining with both Ctip2 and Pax6 markers was performed in E15.5 cortices (Figure R11A). This revealed a band of non-stained, unidentified cells in PDK1$^{fl/fl}$ CRE^{+} mutants that was less prominent in PDK1$^{fl/fl}$ CRE^{-} semimutants and nearly absent in PDK1$^{+/fl}$ CRE^{-} controls. Indeed, cells not stained by either of the markers were significantly higher in PDK1$^{fl/fl}$ CRE^{+} samples than in PDK1$^{fl/fl}$ CRE^{-}, and very reduced in the PDK1$^{+/fl}$ CRE^{-} cortices (Figure R11B).

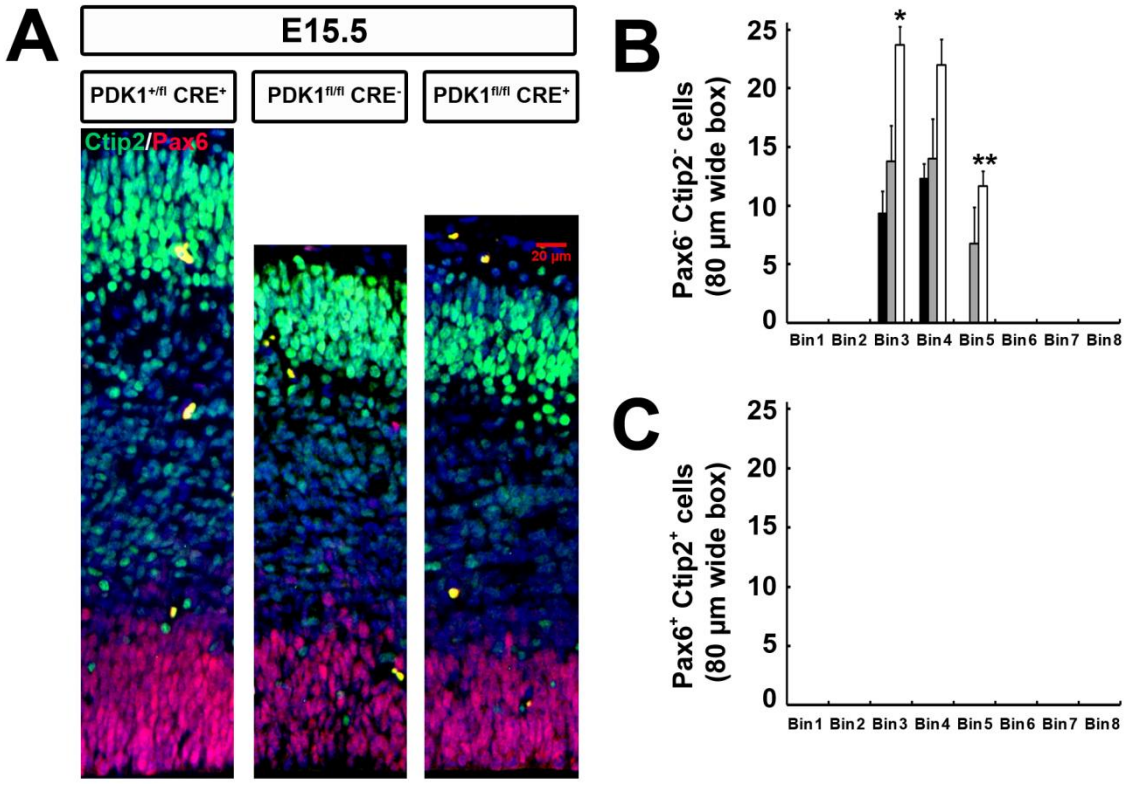

Figure R11: **The PDK1$^{fl/fl}$ CRE^{-} and PDK1$^{fl/fl}$ CRE^{+} embryos have an increased not-identified neuronal sub-population. (A)** Representative epifluorescence microscopy images of E15.5 embryonic brain coronal sections of the indicated genotypes immunostained with Pax6 (red), a marker for apical progenitors, and Ctip2 (green), a marker for the subpopulations of mature neurons that will occupy layer V of the adult neocortex. Hoechst (blue) stains the nucleus. **(B, C)** Binned distribution of the cells (B) not stained, or (C) co-stained both with Pax6 and Ctip2. The cells in 80 µm-wide boxes were quantified and values expressed as the means and standard errors of the mean from three independent sections obtained from three different embryos per genotype. *, P < 0'05; **, P < 0'005 compared to controls

Controls displayed not-stained cells in a small part of the neocortex expanding bins 3 and 4, while the other 2 genotypes showed not-stained cells in bin 5. However, even being closely located populations, no co-staining was detected in any genotype (Figure R11C).

Figure R12 [next page]: **Immature deep layer neurons (Tbr1^{+}) are increased at E15.5 in the PDK1$^{fl/fl}$ CRE^{+} embryos. (A, B)** Representative epifluorescence microscopy images of (A) E14.5 and (B) E15.5 embryonic brain coronal sections of the indicated genotypes immunostained with Pax6 (red), a marker for apical progenitors, and Tbr1 (green), a marker for immature deep layer neurons that will occupy layers V and VI of the adult neocortex. Hoechst (blue) stains the nucleus. **(C-F)** Binned distribution of the cells stained with Tbr1 (C, D) and not stained (E, F) were quantified in E14.5 (C, E) and E15.5 (D, F) samples. **(H-I)** Total number of cells stained with Tbr1 in 80 µm-wide boxes at E14.5 (H) and E15.5 (I). All values are expressed as the means and standard errors of the mean from three independent sections obtained from three different embryos per genotype. *, P < 0'05; **, P < 0'005 compared to controls

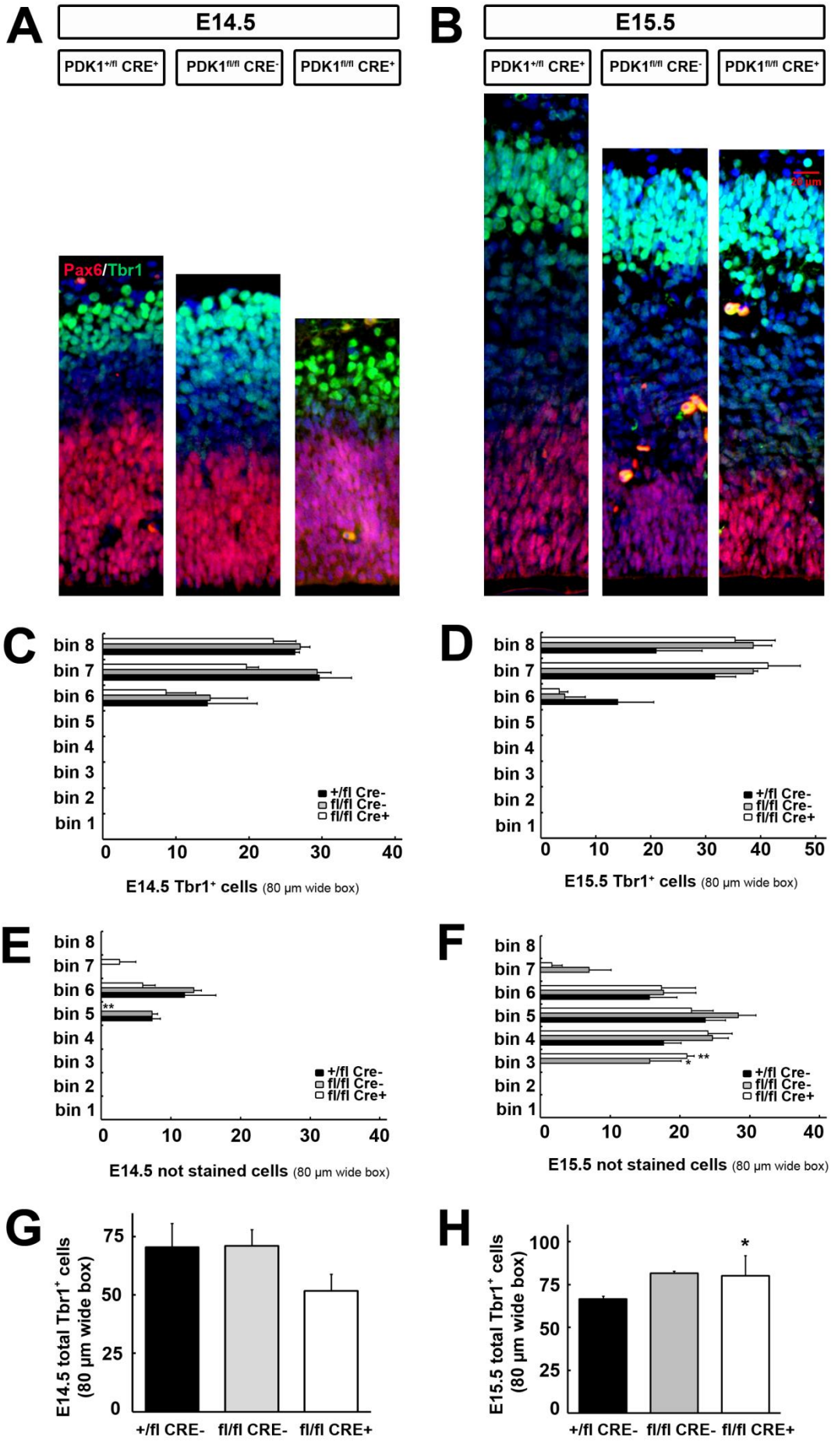
A
E14.5
PDK1+/fl CRE+
PDK1fl/fl CRE-
PDK1fl/fl CRE+
Pax6/Tbr1
B
E15.5
PDK1+/fl CRE+
PDK1fl/fl CRE-
PDK1fl/fl CRE+
20 µm
C
bin 8
bin 7
bin 6
bin 5
bin 4
bin 3
bin 2
bin 1
+/fl Cre-
fl/fl Cre-
fl/fl Cre+
0 10 20 30 40
E14.5 Tbr1+ cells (80 µm wide box)
D
bin 8
bin 7
bin 6
bin 5
bin 4
bin 3
bin 2
bin 1
+/fl Cre-
fl/fl Cre-
fl/fl Cre+
0 10 20 30 40 50
E15.5 Tbr1+ cells (80 µm wide box)
E
bin 8
bin 7
bin 6
bin 5
**
bin 4
bin 3
bin 2
bin 1
+/fl Cre-
fl/fl Cre-
fl/fl Cre+
0 10 20 30 40
E14.5 not stained cells (80 µm wide box)
F
bin 8
bin 7
bin 6
bin 5
bin 4
bin 3
*
**
bin 2
bin 1
+/fl Cre-
fl/fl Cre-
fl/fl Cre+
0 10 20 30 40
E15.5 not stained cells (80 µm wide box)
G
E14.5 total Tbr1+ cells (80 µm wide box)
75
50
25
0
+/fl CRE- fl/fl CRE- fl/fl CRE+
H
E15.5 total Tbr1+ cells (80 µm wide box)
100
75
50
25
0
*
+/fl CRE- fl/fl CRE- fl/fl CRE+

As Ctip2 staining evidenced differences in the neuronal populations amongst genotypes, an evaluation of their precursors, the Tbr1-expressing subpopulation, was necessary. In the adult cortex, Tbr1 is a specific marker for projection neurons residing in layer VI. However, at embryological stages, Tbr1 marks a whole subpopulation of early-born immature neurons that have abandoned Tbr2 expression. Tbr1 populations start appearing at E13.5, peaks at E15.5–17.5, and decreases postnatally (Kolk *et al.*, 2006). Co-staining with Pax6 was used to frame the band where APs are absent. $Tbr1^{+}$ total cell number showed no significant differences at E14.5 (Figure R12G). However, at E15.5, Tbr1-expressing cells were increased in the $PDK1^{fl/fl}$ CRE^{+} mutants (80 ± 12'03) compared to the $PDK1^{fl/fl}$ CRE^{+} controls (66'67 ± 1'61) (Figure R12I). At E14.5 and E15.5, Tbr1 binned positioning was maintained (Figure R12A, R12C, R12D). Additionally, a group of cells not stained by neither of these markers was observed between them. At E14.5, they appeared in the bins 6 and 7 in the $PDK1^{fl/fl}$ CRE^{+} mice, oppositely to the bin 5 and 6 distribution observed in the $PDK1^{fl/fl}$ CRE^{-} and $PDK1^{+/fl}$ CRE^{-} controls (Figure R12E). This band became wider in the E15.5 mutant cortices (Figure R12B). While it was limited to bins 4 to 6 in the $PDK1^{+/fl}$ CRE^{-} controls, in $PDK1^{fl/fl}$ CRE^{-} and $PDK1^{fl/fl}$ CRE^{+} mice it spread from bin 3 to bin 7 (Figure R12F). The identity of the not stained cells remains yet unknown.

Development of an S6K constitutively active construct

CREATION AND CHARACTERIZATION OF $S6K^{T229D/T389D}$ AND $S6K^{T229E/T389D}$

Evidences suggested that some phenotypes overlapped between the conditional PDK1 L155E and the whole body PDK1 K465E knockin mice, such as deficient axonal outgrowth *in vitro*. However, the pathogenic effects were more severe in the PDK1 L155E mutant mice, which included microcephaly and deficient cortical connectivity in the adult mice *in vivo*. This idea contradicts the common believe that PKB is the master kinase regulating many neurodevelopmental processes elicited by PI3K, since cortical defects were observed in spite of normal PKB activation in the PDK1 L155E model. This foreshadowed that the main common effector explaining the phenotypes of the two mice models could be S6K. Indeed, S6K is affected by both mutations, as it is mTORC1- (and thus PKB and PDK1-dependent), but at the same time directly dependent on PDK1 phosphorylation. To prove the relevance or not of this kinase, a constitutively active form was needed. A

constitutively active form of PKB, PKB$^{T308D/S473D}$ was also required as a control to assure whether the effects of the constitutively active form of S6K paralleled those of a constitutively active PKB.

A construct that encoded an S6K form that activated independently of mTORC1 phosphorylation, S6K^{T389D}, was used as a template. Using primers encoding point mutations (Figure R13A), two novel phosphomimetic forms were created by mutating the PDK1-dependent residue (Thr229) to Aspartic (S6K$^{T229D/T389D}$) or Glutamic (S6K$^{T229E/T389D}$) acid. Handily, the Thr229-to-Glu primer was designed so it will also include a new *EcoRI* restriction site only when the mutation is present, which allowed the detection of the mutant form by a simple enzymatic restriction assay. When not present (S6K^{T389D} or S6K$^{T229D/T389D}$), *EcoRI* restriction liberated the whole 1'8 kba insert (Figure R13B). The introduction of the mutation was confirmed by sequencing the plasmids (Figure R13C).

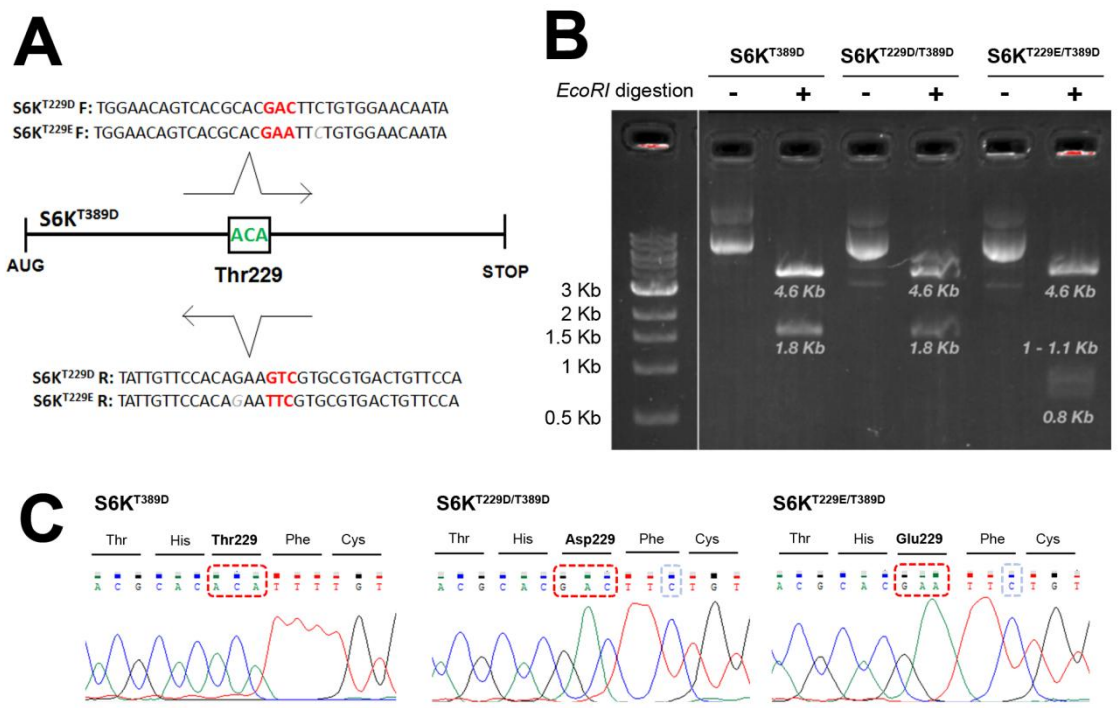

Figure R13: Generation and characterization of the novel double-phosphomimetic forms of S6K. **(A)** Primers used to create the S6K$^{T229D/T389D}$ and the S6K$^{T229E/T389D}$ constructs by directed mutagenesis. The T to C substitution in the double phosphomimetic forms that created a new *EcoRI* site in the S6K$^{T229E/T389D}$ construct is marked with grey italics. **(B)** Restriction map corresponding to the indicated constructs after an *EcoRI* restriction analysis; their lengths are described in Materials and Methods. DNA was amplified in *E. coli*, purified with QIAGen MidiPrep kits and digested for 1 hour at 37 ºC with the indicated restriction enzymes and their appropriate restriction buffers. The product was loaded in an 1% agarose gel stained with RedSafe. **(C)** Identity confirmation by sequencing analysis of the codon corresponding to the Thr229 residue for the S6K^{T389D} template (left panel), S6K$^{T229D/T389D}$ (middle panel) and the S6K$^{T229E/T389D}$ (right panel) constructs. Silent T to C mutation introduced alongside with the mutagenic primers is marked in blue dashed boxes.

To assess whether the novel proteins were indeed constitutively active independently on their upstream activators, a basal condition where no phosphorylation of their downstream substrates could be detected in wild type cells was needed. Thus, the exogenous expression of the new constructs should be sufficient to recover phosphorylation to levels found in cells with the PI3K-PDK1-PKB-S6K pathway active.

The main substrate of S6Ks is rpS6, which is phosphorylated when there is abundance of nutrients (Pende *et al.*, 2004). Thus, different trophic - starving

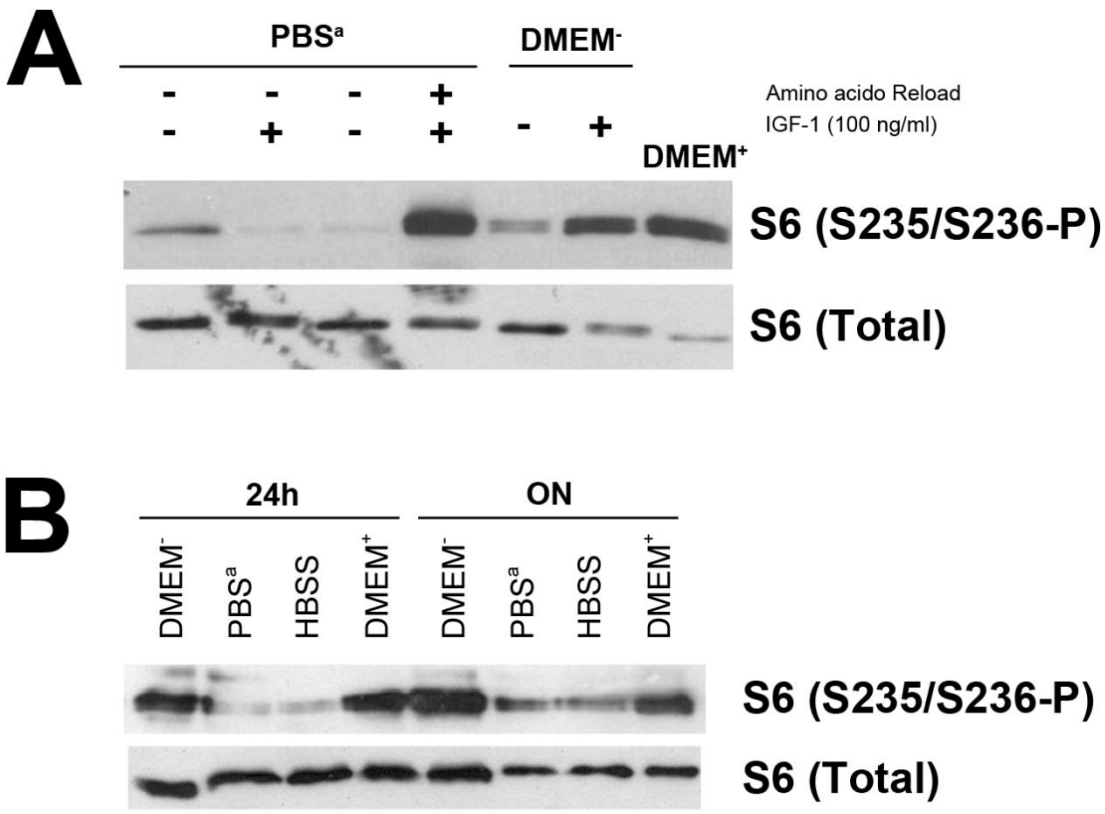

Figure R14: Set up of the conditions to measure phosphorylation of S6 protein. **(A)** HeLa cells were transfected with pCMV5 plasmid for 48 hours. Then, they were starved in PBS^{a} (PBS supplemented with 0.9 mM calcium chloride, 0.5 mM magnesium chloride, 1 g/l glucose and 20 mM HEPES pH 7.4) overnight; PBS^{a} overnight + ReLoad of amino acids for 1 hour (by adding serum-free DMEM + GlutaMAX, to reach a final concentration of 2 mM L-Alanyl-Glutamine); with serum-free DMEM + GlutaMAX overnight; or non-starved; next, cells were stimulated (+) or not (-) with 100 ng/ml of IGF-1 for 30 min. Protein extracts were obtained and analysed by western blot with the indicated antibodies. **(B)** HeLa cells were transfected with pCMV5 empty vector for 48 hours. Then, they were starved in DMEM^{-} (DMEM without serum); supplemented PBS (PBS^{a}), Hanks' Balanced Salt Solution (HBSS) or DMEM supplemented with FBS (DMEM^{+}) for 24 hours or overnight (ON) as indicated. Then, protein extracts were obtained and analysed by western blot with the indicated antibodies.

conditions described in the literature were tested in HeLa cells (Klinkenberg *et al.*, 2012; Martineau *et al.*, 2014; Krall *et al.*, 2016). Since S6K is a direct substrate of mTORC1, amino acid removal and reloading after starvation before stimulation were tested.

Phospho-rpS6 signal was still maintained in DMEM without serum, since it contained the modified amino acid GlutaMax. Instead, starvation with supplemented PBS (PBS^a) suppressed phosphorylation of rpS6 effectively (Figure R14A). In these conditions, amino acid reload step was necessary in order to allow HeLa cells to respond to IGF-1 stimulation (Figure R14A). No differences were observed between overnight or 24-hour starvation (Figure R14B). Thus, incubation with PBS^a overnight followed by amino acid reload using serum-free DMEM supplemented with GlutaMax were chosen as trophic deprivation/stimulation conditions.

The appropriate stimulus to activate the PI3K / PDK1 pathway was then tested in order to reach full rpS6 phosphorylation recovery after the starvation period. IGF-1 was tested at different concentrations and rpS6 phosphorylation was induced efficiently at the highest conditions, so 100 ng/ml was chosen as the concentration to continue with the experiments (Figure R15).

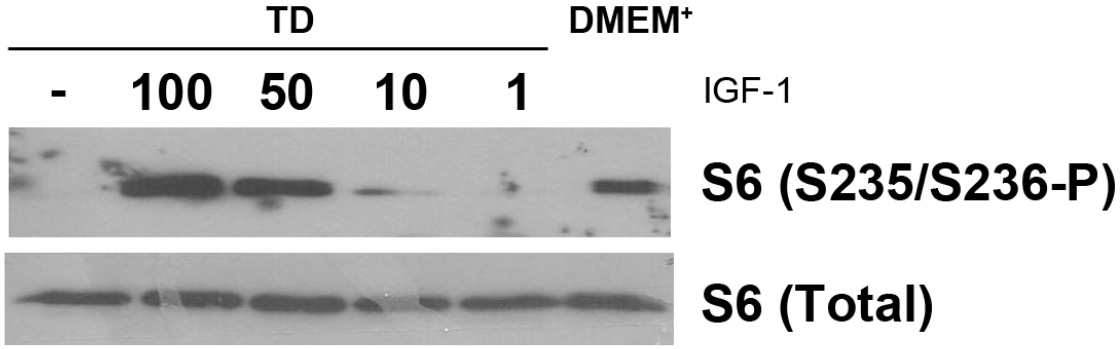

Figure R15: Stimulation of HeLa cells by different concentrations of IGF-1. HeLa cells were transfected with pCMV5 plasmid for 48 hours. Then, they were starved overnight in PBS^a (PBS supplemented with 0.9 mM calcium chloride, 0.5 mM magnesium chloride, 1 g/l glucose and 20 mM HEPES pH 7.4, TD), reloaded with amino acids for 1 hour (by adding serum-free DMEM + GlutaMAX, DMEM+), and stimulated (+) or not (-) with the indicated doses of IGF-1 for 30 min. Then, protein extracts were obtained and analysed by Western Blotting after blotting the indicated antibodies.

Once the assay conditions were set, HeLa cells were transfected with the different constructs and starved as stated above. $S6K^{T229D/T389D}$ and $PKB^{T308D/S473D}$ forms were able to promote the phosphorylation of rpS6 in the absence of both nutrients and IGF stimulation (Figure R16). The control empty vector pCMV5 and,

surprisingly, the S6K$^{T229E/T389D}$ double phosphomimetic form of S6K could not overcome serum withdrawal and did not show any raise in rpS6 phosphorylation signal in the absence of IGF-1.

The PKB pathway was monitored by measuring the phosphorylation levels of the PKB substrate PRAS40 at the specific Thr246 site. As expected, neither of the S6K forms was altering the phospho-PRAS40 levels, which in absence of PI3K stimulation were only increased when the PKB$^{T308D/S473D}$ was expressed (Figure R16).

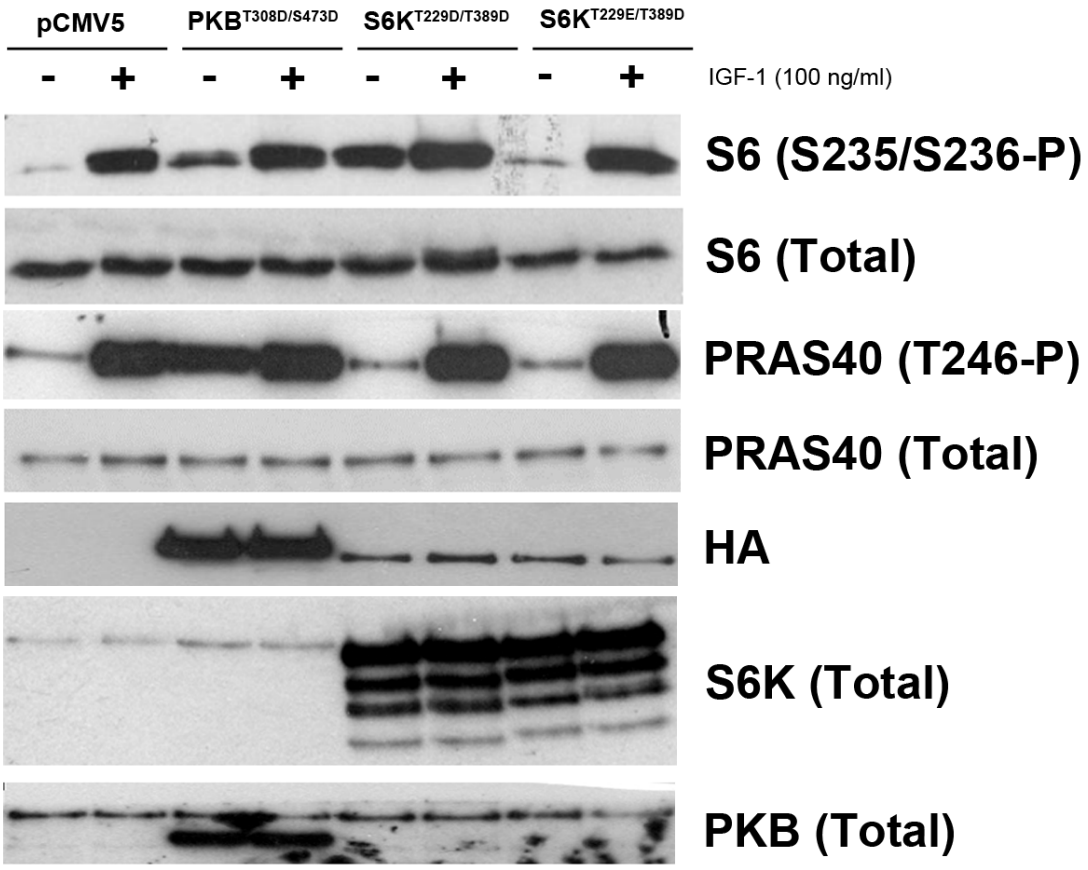

Figure R16: S6K$^{T229D/T389D}$ but not S6K$^{T229E/T389D}$, is constitutively active under trophic deprivation conditions. HeLa cells were transfected with pCMV5 empty vector, PKB$^{T308D/S473D}$, S6K$^{T229D/T389D}$ or S6K$^{T229E/T389D}$ plasmids for 48 hours. Then, they were starved overnight in PBS^{a} (PBS supplemented with 0.9 mM calcium chloride, 0.5 mM magnesium chloride, 1 g/l glucose and 20 mM HEPES pH 7.4), and then reloaded with amino acids for 1 hour (by adding serum-free DMEM + GlutaMAX); next, cells were stimulated (+) or not (-) with 100 ng/ml of IGF-1 for 30 min. Protein extracts were obtained and analysed by western blot with the indicated antibodies.

When confirming the expression of the exogenous proteins with the total antibodies for S6K (Figure R16), a pattern of four bands appeared when cells had been transfected with any of the 3 created forms. These bands ranged from an abundant band of 70 kDa (the endogenous size) to 40 kDa. As the experiments where these plasmids were meant to be conducted in a mice embryo, it became necessary to test whether the mutant proteins will be expressed also in mice cells. pCMV5 empty vector, $S6K^{T229D/T389D}$ and $PKB^{T308D/S473D}$ as a control, were transfected in both HeLa and N2A (a transformed cell line derived from mouse tumours) cell lines in parallel, and at least a three-banded expression pattern was confirmed to be maintained in both cell lines (Figure R17).

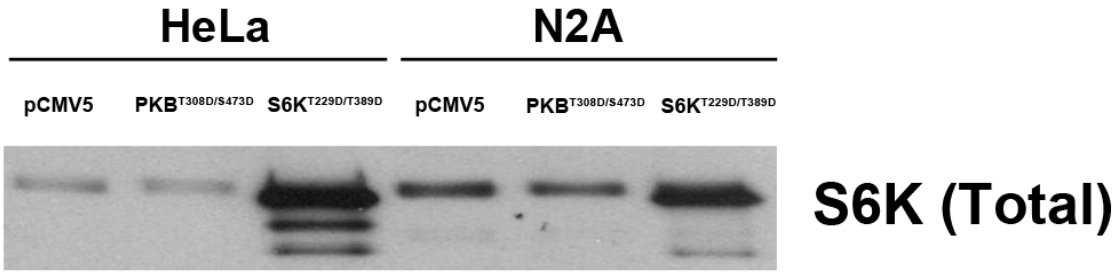

Figure R17: $S6K^{T229D/T389D}$ plasmid expression generated different forms of the protein recognized by the antibody detecting total-S6K. HeLa (derived from human) and Neuro2A (N2A) (derived from mouse) cell lines were transfected with pCMV5, $PKB^{T308D/S473D}$ or $S6K^{T229D/T389D}$ plasmids for 48 hours. Then, protein extracts were obtained and analysed by western blot with the S6K total antibody.

$S6K^{T229D/T389D}$ IS ACTIVE EVEN IN THE PRESENCE OF PDK1 INHIBITOR

It was then required to demonstrate whether the double phosphomimetic S6K mutant forms were also active in the absence of PDK1 activity. As PDK1 is a constitutively active as well as essential kinase, chemical inhibitors rather than genetic depletion were used on HeLa cells transfected with the different constructs and then deprived from serum. In these conditions, IGF-1 must be unable to activate the PI3K pathway since its main effector PDK1 is being blocked by preincubating the cells with specific inhibitors. GSK23334470 was chosen as PDK1 inhibitor, which blocked IGF-1 dependent phosphorylation of the downstream substrate rpS6 in HeLa cells transfected with pCMV5 empty vector in a dose dependent manner (Figure R18).

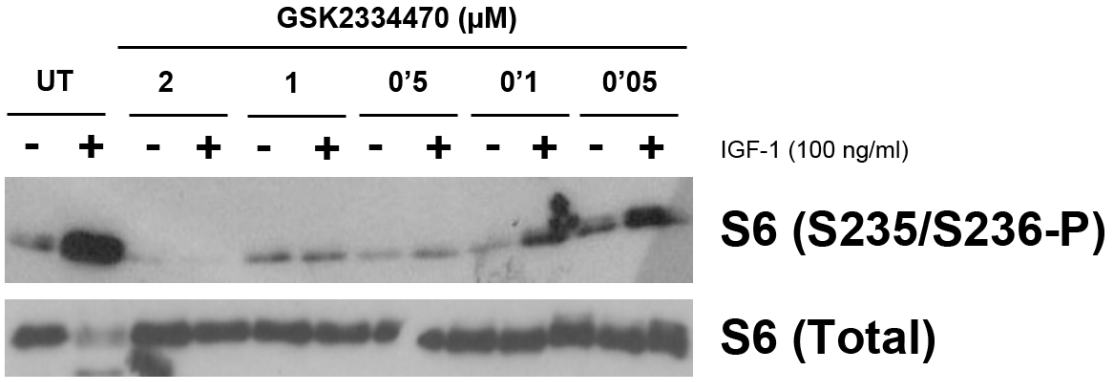

Figure R18: GSK2334470 inhibited the IGF-1 stimulated PI3K/PDK1 pathway in a dose dependent manner. HeLa cells were transfected with the pCMV5 for 48 hours. Then, cells were starved in PBS[a] (PBS supplemented with 0.9 mM calcium chloride, 0.5 mM magnesium chloride, 1 g/l glucose and 20 mM HEPES pH 7.4) overnight and reloaded with amino acids for 1 hour. Cells were next incubated or not (UT) for 45 minutes with the indicated concentrations of the PDK1 inhibitor GSK2334470 diluted in PBS[a]. Then, cells were stimulated (+) or not (-) with 100 ng/ml of IGF-1 for 30 minutes. Protein extracts were obtained and analysed by western blot with the indicated antibodies.

Even upon chemical inhibition of PDK1, constitutively active S6K$^{T229D/T389D}$ expressed exogenously must still be able to phosphorylate its substrates independently of stimuli. Successfully, this construct, but not the single mutant S6K^{T389D}, which retained the Thr229 PDK1 phosphorylation site, was confirmed to be insensitive to PDK1 inhibition (Figure R19).

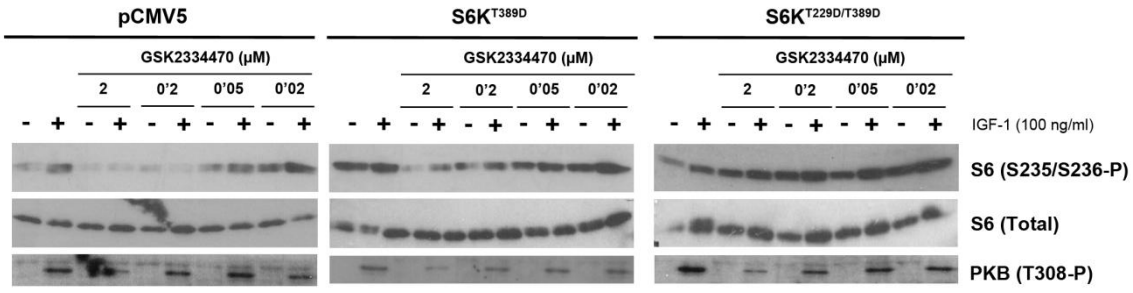

Figure R19: S6K$^{T229D/T389D}$, but not S6K^{T389D} was independent of PDK1 activation. HeLa cells were transfected with the indicated plasmids and allowed to express the exogenous protein for 48 hours. Cells were starved in PBS[a] (PBS supplemented with 0.9 mM calcium chloride, 0.5 mM magnesium chloride, 1 g/l glucose and 20 mM HEPES pH 7.4) overnight and reloaded with amino acids for 1 hour. Cells were next incubated for 45 minutes with the indicated doses of the PDK1 inhibitor GSK2334470. Then, cells were stimulated (+) or not (-) with 100 ng/ml of IGF-1 for 30 minutes. Protein extracts were obtained and analysed by western blot with the indicated antibodies.

As a control, the PKB$^{T308D/S473D}$ construct was tested instead for its ability to phosphorylate its substrate PRAS40 in both the presence of the mTORC1 inhibitor rapamycin and the PDK1 inhibitor GSK2334470. It showed to be fully active independently of both inhibitions (Figure R20).

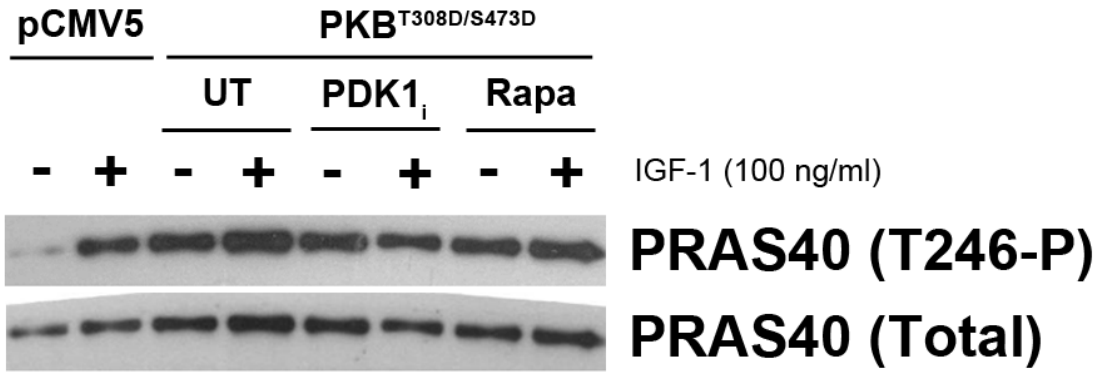

Figure R20: PKB$^{T308D/S473D}$ is independent of mTORC1 and PDK1 activation. HeLa cells were transfected with pCMV5 or PKB$^{T308D/S473D}$ and allowed to express the exogenous protein for 48 hours. Cells were starved in PBS^{a} (PBS supplemented with 0.9 mM calcium chloride, 0.5 mM magnesium chloride, 1 g/l glucose and 20 mM HEPES pH 7.4) overnight and reloaded with amino acids for 1 hour. Then, cells were treated or not (UT) for 45 minutes with 100 nM of the mTORC1 inhibitor rapamycin (Rapa) or with 2 µM of the PDK1 inhibitor GSK2334470 (PDK1$_i$). Then, cells were stimulated (+) or not (-) with 100 ng/ml of IGF-1 for 30 minutes. Protein extracts were obtained and analysed by western blot with the indicated antibodies.

SUBCLONING OF S6K$^{T229E/T389D}$ INTO PCAG PLASMIDS

The constructs were then subcloned in a pCAG-IRES-RFP plasmid appropiate for the *in utero* electroporation (IUE) experiments. S6K$^{T229D/T389D}$ insert could be liberated and subcloned by an orientated and compatible double enzymatic restriction with *SacI* + *ClaI* (Figure R21A). PKB$^{T308D/S473D}$ subcloning was addressed instead as explained in Materials and Methods, due to the internal *SacI* site present in this insert. Briefly, the insert was liberated with *XbaI* at both ends, one of which was added previously by PCR using extended primers. In parallel, the plasmid was opened by a single *NheI* cut. Then, both were ligated without the possibility of directing it, and an enzymatic restriction analysis was used to assess the orientation of the insertion (Figure R21B). Both plasmids were tested for RFP (Figure R21C) and exogenous protein (Figure R21E) expression, which showed to be correct. At 48 hours, homogeneous and maximized levels of protein expression were achieved (Figure R21D).

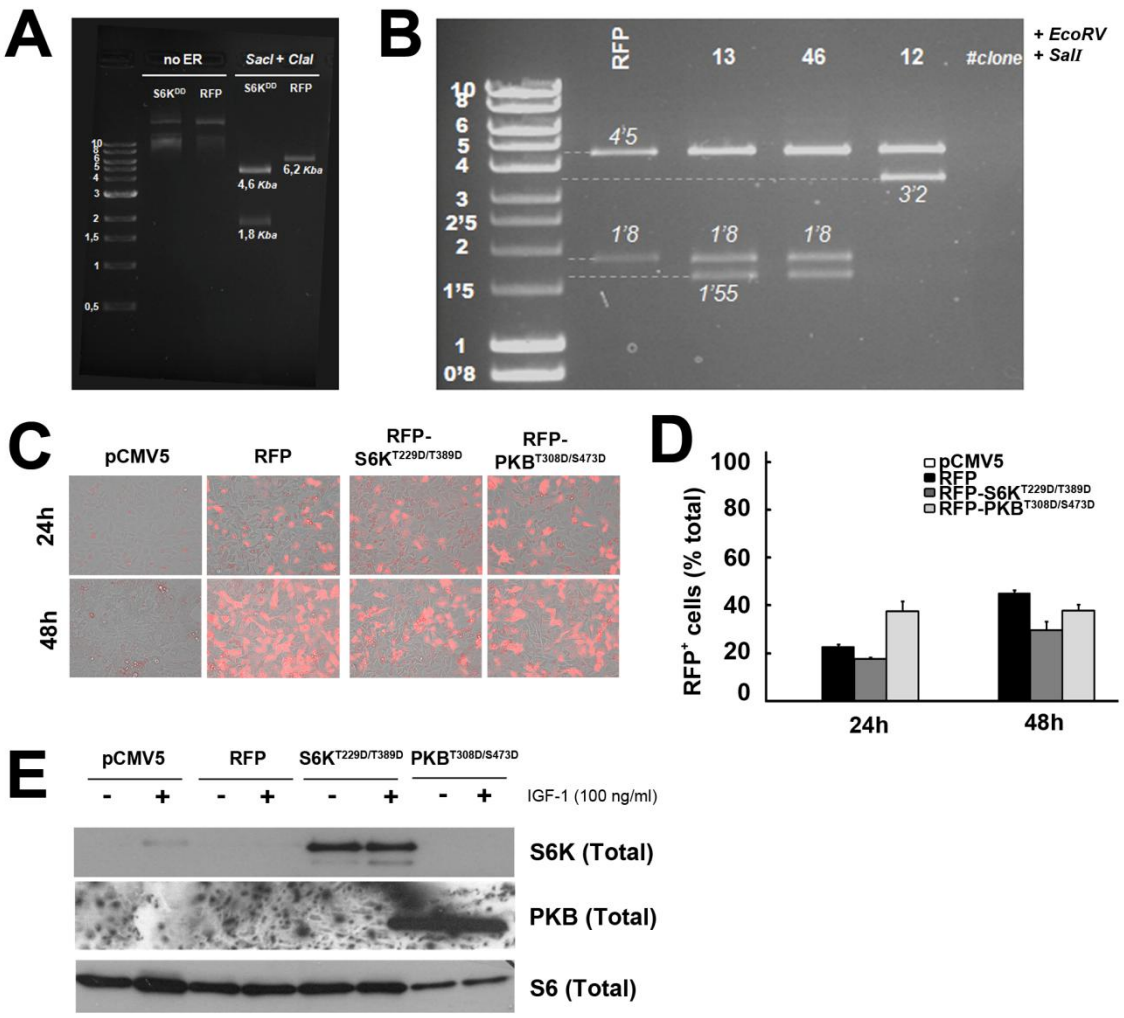

Figure R21: Subcloning PKB$^{T308D/S473D}$ and S6K$^{T229D/T389D}$ inserts inside pCAG plasmids. (A, B) Restriction patterns of the pCAG-RFP (RFP), pCAG-S6K$^{T229D/T389D}$ (S6K^{DD}) (A) and pCAG-PKB$^{T308D/S473D}$ (B) newly-generated constructs after enzymatic restrictions of the indicated clones with the described restriction enzymes; a scheme of the expected restriction maps is shown in Materials and Methods. DNA was amplified in *E. coli*, purified with QIAGen MidiPrep kits and digested for 1 hour at 37 ºC with the indicated restriction enzymes and their appropriate restriction buffers. The product was loaded in an 1% agarose gel stained with RedSafe. **(C)** Representative bright field plus fluorescence microscopy merged images of HeLa cells transfected with pCMV5, pCAG-RFP empty vector (RFP), pCAG-S6K$^{T229D/T389D}$ and pCAG-PKB$^{T308D/S473D}$ for 24 and 48 hours; the Red Fluorescence Protein (RFP) expression is detected. **(D)** Percentage of RFP-expressing cells was obtained by scoring the numbers of total and fluorescent cells from four different fields per well and three wells per condition, and RFP-positive numbers were divided by the total of cells. **(E)** HeLa cells were transfected with the indicated pCMV5 or pCAG plasmids for 48 hours. Cells were starved in PBS^{a} (PBS supplemented with 0.9 mM calcium chloride, 0.5 mM magnesium chloride, 1 g/l glucose and 20 mM HEPES pH 7.4) overnight and reloaded with amino acids for 1 hour. Then, cells were stimulated (+) or not (-) with 100 ng/ml of IGF-1 for 30 minutes. Protein extracts were obtained, and the correct expression of the exogenous proteins was analysed by western blot with the indicated antibodies. Total S6 was used as a control of the loading. *, P < 0'05; **, P < 0'005 compared to controls

Surprisingly, the expression of the empty pCAG-RFP vector, but not pCMV5 vector, induced an increase in the basal phosphorylation of rpS6 in starving conditions, which was also observed when $PKB^{T308D/S473D}$ or $S6K^{T229D/T389D}$ were expressed (Figure R22A, R22C). To rule out than this could arise from transfection toxicity effects, $CaCl_2$ instead of PEI was used, which caused the same results (Figure R22B). Treatment with PEI alone was confirmed to not to induce any rise in the phosphorylation of rpS6 (Figure R22C). On the other hand, RFP did not alter the PKB – dependent cascade, as shown by the phosphorylation of its substrate PRAS40 (Figure R22C). Additional studies have to be conducted to clarify this situation.

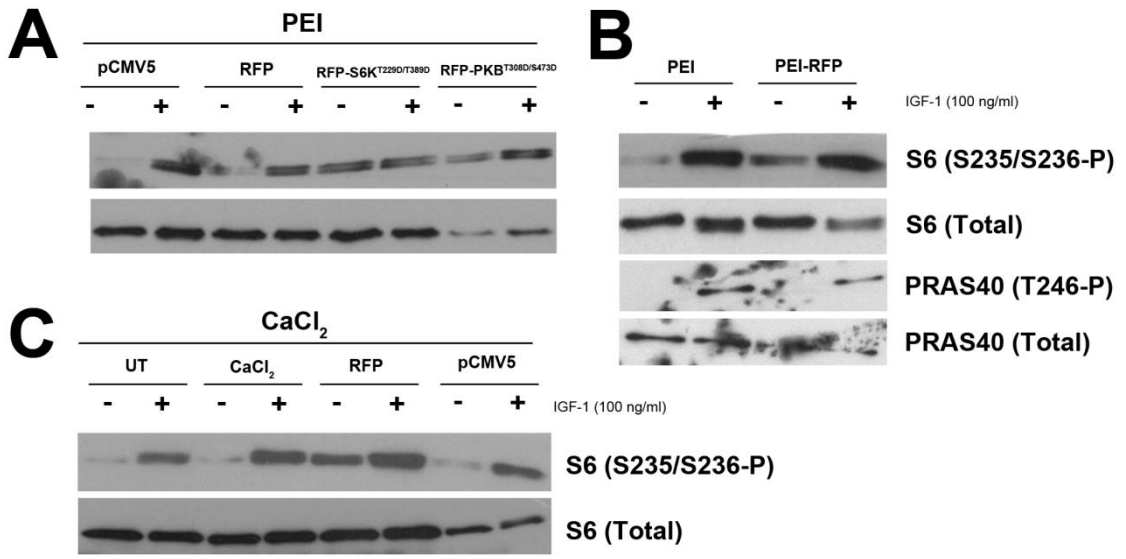

Figure R22: pCAG transfection in HeLa cells increased rpS6 phosphorylation in starving conditions. (A-C) HeLa cells were exposed to transfectant agent alone ($CaCl_2$ for **(B)** and PEI for **(C)**) or agent complexed with the indicated plasmids (A-C) and allowed to express the exogenous protein for 48 hours. Cells were starved in PBS[a] (PBS supplemented with 0.9 mM calcium chloride, 0.5 mM magnesium chloride, 1 g/l glucose and 20 mM HEPES pH 7.4) overnight and reloaded with amino acids for 1 hour. Then, cells were stimulated (+) or not (-) with 100 ng/ml of IGF-1 for 30 minutes. Protein extracts were obtained and analysed by western blot with the indicated antibodies.

DISCUSSION

Microcephaly of the PDK1$^{fl/fl}$ CRE^{+} mice

The results presented above stated that the PDK1$^{fl/fl}$ CRE^{+} adult mice were microcephalic, with brains showing a reduction of about 50% in volume and mass compared to those from the PDK1$^{+/fl}$ CRE^{+} controls (Figure R1B, R1D). Previous studies on neurons purified from E15.5 embryonic cortex suggested that the small brain size of the PDK1$^{fl/fl}$ CRE^{-} and PDK1$^{fl/fl}$ CRE^{+} mice might be mostly due to a reduction in the size of the cells, which were shown to be smaller, rather than to a reduced number of cells, which remained constant (Cordón-Barris *et al.*, 2016). Protein synthesis is indispensable to increase cell size. Thus, amongst all the PDK1 substrates affected by the L155E mutation, S6K, who is a major promoter of protein synthesis (Holz *et al.*, 2005), stands out as the PDK1 substrate candidate and responsible for the PDK1$^{fl/fl}$ CRE^{+} microcephaly. Another major mTORC1-dependent activator of protein synthesis, 4E-BP1, which has an even more prominent role than S6K in regulating translation, should not be involved in this phenotype since it is not a PDK1 target. Nevertheless, 4E-BP1 activity should not have been sufficient to avoid the cell size reduction and consequent microcephaly induced by the PDK1 L155E mutation.

Deficiencies in the mTOR pathway had already been linked to microcephaly. Specifically, brains developed smaller when deficient for *Pdk1*, *Pkb*, *mTOR* or *Raptor* (Liu and Sabatini, 2020). Similar results to the ones reported here were previously obtained with the conditional Nestin-Cre driven elimination of mTOR, which resulted in microcephalic mice (Ka *et al.*, 2014). Microcephaly has also been related with mutations in genes coding for GTPase Activating Proteins, proteins involved in intracellular vesicular trafficking and organization of axonal microtubules (Moffat *et al.*, 2015), but also in the *Pkbγ* gene.

This isoform of PKB, which is the one enriched in the brain, has been proven malfunctioning in a range of developmental cortical malformation syndromes, and was also proposed as a risk factor for microcephaly (Boland *et al.*, 2007) and schizophrenia (Howell, Floyd and Law, 2017). These suggested a critical role of Akt3/PKBγ in the developing human central nervous system, specifically in the attainment of normal brain size. Indeed, PDK1$^{K465E/K465E}$ mutant mice, with reduced PKB activity levels demonstrated to have a reduced brain size (Zurashvili *et al.*, 2013). Strikingly, PDK1$^{fl/fl}$ CRE^{+} mice, with normal PKB activity, also developed microcephaly. The results presented here challenge the literature regarding to some functions attributed to PKB, since these are most likely due to its crucial role in activating mTORC1, which then can regulate in turn downstream important regulators of neurodevelopment. As quoted by (Poopal *et al.*, 2016):

> "While genetic screens are important to identify potentially pathological mutations in the PI3K/mTOR pathway, they do not directly reveal the functional consequences and how signal transduction is affected by a certain mutation in human patient cells. Understanding the exact pathological mechanisms in PI3K/mTOR signalling, which may be the sum of several mutations as well as epigenetic factors, will be essential to identify efficient, disease-targeting therapies" (Poopal *et al.*, 2016).

The activation of S6K1 and PKCs in the PDK1$^{fl/fl}$ CRE^{+} mice

S6K showed, as expected, reduced phosphorylation levels at its activation loop residue Thr229 (Figure R2), as a consequence of the inability of the PDK1 L155E mutated PIF pocket to interact with the S6K phospho-hydrophobic motif docking site. Surprisingly, phosphorylation of the Thr389 residue at the S6K hydrophobic motif, which is under the control of mTORC1, was also decreased to the same extent as that of the activation loop (Figure R2). This can be explained by particular structural intramolecular interactions of the AGC kinases. The phosphorylation in the hydrophobic motif of the AGC kinases is maintained by hiding this phosphate group in their own PIF-pocket (Frödin *et al.*, 2002; Hauge *et al.*, 2007). In addition to avoid dephosphorylation, this interaction promotes structural changes in the αC-helix of the kinase domain that increase the activity by increasing the affinity of the enzyme for ATP molecules (Leroux, Schulze and Biondi, 2018). In the absence of activation loop phosphorylation, the closed conformation is not favoured, which may allow the exposure of the phosphorylated hydrophobic motif site to the action of phosphatases (Collins *et al.*, 2003).

The only PDK1 substrates that showed reduced phosphorylation but also a decrease in their total protein levels in the PDK1$^{fl/fl}$ CRE^{+} samples were the PKC isoforms. PDK1 has a role in PKCs processing and maturation that is independent of agonistic stimulation. When PKCs are synthesized *de novo*, they automatically receive a phosphorylation by PDK1 in their activation loop. The lack of this event in the PDK1$^{fl/fl}$ CRE^{+} cortex made PKCs structurally unstable, which triggers their degradation (Balendran *et al.*, 2000). Thus, the reduced levels of phosphorylation and expression of PKCα found in the PDK1$^{fl/fl}$ CRE^{+} brain and neuronal cell extracts agreed with the current knowledge on PKCs dynamics.

Neurodevelopmental defects of the PDK1$^{fl/fl}$ CRE^{+} mice

The previously described mice models of microcephaly caused by the conditional ablation of mTOR in the neuronal system course with reduced APs proliferation rates at E15.5 and diminished production of both IPs and postmitotic neurons. Additionaly, decreases in neural stem cell proliferation have been reported in schizophrenia patients (Reif *et al.*, 2006). The PDK1$^{fl/fl}$ CRE^{-} and PDK1$^{fl/fl}$ CRE^{+} model mice did not follow this trend, as neither E14.5 nor E15.5 cortices did show a reduction of Pax6^{+} APs (Figure R6G,H). Tbr2^{+} IPs, instead, were generated at a lower rate in the PDK1$^{fl/fl}$ CRE^{+} cortices as early as E14.5, and were still reduced at E15.5 (Figure R5B, R6I). Thus, limited Tbr2^{+} IPs generation could not be explained by a reduction in the number of their APs progenitors, but rather by a reduction in the rate of newly born IPs produced from them.

This agrees with some evidences coming from the *reeler* mouse supporting the hypothesis of a causative link between birth date and cell fate. The reeler (*Reln*) mice is a model that lacks Reelin, an extracellular matrix glycoprotein, which is secreted during the corticogenesis mainly by the Cajal-Retzius cells. These are pyramidal neurons who reside in the marginal zone or layer I, in the surface of the neocortex, above the cortical plate. They tangentially migrate from discrete pallial sources before the preplate even starts to split (Marín *et al.*, 2010). The lack of Reelin in the reeler mice generated cortices with profound disruption of their structure, but this event had no influence on the timing and area distribution during the generation of corticospinal neurons, indicating that the birth date of a premature neuron is what determined its cell fate (Dehay and Kennedy, 2007). Thus, starting from the same pool of progenitors, the resultant number of daughter cells shall be equivalent. This puts the focus on the first reduced pool observed in the the PDK1 L155E mutant mice: the Tbr2^{+} population (Figure R5), which at E14.5 was already being produced at diminished amounts (Figure R6I).

The possibility that in the PDK1$^{fl/fl}$ CRE^{+} mice the expression levels of either Pax6 or Tbr2 rather than the number of cells expressing these markers were reduced can be ruled out by comparing their phenotypes with the ones of PAX6 and TBR2 deficient brains. Humans carrying mutations on those genes suffer from a pathology called polymicrogyria due to defects in neuronal migration, differentiation and proliferation of neural progenitors (Moffat *et al.*, 2015). Polymicrogyria is a developmental disorder where the brain develops multiple small gyri that finally lead to an excessive folding of the brain with small furrows. Polymicrogyria can appear

focally, unilaterally or bilaterally and, in concordance, symptoms course from non-detected to severe intellectual disability. In embryonic samples of either PAX6 or TBR2 deficient mice, polymicrogyria is anatomically easily detectable, as they developed ventriculomegaly and a concordantly drastically thinner cortical neuroepithelium (Stottmann *et al.*, 2013). Interestingly, the TBR2 silencing mutation coursed with a polymicrogyria that was accompanied by microcephaly, pointing at a possible relevant role of this population of cells in generating brains with the appropriate size (Baala *et al.*, 2007).

The reduced $Tbr2^{+}$ cells generation could not even be due to diminished proliferation of their progenitors, as APs were all engaged in an active cell cycle in all the genotypes analysed at both E14.5 and E15.5 (Figure R7A, R7B), as visualized by the ki67 staining. However, numerical differences appeared in the percentage of proliferating cells ($ki67^{+}$) that were no APs ($Pax6^{-}$) cells, which could include the $Tbr2^{+}$ IPs, amongst others. This population was increased at E14.5 in the $PDK1^{fl/fl}$ CRE^{+} mice when compared to the $PDK1^{fl/fl}$ CRE^{+} controls (Figure R7C) but reduced at E15.5 (Figure R7H). The results from E15.5 cortices seeded *in vitro* confirmed that $PDK1^{fl/fl}$ CRE^{-} and $PDK1^{fl/fl}$ CRE^{+} neurons (without differentiating between populations) were less proliferative in total than $PDK1^{+/fl}$ CRE^{-} controls (Figure R3A, R3B).

Later, when comparing the non-APs ($Pax6^{-}$) that were proliferating ($ki67^{+}$), only E14.5 showed an increase in their percentage (Figure R7F), while E15.5 changes were not statistically significant (Figure R7I). This suggests that the population that had a greater role in the drop of the proliferative rate at E15.5 in the $PDK1^{fl/fl}$ CRE^{+} *in vitro* neurons were the APs, even if their number was not significantly diminished when statistically assessed (Figure R6H). The thickness of the layer occupied by these $ki67^{+}$ cells was also diminished at this age in the $PDK1^{fl/fl}$ CRE^{+} mice (Figure R7J), but not at E14.5 (Figure R7E).

Altogether, the results showed that cells which were proliferating at E14.5 in the $PDK1^{fl/fl}$ CRE^{+} neocortex had exited the cell cycle one day later (Figure R7C, R7H). The percentage of $Pax6^{-}$ cells that were proliferating ($ki67^{+}$) decreased from E14.5 to E15.5 in all the genotypes (Figure R7F, R7K), but more markedly in the $PDK1^{fl/fl}$ CRE^{+} neurons (30'55% ± 3'31) than in the $PDK1^{+/fl}$ CRE^{-} controls (17'88% ± 4'24) (Figure D1). These cells were not undergoing programmed cell death, as controlled with an active caspase-3 staining, a marker for active apoptotic processes, which were spurious and equivalent for the three genotypes (Figure R4A, R4C). Neurons from E15.5 cortices that were seeded *in vitro* retrieved an equivalent result (Figure R3A, R3C). Thus, a possible explanation was a premature generation of immature neurons at E14.5 that had exited the active cell cycle in the $PDK1^{fl/fl}$ CRE^{+} mice.

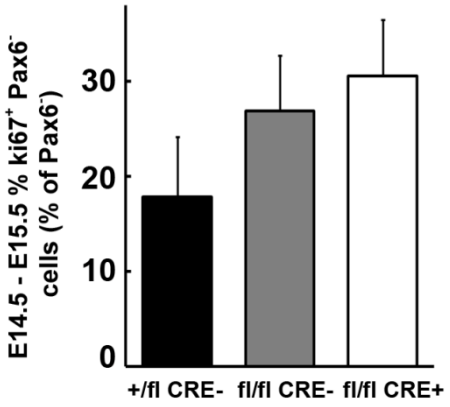

Figure D1: Increased drop of proliferation of the PDK1$^{fl/fl}$ CRE^{+} neurons. Percentage of decrease from E14.5 to E15.5 in the number of proliferating cells (ki67^{+}) that are not apical progenitors (Pax6^{-}) in relation to the total Pax6^{-} cells per field.

Even if all the APs were dividing, proliferating out of phase could also have consequences in neurodevelopmental processes. Differential times spent in the different phases of the cell cycle determine the fate of the daughter cells (neurogenic or self-renewal) (Arai *et al.*, 2011). PDK1$^{fl/fl}$ CRE^{+} APs were less active in mitosis and presented a preference for a punctuated pattern of staining (as did APs from the PDK1$^{fl/fl}$ CRE^{-} samples) when compared to the heterogeneous distribution in the PDK1$^{+/fl}$ CRE^{-} controls (Figure R8), although it did not reached statistical significance. The phosphorylation of H3 at Ser10 is strongly related to the chromosome condensation status. Because of that, a punctuated distribution indicated that cells were at a late G_2/M stages, because phosphorylation of histone H3 could had only occurred on pericentromeric chromatin. As mitosis proceeds, it spreads along the chromosomes, and reaches a peak covering the whole genome at prophase. Finally, at the end of mitosis, histone H3 is dephosphorylated (Prigent and Dimitrov, 2003). Thus, deficient activity of PDK1 increased the percentage of mitotic cells that are just entering mitosis at E15.5, while a higher number of cells are at prophase in the PDK1$^{+/fl}$ CRE^{-} controls. This deffects could arise from the step before mitosis, the S-phase, taking longer at E14.5 in PDK1 mutant samples. Longer S-phase is believed to generate renewing daughters, but E15.5 PDK1$^{fl/fl}$ CRE^{-} and PDK1$^{fl/fl}$ CRE^{+} cortices did not exhibit an increased Pax6^{+} nor Tbr2^{+} pool of cells, quite the opposite, as Pax6^{+} APs did not show any significant differences between genotypes, and Tbr2^{+} were diminished at both E14.5 and E15.5 in the mutant mice (Figure R5B, Figure R6H). EdU incorporation assays did not reveal any significant difference amongst the three genotypes analysed indicating changes in the active S-phase at E15.5 (Figure R9), so clearly other dynamic experiments (for example, with BrdU injection at different gestation times and sacrificing times) have to be conducted to obtain any conclusion about this.

Additional information about the cell cycle stage of steady-fixed samples could be obtained with high-resolution pictures. A combined staining with proliferating cell nuclear antigen (PCNA), which unfortunately could not be used in this study, and ki-67 could allow to accurately determining the proportion of cells in each phase of the

cell-cycle. Four distinct populations of cells could be distingished based on their labelling: cells whose nuclei exhibit small punctuate PCNA labelling (early S phase cells), nuclei with large punctuate PCNA labelling (late S phase cells), cells with ki-67 dots throughout the nucleus (G_1 phase), or nucleus stained completely by ki67 in cells are undergoing metaphase or anaphase (G_2 phase) (Ghule *et al.*, 2007; Filion *et al.*, 2009; Fousse *et al.*, 2019).

However, in different cellular contexts, PDK1 has already been related with the cell cycle control. In the haematopoietic system, PDK1 demonstrated to modulate the cell cycle because PDK1 knockout reduced the ability of pre-B cells to exit the $S/G_2/M$ phase of the cell cycle. This was explained because PDK1 deficiency reduced the levels of Pax5, which curiously is another member of the Paired box (Pax) family, such as Pax6. The pro-survival gene Bcl2A1 was also affected, and restoring the expression of both genes together by transfection was necessary to reduce the number of cells blocked in the cell cycle in PDK1 knockout pro-B cells (Venigalla *et al.*, 2013). However, this mechanism cannot be extrapolated to the neural tissue, as B-cells developmental program is linked to their ability to initiate or not the recombination of the light chain that they need to produce.

Another possibility is that there is a defect in the transitioning step from $Pax6^+$ APs to $Tbr2^+$ IPs when PDK1 is not fully active The $PDK1^{fl/fl}$ CRE^+ mutant mice had somehow affected the progressive specification from neocortical progenitors to projection neurons, guided by the transcription factors Pax6 → Tbr2 → Tbr1 cascade expressed sequentially in the RGPs. A recent work has described how this cascade is regulated by epigenetic factors, with these three transcription factors forming an intricate feedforward cascade that also included direct feedback repression (Elsen *et al.*, 2018). However, direct neurogenesis has not to be forgotten, as $Pax6^+$ progenitors can generate immature neurons directly at all ages, exhausting in this way their own pool.

Currently, four categories of epigenetic mechanisms are recognized: DNA methylation / demethylation; histone covalent modifications such as lysine acetylation and methylation; ATPase-dependent chromatin remodelling; and non-coding RNA. Both S6K1 and S6K2 have shown to regulate transcriptional factors, and p70-S6K1 has even shown to translocate to the nucleus during different stages of the cell cycle (Rosner and Hengstschla, 2011). Even if S6K cannot bind DNA directly, many regulatory factors function by physically being recruited and targeting specific genes to be epigenetically modified. The most interesting result regarding the $PDK1^{fl/fl}$ CRE^+ paradigm appeared recently, when bioinformatical analysis and immunocoprecipitation assays in breast carcinoma MCF-7 cells revealed the existence of several phosphorylation sites in the TBR2 protein accomplishing the consensus for S6K1, suggesting that TBR2 could be a target for phosphorylation

and regulation by S6K1 (Kosach *et al.*, 2018). Even rpS6 itself has been recently related to histone modification in *Arabidopsis Thaliana,* which will modulate rRNA synthesis and rDNA transcription (Biever, Valjent and Puighermanal, 2015), an effect that might be dependent on the phosphorylation state of rpS6.

Pax6 directly represses its own transcription (Manuel *et al.*, 2007), while directly activating Tbr2 expression (Sansom *et al.*, 2009). Tbr2, in turn, binds and represses both its own plus Pax6 gene expression (Elsen *et al.*, 2018). Because of that, Pax6 null neocortex displayed an expansion of their ventral progenitors, which was accompanied by a reduction in the number of Tbr2 intermediate progenitors (Quinn *et al.*, 2007). The lack of Pax6 caused a premature depletion of the progenitor pool caused by a greater-than-normal proportion of newly divided cells exiting the cell cycle, starting as early as E12.5. The $PDK1^{fl/fl}$ CRE^{+} demonstrated to express Pax6 at the same levels than the $PDK1^{+/fl}$ CRE^{-} controls (Figure R6), and exhibited a similar number of cells amongst the three genotypes at both studied ages (E14.5 and E15.5). Thus, altered levels of Pax6 expression produced by the L155E mutation can be ruled-out.

Other key transcription factors linked to the Pax6 → Tbr2 transition included the transcription factor Neurogenin2 (Neurog2), whose expression is directly activated by Pax6, which in turn directly activates Tbr2's expression (Hevner, 2019). Neurog2 shares with Tbr2 a large fraction of binding sites along the genome, and they may coordinately regulate gene expression (Sessa *et al.*, 2017). GSK3β, a substrate of S6K but also for a number of other PDK1 substrate kinases, showed to phosphorylate Neurog2 and regulate its preference for an homodimeric or an heterodimeric quaternary structure, which had differential abilities to activate the neuronal differentiation genes (Li *et al.*, 2012). Post-translational control of the active lifetime of neurogenic transcription factors's also determines the numbers and identities of neurons specified during development, and even subtle quantitative interference with their phosphorylation state affected neuronal cell fate. The proper control of the duration of proneural protein activity is required for a correct neuronal development (Quan *et al.*, 2016). GSK3β, which is constitutively active, becomes inhibited by phosphorylations performed by a variety of PDK1 substrates. Thus, the PDK1 L155E mutation could lead to an overactivity of GSK3β that in turn reduced the opportunities of Neurog2 to be active by maintaining it phosphorylated and thus forming non-proneurogenic heterodimers. This decreased time windows for neurogenic divisions could led to a reduced production of Tbr2-expressing IPs, as observed in the $PDK1^{fl/fl}$ CRE^{+} cortices (Figure R5). However, GSK3β activity can also be regulated by other pathways other than PI3K, such as canonical Wnt.

GSK3β has indeed been pointed out as the key kinase regulating the mTOR-dependent APs proliferation in other mice models (Ka *et al.*, 2014). Indeed, Nestin-Cre GSK3β-deleted mice showed an ectopical (far away from the ventricle) activation of S6K and phosphorylation of its substrate rpS6, which coursed with hyperproliferation of the neural progenitors. The Nestin-Cre GSK3β-deleted mice are equivalent to an always-inactive GSK3β, which in physiological conditions is accomplished when phosphorylated; this is the opposite condition to the one caused by the expression of the PDK1 L155E mutant form, which leads to the inactivation of some of the GSK3 upstream inhibitory kinases, such as S6K, aPKCs and PKAs. Accordingly, GSK3β overactivation through PDK1 deficiency in the model studied here led to hypoproliferation of the progenitors. Chemically inhibiting mTOR in the Nestin-Cre GSK3β-deleted mice recovered the normal proliferating rates of the neurons, pointing again at an mTOR-downstream protein as the important regulator of progenitor proliferation. However, the substrates used in this work to monitor mTOR activity were usually phospho-S6K and phospho-rpS6 as its downstream substrates, but this approach could have been masking an autonomous effect of S6K in the regulation of neural progenitor proliferation. Not in vain, GSK3β is a S6K direct substrate as well. The results presented here complement this idea: when the major phosphorylator of rpS6, S6K, is not activated, $PDK1^{fl/fl}$ CRE^{+} brains developed microcephalic.

GSK3β had also a demonstrated role on neuronal progenitor proliferation in a Disrupted in Schizophrenia 1 (DISC1) model mice, a protein whose loss of function is associated with schizophrenia. DISC1 inhibited GSK3β through a direct interaction, and when DISC1 was down-regulated to simulate the pathology, an unleashed GSK3β activity was detected and accompanied by a reduction in the taxes of neuronal progenitors' proliferation. Chemical inhibition of GSK3β normalized back the situation and even cured the behavioural defects showed by these model mice (Mao *et al.*, 2009). With this enzyme being constitutively active when unphosphorylated, the $PDK1^{fl/fl}$ CRE^{+} progenitors might be affected by the uninhibited GSK3β activity, as observed in our results (Figure R5, R6, R8).

When elucubrating about how the PDK1 L155E mutation could be affecting $Tbr2^{+}$ generation, it is necessary to notice that not all IPs are equal. The Tbr2-positive cells start appearing in the proliferative zones from E11.5 to the end of the neurogenesis, with a peak of presence from E13.5 to E16.5, corresponding to the peaks of neurogenesis (Englund, 2005). However, IPs destined to produce lower cortical layers appear early in corticogenesis, by E11.5. Later on, IPs' laminar fates get restricted to generate upper layers neurons (Mihalas *et al.*, 2016). Previous works had already found, by an unbiased single-cell transcriptome analysis of E14.5 mouse cortex, that the VZ/SVZ contained two subtypes of IPs. Although both IP subtypes expressed Tbr2, one of them was enriched in neuronal differentiation

markers, and *in situ* hybridization located them in the SVZ, whereas less differentiated IPs were mainly in the VZ (Kawaguchi *et al.*, 2008). So, an hypothesis can be made that in the PDK1$^{fl/fl}$ CRE^{+} embryos, whose Tbr2^{+} IPs appeared further away from the ventricle (Figure R5), the more pluripotent population of the IPs is missing. This could be addressed by studying their morphologies, as these two populations are distinguishable: radial bipolar, or 'pin-like', IPs located in the VZ exhibit apical processes initially contacting the ventricular surface, and correspond to the molecularly less differentiated IP subtype. Multipolar IPs, instead, are located in the SVZ, have multiple short processes that extend and retract dynamically in all directions and represent the more neuronally differentiated IP subtype (Hevner, 2019).

Tbr2 was found to be necessary for differentiation, but not genesis, of IPs (Mihalas *et al.*, 2016). The destiny of the cells that started expressing Tbr2 at each developmental day was tracked until they completed the embryological neurodevelopment (at P0) thanks to a conditional coupled expression of the tdTomato red fluorescent protein. This study demonstrated that Tbr2^{+} IPs born from mid-neurogenesis (E13.5–E14.5) contributed widely to lower and upper layer postmitotic neurons, whereas late IPs (born at E15.5 or E16.5) produced upper-layer neurons selectively (Mihalas *et al.*, 2016). Interestingly, progenitor neurogenesis become less responsive at E14.5 to the differentiation signals of Neurog2 (Li *et al.*, 2012). According to these reported results, the reduced pool of Tbr2^{+} cells observed in the PDK1$^{fl/fl}$ CRE^{+} at E14.5 and E15.5 have a restricted capacity to generate Satb2^{+} (specific marker for callosal projection neurons) and Cux1^{+} (specific marker for layers II/III to IV) neurons. This last population showed developmental alterations in the PDK1$^{fl/fl}$ CRE^{+} adult brain, as they were found to be compacted in layer IV (Cordón-Barris *et al.*, 2016). However, the Tbr2^{+} IPs that generated the observed increased pool of Tbr1^{+} (Figure R12) and deficient Ctip2^{+} (Figure R10) populations of the PDK1$^{fl/fl}$ CRE^{+} embryos had born from E11.5 or E12.5, respectively, to E13.5 (Mihalas *et al.*, 2016). Thus, PDK1 full activity is necessary from the first stages of neurogenesis; otherwise, defects in neurodevelopment appear.

The reduction of the IPs population in the PDK1$^{fl/fl}$ CRE^{+} brains cannot come from a reduction in Tbr2 levels of expression. Tbr2 is known to repress Tbr1 expression and differentiation (Sessa *et al.*, 2017) and, as a consequence, adult mice lacking Tbr2 show a significant increased number of Ctip2^{+} neurons at layer V at the expense of a 25% layer VI Tbr1^{+} and 50% layer II-IV Cux1^{+} decrease at P0 (Mihalas *et al.*, 2016); by contrast, the effects on the adult PDK1$^{fl/fl}$ CRE^{+} mice were not that dramatic (Cordón-Barris *et al.*, 2016). Also, Tbr2 knockout mice exhibited opposite behavioural phenotypes when compared to the PDK1$^{fl/fl}$ CRE^{+} mice, since they are aggressive, hyperactive and have increased exploratory behaviour (Arnold

et al., 2008). In the PDK1$^{fl/fl}$ CRE^{+} mice, an increased Tbr1^{+} cell number is observed at E15.5 (Figure R12H), but it is accompanied by a decrease in the Ctip2^{+} population at the same age (Figure R10H). Thus, a retarded specification of immature neurons to specific subpopulations could account for the results found in the PDK1$^{fl/fl}$ CRE^{+} mice at this age.

Finally, the decrease in Tbr2^{+} population during the embryological development of PDK1$^{fl/fl}$ CRE^{+} mice could be the reason of the deficient connectivity of the PDK1$^{fl/fl}$ CRE^{+} adult mice. IPs have been proven to secrete Cxcl12, a factor that guides and stimulate the intracortical growth of thalamic axons that have entered the cortex tangentially through the IZ and express its receptor Cxcr4 (Abe *et al.*, 2015).

When comparing the results obtained with the PDK1$^{fl/fl}$ CRE^{+} model with the Pax6- or Tbr2-null mice, all points out to a deficit in cell number production rather than in protein levels expression. In neurodevelopment, the generation of new cells is highly related to the cell cycle and the mitotic spindle orientation, as debated in other parts of this discussion.

However, the hypothesis of a premature maturation of progenitors to immature neurons during the PDK1$^{fl/fl}$ CRE^{-} and PDK1$^{fl/fl}$ CRE^{+} neurodevelopment, and the consequential accumulation of these late ones at earlier stages could be ruled out, due to the reduced number of DCX positive immature newly born neurons progenitors in the PDK1$^{fl/fl}$ CRE^{+} brains at E15.5 (Figure R4A, R4B) and the normal number of Tbr1^{+} immature deep layer neurons of the E14.5 PDK1$^{fl/fl}$ CRE^{+} cortex (Figure R12G). The hypothesis of an even more accelerated maturation, that trespassed IPs to specific neuronal subpopulations at a high accelerated time could also be ruled out because of the lower number of Ctip2^{+} labelled cells presented by the PDK1$^{fl/fl}$ CRE^{-} and the PDK1$^{fl/fl}$ CRE^{+} cortices at both E14.5 and E15.5 when compared to the PDK1$^{+/fl}$ CRE^{-} controls (Figure R10G, R10H). On the contrary, the appearance of specific subpopulations of neurons seemed to be delayed in the PDK1$^{fl/fl}$ CRE^{+} brains, as Tbr1^{+} population suffered an expansion of its number in the PDK1$^{fl/fl}$ CRE^{+} mutant mice at E15.5 at the expense of their progeny Ctip2^{+}, which were diminished at that same age (Figure R10H, R12H).

However, the distribution of Ctip2^{+} neurons was largely unchanged at P0 in the the Nestin-Cre PDK1 conditional deficient mice (Itoh *et al.*, 2016), indicating that either the generation of this subpopulation is delayed in the PDK1$^{fl/fl}$ CRE^{+} mice, but could normalize at postnatal developmental stages, or that the specification of this subpopulation is a PKB-dependent event. In their model, instead, the absence of PDK1 displaced the Cux1^{+} population (a marker expressed in neurons of layers II–IV (Molyneaux *et al.*, 2007) from the upper layers they were supposed to be to deeper layers in the mutant brain. Cux1, however, has not been examined in the

PDK1$^{fl/fl}$ CRE^{+} mice expressing the PIF-pocket specific mutation. Interestingly, when these authors manipulated exclusively PKB but not PDK1 by forcing the expression of a dominant-negative inactive kinase form, it had a larger effect on post-mitotic populations at E17.5 than at E15.5. Then, it was confirmed that PDK1 was required cell autonomously in the postmitotic neurons, as its deficiency altered their final laminal positioning.

Thus, the results presented here tend to confirm that the PDK1$^{fl/fl}$ CRE^{+} mice suffered from a problem with the early expansion wave of Tbr2^{+} IPs that affected the lower layers subpopulations of immature (Tbr1^{+}) and specific (Ctip2^{+}) neurons, while the developing program remained intact. However, results from other works (Itoh *et al.*, 2016; Mihalas *et al.*, 2016) push an interest on checking the upper layers populations in the PDK1$^{fl/fl}$ CRE^{+} mice. This can be done by using the staining with specific markers such as Cux1 (immature upper layer marker) or Cux2, whose pattern was at first confusing to analyse, as postnatally it specifically stained neurons from layers II-IV, but during embryological development it can be found in a subset of cells in the SVZ (Molyneaux *et al.*, 2007). After knowing the results from (Kawaguchi *et al.*, 2008), the presence of Cux2^{+} in SVZ could be a mark for IPs enriched in this differentiation factors that are destined to produce this kind of neurons. Upper layer immature neurons should be a population to explore, as PDK1$^{fl/fl}$ CRE^{+} embryos seem to lack the Tbr2^{+} IPs born in the early neurogenesis (E11.5 to E13.5), located closer to the VZ (Figure R5), which are the progenitors of the upper cortical layers (Mihalas *et al.*, 2016).

A possibility is that, when analysing these markers, the positive cells turn to be the unmarked population that was increased in the PDK1$^{fl/fl}$ CRE^{+} embryos when compared to the PDK1$^{+/fl}$ CRE^{-} controls (Figure R11, Figure R12F), in which the presence of Ctip2^{+} cells was favoured instead. This increase could have come from an increased Tbr2^{+} expansion as early as E11.5 to E13.5 that generated a greater-than-normal number of IPs destined to produce immature upper layer cells thereby disbalancing the pool of remaining Tbr2^{+} IPs and exhausting in part the ones that should have been destined to produce lower layers neurons stained with Ctip2^{+}. Again, why the production of these upper layer immature neurons was favoured could be a cell cycle or mitotic spindle orientation issue. Otherwise, other possible identities could include a massive infiltration of glutamatergic neurons.

It cannot be ruled out that the effects seen by the PDK1 L155E expression are due to the inability of cortical neurons to migrate radially to the pial surfaces. This process, called locomotion, is a unique mode of neuronal migration in which cells first stabilize and elongate their leading process. Then, the centrosome of the newly generated daughters has to move forward from the perinuclear region into the leading process, carrying the nucleus with it and retracting the cell rear. Genes that

control the coupling of the centrosome with the nucleus have been found mutated in human neurological diseases such as lissencephaly, a brain malformation characterized by the absence of normal convolutions (folds) in the cerebral cortex, associated with microcephaly and severe psychomotor retardation [reviewed in (Marín *et al.*, 2010)].

PDK1 has been demonstrated to regulate the speed of locomotion of mouse neocortical neurons through the cortical plate (Itoh *et al.*, 2016). Nestin-Cre conditional ablation of PDK1 in the neural progenitor cells slowed down neuronal locomotion from E15.5 on, as shown by a time-lapse neuronal tracking of brain slices injected with BrdU. When trying to confirm these results by *in utero* electroporing a WT, a dominant-negative (KN) or a constitutively active (ΔPH) forms of PKB, similar yet not equal results were observed. First of all, the effects of these plasmids were only detectable after E17.5, when all neurons had already become postmitotic (Molyneaux *et al.*, 2007). KN inhibited and WT increased the number of cells that had enter and advanced through the cortical plate. However, the ΔPH electroporation completely abrogated the migration of the neurons, stacking them unable to enter the cortical plate. When *in utero* electroporation was done on $Nex^{Cre/+}$ embryos at E15.5, where plasmids will only be expressed in postmitotic neurons, the effects on radial migration became clear-cut: overexpression of KN reduced and WT increased migration speed. This work also evaluated if GSK3β was mediating these effects and found that phosphorylation of GSK3β by PKB was dispensable for radial migration and that PKB and GSK3β regulated radial neuronal migration by independent mechanisms. The results of this paper opened the door for S6K, a substrate controlled by both PDK1 and PKB, and a natural kinase for GSK3β, as a possible regulator of neuronal radial migration in neural progenitors before they become postmitotic neurons.

The authors found that the effects on radial migration were PDK1-mediated and acted at the microtubules level, possibly regulating the formation of the cytoplasmic dynein/dynactin complex that coordinated movement of the nucleus and centrosome (Itoh *et al.*, 2016). In this sense, there are accumulating evidences that PDK1 could control cell migration processes, from cell polarization to actin cytoskeleton and focal adhesion regulation, at least in the field of cancer cell invasion and dissemination [reviewed in (Di Blasio *et al.*, 2017)]. S6K specifically had also already proven to localize, bind and phosphorylate actin filaments of the cytoskeleton, to regulate cell migration and to promote filament crosslinking and stabilization (Berven, Willard and Crouch, 2004; Ip *et al.*, 2011).

The importance of PDK1 controlling the radial migration speed of immature glutamatergic neurons is even more relevant when realising that the proposal by Dehay on 2007 (Dehay and Kennedy, 2007) has still not been clearly clarified: is

the day that neurons are born who determines their final identity, or is it the local layer they position when they born (possibly due external cues)? While it was traditionally though that there was a precise relationship between the temporal order in which the various neuronal cell types are generated and their spatial distribution in the neocortex, evidences show that positioning-dependent layer identity acquisition could happen in interneurons (Lodato and Arlotta, 2015; Oishi *et al.*, 2016). However, the processes defining the identity of both excitatory and inhibitory neurons could not be comparable, as the final positioning of interneurons is completed in postnatal days and even includes a round of massive programmed cell death, events that do not happen in the glutamatergic population. Nevertheless, if true, minor changes in migration speed could lead to an incorrect neuronal placement and disorganized layer formation by unwillingly changing the post-migratory environment.

The strongest external factor that orchestrates the choice between renewal or differentiating divisions is the levels of stimulation of the Slit-Robo signalling, being Slit a secreted protein and Robo its receptor. Indeed, Robo or Slit mutants enhanced to production of IPs, suggesting that Slit/Robo signalling modulates the transition between primary and intermediate progenitors (Borrell *et al.*, 2012). Increasing Robo1 and Robo2 expression demonstrated to be necessary and sufficient to elicit direct neurogenesis in APs and impair the formation of superficial layer neurons in favour of deep layers. The importance of this signalling is so big that an attenuation of Robo stimulus during amniote evolution is believed to be the factor allowing the expansion and increased complexity of the mammalian cerebral cortex (Cárdenas *et al.*, 2018). PI3K signalling pathway has proven to regulate Slit / Robo signalling during angiogenesis and in breast cancer (Karar and Maity, 2011; Gu *et al.*, 2015).

The S6K$^{T229D/T389D}$ constitutively active construct

Testing the relevance of S6K in neurodevelopment required the phenotypic rescue by using a constitutively active form. At the time, partially constitutively active constructs had been created by hijacking the Thr389 phosphorylation requirement by mTORC1 (Pearson *et al.*, 1995; Alessi *et al.*, 1998). It was required first to overcome the autoinhibition that the unphosphorylated C-terminus domain of S6K exerts on the whole protein. Even before the structural analysis of S6K was completed, the deletion of specific amino acids had proved to be more or less detrimental in activating the catalytic domain of the enzyme, and in turning it more or less resistant to rapamycin treatment (Mahalingam and Templeton, 1996). To

reach this aim, different groups followed different strategies. Alessi's group introduced two STOP codons in the sequence of the construct that directly left the autoinhibitory domain out of the translated protein. The protein was structurally stable and functional, as demonstrated in *in vitro* radioincorporation assays. Thomas' group instead, avoided eliminating the autoinhibitory domain but mutated the four amino acids that have to be necessarily phosphorylated to activate the protein (Ser411, Ser418 and Ser424 in the autoinhibitory domain, plus Thr389), into aspartic or glutamic acids. This S6K1-E389D_3E construct demonstrated to be partially resistant to rapamycin, and inducible by insulin. The version described by (Alessi *et al.*, 1998) was chosen as it proved to be more insensitive to rapamycin; besides that, the phosphorylation of the residues of the autoinhibitory domain could have an effect in re-directing substrate specificity of S6K in different tissues (Arif *et al.*, 2019).

However, all the previous works using these so-called constitutively active kinase forms still relied on the phosphorylation of Thr229 by PDK1. Since PDK1 is a constitutively active enzyme (Casamayor, Morrice and Alessi, 1999), PDK1 activity is taken for granted in any cellular or animal model, except for the PDK1 knockout and the few conditional tissue-specific PDK1 L155E knockin models (Collins *et al.*, 2003; Kelly *et al.*, 2007), including the one studied here. Because of that, the $S6K^{T229D/T389D}$ is a novel creation not described before.

Starvation conditions had to be carefully chosen, as S6K is directly regulated by mTORC1, which is at the same time a sensor for nutrients but also amino acids. Cellular amino acid uptake itself is critical for mTOR complex 1 (mTORC1) activation, and it is a complexly regulated process. The intracellular presence of certain amino acids such as glutamine could activate protein synthesis in nutrient deprivation conditions, by acting as an exchange factor to provide the cells with the rest of amino acids and activate mTORC1 (Nicklin *et al.*, 2009). Serum-free medium is usually supplemented with amino acids, such it is the case of the GlutaMax, a stabilized form of L-glutamine formulated as an L-alanine-L-glutamine dipeptide. Thus, amino acid free starvation was tested, which resulted in a more robust reduction of rpS6 phosphorylation when compared alongside to serum withdrawal (Figure R14A). Optimal stimulation conditions were also set up (Figure R15). In amino acid and serum withdrawal conditions, the $S6K^{T229D/T389D}$ construct, but not the $S6K^{T229E/T389D}$ one, was able to induce the phosphorylation of the rpS6 protein autonomously. $S6K^{T389D}$ single mutant also failed to phosphorylate the rpS6 protein in the absence of stimulation of the PI3K/PDK1 pathway (Figure R16). A unspecific interference of the constitutively active S6K constructs with other pathways, and specifically with the PKB-driven pathway, was checked by monitoring the phosphorylation of the PKB-specific substrate PRAS40. Moreover, the constitutive activity of the $PKB^{T308D/S473D}$ construct was also confirmed. As

expected, none of the S6K construct had any effect on PRAS40 phosphorylation, while $PKB^{T308D/S473D}$ expression phosphorylated PRAS40 even in absence of nutrients (Figure R16).

The results confirmed that mutating Thr229 to an aspartic or a glutamic acid was not equivalent (Figure R16), a fact that had usually been not even considered in the field of phosphomimetic construction. In the $S6K^{T389D}$ case, the mutation to a glutamic acid ($S6K^{T229E/T389D}$) resulted in a protein that did not gained any additional function compared to the template one. Instead, mutation to aspartic acid ($S6K^{T229D/T389D}$) achieved the expected gain of function. A possible explanation comes from the differences in the structure of glutamic and aspartic acid. Glutamic acid is bigger in size than aspartic acid, as it has an additional methylene group in its side chain. Threonine is a small amino acid, more structurally similar in size to aspartic acid. The extra methylene group of glutamic acid could compromise the T-loop restructuration of S6K because it could be physically clashing or getting too close to other residue/-s, thereby creating new repelling interactions that disfavour the active conformation of the enzyme. Finally, the $S6K^{T229D/T389D}$ construct was used to continue on with the experiments, while the $S6K^{T229E/T389D}$ was abandoned.

Interestingly, the detection of total S6K protein levels in cells transfected with any of the 3 exogenous forms of p70 kinase exhibited a particular pattern of bands, ranging from 70 kDa (the endogenous size) to 40 kDa (Figure R16). This phenomenon was also observed when these constructs were expressed in the N2A mice cells (Figure R17). When the sequence of the insert of the original plasmid was checked, the presence of alternative methionine starts codons besides the expected one was noticed. This could generate smaller versions of S6K that won't be missing the active site, neither the T-loop. The expected molecular weight of the proteins generated by these internal methionines and the weight of the unknown bands matched together. This hypothesis matches with the fact that HA detection retrieved always a single band for each plasmid (Figure R16), as smaller versions will not express the epitope, encoded in the 5' end of the casette. However, the expression of a myriad of alternative versions is undesired. This problem could be solved by introducing the S6K natural 5' UTR before the beginning of the translation initiation codon in order to promote the expression of the full-length protein. However, the incorporation of the N-terminal hemagglutinin (HA) epitope might compromise the approach (Fukushima *et al.*, 2012).

Both HeLa cells as well as N2A cells express an active PDK1 enzyme. To check whether the $S6K^{T229D/T389D}$ construct was constitutively active independently of PDK1 activity, PDK1 was inactivated by chemical inhibition with the GSK23334470 compound in a dose-dependent fashion, with a strong inhibition at 2 μM, and whose effect was lost at 0'05 μM (Figure R18).

Different doses where PDK1 was strongly (2 μM), mildly (0'2 μM) or weakly (0'05 μM) inhibited were then tested together with the exogenous expression of the $S6K^{T389D}$ and the $S6K^{T229D/T389D}$ proteins and compared to control cells transfected with the empty vector. pCMV5-transfected cells after GSK23334470 preincubation could only phosphorylate rpS6 at the lowest doses of inhibitor. At 2 μM or 0'2 μM, they were unable to respond to the stimulation of PI3K/PDK1 by IGF-1 (Figure R19). By contrast, $S6K^{T229D/T389D}$ demonstrated to be active even after the preincubation with the highest concentration of PDK1, proving its ability to work independently of PDK1 and also independently of the stimulation of the PI3K/PDK1 pathway by IGF-1 (Figure R19). $S6K^{T389D}$, instead, was unable to phosphorylate rpS6 in the presence of GSK23334470 only if IGF-1 was not added. However, when the PI3K/PDK1 pathway was stimulated, that overcomed PDK1 inhibition and rpS6 was phosphorylated, weakly at 2 μM but stronger at 0'2 μM of the PDK1 inhibitor. Kinases other than S6K that are capable to phosphorylate rpS6 were not responsible for this result, as they were also present in the HeLa cells transfected with the pCMV5 empty vector.

Thus, this could be an artefact due to the levels of over expression of total S6K protein when compared to cells transfected with pCMV5 (Figure R16), which escaped somehow PDK1 inhibition. Even if $S6K^{T389D}$ is not expected to function in the absence of PDK1 activity, the results described here are important when translating the use of this plasmid from *in vitro* experiments to *in utero* electroporations. In the embryonic progenitor area, PI3K/PDK1 pathway will be continuously stimulated by the presence of BDNF during embyogenesis (Fukumitsu *et al.*, 2006). Thus, if an increase in $S6K^{T389D}$ levels alone due to the *in utero* injection is able to recover normal levels of rpS6 phophorylation, false positive results could be obtained with the $S6K^{T229D/T389D}$ electroporation. On the other hand, the fact that the $S6K^{T229D/T389D}$ plasmid is active in the absence of IGF-1 while $S6K^{T389D}$ is not, is a promising result, since the $PDK1^{fl/fl}$ CRE^{+} embryos will have no PDK1 activity at all towards S6K, no matter the levels expressed in the cells. However, these results indicate that $S6K^{T389D}$ plasmid should be included in parallel with $S6K^{T229D/T389D}$ as a control during the *in utero* electroporations experiments, alongside with the $PKB^{T308D/S473D}$ plasmid.

Other experimental methodologies could be tested such as *in vitro* kinase assays, where only the studied kinase, a substrate (that can be a generic phosphorylatable peptide) and traceable radioactive ATP are added. Results measure how many radioactive phosphates had been incorporated by the studied kinase to the peptidic substrate, which is attached to a washable membrane and radiometrically measured. These experiments eliminate any possible cellular interferences and could be a useful tool to truly assess the constitutive activity of the novel construct generated here.

In the three transfections, interference with the PKB-specific pathway was checked by controlling the phosphorylation of the PDK1-dependent Thr308 residue. However, the PDK1 – PKB interaction has been actively improved by evolution. Indeed, since the amoebozoans-metazoans diverge, PKB acquired an additional domain, the PH domain, only to ensure immediate co-localization with PDK1 in response to PtdIns(3,4,5)P_3 raises. This enabled activating PKB with high efficiency, which allowed the recruitment of additional cellular substrates regulating novel functions, such as complex neuronal morphogenesis (Zhou *et al.*, 2014). Thus, it could be expected that higher doses were necessary to completely abolish PKB's Thr308 than S6K's Thr229 phosphorylation. Indeed, 2 μM GSK23334470 diminished but not completely abolished Thr308 phosphorylation in the presence of IGF-1. Importantly, the expression of any of the S6K plasmids increased the phosphorylation of this PKB residue (Figure R19).

The $PKB^{T308D/S473D}$ constitutive activity was confirmed to be independent of PDK1 (up to 2 μM GSK23334470 inhibition) and mTORC1 and thus nutrient signalling (inhibited with 100 nM rapamycin). This plasmid was able to phosphorylate its specific substrate PRAS40 in all the conditions tested (Figure R20).

However, when the constructs were subcloned into pCAG-IRES-RFP plasmids, the expression of the empty plasmid itself induced an increase in the basal phosphorylation of rpS6 in starving conditions, and this was observed using different transfection agents (Figure R22). pCAG plasmids are mammalian expression vectors used for cloning and expressing genes under the CAG promoter. This promoter is synthetic and drives high levels of expression in mammals. It was constructed based on sequences coming from the cytomegalovirus (CMV) early enhancer element, the promoter, first exon and the first intron of chicken beta-actin gene and the splice acceptor of the rabbit beta-globin gene (Niwa, Yamamura and Miyazaki, 1991). Previous studies had used pCAGSS plasmids to transfect different elements of the PI3K/PKB/S6K/GSK3β-related pathway and had not reported inconveniences, even though phosphorylation levels of rpS6 where not measured in these studies (Gong *et al.*, 2015; Itoh *et al.*, 2016).

mTOR-related brain developmental pathologies

Abnormal PI3K signalling has demonstrated to be related with a variety of neurodevelopmental disorders, including schizophrenia, autism and developmental delay (Hood *et al.*, 2019). The current knowledge suggests that the enhancement of

the PI3K-PKB-mTORC1 signalling pathway leads to an increased proliferation of progenitors and excessive dendritic branching, whereas suppression exhibits the opposite consequences (Wang *et al.*, 2017). When trying to identify a key kinase in these alterations PKB, or mTORC1 itself, have emerged highlighted.

Dysregulation of the mTORC1 pathway is associated with a set of characteristic neurodevelopmental diseases, collectively termed 'mTORopathies', which include epilepsy, focal cortical dysplasia, macrocephaly or megalencephaly and cognitive and social defects (Liu and Sabatini, 2020). Downregulation of mTORC1 or mTORC2 in the nervous system perturbs cell and organ size and disrupts the cortical architecture of the brain. The synaptic activity, so relevant for the formation and maintenance of functional neuronal connections, is also regulated by mTORC1, who mostly relies on its substrates 4E- BP1 and S6K1 to strengthen or weaken a given neuronal circuit (Liu and Sabatini, 2020). However, the specific proteins of the pathway whose genes bear mutations in these neurodevelopmental diseases included other proteins besides the mTOR kinase and the components of both mTORC1 and 2 complexes, such as PI3K, PTEN, PKB or GATOR.

Deep whole-exome sequencing had repeatedly identified somatic mutations of genes involved in the mTOR and the PI3K/PKB pathways causing malformations of cortical development that lead to hemimegalencephaly (Moffat *et al.*, 2015). Interestingly, paired DNA samples of patients with this disease were extracted from blood and dysplastic brain tissue, which was surgically removed to treat drug-resistant epilepsy, and processed by next-generation sequencing approaches. From this it was concluded that not only mutations in mTORC1 were producing this disease by affecting neuronal migration, but also identified RPS6 as a direct potential novel disease-related gene. Indeed, a somatic variant in the RPS6 gene called p.R232H was identified. When expressed in embryonic rat brains, it prompted an increase in cell proliferation in neuronal progenitors located in the ventricular zone, as seen by both pH3 and ki67 stainings. The coexpression with the pathogenic variants of mTOR worsened the phenotype observed at embryonic stages and partially phenocopied cytological anomalies observed in the hemimegalencephalic brain tissue (Pelorosso *et al.*, 2019).

S6K itself, separately from mTORC1 or PKB, has already gained its first *solo* function in a neurodevelopmental process. Specifically, using human neural stem cells system, the abolition or constitutive activation of S6K (with exogenous forms) alone controlled the percentage of neurons that differentiated to the dopaminergic lineage: non-active S6K impaired it and constitutively active promoted it. Interestingly, chemically inhibiting PKB and mTORC1 caused the same results as abolishing S6K alone (Petritsch *et al.*, 2000; Mitchell *et al.*, 2015; Lee *et al.*, 2016),

and this could have explained the results reported in many studies before (Biever, Valjent and Puighermanal, 2015).

However, in neurons, phosphorylation of rpS6 was dispensable for overall protein synthesis (Puighermanal *et al.*, 2017), as demonstrated before in other tissues in the whole body non-phosphorylable knockin mice mutants of rpS6 (Ruvinsky *et al.*, 2005). Instead, it had a regulatory effect on specific subsets of mitochondria-related mRNAs in specific brain areas which did not include the cortex (Puighermanal *et al.*, 2017). These mice had an enhanced novelty-induced locomotor activity, exactly the opposite effect that the one found in the $PDK1^{fl/fl}$ CRE^{+} mice, which hyper reacted when handled and froze when exposed to an open-field test (Cordón-Barris *et al.*, 2016). These results are surprising, as rpS6 phosphorylation in the adult $PDK1^{fl/fl}$ CRE^{+} mice whole-brain extracts is reduced by 90% (Figure R2), mimicking the lack of phosphorylation of Ruvinsky's mice. However, the striatum (the structure more related to controlling locomotion) was not specifically analyzed by Cordon-Barris and co-workers.

On the other hand, brains deficient for *Pdk1*, *Pkb*, *mTOR*, and *Raptor* all exhibited microcephaly. Results similar to the ones described here had been obtained previously when eliminating upstreams activators of S6K. Indeed, the conditional Nestin-Cre driven elimination of mTOR resulted in microcephalic mice with reduced APs proliferation rates at E15.5 and diminished production of both IPs and postmitotic neurons, accompanied by an aberrant cell cycle progression (Ka *et al.*, 2014). Cell cycle missregulation in APs had been found underlying microcephaly, as shown by a Brap floxed mice model conditionally ablated in these progenitors (Lanctot *et al.*, 2017). Brap is a Ras-Erk signalling modulator with ubiquitin E3 ligase activity that ultimately regulates the levels of a cyclin-dependent kinase inhibitor family member, $p27^{Kip1}$. These mice showed to have a truncated G_1 phase and a consequently premature and hindered S-phase entry, which greatly arrested G_2 phase and prolonged the cell cycle of the apical progenitors. This impeded neuronal differentiation and finally culminated in microcephaly.

S6K has shown evidences to be controlled by the cell cycle. Specifically, the p70-S6K1 isoform is known to translocate from its regular cytoplasmatic location to the nucleus during mid G_1 phase after being hyperphosphorylated by mTORC1 (Rosner and Hengstschla, 2011). An essential function for p70-S6K1 in this cell cycle phase had already been detected (Lane *et al.*, 1993). p70-S6K1 was the only of the 3 S6K isoforms with a differential subcellular location controlled by mTOR, while p85 and p31 maintained their described basal cytoplasmatic and nuclear locations, respectively (Rosner and Hengstschla, 2011). The relevance of the Thr389 residue phosphorylation in this process was demonstrated by chemical inhibition of mTORC1 which avoided p70-S6K1 translocation, and TSC2-specific

ablation with small interference RNA, which induced an only nuclear localization of the p70 kinase at earlier stages such as in G_0/G_1.

Factors such as TGF-β, which inhibits G_1/S progression in a variety of eukaryotic cell types, acts by indirectly repressing p70-S6K1. TGF-β induced the formation and stabilization of complexes between this kinase and the protein phosphatase 2A (PP2A), leading to S6K-dephosphorylation and G_1 cell cycle arrest. However, S6K dephosphorylation was not sufficient but only rate-limiting in mediating G_1 arrest, as other TGF-β-activated effectors such as Smad2/3 were also necessary for this process (Petritsch *et al.*, 2000).

A direct role of S6K in enabling S-phase progression is phosphorylating and activating the carbamoyl-phosphate synthetase 2, aspartate transcarbamylase, and dihydroorotase (CAD). CAD catalyses the first three steps in de novo pyrimidine synthesis, necessaries for DNA synthesis. When CAD was phosphorylated at Ser1489, it oligomerized and became active. In that work, inhibiting S6K chemically with PF-4708671 directly delayed cell cycle progression (Benjamin *et al.*, 2011). The high relevance of S6K was consistent with previous reports stating that rapamycin inhibited DNA synthesis independently of the other major mTORC1 direct substrate, 4E-BP1 (Dowling *et al.*, 2010; Espeillac *et al.*, 2011). However, other studies based on dose-dependent rapamycin treatments reported that 4E-BP1 was required for a complete G_1 cell cycle arrest, pointing at 4E-BP1 as a critical target when trying to block cell cycle progression (Chatterjee *et al.*, 2015). Also, Ohanna *et al* found that myoblasts with ablated S6K1 were smaller in size but could proliferate normally, thereby excluding S6K1 as a member of the cell cycle control machinery (Ohanna *et al.*, 2005).

Elevated S6 phosphorylation levels have been proposed as a marker of neurodevelopmental pathologies, in this case autism (Poopal *et al.*, 2016). The pathological relevance of increased S6 phosphorylation levels alone, with independence of the activation status of their upstream pathways, was demonstrated when one patient from the AGRE collection showed this rise, whereas his healthy sister did not have increased S6 phosphorylation.

Another piece of evidence suggesting that the major effector of the PDK1 L155E mutation can be narrowed to one of the many proteins regulated by the mTOR cascade came from the status of the interneuron populations of the adult mice. Indeed, conditionally deleting the mTOR gene specifically in mice interneuron progenitors and their derived progeny markedly reduced the number of interneurons in the cerebral cortex (Ka *et al.*, 2017). This phenotype was not observed in the $PDK1^{fl/fl}$ CRE^{+} adult brains, whereas only the layer location of these cells was changed respect to the control (Cordón-Barris *et al.*, 2016).

However, a recent transposon-mediated somatic mutagenesis screen in mice neglected S6K as a candidate to generate malformations of cortical development diseases (Lu *et al.*, 2018).

Many of the schizophrenia risk factors described in the literature were related to key neurodevelopmental genes that converged on PKB/mTOR signalling, and several studies supported a direct involvement of the PKB1/GSK3β/mTOR pathway in schizophrenia and proposed them as targets for pharmacological treatment (Emamian *et al.*, 2004; Emamian, 2012; Law *et al.*, 2012; Papaleo *et al.*, 2016) . Effectively, a variety of genetic susceptibility factors for this disorder such as Neuregulin-1 (NRG1) and its receptor ErbB4, NRG1 paralog Neuregulin-3 (NRG3), Disrupted-in-Schizophrenia-1 (DISC1) and Dysbindin-1, regulated or signalled through the PI3K/PKB pathway (Enriquez-Barreto and Morales, 2016), sometimes even synergizing directly at the beginning of the pathway by binding the PI3K catalytic subunit p110δ. Accordingly, increases in p110δ levels had also been related to schizophrenia (Law *et al.*, 2012). p110δ gene is regulated in a developmental-specific manner, with some of its alternative transcripts being generated preferentially in the subventricular zone of the foetal brain (Hood *et al.*, 2019).

The relevant role of PKB in the cortical neurodevelopmental is out of discussion. Cortical neurons seeded in vitro expressing the PDK1$^{K465E/K465E}$ mutation reducing specifically PKB activity showed impaired neuronal growth and differentiation (Zurashvili *et al.*, 2013). A forebrain-specific conditional ablation of PDK1 in excitatory neurons of the cortex displayed a massive neuron loss and increased apoptosis together with deficits on several behavioural tasks. These results highlighted the essential role of PKB-mediated signalling in the maintenance of neuronal survival during cortical development (Xu *et al.*, 2017) . However, after neurodevelopment, a decreased activity of PKB (such the one showed by the PDK1$^{K465E/K465E}$ mice) could result even beneficial and protect neurons against endoplasmic reticulum stressors or attenuate the unfolding protein response, giving neurons a resistance against amyloid-β oligomers (Yang *et al.*, 2018).

Other comments about PDK1 substrates in literature

PKCs: Previous studies allowed to rule out the PKCs as major effectors of the PDK1 L155E mutation. A *Nestin*-Cre *Prkci* neural-specific deficient mice was

created and described. These mice died within 1 month after birth due to hydrocephaly. The study of their developing brains revealed expanded proliferating ventricular and subventricular zones and disrupted pseudostratified neuroepithelial structure. Apical adherent junctions in radial glial cells were lost, resulting in the displacement of these cells beyond the progenitor zone cells and their intermingling with $Tuj1^{+}$- differentiated neuronal zones. Surprisingly, neurogenesis was not affected at any stage (Imai *et al.*, 2006; Hapak, Rothlin and Ghosh, 2018). The $PDK1^{fl/fl}$ CRE^{+}, instead, conserved the differentiated layering between progenitors and differentiated neurons, but neurons were generated at lower rates (Figure R6, R10, R11).

GSK3β: GSK3β, a downstream effector (but not a substrate) of PDK1 participates in the control of the proneural protein Neurog2, as explained above (Li *et al.*, 2012). However, the GSK3β phosphorylation sites are located outside of the bHLH domain of Neurog2. This is the motif that has demonstrated to be evolutionary conserved from *Drosophila* to all vertebrates amongst all proneural genes/factors, relevant as an on/off switch for *in vivo* DNA binding and transcriptional activity of all proneural proteins, and essential for the rapid termination of the fate specification functions in early neural progenitors (Guillemot *et al.*, 2017).

RSKs: RSKs has also been directly involved in the regulation of cell-cycle progression and cell proliferation. RSK1 and RSK2 may also regulate G_1 phase progression by controlling the activity of the CDK2 (cyclin-dependent kinase 2) inhibitor $p27^{kip1}$. RSK also mediates cell-cycle progression by negatively regulating GSK3β, which targets the proto-oncogen c-Myc and cyclin D1 for degradation. Inhibition of RSK2 activity prevented the kinetochore localization of a couple of proliferation suppressors (Mad1 and Mad2), suggesting that RSK2 participated in the spindle assembly checkpoint (Romeo, Zhang and Roux, 2012) (Vigneron *et al.*, 2010). Also importantly, RSKs demonstrated during *Xenopus laevis* oocyte maturation to be able to phosphorylate rpS6 whenever necessary during periods where S6K1/2 is still inactive (Schwab *et al.*, 1999; Anjum and Blenis, 2008).

SGK1: PKB-independent manners to activate mTORC1 have been described, where SGK1, another PDK1 direct substrate, phosphorylates TSC2. This was detected in cancer cells that developed resistance to PI3Kα inhibitors, and PDK1 blockade restored sensitivity to the former therapies (Castel *et al.*, 2016). This showed that PDK1 is an important agent on its own to keep in mind, not only as a third leg in “others” (named PI3K and PKB) game. However, this recently discovered loop allowing mTORC1 activation in the absence of PDK1, which could be acting in the $PDK1^{K465E/K465}$ mice and brain, will still be unable to work in the $PDK1^{fl/fl}$ L155E Nestin-Cre conditional mice, as SGK1 will be even more affected than PKB by the PDK1 PIF pocket mutation.

Working with the PDK1$^{fl/fl}$ CRE^{+} mouse model

The major problematics of working with the PDK1$^{fl/fl}$ CRE^{+} model were both the lower frequency of birth of the PDK1$^{fl/fl}$ (Cordón-Barris *et al.*, 2016), and also the necessity of crossing this line with a CRE-expressing model. These steps led to a reduced and complicated obtention of enough sample for experiments, with litters that could contain no mutant or semimutant at all and would then invalidate the experiment. Future perspectives in this study could be the use of brain organoids (Quadrato *et al.*, 2017). These are *in vitro* three-dimensional models of the developing brain established by seeding initial embryoid bodies of pluripotent stem cells and using BDNF in the final differentiation medium. They are large self-patterning systems and have the potential to generate a vast cellular diversity of endogenous tissue, from neuroepithelial cells to proliferative precursors, astroglia, retina and more. Their ability to fully recapitulate the regional complexity, cellular diversity and circuit functionality of the brain is largely untested, but some results could be obtained using these models. To the date, they have proven useful to study neural progenitor dysfunction occurring during early stages of brain development leading to microcephaly-associated phenotypes, where clear structures mimicking the neocortex and expressing Pax6, Tbr2 or Tbr1 were described and quantified (Lancaster *et al.*, 2013).

A special attention has to be paid on the mice deleter model used in this study. The Nestin-Cre generated by at Günther Schütz lab (Tronche *et al.*, 1999), the one available from Jackson Laboratories, claimed that Cre expression, and thus recombination, commenced in the neural stem cells (NSCs) and IP during embryogenesis. However, 2012 results demonstrated that recombination rate driven by Nestin was extremely insufficient in the VZ and SVZ of the neocortex during early (E12.5) and mid stages of forebrain development (E14.5), and that it only reached sufficiency during late embryonic and early postnatal periods (Liang, Hippenmeyer and Ghashghaei, 2012). As a control and alternative, the authors used and proposed targeting the CNS using the Emx1-Cre line, which showed robust recombination and transgene expression in NSCs and IPs as early as E12.5 (Gorski *et al.*, 2002). However, other studies using Nestin-Cre-mediated deletion of PDK1 have shown complete abrogation of the expression of the protein at E15.5 (Watatani *et al.*, 2012).

Finally, if trying to translate the results of this study to human neurodevelopment of schizophrenia, differences amongst primate and mouse cortices have to be considered. The primate cortex is more complex than the rodent's one, as a new enlarged supragranular compartment appears called the outer subventricular zone

(OSVZ), which only exists in primates. This OSVZ is a novel germinal zone that emerges from the germinal zones already described in the rodent, but additional NPC types can be found and they inter-related forming non-hierarchical lineages. In addition, the OSVZ regulatory mechanisms rely strongly on the use of miRNAs that evolved uniquely in primate cortices (Paridaen and Huttner, 2014; Dehay, Kennedy and Kosik, 2015).

However, importantly, a conserved feature amongst small rodents and primates is the role of $Tbr2^+$ IPs. IPs are abundant in both species, and Tbr2 is specifically expressed in IPs in a similar way that does in small rodents. However, in gyrencephalic species (which mice are not), $Tbr2^+$ have an additional role in the structural formation of the brain, as these cells are most abundant beneath growing gyri, and experimental interference with Tbr2 expression impairs cortical folding (Hevner, 2019). The vast majority of RG-enriched genes are similarly expressed in mouse and human, and the ones that displayed the highest differential expression between species were genes highly expressed in human but missing in mouse (Silbereis *et al.*, 2016).

Finally, the potential of this mouse model is remarkable. The PIF pocket of PDK1 is gaining attention as it has a great potential to allosterically modulate the activity of PDK1, avoiding the necessity for inhibitors of the catalytic site, which tend to be ATP-competitive and thus less specific (Leroux and Biondi, 2020). Allosteric modulators (both inhibitors and activators) have then less side effect and lower toxicity. The activators stabilize the activation loop and ATP binding site of PDK1 by modifying the closure angle of the PIF-pocket to these structures, while the inhibitors cause a realignment of the helices αB and αC that inhibited PDK1 activity. Till date, seven classes of PDK1 allosteric modulators have been reported based on their chemical structure, most of them being PDK1 activators (Xu *et al.*, 2019).

Studies in pregnant mice reported that developmental inhibition of GSK3β rescued behavioural and neurophysiological deficits in a mouse model of schizophrenia predisposition. The authors reported that the use of pharmacological GSK3β antagonists during postnatal development can rescue axonal outgrowth in the 22q11.2 deletion model. This treatment also restored functional and behavioural impairments of the mice (Tamura *et al.*, 2016). This study highlighted the potential of early pharmacological interventions for restoring neural circuit dysfunction in neurodevelopmental disorders.

CONCLUSIONS

1. PDK1$^{fl/fl}$ CRE^{-} and PDK1$^{fl/fl}$ CRE^{+} are microcephalic at their adulthood; in the PDK1$^{fl/fl}$ CRE^{+} mice, microcephaly is already observed at embryological day E15.5.

2. PDK1$^{fl/fl}$ CRE^{-} and PDK1$^{fl/fl}$ CRE^{+} mice exhibit reduced level of phosphorylation of rpS6 at Ser235/236 and S6K at Thr389 in whole adult brain extracts and E15.5 neurons seeded *in vitro*, both in starvation conditions and after stimulation of the PI3K/PDK1 pathway with BDNF. S6K phosphorylation at Thr229 is reduced in these two genotypes in the whole brain extracts and in starving neurons seeded *in vitro*, but only PDK1$^{fl/fl}$ CRE^{+} neurons fail to phosphorylate this residue after stimulation with BDNF.

3. PDK1$^{fl/fl}$ CRE^{+} mice show reduced protein levels of total PKCα with further decreased phosphorylation levels at the Thr497 residue in whole adult brain extracts and in extracts from E15.5 neurons seeded *in vitro*, both in starvation conditions and after stimulation of the PI3K/PDK1 pathway with BDNF. PDK1$^{fl/fl}$ CRE^{-} neurons exhibit normal phosphorylation and total PKCa protein levels when compared with the PDK1$^{+/fl}$ CRE^{-} controls.

4. Neuronal expression of the PDK1 L155E mutant protein in the PDK1$^{fl/fl}$ CRE^{+} mice does not induce apoptosis in E15.5 cortical neurons seeded *in vitro* neither in cortical tissues of the same age.

5. E15.5 cortical neurons from the PDK1$^{fl/fl}$ CRE^{-} and PDK1$^{fl/fl}$ CRE^{+} mice are less proliferative than those from the PDK1$^{+/fl}$ CRE^{-} controls at 1 day *in vitro* (DIV). For the three genotypes, proliferation stops after 4 DIVs.

6. The Tbr2^{+} intermediate progenitors of the PDK1$^{fl/fl}$ CRE^{-} and PDK1$^{fl/fl}$ CRE^{+} mice at E14.5 and E15.5 are less abundant than those of the PDK1$^{+/fl}$ CRE^{-} controls, and at E15.5 they are located further away from the ventricle.

7. The number of Pax6^{+} apical progenitors is not different in the three analysed genotypes neither at E14.5 nor at E15.5.

8. The totality of the Pax6^{+} apical progenitors of the three analysed genotypes are proliferating at both E14.5 and E15.5.

9. The percentage of proliferative cells that are non-AP cells is reduced at E14.5 but increased at E15.5 in the PDK1$^{fl/fl}$ CRE^{+} mice when compared with the PDK1$^{+/fl}$ CRE^{-} controls.

10. The percentage of Pax6^{+} APs that are undergoing mitosis at E15.5 is decreased in the PDK1$^{fl/fl}$ CRE^{-} and the PDK1$^{fl/fl}$ CRE^{+} mice compared to the

PDK1$^{+/fl}$ CRE^{-} controls. The number of Pax6^{-} mitotic cells, however, shows no differences amongst the three genotypes.

11. The percentage of E15.5 cortical neurons seeded *in vitro* incorporating the thymidine analogous base 5-ethynyl-2'-deoxyuridine (EdU) showed no differences between the three analysed genotypes.

12. The number of Ctip2^{+} neurons generated at both E14.5 and E15.5 in the PDK1$^{fl/fl}$ CRE^{+} mice are decreased compared to the PDK1$^{+/fl}$ CRE^{-} controls. This population is also displaced away from the ventricle at E14.5.

13. At E15.5, the population of neurons that are not stained by neither Pax6 nor Ctip2 is increased in the PDK1$^{fl/fl}$ CRE^{+} cortices when compared to the PDK1$^{+/fl}$ CRE^{-} controls.

14. The PDK1$^{fl/fl}$ CRE^{+} mice generate an increased population of immature deep layer neurons marked by Tbr1^{+} at E15.5.

15. At E14.5, the population of neurons that are not stained by neither Pax6 nor Tbr1 is found closer to the pia in the PDK1$^{fl/fl}$ CRE^{+} cortices than in the PDK1$^{fl/fl}$ CRE^{-} or the PDK1$^{+/fl}$ CRE^{-} controls. At E15.5, this population of neurons that are not stained by neither Pax6 nor Ctip2 is concentrated in a narrow area in the PDK1$^{+/fl}$ CRE^{-} controls, while it spreads into a wider region in the PDK1$^{fl/fl}$ CRE^{-} and the PDK1$^{fl/fl}$ CRE^{+} embryos.

16. S6K$^{T229D/T389D}$, but not S6K$^{T229E/T389D}$ nor S6K^{T389D}, are able to phosphorylate rpS6 in Hela cells starved overnight in the absence of PI3K/PDK1 stimulation. PKB$^{T308D/S473D}$ shows a reduced capacity of inducing this phosphorylation in the same conditions.

17. S6K$^{T229D/T389D}$, S6K$^{T229E/T389D}$ and S6K^{T389D} do not phosphorylate the PKB specific substrate PRAS40 in Hela cells starved overnight in the absence of PI3K/PDK1 stimulation. PKB$^{T308D/S473D}$ is capable of phosphorylating PRAS40 in the same conditions.

18. The exogenous expression of S6K$^{T229D/T389D}$, S6K$^{T229E/T389D}$ and S6K^{T389D} in Hela cells generates a pattern of bands that are detected by the anti-total S6K antibody and that range from 70 kDa to 40 kDa. This pattern is observed in both human Hela and mice N2A cell lines.

19. The PDK1 inhibitor GSK2334470 inhibited rpS6 phosphorylation in Hela cells starved overnight in the absence of PI3K/PDK1 stimulation in a dose dependent manner.

20. The exogenously expressed $S6K^{T229D/T389D}$ protein phosphorylates rpS6 even in the presence of 2 μM of the PDK1 inhibitor GSK2334470 in Hela cells starved overnight in the absence of PI3K/PDK1 stimulation. $S6K^{T389D}$ protein phosphorylates rpS6 only when the PI3K/PDK1 pathway is stimulated with IGF-1. Hela cells transfected with the empty vector pCMV5 and starved overnight cannot phosphorylate rpS6 in the presence of 2 μM or 0'2 μM of the PDK1 inhibitor GSK2334470 even upon PI3K/PDK1 stimulation with IGF-1.

21. 0'2 μM of the PDK1 inhibitor GSK2334470 did not inhibited PKB Thr308 phosphorylation by PDK1 in Hela cells starved overnight when stimulated with IGF-1.

22. Pre-incubation with 2 μM of the PDK1 inhibitor GSK2334470 or 100 nM of the mTORC1 inhibitor rapamycin did not affect the capacity of $PKB^{T308D/S473D}$ to phosphorylate PRAS40 in Hela cells starved overnight without stimulation of the PI3K/PDK1 pathway.

23. The transfection of pCAG-RFP empty vector increases rpS6 phosphorylation in Hela cells starved overnight without stimulation of the PI3K/PDK1 pathway, independently of the transfectant reagent used. The expression of this plasmid has no effect on the phosphorylation of PRAS40 in the same conditions.

PUBLICATIONS DERIVED FROM THE THESIS

Cordón-Barris L, **Pascual-Guiral S**, Yang S, Giménez-Llort L, Lope-Piedrafita S, Niemeyer C, Claro E, Lizcano JM, Bayascas JR. Mutation of the 3-Phosphoinositide-Dependent Protein Kinase 1 (PDK1) Substrate-Docking Site in the Developing Brain Causes Microcephaly with Abnormal Brain Morphogenesis Independently of Akt, Leading to Impaired Cognition and Disruptive Behaviors. Mol Cell Biol. 2016 Nov 14;36(23):2967-2982.

Yang S, **Pascual-Guiral S**, Ponce R, Giménez-Llort L, Baltrons MA, Arancio O, Palacio JR, Clos VM, Yuste VJ, Bayascas JR. Reducing the Levels of Akt Activation by PDK1 Knock-in Mutation Protects Neuronal Cultures against Synthetic Amyloid-Beta Peptides. Front Aging Neurosci. 2018 Jan 8;9:435.

BIBLIOGRAPHY

A

Abe, P. *et al.* (2015) 'Intermediate progenitors facilitate intracortical progression of thalamocortical axons and interneurons through CXCL12 chemokine signaling', *Journal of Neuroscience*, 35(38), pp. 13053–13063. doi: 10.1523/JNEUROSCI.1488-15.2015.

Alessi, D. *et al.* (1998) '3-phosphoinositide-dependent protein kinase 1 (PDK1) phosphorylates and activates the p70 S6 kinase in vivo and in vitro', *Current Biology*, 8(2), pp. 69–81. doi: 10.1016/S0960-9822(98)70037-5.

Alessi, D. R. *et al.* (1996) 'Mechanism of activation of protein kinase B by insulin and IGF-1', *EMBO Journal*, 15(23), pp. 6541–6551. doi: 10.1002/j.1460-2075.1996.tb01045.x.

Alessi, D. R. *et al.* (1997) 'Characterization of a 3-phosphoinositide-dependent protein kinase which phosphorylates and activates protein kinase Bα', *Current Biology*, 7(4), pp. 261–269. doi: 10.1016/s0960-9822(06)00122-9.

Ali, F. *et al.* (2011) 'Cell cycle-regulated multi-site phosphorylation of neurogenin 2 coordinates cell cycling with differentiation during neurogenesis', *Development*, 138(19), pp. 4267–4277. doi: 10.1242/dev.067900.

Anderson, S. A. *et al.* (1997) 'Interneuron migration from basal forebrain to neocortex: Dependence on Dlx genes', *Science*, 278(5337), pp. 474–476. doi: 10.1126/science.278.5337.474.

Anglada-Huguet, M. *et al.* (2016) 'Loss of striatal 90-kDa ribosomal S6 kinase (Rsk) is a key factor for motor, synaptic and transcription dysfunction in Huntington's disease', *Biochimica et Biophysica Acta - Molecular Basis of Disease*, 1862(7), pp. 1255–1266. doi: 10.1016/j.bbadis.2016.04.002.

Anjum, R. and Blenis, J. (2008) 'The RSK family of kinases: Emerging roles in cellular signalling', *Nature Reviews Molecular Cell Biology*, 9(10), pp. 747–758. doi: 10.1038/nrm2509.

Arai, Y. *et al.* (2011) 'Neural stem and progenitor cells shorten S-phase on commitment to neuron production', *Nature Communications*, 2, p. 154. doi: 10.1038/ncomms1155.

Arencibia, J. M. *et al.* (2013) 'AGC protein kinases: From structural mechanism of regulation to allosteric drug development for the treatment of human diseases', *Biochimica et Biophysica Acta - Proteins and Proteomics*, 1834(7), pp. 1302–1321. doi: 10.1016/j.bbapap.2013.03.010.

Arif, A. *et al.* (2019) 'Multisite Phosphorylation of S6K1 Directs a Kinase Phospho-code that Determines Substrate Selection', *Molecular Cell*, 73(3), pp. 446-457.e6. doi: 10.1016/j.molcel.2018.11.017.

Arlotta, P. *et al.* (2005) 'Neuronal subtype-specific genes that control corticospinal motor neuron development in vivo', *Neuron*, 45(2), pp. 207–221. doi: 10.1016/j.neuron.2004.12.036.

Arnold, S. J. *et al.* (2008) 'The T-box transcription factor Eomes/Tbr2 regulates

neurogenesis in the cortical subventricular zone', *Genes and Development*, 22(18), pp. 2479–2484. doi: 10.1101/gad.475408.
Arthur, J. S. C. (2008) 'MSK activation and physiological roles', *Frontiers in bioscience*, 13, pp. 5866–5879. doi: 10.2741/3122.
Averous, J. *et al.* (2014) 'Requirement for lysosomal localization of mTOR for its activation differs between leucine and other amino acids', *Cellular Signalling*, 26(9), pp. 1918–1927. doi: 10.1016/j.cellsig.2014.04.019.
Averous, J. *et al.* (2016) 'GCN2 contributes to mTORC1 inhibition by leucine deprivation through an ATF4 independent mechanism', *Scientific Reports*, 6, p. 27698. doi: 10.1038/srep27698.
Azim, E. *et al.* (2009) 'SOX6 controls dorsal progenitor identity and interneuron diversity during neocortical development', *Nature Neuroscience*, 12(10), pp. 1238–1247. doi: 10.1038/nn.2387.

B

Baala, L. *et al.* (2007) 'Homozygous silencing of T-box transcription factor EOMES leads to microcephaly with polymicrogyria and corpus callosum agenesis', *Nature Genetics*, 39(4), pp. 454–456. doi: 10.1038/ng1993.
Balendran, A. *et al.* (1999) 'Evidence that 3-phosphoinositide-dependent protein kinase-1 mediates phosphorylation of p70 S6 kinase in vivo at Thr-412 as well as Thr-252', *Journal of Biological Chemistry*, 274(52), pp. 37400–37406. doi: 10.1074/jbc.274.52.37400.
Balendran, A. *et al.* (2000) 'Further evidence that 3-phosphoinositide-dependent protein kinase-1 (PDK1) is required for the stability and phosphorylation of protein kinase C (PKC) isoforms', *FEBS Letters*, 484(3), pp. 217–223. doi: 10.1016/S0014-5793(00)02162-1.
Banerjee, P. *et al.* (2006) 'Molecular structure of a major insulin/mitogen-activated 70-kDa S6 protein kinase', *Proceedings of the National Academy of Sciences*, 87(21), pp. 8550–8554. doi: 10.1073/pnas.87.21.8550.
Bartolini, G. *et al.* (2017) 'Neuregulin 3 Mediates Cortical Plate Invasion and Laminar Allocation of GABAergic Interneurons Article Neuregulin 3 Mediates Cortical Plate Invasion and Laminar Allocation of GABAergic Interneurons', *Cell reports*, 18(5), pp. 1157–1170. doi: 10.1016/j.celrep.2016.12.089.
Basnet, R. *et al.* (2018) 'Serum and glucocorticoid inducible protein kinases (SGKs): a potential target for cancer intervention', *Acta Pharmaceutica Sinica B*, pp. 767–771. doi: 10.1016/j.apsb.2018.07.001.
Bayascas, J. R. *et al.* (2006) 'Evaluation of approaches to generation of tissue-specific knock-in mice', *Journal of Biological Chemistry*, 281(39), pp. 28772–28781. doi: 10.1074/jbc.M606789200.
Bayascas, J. R. *et al.* (2008) 'Mutation of the PDK1 PH Domain Inhibits Protein Kinase B/Akt, Leading to Small Size and Insulin Resistance', *Molecular and Cellular*

Biology, 28(10), pp. 3258–3272. doi: 10.1128/mcb.02032-07.
Bayascas, J. R. (2010) 'PDK1: the major transducer of PI 3-kinase actions.', *Current topics in microbiology and immunology*, 346, pp. 9–29. doi: 10.1007/82_2010_43.
Bayer, T. A., Falkai, P. and Maier, W. (1999) 'Genetic and non-genetic vulnerability factors in schizophrenia: The basis of the "Two hit hypothesis"', *Journal of Psychiatric Research*, 33(6), pp. 543–548. doi: 10.1016/S0022-3956(99)00039-4.
Beaulieu, J. M. *et al.* (2004) 'Lithium antagonizes dopamine-dependent behaviors mediated by an AKT/glycogen synthase kinase 3 signaling cascade', *Proceedings of the National Academy of Sciences of the United States of America*, 101(14), pp. 5099–5104. doi: 10.1073/pnas.0307921101.
Beck, E. C. and Burns, B. D. (1959) 'The Mammalian Cerebral Cortex', *The American Journal of Psychology*, 72(4), p. 655. doi: 10.2307/1419527.
Ben-Hur, V. *et al.* (2013) 'S6K1 Alternative Splicing Modulates Its Oncogenic Activity and Regulates mTORC1', *Cell Reports*, 3(1), pp. 103–115. doi: 10.1016/j.celrep.2012.11.020.
Ben-Sahra, I. *et al.* (2013) 'Stimulation of de novo pyrimidine synthesis by growth signaling through mTOR and S6K1', *Science*, 339(6125), pp. 1323–1328. doi: 10.1126/science.1228792.
Benjamin, D. *et al.* (2011) 'Rapamycin passes the torch: a new generation of mTOR inhibitors', *Nature reviews Drug discovery*, 10(11), pp. 868–880. doi: 10.1038/nrd3531.
Bernal, A. and Arranz, L. (2018) 'Nestin - expressing progenitor cells : function , identity and therapeutic implications', *Cellular and Molecular Life Sciences*. Springer International Publishing, 75(12), pp. 2177–2195. doi: 10.1007/s00018-018-2794-z.
Berven, L. A., Willard, F. S. and Crouch, M. F. (2004) 'Role of the p70S6K pathway in regulating the actin cytoskeleton and cell migration', *Experimental Cell Research*, 296(2), pp. 183–195. doi: 10.1016/j.yexcr.2003.12.032.
Biever, A., Valjent, E. and Puighermanal, E. (2015) 'Ribosomal protein S6 phosphorylation in the nervous system: From regulation to function', *Frontiers in Molecular Neuroscience*, 8, p. 75. doi: 10.3389/fnmol.2015.00075.
Biondi, R. M. *et al.* (2000) 'Identification of a pocket in the PDK1 kinase domain that interacts with PIF and the C-terminal residues of PKA', *EMBO Journal*, 19(5), pp. 979–988. doi: 10.1093/emboj/19.5.979.
Biondi, R. M. *et al.* (2001) 'The PIF-binding pocket in PDK1 is essential for activation of S6K and SGK, but not PKB', *EMBO Journal*, 20(16), pp. 4380–4390. doi: 10.1093/emboj/20.16.4380.
Biondi, R. M. *et al.* (2002) 'High resolution crystal structure of the human PDK1 catalytic domain defines the regulatory phosphopeptide docking site', *EMBO Journal*, 21(16), pp. 4219–4228. doi: 10.1093/emboj/cdf437.
Bjørbaek, C., Zhao, Y. and Moller, D. E. (1995) 'Divergent functional roles for

p90rsk kinase domains', *The Journal of biological chemistry*, 270(32), pp. 18848–18852. doi: 10.1074/jbc.270.32.18848.
Di Blasio, L. *et al.* (2017) 'Serine/threonine kinase 3-phosphoinositide-dependent protein kinase-1 (PDK1) as a key regulator of cell migration and cancer dissemination', *Cancers*, 9(3), p. 25. doi: 10.3390/cancers9030025.
Boland, E. *et al.* (2007) 'Mapping of deletion and translocation breakpoints in 1q44 implicates the serine/threonine kinase AKT3 in postnatal microcephaly and agenesis of the corpus callosum', *American Journal of Human Genetics*, 81(2), pp. 292–303. doi: 10.1086/519999.
Bond, J. *et al.* (2002) 'ASPM is a major determinant of cerebral cortical size', *Nature Genetics*, 32(2), pp. 316–320. doi: 10.1038/ng995.
Borrell, V. *et al.* (2012) 'Slit/Robo Signaling Modulates the Proliferation of Central Nervous System Progenitors', *Neuron*, 76(2), pp. 338–352. doi: 10.1016/j.neuron.2012.08.003.
Bortone, D. and Polleux, F. (2009) 'KCC2 Expression Promotes the Termination of Cortical Interneuron Migration in a Voltage-Sensitive Calcium-Dependent Manner', *Neuron*, 62(1), pp. 53–71. doi: 10.1016/j.neuron.2009.01.034.
Britanova, O. *et al.* (2005) 'Novel transcription factor Satb2 interacts with matrix attachment region DNA elements in a tissue-specific manner and demonstrates cell-type-dependent expression in the developing mouse CNS', *European Journal of Neuroscience*, 21(3), pp. 658–668. doi: 10.1111/j.1460-9568.2005.03897.x.
Britanova, O. *et al.* (2008) 'Satb2 Is a Postmitotic Determinant for Upper-Layer Neuron Specification in the Neocortex', *Neuron*, 57(3), pp. 378–392. doi: 10.1016/j.neuron.2007.12.028.
Brunet, A. *et al.* (1999) 'Akt promotes cell survival by phosphorylating and inhibiting a forkhead transcription factor', *Cell*, 96(6), pp. 857–868. doi: 10.1016/S0092-8674(00)80595-4.
Brunet, A. *et al.* (2001) 'Protein Kinase SGK Mediates Survival Signals by Phosphorylating the Forkhead Transcription Factor FKHRL1 (FOXO3a)', *Molecular and Cellular Biology*, 21(3), pp. 952–965. doi: 10.1128/mcb.21.3.952-965.2001.
Burnett, P. E. *et al.* (1998) 'RAFT1 phosphorylation of the translational regulators p70 S6 kinase and 4E-BP1', *Proceedings of the National Academy of Sciences of the United States of America*, 95(4), pp. 1432–1437. doi: 10.1073/pnas.95.4.1432.

C

Calegari, F. *et al.* (2005) 'Selective Lengthening of the Cell Cycle in the Neurogenic Subpopulation of Neural Progenitor Cells during Mouse Brain Development', *Journal of Neuroscience*, 25(28), pp. 6533–6538. doi: 10.1523/JNEUROSCI.0778-05.2005.
Calegari, F. and Huttner, W. B. (2003) 'An inhibition of cyclin-dependent kinases that lengthens, but does not arrest, neuroepithelial cell cycle induces premature

neurogenesis', *Journal of Cell Science*, 116(24), pp. 4947–4955. doi: 10.1242/jcs.00825.
Cárdenas, A. *et al.* (2018) 'Evolution of Cortical Neurogenesis in Amniotes Controlled by Robo Signaling Levels', *Cell*, 174(3), pp. 590-606.e21. doi: 10.1016/j.cell.2018.06.007.
Casamayor, A., Morrice, N. A. and Alessi, D. R. (1999) 'Phosphorylation of Ser-241 is essential for the activity of 3-phosphoinositide-dependent protein kinase-1: identification of five sites of phosphorylation in vivo', *The Biochemical journal*, 342(Pt 2), pp. 287–292.
Castel, P. *et al.* (2016) 'PDK1-SGK1 Signaling Sustains AKT-Independent mTORC1 Activation and Confers Resistance to PI3Kα Inhibition', *Cancer Cell*, 30(2), pp. 229–242. doi: 10.1016/j.ccell.2016.06.004.
De Cesare, D. *et al.* (1998) 'Rsk-2 activity is necessary for epidermal growth factor-induced phosphorylation of CREB protein and transcription of c-fos gene', *Proceedings of the National Academy of Sciences of the United States of America*, 95(21), pp. 12202–12207. doi: 10.1073/pnas.95.21.12202.
Chalhoub, N. *et al.* (2009) 'Cell type specificity of PI3K signaling in Pdk1- and Pten-deficient brains', *Genes and Development*, 23(14), pp. 1619–1624. doi: 10.1101/gad.1799609.
Chang, H. W. *et al.* (1997) 'Transformation of chicken cells by the gene encoding the catalytic subunit of PI 3-kinase', *Science*, 276(5320), pp. 1848–1850. doi: 10.1126/science.276.5320.1848.
Chatterjee, A. *et al.* (2015) 'Rapamycin-induced G1 cell cycle arrest employs both TGF-β and Rb pathways', *Cancer Letters*, 360(2), pp. 134–140. doi: 10.1016/j.canlet.2015.01.043.
Chauvin, C. *et al.* (2014) 'Ribosomal protein S6 kinase activity controls the ribosome biogenesis transcriptional program', *Oncogene*, 33(4), pp. 474–483. doi: 10.1038/onc.2012.606.
Chen, B. *et al.* (2008) 'The Fezf2-Ctip2 genetic pathway regulates the fate choice of subcortical projection neurons in the developing cerebral cortex', *Proceedings of the National Academy of Sciences of the United States of America*, 105(32), pp. 11382–11387. doi: 10.1073/pnas.0804918105.
Chen, R. H., Sarnecki, C. and Blenis, J. (1992) 'Nuclear localization and regulation of erk- and rsk-encoded protein kinases.', *Molecular and Cellular Biology*, 12(3), pp. 915–927. doi: 10.1128/mcb.12.3.915.
Chittajallu, R. and Isaac, J. T. R. (2010) 'Emergence of cortical inhibition by coordinated sensory-driven plasticity at distinct synaptic loci', *Nature Neuroscience*, 13(10), pp. 1240–1248. doi: 10.1038/nn.2639.
Chun, J. *et al.* (2004) '14-3-3 protein mediates phosphorylation of microtubule-associated protein Tau by serum- and glucocorticoid-induced protein kinase 1', *Molecules and Cells*, 18(3), pp. 360–368.
Chung, J. *et al.* (1992) 'Rapamycin-FKBP specifically blocks growth-dependent

activation of and signaling by the 70 kd S6 protein kinases', *Cell*, 69(7), pp. 1227–1236. doi: 10.1016/0092-8674(92)90643-q.
Collins, B. J. *et al.* (2003) 'In vivo role of the PIF-binding docking site of PDK1 defined by knock-in mutation', *EMBO Journal*, 22(16), pp. 4202–4211. doi: 10.1093/emboj/cdg407.
Collins, B. J. *et al.* (2005) 'In vivo role of the phosphate groove of PDK1 defined by knockin mutation', *Journal of Cell Science*, 118(21), pp. 5023–5034. doi: 10.1242/jcs.02617.
Cordón-Barris, L. *et al.* (2016) 'Mutation of the 3-Phosphoinositide-Dependent Protein Kinase 1 (PDK1) Substrate-Docking Site in the Developing Brain Causes Microcephaly with Abnormal Brain Morphogenesis Independently of Akt, Leading to Impaired Cognition and Disruptive Behaviors', *Molecular and Cellular Biology*, 36(23), pp. 2967–2982. doi: 10.1128/mcb.00230-16.
Coronado, D. *et al.* (2013) 'A short G1 phase is an intrinsic determinant of naïve embryonic stem cell pluripotency', *Stem Cell Research*, 10(1), pp. 118–131. doi: 10.1016/j.scr.2012.10.004.
Cross, D. A. E. *et al.* (1995) 'Inhibition of glycogen synthase kinase-3 by insulin mediated by protein kinase B', *Nature*, 378(6559), pp. 785–789. doi: 10.1038/378785a0.
Currie, R. A. *et al.* (1999) 'Role of phosphatidylinositol 3,4,5-trisphosphate in regulating the activity and localization of 3-phosphoinositide-dependent protein kinase-1', *The Biochemical journal*, 337(Pt 3), pp. 575–583.

D

Dahlstrand, J., Lardelli, M. and Lendahl, U. (1995) 'Nestin mRNA expression correlates with the central nervous system progenitor cell state in many, but not all, regions of developing central nervous system', *Brain Research Developmental Brain Research*. Netherlands, 84(1), pp. 109–129. doi: 10.1016/0165-3806(94)00162-s.
Dajas-Bailador, F. *et al.* (2014) 'Regulation of axon growth by the JIP1-AKT axis', *Journal of Cell Science*, 127(1), pp. 230–239. doi: 10.1242/jcs.137208.
Dalby, K. N. *et al.* (1998) 'Identification of regulatory phosphorylation sites in mitogen-activated protein kinase (MAPK)-activated protein kinase-1a/p90(rsk) that are inducible by MAPK', *Journal of Biological Chemistry*, 273(3), pp. 1496–1505. doi: 10.1074/jbc.273.3.1496.
Deak, M. *et al.* (1998) 'Mitogen- and stress-activated protein kinase-1 (MSK1) is directly activated by MAPK and SAPK2/p38, and may mediate activation of CREB', *EMBO Journal*, 17(15), pp. 4426–4441. doi: 10.1093/emboj/17.15.4426.
Dehay, C. and Kennedy, H. (2007) 'Cell-cycle control and cortical development', *Nature Reviews Neuroscience*, 8(6), pp. 438–450. doi: 10.1038/nrn2097.
Dehay, C., Kennedy, H. and Kosik, K. S. (2015) 'The Outer Subventricular Zone

and Primate-Specific Cortical Complexification', *Neuron*, 85(4), pp. 683–694. doi: 10.1016/j.neuron.2014.12.060.
Dekker, J. (2014) 'Two ways to fold the genome during the cell cycle: insights obtained with chromosome conformation capture', *Epigenetics & chromatin*, 7(1), p. 25. doi: 10.1186/1756-8935-7-25.
Dennis, M. D., Jefferson, L. S. and Kimball, S. R. (2012) 'Role of p70S6K1-mediated phosphorylation of eIF4B and PDCD4 proteins in the regulation of protein synthesis', *Journal of Biological Chemistry*, 287(51), pp. 42890–42899. doi: 10.1074/jbc.M112.404822.
Depeursinge, A. *et al.* (2010) 'Fusing Visual and Clinical Information for Lung Tissue Classification in HRCT Data', *Artificial Intelligence in Medicine*, 50(1), pp. 13–21. doi: 10.1016/j.
Deyoung, M. P. *et al.* (2008) 'Hypoxia regulates TSC1/2-mTOR signaling and tumor suppression through REDD1-mediated 14-3-3 shuttling', *Genes and Development*, 22(2), pp. 239–251. doi: 10.1101/gad.1617608.
Dibble, C. C. and Cantley, L. C. (2015) 'Regulation of mTORC1 by PI3K signaling', *Trends in cell biology*, 25(9), pp. 545–555. doi: 10.1016/j.tcb.2015.06.002.
Dominguez, M. H., Ayoub, A. E. and Rakic, P. (2013) 'POU-III transcription factors (Brn1, Brn2, and Oct6) influence neurogenesis, molecular identity, and migratory destination of upper-layer cells of the cerebral cortex', *Cerebral Cortex*, 23(11), pp. 2632–2643. doi: 10.1093/cercor/bhs252.
Dowling, R. J. O. *et al.* (2010) 'mTORC1-mediated cell proliferation, but not cell growth, controlled by the 4E-BPs', *Science*, 328(5982), pp. 1172–1176.
Duda, P. *et al.* (2018) 'Targeting GSK3 signaling as a potential therapy of neurodegenerative diseases and aging', *Expert Opinion on Therapeutic Targets*, pp. 833–848. doi: 10.1080/14728222.2018.1526925.
Dümmler, B. A. *et al.* (2005) 'Functional characterization of human RSK4, a new 90-kDa ribosomal S6 kinase, reveals constitutive activation in most cell types', *Journal of Biological Chemistry*, 280(14), pp. 13304–13314. doi: 10.1074/jbc.M408194200.

E

Ebner, M. *et al.* (2017) 'Localization of mTORC2 activity inside cells', *Journal of Cell Biology*, 216(2), pp. 343–353. doi: 10.1083/jcb.201610060.
Elsen, G. E. *et al.* (2018) 'The epigenetic factor landscape of developing neocortex is regulated by transcription factors Pax6→ Tbr2→ Tbr1', *Frontiers in Neuroscience*, 12, p. 571. doi: 10.3389/fnins.2018.00571.
Emamian, E. S. *et al.* (2004) 'Convergent evidence for impaired AKT1-GSK3β signaling in schizophrenia', *Nature Genetics*, 36(2), pp. 131–137. doi: 10.1038/ng1296.
Emamian, E. S. (2012) 'AKT/GSK3 signaling pathway and schizophrenia', *Frontiers*

in Molecular Neuroscience, 5, p. 33. doi: 10.3389/fnmol.2012.00033.
Engelman, J. A. (2009) 'Targeting PI3K signalling in cancer: Opportunities, challenges and limitations', *Nature Reviews Cancer*, 9(8), pp. 550–562. doi: 10.1038/nrc2664.
Englund, C. (2005) 'Pax6, Tbr2, and Tbr1 Are Expressed Sequentially by Radial Glia, Intermediate Progenitor Cells, and Postmitotic Neurons in Developing Neocortex', *Journal of Neuroscience*, 25(1), pp. 247–251. doi: 10.1523/JNEUROSCI.2899-04.2005.
Enriquez-Barreto, L. and Morales, M. (2016) 'The PI3K signaling pathway as a pharmacological target in Autism related disorders and Schizophrenia', *Molecular and Cellular Therapies*, 4, p. 2. doi: 10.1186/s40591-016-0047-9.
Erikson, E. and Maller, J. L. (1985) 'A protein kinase from Xenopus eggs specific for ribosomal protein S6', *Proceedings of the National Academy of Sciences of the United States of America*, 82(3), pp. 742–746. doi: 10.1073/pnas.82.3.742.
Espeillac, C. *et al.* (2011) 'S6 kinase 1 is required for rapamycin-sensitive liver proliferation after mouse hepatectomy', *Journal of Clinical Investigation*, 121(7), pp. 2821–2832. doi: 10.1172/JCI44203.

F

Filer, D. *et al.* (2017) 'RNA polymerase III limits longevity downstream of TORC1', *Nature*, 552(7684), pp. 263–267. doi: 10.1038/nature25007.
Filion, T. M. *et al.* (2009) 'Survival responses of human embryonic stem cells to DNA damage', *Journal of Cellular Physiology*, 220(3), pp. 586–592. doi: 10.1002/jcp.21735.
Fish, J. L. *et al.* (2006) 'Aspm specifically maintains symmetric proliferative divisions of neuroepithelial cells', *Proceedings of the National Academy of Sciences of the United States of America*, 103(27), pp. 10438–10443. doi: 10.1073/pnas.0604066103.
Fisher, T. L. and Blenis, J. (1996) 'Evidence for two catalytically active kinase domains in pp90rsk.', *Molecular and Cellular Biology*, 16(3), pp. 1212–1219. doi: 10.1128/mcb.16.3.1212.
Fousse, J. *et al.* (2019) 'Developmental changes in interkinetic nuclear migration dynamics with respect to cell-cycle progression in the mouse cerebral cortex ventricular zone', *Journal of Comparative Neurology*, 527(10), pp. 1545–1557. doi: 10.1002/cne.24641.
Francis, F. *et al.* (1999) 'Doublecortin is a developmentally regulated, microtubule-associated protein expressed in migrating and differentiating neurons', *Neuron*, 23(2), pp. 247–256. doi: 10.1016/S0896-6273(00)80777-1.
Franco, S. J. *et al.* (2012) 'Fate-restricted neural progenitors in the mammalian cerebral cortex.', *Science*, 337(6095), pp. 746–749. doi: 10.1126/science.1223616.
Frödin, M. *et al.* (2000) 'A phosphoserine-regulated docking site in the protein

kinase RSK2 that recruits and activates PDK1', *EMBO Journal*, 19(12), pp. 2924–2934. doi: 10.1093/emboj/19.12.2924.
Frödin, M. *et al.* (2002) 'A phosphoserine/threonine-binding pocket in AGC kinases and PDK1 mediates activation by hydrophobic motif phosphorylation', *EMBO Journal*, 21(20), pp. 5396–5407. doi: 10.1093/emboj/cdf551.
Fukumitsu, H. *et al.* (2006) 'Brain-derived neurotrophic factor participates in determination of neuronal laminar fate in the developing mouse cerebral cortex', *Journal of Neuroscience*, 26(51), pp. 13218–13230. doi: 10.1523/JNEUROSCI.4251-06.2006.
Fukushima, M. *et al.* (2012) 'Alternative translation initiation gives rise to two isoforms of Orai1 with distinct plasma membrane mobilities', *Journal of Cell Science*, 125(18), pp. 4354–4361. doi: 10.1242/jcs.104919.

G

Gao, T., Toker, A. and Newton, A. C. (2001) 'The Carboxyl Terminus of Protein Kinase C Provides a Switch to Regulate Its Interaction with the Phosphoinositide-dependent Kinase, PDK-1', *Journal of Biological Chemistry*, 276(22), pp. 19588–19596. doi: 10.1074/jbc.M101357200.
Garcez, P. P. *et al.* (2015) 'Cenpj/CPAP regulates progenitor divisions and neuronal migration in the cerebral cortex downstream of Ascl1', *Nature communications*, 6, p. 6474. doi: 10.1038/ncomms7474.
García-Martínez, J. M. and Alessi, D. R. (2008) 'mTOR complex 2 (mTORC2) controls hydrophobic motif phosphorylation and activation of serum- and glucocorticoid-induced protein kinase 1 (SGK1).', *The Biochemical journal*, 416(3), pp. 375–385. doi: 10.1042/BJ20081668.
Gavériaux-Ruff, C. and Kieffer, B. L. (2007) 'Conditional gene targeting in the mouse nervous system: Insights into brain function and diseases', *Pharmacology and Therapeutics*, pp. 619–634. doi: 10.1016/j.pharmthera.2006.12.003.
Ghosh, S. *et al.* (2008) 'Instructive role of aPKCζ subcellular localization in the assembly of adherens junctions in neural progenitors', *Proceedings of the National Academy of Sciences of the United States of America*, 105(1), pp. 335–340. doi: 10.1073/pnas.0705713105.
Ghule, P. N. *et al.* (2007) 'Cell cycle dependent phosphorylation and subnuclear organization of the histone gene regulator p220NPAT in human embryonic stem cells', *Journal of Cellular Physiology*, 213(1), pp. 9–17. doi: 10.1002/jcp.21119.
Gibert-Rahola, J. and Villena-Rodriguez, A. (2014) 'Glutamatergic drugs for schizophrenia treatment', *Actas Espanolas de Psiquiatria*, 42(5), pp. 234–241.
Gong, X. *et al.* (2015) 'Activating the translational repressor 4E-BP or reducing S6K-GSK3β activity prevents accelerated axon growth induced by hyperactive mTOR in vivo', *Human Molecular Genetics*, 24(20), pp. 5746–5758. doi: 10.1093/hmg/ddv295.

Gonzales, K. A. U. *et al.* (2015) 'Deterministic Restriction on Pluripotent State Dissolution by Cell-Cycle Pathways Article Deterministic Restriction on Pluripotent State Dissolution by Cell-Cycle Pathways', *Cell*, 162(3), pp. 564–579. doi: 10.1016/j.cell.2015.07.001.
Gorski, J. A. *et al.* (2002) 'Cortical excitatory neurons and glia, but not GABAergic neurons, are produced in the Emx1-expressing lineage', *Journal of Neuroscience*, 22(15), pp. 6309–6314. doi: 10.1523/jneurosci.22-15-06309.2002.
Greig, L. C. *et al.* (2013) 'Molecular logic of neocortical projection neuron specification, development and diversity.', *Nature Reviews Neuroscience*, 14(11), pp. 755–69. doi: 10.1038/nrn3586.
Grove, J. R. *et al.* (1991) 'Cloning and expression of two human p70 S6 kinase polypeptides differing only at their amino termini.', *Molecular and Cellular Biology*, 11(11), pp. 5541–5550. doi: 10.1128/mcb.11.11.5541.
Gu, F. *et al.* (2015) 'Function of Slit/Robo signaling in breast cancer.', *Frontiers of medicine*, 9(4), pp. 431–436. doi: 10.1007/s11684-015-0416-9.
Gu, X. *et al.* (2017) 'SAMTOR is an S-adenosylmethionine sensor for the mTORC1 pathway', *Science*, 358(6364), pp. 813–818. doi: 10.1126/science.aao3265.
Guillemot, F. *et al.* (2017) 'Beyond proneural: emerging functions and regulations of proneural proteins', *Current Opinion in Neurobiology*, 42, pp. 93–101. doi: 10.1016/j.conb.2016.11.011.
Gundersen, H. J. and Jensen, E. B. (1987) 'The efficiency of systematic sampling in stereology and its prediction.', *Journal of microscopy*, 147(Pt 3), pp. 229–263. doi: 10.1111/j.1365-2818.1987.tb02837.x.
Guo, C. *et al.* (2013) 'Fezf2 expression identifies a multipotent progenitor for neocortical projection neurons, astrocytes, and oligodendrocytes', *Neuron*, 80(5), pp. 1167–1174. doi: 10.1016/j.neuron.2013.09.037.

H

Han, W. *et al.* (2011) 'TBR1 directly represses Fezf2 to control the laminar origin and development of the corticospinal tract', *Proceedings of the National Academy of Sciences of the United States of America*, 108(7), pp. 3041–3046. doi: 10.1073/pnas.1016723108.
Hanks, S. K. and Hunter, T. (1995) 'Protein kinases 6. The eukaryotic protein kinase superfamily: kinase (catalytic) domain structure and classification.', *FASEB journal : official publication of the Federation of American Societies for Experimental Biology*, 9(8), pp. 576–596.
Hapak, S. M., Rothlin, C. V and Ghosh, S. (2018) 'PAR3 – PAR6 – atypical PKC polarity complex proteins in neuronal polarization', *Cellular and Molecular Life Sciences*, 75(15), pp. 2735–2761. doi: 10.1007/s00018-018-2828-6.
Harada, H. *et al.* (2001) 'p70S6 kinase signals cell survival as well as growth, inactivating the pro-apoptotic molecule BAD', *Proceedings of the National Academy*

of Sciences of the United States of America, 98(17), pp. 9666–9670. doi: 10.1073/pnas.171301998.
Harb, K. *et al.* (2015) 'Area-specific development of distinct projection neuron subclasses is regulated by postnatal epigenetic modifications', *eLIFE*, 5, p. e09531. doi: 10.7554/eLife.09531.
Hashimoto, N. *et al.* (2006) 'Ablation of PDK1 in pancreatic β cells induces diabetes as a result of loss of β cell mass', *Nature Genetics*, 38(5), pp. 589–593. doi: 10.1038/ng1774.
Haubensak, W. *et al.* (2004) 'Neurons arise in the basal neuroepithelium of the early mammalian telencephalon: A major site of neurogenesis', *Proceedings of the National Academy of Sciences of the United States of America*, 101(9), pp. 3196–3201. doi: 10.1073/pnas.0308600100.
Hauge, C. *et al.* (2007) 'Mechanism for activation of the growth factor-activated AGC kinases by turn motif phosphorylation', *EMBO Journal*, 26(9), pp. 2251–2261. doi: 10.1038/sj.emboj.7601682.
Hauge, C. and Frödin, M. (2006) 'RSK and MSK in MAP kinase signalling', *Journal of Cell Science*, 119(15), pp. 3021–3023. doi: 10.1242/jcs.02950.
He, S. *et al.* (2015) 'Inside-Out Radial Migration Facilitates Lineage-Dependent Neocortical Microcircuit Assembly', *Neuron*, 86(5), pp. 1159–1166. doi: 10.1016/j.neuron.2015.05.002.
Heins, N. *et al.* (2002) 'Glial cells generate neurons: The role of the transcription factor Pax6', *Nature Neuroscience*, 5(4), pp. 308–315. doi: 10.1038/nn828.
Heras-Martínez, G. de las *et al.* (2019) 'A Complex Interplay of Anionic Phospholipid Binding Regulates 3'-Phosphoinositide-Dependent-Kinase-1 Homodimer Activation', *Scientific Reports*, 9(1), p. 14527. doi: 10.1038/s41598-019-50742-8.
Hevner, R. F. (2019) 'Intermediate progenitors and Tbr2 in cortical development', *Journal of Anatomy*, pp. 616–625. doi: 10.1111/joa.12939.
Hinton, H. J., Alessi, D. R. and Cantrell, D. A. (2004) 'The serine kinase phosphoinositide-dependent kinase 1 (PDK1) regulates T cell development', *Nature Immunology*, 5(5), pp. 539–545. doi: 10.1038/ni1062.
Hirai, H. (2018) 'Protein Kinase C in the Cerebellum: Its Significance and Remaining Conundrums', *Cerebellum*, 17(1), pp. 23–27. doi: 10.1007/s12311-017-0898-x.
Holz, M. K. *et al.* (2005) 'mTOR and S6K1 mediate assembly of the translation preinitiation complex through dynamic protein interchange and ordered phosphorylation events', *Cell*, 123(4), pp. 569–580. doi: 10.1016/j.cell.2005.10.024.
Hong, S. *et al.* (2014) 'Cross-talk between sirtuin and mammalian target of rapamycin complex 1 (mTORC1) signaling in the regulation of S6 kinase 1 (S6K1) phosphorylation', *Journal of Biological Chemistry*, 289(19), pp. 13132–13141. doi: 10.1074/jbc.M113.520734.
Hood, V. L. *et al.* (2019) 'Transcription of PIK3CD in human brain and

schizophrenia: Regulation by proinflammatory cytokines', *Human Molecular Genetics*, 28(19), pp. 3188–3198. doi: 10.1093/hmg/ddz144.
Howell, K. R., Floyd, K. and Law, A. J. (2017) 'PKBγ/AKT3 loss-of-function causes learning and memory deficits and deregulation of AKT/mTORC2 signaling: Relevance for schizophrenia', *PLoS ONE*, 12(5), pp. 1–21. doi: 10.1371/journal.pone.0175993.
Howes, O., McCutcheon, R. and Stone, J. (2015) 'Glutamate and dopamine in schizophrenia: An update for the 21st century', *Journal of Psychopharmacology*, pp. 97–115. doi: 10.1177/0269881114563634.
Huurne, M. *et al.* (2017) 'Distinct Cell-Cycle Control in Two Different States of Mouse Pluripotency Brief Report Distinct Cell-Cycle Control in Two Different States of Mouse Pluripotency', *Stem Cell*, 21(4), pp. 449-455.e4. doi: 10.1016/j.stem.2017.09.004.

I

Iacopetti, P. *et al.* (1999) 'Expression of the antiproliferative gene TIS21 at the onset of neurogenesis identifies single neuroepithelial cells that switch from proliferative to neuron-generating division.', *Proceedings of the National Academy of Sciences of the United States of America*, 96(8), pp. 4639–4644. doi: 10.1073/pnas.96.8.4639.
Ikenoue, T. *et al.* (2008) 'Essential function of TORC2 in PKC and Akt turn motif phosphorylation, maturation and signalling', *EMBO Journal*, 27(14), pp. 1919–1931. doi: 10.1038/emboj.2008.119.
Imai, F. *et al.* (2006) 'Inactivation of aPKClambda results in the loss of adherens junctions in neuroepithelial cells without affecting neurogenesis in mouse neocortex', *Development*, 133(9), pp. 1735–1744. doi: 10.1242/dev.02389.
Inada, H. *et al.* (2011) 'GABA regulates the multidirectional tangential migration of GABAergic interneurons in living neonatal mice', *PLoS ONE*, 6(12), p. e27048. doi: 10.1371/journal.pone.0027048.
Inoki, K., Zhu, T. and Guan, K. L. (2003) 'TSC2 Mediates Cellular Energy Response to Control Cell Growth and Survival', *Cell*, 115(5), pp. 577–590. doi: 10.1016/S0092-8674(03)00929-2.
Ip, C. K. M. *et al.* (2011) 'P70 S6 kinase in the control of actin cytoskeleton dynamics and directed migration of ovarian cancer cells', *Oncogene*, 30(21), pp. 2420–2432. doi: 10.1038/onc.2010.615.
Iqbal, S., Howard, S. and LoGrasso, P. V. (2015) 'Serum- and Glucocorticoid-Inducible Kinase 1 Confers Protection in Cell-Based and in In Vivo Neurotoxin Models via the c-Jun N-Terminal Kinase Signaling Pathway', *Molecular and Cellular Biology*, 35(11), pp. 1992–2006. doi: 10.1128/mcb.01510-14.
Itoh, Y. *et al.* (2016) 'PDK1–Akt pathway regulates radial neuronal migration and microtubules in the developing mouse neocortex', *Proceedings of the National*

Academy of Sciences, 113(21), pp. E2955–E2964. doi: 10.1073/pnas.1516321113.

J

Jensen, C. J. *et al.* (1999) '90-kDa ribosomal S6 kinase is phosphorylated and activated by 3- phosphoinositide-dependent protein kinase-1', *Journal of Biological Chemistry*, 274(38), pp. 27168–27176. doi: 10.1074/jbc.274.38.27168.
Jiang, M. and Chen, G. (2006) 'High Ca2+-phosphate transfection efficiency in low-density neuronal cultures', *Nature Protocols*, 1(2), pp. 695–700. doi: 10.1038/nprot.2006.86.
Jiao, S. and Li, Z. (2011) 'Nonapoptotic Function of BAD and BAX in Long-Term Depression of Synaptic Transmission', *Neuron*, 70(4), pp. 758–772. doi: 10.1016/j.neuron.2011.04.004.
Jiménez, C. *et al.* (2002) 'The p85 regulatory subunit controls sequential activation of phosphoinositide 3-kinase by Tyr kinases and Ras', *Journal of Biological Chemistry*, 277(44), pp. 41556–41562. doi: 10.1074/jbc.M205893200.
Jones, S. W. *et al.* (1988) 'A Xenopus ribosomal protein S6 kinase has two apparent kinase domains that are each similar to distinct protein kinases', *Proceedings of the National Academy of Sciences of the United States of America*, 85(10), pp. 3377–3381. doi: 10.1073/pnas.85.10.3377.

K

Ka, M. *et al.* (2014) 'mTOR regulates brain morphogenesis by mediating GSK3 signaling', *Development*, 141(21), pp. 4076–86. doi: 10.1242/dev.108282.
Ka, M. *et al.* (2017) 'MTOR controls genesis and autophagy of GABAergic interneurons during brain development', *Autophagy*, 13(8), pp. 1348–1363. doi: 10.1080/15548627.2017.1327927.
Karar, J. and Maity, A. (2011) 'PI3K/AKT/mTOR Pathway in Angiogenesis', *Frontiers in molecular neuroscience*, 4, p. 51. doi: 10.3389/fnmol.2011.00051.
Kawaguchi, A. *et al.* (2008) 'Single-cell gene profiling defines differential progenitor subclasses in mammalian neurogenesis', *Development*, 135(18), pp. 3113–3124. doi: 10.1242/dev.022616.
Kelly, A. P. *et al.* (2007) 'Notch-induced T cell development requires phosphoinositide-dependent kinase 1', *EMBO Journal*, 26(14), pp. 3441–3450. doi: 10.1038/sj.emboj.7601761.
Kilkenny, C. *et al.* (2010) 'Improving bioscience research reporting: The ARRIVE guidelines for reporting animal research', *Journal of Pharmacology and Pharmacotherapeutics*, 1(2), p. 94. doi: 10.4103/0976-500x.72351.
Klinkenberg, M. *et al.* (2012) 'Restriction of trophic factors and nutrients induces PARKIN expression', *Neurogenetics*, 13(1), pp. 9–21. doi: 10.1007/s10048-011-

0303-8.
Kochunov, P. and Hong, L. E. (2014) 'Neurodevelopmental and neurodegenerative models of schizophrenia: White matter at the center stage', *Schizophrenia Bulletin*, 40(4), pp. 721–728. doi: 10.1093/schbul/sbu070.
Kolk, S. M. *et al.* (2006) 'A unique subpopulation of Tbr1-expressing deep layer neurons in the developing cerebral cortex', *Molecular and Cellular Neuroscience*, pp. 200–214. doi: 10.1016/j.mcn.2005.08.022.
Komander, D. *et al.* (2004) 'Structural insights into the regulation of PDK1 by phosphoinositides and inositol phosphates', *EMBO Journal*, 23(20), pp. 3918–3928. doi: 10.1038/sj.emboj.7600379.
Komander, D. *et al.* (2005) 'Role of T-loop phosphorylation in PDK1 activation, stability, and substrate binding', *Journal of Biological Chemistry*, 280(19), pp. 18797–18802. doi: 10.1074/jbc.M500977200.
Kosach, V. *et al.* (2018) 'Nucleocytoplasmic distribution of S6K1 depends on the density and motility of MCF-7 cells in vitro', *F1000Research*, 7, p. 1332. doi: 10.12688/f1000research.15447.1.
Kosodo, Y. *et al.* (2004) 'Asymmetric distribution of the apical plasma membrane during neurogenic divisions of mamalian neuroepithelial cells', *EMBO Journal*, 23(11), pp. 2314–2324. doi: 10.1038/sj.emboj.7600223.
Kovalski, J. R. *et al.* (2019) 'The Functional Proximal Proteome of Oncogenic Ras Includes mTORC2', *Molecular Cell*, 73(4), pp. 830-844.e12. doi: 10.1016/j.molcel.2018.12.001.
Krall, A. S. *et al.* (2016) 'Asparagine promotes cancer cell proliferation through use as an amino acid exchange factor', *Nature Communications*, 7, p. 11457. doi: 10.1038/ncomms11457.
Kriegstein, A. R. and Noctor, S. C. (2004) 'Patterns of neuronal migration in the embryonic cortex.', *Trends in neurosciences*, 27(7), pp. 392–399. doi: 10.1016/j.tins.2004.05.001.
Kumamoto, T. *et al.* (2013) 'Foxg1 coordinates the switch from nonradially to radially migrating glutamatergic subtypes in the neocortex through spatiotemporal repression', *Cell Reports*, 3(3), pp. 931–945. doi: 10.1016/j.celrep.2013.02.023.
Kurebayashi, Y. *et al.* (2012) 'PI3K-Akt-mTORC1-S6K1/2 Axis Controls Th17 Differentiation by Regulating Gfi1 Expression and Nuclear Translocation of RORγ', *Cell Reports*, 1(4), pp. 360–373. doi: 10.1016/j.celrep.2012.02.007.

L

Lakomá, J., Garcia-Alonso, L. and Luque, J. M. (2011) 'Reelin sets the pace of neocortical neurogenesis', *Development*, 138(23), pp. 5223–5234. doi: 10.1242/dev.063776.
Lancaster, M. A. *et al.* (2013) 'Cerebral organoids model human brain development and microcephaly', *Nature*, 501(7467), pp. 373–379. doi: 10.1038/nature12517.

Lancaster, M. A. and Knoblich, J. A. (2012) 'Spindle orientation in mammalian cerebral cortical development', *Current Opinion in Neurobiology*, pp. 737–746. doi: 10.1016/j.conb.2012.04.003.
Lanctot, A. A. *et al.* (2017) 'Loss of Brap Results in Premature G1/S Phase Transition and Impeded Neural Progenitor Differentiation', *Cell Reports*, 20(5), pp. 1148–1160. doi: 10.1016/j.celrep.2017.07.018.
Lane, H. A. *et al.* (1993) 'p70s6k function is essential for G1 progression', *Nature*, 363(6425), pp. 170–172. doi: 10.1038/363170a0.
Lang, F. *et al.* (2010) 'Significance of SGK1 in the regulation of neuronal function', *Journal of Physiology*, pp. 3349–3354. doi: 10.1113/jphysiol.2010.190926.
Lara, R., Seckl, M. J. and Pardo, O. E. (2013) 'The p90 RSK family members: Common functions and isoform specificity', *Cancer Research*, pp. 5301–5308. doi: 10.1158/0008-5472.CAN-12-4448.
Lavdas, A. A. *et al.* (1999) 'The medial ganglionic eminence gives rise to a population of early neurons in the developing cerebral cortex', *Journal of Neuroscience*, 19(18), pp. 7881–7888. doi: 10.1523/jneurosci.19-18-07881.1999.
Law, A. J. *et al.* (2012) 'Neuregulin 1-ErbB4-PI3K signaling in schizophrenia and phosphoinositide 3-kinase-p110δ inhibition as a potential therapeutic strategy', *Proceedings of the National Academy of Sciences of the United States of America*, 109(30), pp. 12165–12170. doi: 10.1073/pnas.1206118109.
Lawlor, M. A. *et al.* (2002) 'Essential role of PDK1 in regulating cell size and development in mice', *EMBO Journal*, 21(14), pp. 3728–3738. doi: 10.1093/emboj/cdf387.
Lee, J. E. *et al.* (2016) 'S6K Promotes Dopaminergic Neuronal Differentiation Through PI3K/Akt/mTOR-Dependent Signaling Pathways in Human Neural Stem Cells', *Molecular Neurobiology*, 53(6), pp. 3771–3782. doi: 10.1007/s12035-015-9325-9.
Leroux, A. E. *et al.* (2019) 'Allosteric Regulation of Protein Kinases Downstream of PI3-Kinase Signalling', *Advances in experimental medicine and biology*. United States, 1163, pp. 279–311. doi: 10.1007/978-981-13-8719-7_12.
Leroux, A. E. and Biondi, R. M. (2020) 'Renaissance of Allostery to Disrupt Protein Kinase Interactions', *Trends in Biochemical Sciences*, 45(1), pp. 27–41. doi: 10.1016/j.tibs.2019.09.007.
Leroux, A. E., Schulze, J. O. and Biondi, R. M. (2018) 'AGC kinases, mechanisms of regulation and innovative drug development', *Seminars in Cancer Biology*. Elsevier, 48(May 2017), pp. 1–17. doi: 10.1016/j.semcancer.2017.05.011.
Levenga, J. *et al.* (2017) 'AKT isoforms have distinct hippocampal expression and roles in synaptic plasticity', *eLife*, 6, p. e30640. doi: 10.7554/eLife.30640.
Lewis, D. A. (2014) 'Inhibitory neurons in human cortical circuits: Substrate for cognitive dysfunction in schizophrenia', *Current Opinion in Neurobiology*, pp. 22–26. doi: 10.1016/j.conb.2013.11.003.
Li, G. *et al.* (2008) 'Regional distribution of cortical interneurons and development of

inhibitory tone are regulated by Cxcl12/Cxcr4 signaling', *Journal of Neuroscience*, 28(5), pp. 1085–1098. doi: 10.1523/JNEUROSCI.4602-07.2008.
Li, S. *et al.* (2012) 'GSK3 Temporally Regulates Neurogenin 2 Proneural Activity in the Neocortex', *Journal of Neuroscience*, 32(23), pp. 7791–7805. doi: 10.1523/JNEUROSCI.1309-12.2012.
Liang, H., Hippenmeyer, S. and Ghashghaei, H. T. (2012) 'A Nestin-cre transgenic mouse is insufficient for recombination in early embryonic neural progenitors', *Biology Open*, 1(12), pp. 1200–1203. doi: 10.1242/bio.20122287.
Lim, L. *et al.* (2018) 'Development and Functional Diversification of Cortical Interneurons', *Neuron*, 100(2), pp. 294–313. doi: 10.1016/j.neuron.2018.10.009.
Liu, G. Y. and Sabatini, D. M. (2020) 'mTOR at the nexus of nutrition, growth, ageing and disease', *Nature Reviews Molecular Cell Biology*, 21(4), pp. 183–203. doi: 10.1038/s41580-019-0199-y.
Liu, P. *et al.* (2015) 'Ptdins(3,4,5) P3 -dependent activation of the mTORC2 kinase complex', *Cancer Discovery*, 5(11), pp. 1194–11209. doi: 10.1158/2159-8290.CD-15-0460.
Lizcano, J. M. and Alessi, D. R. (2002) 'The insulin signalling pathway', *Current Biology*, pp. 10–13. doi: 10.1016/S0960-9822(02)00777-7.
Lodato, S. *et al.* (2011) 'Excitatory Projection Neuron Subtypes Control the Distribution of Local Inhibitory Interneurons in the Cerebral Cortex', *Neuron*, 69(4), pp. 763–779. doi: 10.1016/j.neuron.2011.01.015.
Lodato, S. and Arlotta, P. (2015) 'Generating Neuronal Diversity in the Mammalian Cerebral Cortex', *Annual Review of Cell and Developmental Biology*, 31(1), pp. 699–720. doi: 10.1146/annurev-cellbio-100814-125353.
López-Bendito, G. *et al.* (2008) 'Chemokine signaling controls intracortical migration and final distribution of GABAergic interneurons', *Journal of Neuroscience*, 28(7), pp. 1613–1624. doi: 10.1523/JNEUROSCI.4651-07.2008.
Lopez-Garcia, L. A. *et al.* (2011) 'Allosteric regulation of protein kinase PKCζ by the N-terminal C1 domain and small compounds to the PIF-pocket', *Chemistry and Biology*, 18(11), pp. 1463–1473. doi: 10.1016/j.chembiol.2011.08.010.
Lu, I. L. *et al.* (2018) 'Identification of genes associated with cortical malformation using a transposon-mediated somatic mutagenesis screen in mice', *Nature Communications*, 9(1), p. 2498. doi: 10.1038/s41467-018-04880-8.
Lučic, I. *et al.* (2018) 'Conformational sampling of membranes by Akt controls its activation and inactivation', *Proceedings of the National Academy of Sciences of the United States of America*, 115(17), pp. E3940–E3949. doi: 10.1073/pnas.1716109115.
Lukaszewicz, A. *et al.* (2002) 'Contrasting effects of basic fibroblast growth factor and neurotrophin 3 on cell cycle kinetics of mouse cortical stem cells', *Journal of Neuroscience*, 22(15), pp. 6610–6622. doi: 10.1523/jneurosci.22-15-06610.2002.

M

Ma, L. *et al.* (2005) 'Phosphorylation and functional inactivation of TSC2 by Erk: Implications for tuberous sclerosis and cancer pathogenesis', *Cell*, 121(2), pp. 179–193. doi: 10.1016/j.cell.2005.02.031.
Mahalingam, M. and Templeton, D. J. (1996) 'Constitutive activation of S6 kinase by deletion of amino-terminal autoinhibitory and rapamycin sensitivity domains.', *Molecular and Cellular Biology*, 16(1), pp. 405–413. doi: 10.1128/mcb.16.1.405.
Malatesta, P., Hartfuss, E. and Götz, M. (2000) 'Isolation of radial glial cells by fluorescent-activated cell sorting reveals a neuronal lineage.', *Development*, 127(24), pp. 5253–5263.
Manuel, M. *et al.* (2007) 'Controlled overexpression of Pax6 in vivo negatively auto-regulates the Pax6 locus, causing cell-autonomous defects of late cortical progenitor proliferation with little effect on cortical arealization', *Development*, 134(3), pp. 545–555. doi: 10.1242/dev.02764.
Mao, Y. *et al.* (2009) 'Disrupted in Schizophrenia 1 Regulates Neuronal Progenitor Proliferation via Modulation of GSK3 b / b -Catenin Signaling', *Cell*, 136(6), pp. 1017–1031. doi: 10.1016/j.cell.2008.12.044.
Marín, O. *et al.* (2003) 'Directional guidance of interneuron migration to the cerebral cortex relies on subcortical Slit1/2-independent repulsion and cortical attraction', *Development*, pp. 1889–1901. doi: 10.1242/dev.00417.
Marín, O. *et al.* (2010) 'Guiding neuronal cell migrations.', *Cold Spring Harbor perspectives in biology*, 2(2), p. a001834. doi: 10.1101/cshperspect.a001834.
Marín, O. (2013) 'Cellular and molecular mechanisms controlling the migration of neocortical interneurons', *European Journal of Neuroscience*, 38(1), pp. 2019–2029. doi: 10.1111/ejn.12225.
Martineau, Y. *et al.* (2014) 'Control of Paip1-Eukayrotic Translation Initiation Factor 3 Interaction by Amino Acids through S6 Kinase', *Molecular and Cellular Biology*, 34(6), pp. 1046–1053. doi: 10.1128/mcb.01079-13.
Masters, T. A. *et al.* (2010) 'Regulation of 3-phosphoinositide-dependent protein kinase 1 activity by homodimerization in live cells', *Science signaling*, 3(145), p. ra78. doi: 10.1126/scisignal.2000738.
McCoy, C. E. *et al.* (2005) 'MSK1 activity is controlled by multiple phosphorylation sites', *Biochemical Journal*, 387(2), pp. 507–517. doi: 10.1042/BJ20041501.
McGuire, P. *et al.* (2008) 'Functional neuroimaging in schizophrenia: diagnosis and drug discovery', *Trends in pharmacological sciences*. England, 29(2), pp. 91–98. doi: 10.1016/j.tips.2007.11.005.
McKenna, W. L. *et al.* (2011) 'Tbr1 and Fezf2 regulate alternate corticofugal neuronal identities during neocortical development', *Journal of Neuroscience*, 31(2), pp. 549–564. doi: 10.1523/JNEUROSCI.4131-10.2011.
McManus, E. J. *et al.* (2004) 'The in vivo role of PtdIns(3,4,5)P3 binding to PDK1 PH domain defined by knockin mutation', *EMBO Journal*, 23(10), pp. 2071–2082.

doi: 10.1038/sj.emboj.7600218.
Mcquin, C. *et al.* (2018) 'CellProfiler 3.0: Next-generation image processing for biology', *PLoS Biology*, 16(7), p. e2005970.
Meng, D. *et al.* (2020) 'Glutamine and asparagine activate mTORC1 independently of Rag GTPases', *The Journal of biological chemistry*, 295(10), pp. 2890–2899. doi: 10.1074/jbc.AC119.011578.
Meng, P. *et al.* (2019) 'Leonurine promotes neurite outgrowth and neurotrophic activity by modulating the GR/SGK1 signaling pathway in cultured PC12 cells', *NeuroReport*, 30(4), pp. 247–254. doi: 10.1097/WNR.0000000000001180.
Mihalas, A. B. *et al.* (2016) 'Intermediate Progenitor Cohorts Differentially Generate Cortical Layers and Require Tbr2 for Timely Acquisition of Neuronal Subtype Identity', *Cell Reports*, 16(1), pp. 92–105. doi: 10.1016/j.celrep.2016.05.072.
Mitchell, N. C. *et al.* (2015) 'S6 Kinase is essential for MYC-dependent rDNA transcription in Drosophila', *Cellular Signalling*, 27(10), pp. 2045–2053. doi: 10.1016/j.cellsig.2015.07.018.
Miyata, T. *et al.* (2001) 'Asymmetric inheritance of radial glial fibers by cortical neurons', *Neuron*, 31(5), pp. 727–741. doi: 10.1016/S0896-6273(01)00420-2.
Miyata, T. *et al.* (2004) 'Asymmetric production of surface-dividing and non-surface-dividing cortical progenitor cells', *Development*, 131(13), pp. 3133–3145. doi: 10.1242/dev.01173.
Moffat, J. J. *et al.* (2015) 'Genes and brain malformations associated with abnormal neuron positioning', *Molecular Brain*, p. 72. doi: 10.1186/s13041-015-0164-4.
Molyneaux, B. J. *et al.* (2007) 'Neuronal subtype specification in the cerebral cortex', *Nature Reviews Neuroscience*, 8(6), pp. 427–437. doi: 10.1038/nrn2151.
Mora, A. *et al.* (2003) 'Deficiency of PDK1 in cardiac muscle results in heart failure and increased sensitivity to hypoxia', *EMBO Journal*, 22(18), pp. 4666–4676. doi: 10.1093/emboj/cdg469.
Mora, A. *et al.* (2004) 'PDK1, the master regulator of AGC kinase signal transduction', *Seminars in Cell and Developmental Biology*, 15(2), pp. 161–170. doi: 10.1016/j.semcdb.2003.12.022.
Mora, A. *et al.* (2005) 'Deficiency of PDK1 in liver results in glucose intolerance, impairment of insulin-regulated gene expression and liver failure', *The Biochemical journal*, 385(Pt 3), pp. 639–648. doi: 10.1042/BJ20041782.
Muzio, L. and Mallamaci, A. (2003) 'Emx1, Emx2 and Pax6 in specification, regionalization and arealization of the cerebral cortex', *Cerebral Cortex*, 13(6), pp. 641–647. doi: 10.1093/cercor/13.6.641.

N

Nagy, A. (2000) 'Cre recombinase: The universal reagent for genome tailoring', *Genesis*, 26(2), pp. 99–109. doi: 10.1002/(SICI)1526-968X(200002)26:2<99::AID-GENE1>3.0.CO;2-B.

Naqvi, S., Martin, K. J. and Arthur, J. S. C. (2014) 'CREB phosphorylation at Ser133 regulates transcription via distinct mechanisms downstream of cAMP and MAPK signalling', *Biochemical Journal*, 458(3), pp. 469–479. doi: 10.1042/BJ20131115.
Nicklin, P. *et al.* (2009) 'Bidirectional Transport of Amino Acids Regulates mTOR and Autophagy', *Cell*, 136(3), pp. 521–534. doi: 10.1016/j.cell.2008.11.044.
Nieto, R., Kukuljan, M. and Silva, H. (2013) 'BDNF and schizophrenia: From neurodevelopment to neuronal plasticity, learning, and memory', *Frontiers in Psychiatry*, p. 45. doi: 10.3389/fpsyt.2013.00045.
Niwa, H., Yamamura, K. and Miyazaki, J. (1991) 'Efficient selection for high-expression transfectants with a novel eukaryotic vector', *Gene*, 108(2), pp. 193–199. doi: 10.1016/0378-1119(91)90434-d.
Noctor, S. C. *et al.* (2004) 'Cortical neurons arise in symmetric and asymmetric division zones and migrate through specific phases', *Nature Neuroscience*, 7(2), pp. 136–144. doi: 10.1038/nn1172.
Noctor SC, Flint AC, Weissman TA, Dammerman RS, K. A. (2001) 'Neurons derived from radial glial cells establish radial units in neocortex', *Nature*, 409(6821), pp. 714–720.
Noorolyai, S. *et al.* (2019) 'The relation between PI3K/AKT signalling pathway and cancer', *Gene*, pp. 120–128. doi: 10.1016/j.gene.2019.02.076.
Numakawa, T. *et al.* (2013) 'Brain-derived neurotrophic factor and glucocorticoids: Reciprocal influence on the central nervous system', *Neuroscience*, pp. 157–172. doi: 10.1016/j.neuroscience.2012.09.073.

O

Ohanna, M. *et al.* (2005) 'Atrophy of S6K1-/- skeletal muscle cells reveals distinct mTOR effectors for cell cycle and size control', *Nature Cell Biology*, 7(3), pp. 286–294. doi: 10.1038/ncb1231.
Oishi, K. *et al.* (2016) 'Identity of neocortical layer 4 neurons is specified through correct positioning into the cortex', *eLife*, 5, p. e10907. doi: 10.7554/eLife.10907.
Orike, N. *et al.* (2001) 'Role of PI 3-kinase, Akt and Bcl-2-related proteins in sustaining the survival of neurotrophic factor-independent adult sympathetic neurons', *Journal of Cell Biology*, 154(5), pp. 995–1005. doi: 10.1083/jcb.200101068.

P

Papaleo, F. *et al.* (2016) 'Behavioral, neurophysiological, and synaptic impairment in a transgenic neuregulin1 (NRG1-IV) murine schizophrenia model', *Journal of Neuroscience*, 36(17), pp. 4859–4875. doi: 10.1523/JNEUROSCI.4632-15.2016.

Paradis, S. *et al.* (1999) 'A PDK1 homolog is necessary and sufficient to transduce AGE-1 PI3 kinase signals that regulate diapause in Caenorhabditis elegans', *Genes and Development*, 13(11), pp. 1438–1452. doi: 10.1101/gad.13.11.1438.
Pardo, O. E. and Seckl, M. J. (2013) 'S6K2: The neglected S6 kinase family member', *Frontiers in Oncology*, p. 191. doi: 10.3389/fonc.2013.00191.
Paridaen, J. T. and Huttner, W. B. (2014) 'Neurogenesis during development of the vertebrate central nervous system', *EMBO Reports*, pp. 351–364. doi: 10.1002/embr.201438447.
Park, M. K. *et al.* (2019) 'PTEN self-regulates through USP11 via the PI3K-FOXO pathway to stabilize tumor suppression', *Nature Communications*, 10(1), p. 636. doi: 10.1038/s41467-019-08481-x.
Pauklin, S. and Vallier, L. (2013) 'The cell-cycle state of stem cells determines cell fate propensity', *Cell*, 155(1), pp. 135–47. doi: 10.1016/j.cell.2013.08.031.
Pearce, L. R., Komander, D. and Alessi, D. R. (2010) 'The nuts and bolts of AGC protein kinases', *Nature Reviews Molecular Cell Biology*, 11(1), pp. 9–22. doi: 10.1038/nrm2822.
Pearson, R. B. *et al.* (1995) 'The principal target of rapamycin-induced p70s6k inactivation is a novel phosphorylation site within conserved hydrophobic domain', *EMBO Journal*, 14(21), pp. 5279–5287. doi: 10.1002/j.1460-2075.1995.tb00212.x.
Pelorosso, C. *et al.* (2019) 'Somatic double-hit in MTOR and RPS6 in hemimegalencephaly with intractable epilepsy.', *Human molecular genetics*, 28(22), pp. 3755–3765. doi: 10.1093/hmg/ddz194.
Pende, M. *et al.* (2004) 'S6K1(-/-)/S6K2(-/-) Mice Exhibit Perinatal Lethality and Rapamycin-Sensitive 5 J -Terminal Oligopyrimidine mRNA Translation and Reveal a Mitogen-Activated Protein Kinase-Dependent S6 Kinase Pathway', *Molecular and Cellular Biology*, 24(8), pp. 3112–3124. doi: 10.1128/MCB.24.8.3112.
Petritsch, C. *et al.* (2000) 'TGF-β inhibits p70 S6 kinase via protein phosphatase 2A to induce G1 arrest', *Genes and Development*, 14(24), pp. 3093–3101. doi: 10.1101/gad.854200.
del Pino, I., Rico, B. and Marín, O. (2018) 'Neural circuit dysfunction in mouse models of neurodevelopmental disorders', *Current Opinion in Neurobiology*, 48, pp. 174–182. doi: 10.1016/j.conb.2017.12.013.
Pla, R. *et al.* (2006) 'Layer acquisition by cortical GABAergic interneurons is independent of reelin signaling', *Journal of Neuroscience*, 26(26), pp. 6924–6934. doi: 10.1523/JNEUROSCI.0245-06.2006.
Polleux, F. *et al.* (1997) 'Regulation of neuroblast cell-cycle kinetics plays a crucial role in the generation of unique features of neocortical areas', *Journal of Neuroscience*, 17(20), pp. 7763–7783. doi: 10.1523/jneurosci.17-20-07763.1997.
Polleux, F. *et al.* (2002) 'Control of cortical interneuron migration by neurotrophins and PI3-kinase signaling', *Development*, pp. 3147–3160.
Poopal, A. C. *et al.* (2016) 'Increased expression of the PI3K catalytic subunit p110δ underlies elevated S6 phosphorylation and protein synthesis in an individual

with autism from a multiplex family', *Molecular autism*, 7, p. 3. doi: 10.1186/s13229-015-0066-4.
Postel, M. *et al.* (2019) 'A multiscale mathematical model of cell dynamics during neurogenesis in the mouse cerebral cortex', *BMC Bioinformatics*, 20(1), p. 470. doi: 10.1186/s12859-019-3018-8.
Price, D. J., Mukhopadhyay, N. K. and Avruch, J. (1991) 'Insulin-activated protein kinases phosphorylate a pseudosubstrate synthetic peptide inhibitor of the p70 S6 kinase', *Journal of Biological Chemistry*, 266(25), pp. 16281–16284.
Prigent, C. and Dimitrov, S. (2003) 'Phosphorylation of serine 10 in histone H3, what for?', *Journal of Cell Science*, 116(18), pp. 3677–3685. doi: 10.1242/jcs.00735.
Puighermanal, E. *et al.* (2017) 'Ribosomal protein s6 phosphorylation is involved in novelty-induced locomotion, synaptic plasticity and mRNA translation', *Frontiers in Molecular Neuroscience*, 10, p. 419. doi: 10.3389/fnmol.2017.00419.
Pullen, N. *et al.* (1998) 'Phosphorylation and activation of p70(s6k) by PDK1', *Science*, 279(5351), pp. 707–710. doi: 10.1126/science.279.5351.707.

Q

Quadrato, G. *et al.* (2017) 'Cell diversity and network dynamics in photosensitive human brain organoids', *Nature*, 545(7652), pp. 48–53. doi: 10.1038/nature22047.
Quan, X. J. *et al.* (2016) 'Post-translational Control of the Temporal Dynamics of Transcription Factor Activity Regulates Neurogenesis', *Cell*, 164(3), pp. 460–475. doi: 10.1016/j.cell.2015.12.048.
Quinn, J. C. *et al.* (2007) 'Pax6 controls cerebral cortical cell number by regulating exit from the cell cycle and specifies cortical cell identity by a cell autonomous mechanism', *Developmental Biology*, 302(1), pp. 50–65. doi: 10.1016/j.ydbio.2006.08.035.

R

Rai, S. N. *et al.* (2019) 'The Role of PI3K / Akt and ERK in Neurodegenerative Disorders', *Neurotoxicity Research*, 35(3), pp. 775–795. doi: 10.1007/s12640-019-0003-y.
Rakic, P. (2003) 'Developmental and evolutionary adaptations of cortical radial glia', *Cerebral Cortex*, pp. 541–549. doi: 10.1093/cercor/13.6.541.
Reichardt, L. F. (2006) 'Neurotrophin-regulated signalling pathways', *Philosophical Transactions of the Royal Society B: Biological Sciences*, pp. 1545–1564. doi: 10.1098/rstb.2006.1894.
Reif, A. *et al.* (2006) 'Neural stem cell proliferation is decreased in schizophrenia, but not in depression', *Molecular Psychiatry*, 11(5), pp. 514–522. doi:

10.1038/sj.mp.4001791.
Rettenmaier, T. J. *et al.* (2014) 'A small-molecule mimic of a peptide docking motif inhibits the protein kinase PDK1', *Proceedings of the National Academy of Sciences of the United States of America*, 111(52), pp. 18590–18595. doi: 10.1073/pnas.1415365112.
Reyskens, K. M. S. E. and Arthur, J. S. C. (2016) 'Emerging roles of the mitogen and stress activated kinases MSK1 and MSK2', *Frontiers in Cell and Developmental Biology*, p. 56. doi: 10.3389/fcell.2016.00056.
Richards, S. A. *et al.* (2001) 'Characterization of Regulatory Events Associated with Membrane Targeting of p90 Ribosomal S6 Kinase 1', *Molecular and Cellular Biology*, 21(21), pp. 7470–7480. doi: 10.1128/mcb.21.21.7470-7480.2001.
Robertson, H., Hayes, J. D. and Sutherland, C. (2018) 'A partnership with the proteasome; the destructive nature of GSK3', *Biochemical Pharmacology*, pp. 77–92. doi: 10.1016/j.bcp.2017.10.016.
Rogala, K. B. *et al.* (2019) 'Structural basis for the docking of mTORC1 on the lysosomal surface', *Science*, 366(6464), pp. 468–475. doi: 10.1126/science.aay0166.
Romeo, Y., Zhang, X. and Roux, P. P. (2012) 'Regulation and function of the RSK family of protein kinases', *Biochemical Journal*, pp. 553–569. doi: 10.1042/BJ20110289.
Romero-Grimaldi, C., Moreno-López, B. and Estrada, C. (2008) 'Age-Dependent Effect of Nitric Oxide on Subventricular Zone and Olfactory Bulb', *Journal of Comparative Neurology*, 506(2), pp. 339–46. doi: 10.1002/cne.
Rosner, M. and Hengstschla, M. (2011) 'Nucleocytoplasmic localization of p70 S6K1 , but not of its isoforms p85 and p31 , is regulated by TSC2 / mTOR', *Oncogene*, 30(44), pp. 4509–4522. doi: 10.1038/onc.2011.165.
Roux, P. P. *et al.* (2004) 'Tumor-promoting phorbol esters and activated Ras inactivate the tuberous sclerosis tumor suppressor complex via p90 ribosomal S6 kinase', *Proceedings of the National Academy of Sciences of the United States of America*, 101(37), pp. 13489–13494. doi: 10.1073/pnas.0405659101.
Roux, P. P. *et al.* (2007) 'RAS/ERK signaling promotes site-specific ribosomal protein S6 phosphorylation via RSK and stimulates cap-dependent translation', *Journal of Biological Chemistry*, 282(19), pp. 14056–14064. doi: 10.1074/jbc.M700906200.
Rueda, P. *et al.* (2008) 'The CXCL12γ chemokine displays unprecedented structural and functional properties that make it a paradigm of chemoattractant proteins', *PLoS ONE*, 3(7), p. e2543. doi: 10.1371/journal.pone.0002543.
Ruvinsky, I. *et al.* (2005) 'Ribosomal protein S6 phosphorylation is a determinant of cell size and glucose homeostasis', *Genes and Development*, 19(18), pp. 2199–2211. doi: 10.1101/gad.351605.

S

Saha, S. *et al.* (2005) 'A systematic review of the prevalence of schizophrenia', *PLoS Medicine*, pp. 0413–0433. doi: 10.1371/journal.pmed.0020141.
Sakoda, H. *et al.* (2003) 'Differing roles of Akt and serum- and glucocorticoid-regulated kinase in glucose metabolism, DNA synthesis, and oncogenic activity', *Journal of Biological Chemistry*, 278(28), pp. 25802–25807. doi: 10.1074/jbc.M301127200.
Salic, A. and Mitchison, T. J. (2008) 'A chemical method for fast and sensitive detection of DNA synthesis in vivo.', *Proceedings of the National Academy of Sciences of the United States of America*, 105(7), pp. 2415–2420. doi: 10.1073/pnas.0712168105.
Sancak, Y. *et al.* (2007) 'PRAS40 Is an Insulin-Regulated Inhibitor of the mTORC1 Protein Kinase', *Molecular Cell*, 25(6), pp. 903–915. doi: 10.1016/j.molcel.2007.03.003.
Sancak, Y. *et al.* (2008) 'The rag GTPases bind raptor and mediate amino acid signaling to mTORC1', *Science*, 320(5882), pp. 1496–1501. doi: 10.1126/science.1157535.
Sánchez-Alcañiz, J. A. *et al.* (2011) 'Cxcr7 Controls Neuronal Migration by Regulating Chemokine Responsiveness', *Neuron*, 69(1), pp. 77–90. doi: 10.1016/j.neuron.2010.12.006.
Sansom, S. N. *et al.* (2009) 'The level of the transcription factor Pax6 is essential for controlling the balance between neural stem cell self-renewal and neurogenesis', *PLoS Genetics*, 5(6), p. e1000511. doi: 10.1371/journal.pgen.1000511.
Schwab, M. S. *et al.* (1999) 'p70 S6K Controls Selective mRNA Translation during Oocyte Maturation and Early Embryogenesis in Xenopus laevis', *Molecular and Cellular Biology*, 19(4), pp. 2485–2494.
Sessa, A. *et al.* (2008) 'Tbr2 Directs Conversion of Radial Glia into Basal Precursors and Guides Neuronal Amplification by Indirect Neurogenesis in the Developing Neocortex', *Neuron*, 60(1), pp. 56–69. doi: 10.1016/j.neuron.2008.09.028.
Sessa, A. *et al.* (2017) 'The Tbr2 Molecular Network Controls Cortical Neuronal Differentiation Through Complementary Genetic and Epigenetic Pathways', *Cerebral Cortex*, 27(6), pp. 3378–3396. doi: 10.1093/cercor/bhw270.
Shah, O. J., Wang, Z. and Hunter, T. (2004) 'Inappropriate activation of the TSC/Rheb/mTOR/S6K cassette induces IRS1/2 depletion, insulin resistance, and cell survival deficiencies.', *Current biology*. England, 14(18), pp. 1650–1656. doi: 10.1016/j.cub.2004.08.026.
Shen, J. *et al.* (1999) 'Determination of the rate of the glutamate/glutamine cycle in the human brain by in vivo 13C NMR', *Proceedings of the National Academy of Sciences of the United States of America*, 96(14), pp. 8235–8240. doi:

10.1073/pnas.96.14.8235.
Shen, K., Choe, A. and Sabatini, D. M. (2017) 'Intersubunit Crosstalk in the Rag GTPase Heterodimer Enables mTORC1 to Respond Rapidly to Amino Acid Availability', *Molecular Cell*, 68(3), pp. 552-565.e8. doi: 10.1016/j.molcel.2017.09.026.
Shi, S. H., Jan, L. Y. and Jan, Y. N. (2003) 'Hippocampal neuronal polarity specified by spatially localized mPar3/mPar6 and PI 3-kinase activity', *Cell*, pp. 63–75. doi: 10.1016/S0092-8674(02)01249-7.
Silbereis, J. C. *et al.* (2016) 'The Cellular and Molecular Landscapes of the Developing Human Central Nervous System', *Neuron*, pp. 248–68. doi: 10.1016/j.neuron.2015.12.008.
Silva, C. G. *et al.* (2018) 'Cell-Intrinsic Control of Interneuron Migration Drives Cortical Morphogenesis', *Cell*, 172(5), pp. 1063-1078.e19. doi: 10.1016/j.cell.2018.01.031.
Smith, J. A. *et al.* (1999) 'Identification of an extracellular signal-regulated kinase (ERK) docking site in ribosomal S6 kinase, a sequence critical for activation by ERK in vivo', *Journal of Biological Chemistry*, 274(5), pp. 2893–2898. doi: 10.1074/jbc.274.5.2893.
Southwell, D. G. *et al.* (2012) 'Intrinsically determined cell death of developing cortical interneurons', *Nature*, 490(7422), pp. 109–113. doi: 10.1038/nature11523.
Staal, S. P., Hartley, J. W. and Rowe, W. P. (1977) 'Isolation of transforming murine leukemia viruses from mice with a high incidence of spontaneous lymphoma', *Proceedings of the National Academy of Sciences of the United States of America*, 74(7), pp. 3065–3067. doi: 10.1073/pnas.74.7.3065.
Stone, J. M. *et al.* (2010) 'Altered relationship between hippocampal glutamate levels and striatal dopamine function in subjects at ultra high risk of psychosis', *Biological Psychiatry*. Elsevier Inc., 68(7), pp. 599–602. doi: 10.1016/j.biopsych.2010.05.034.
Stone, J. M., Morrison, P. D. and Pilowsky, L. S. (2007) 'Glutamate and dopamine dysregulation in schizophrenia--a synthesis and selective review.', *Journal of psychopharmacology*. United States, 21(4), pp. 440–452. doi: 10.1177/0269881106073126.
Stottmann, R. W. *et al.* (2013) 'A mutation in Tubb2b, a human polymicrogyria gene, leads to lethality and abnormal cortical development in the mouse', *Human Molecular Genetics*, 22(20), pp. 4053–4063. doi: 10.1093/hmg/ddt255.
Stumm, R. K. *et al.* (2003) 'CXCR4 regulates interneuron migration in the developing neocortex', *Journal of Neuroscience*, 23(12), pp. 5123–5130. doi: 10.1523/jneurosci.23-12-05123.2003.

T

Tamamaki, N. *et al.* (2003) 'Evidence that Sema3A and Sema3F regulate the

migration of GABAergic neurons in the developing neocortex', *Journal of Comparative Neurology*, 455(2), pp. 238–248. doi: 10.1002/cne.10476.
Tamamaki, N., Fujimori, K. E. and Takauji, R. (1997) 'Origin and route of tangentially migrating neurons in the developing neocortical intermediate zone', *Journal of Neuroscience*, 17(21), pp. 8313–8323. doi: 10.1523/jneurosci.17-21-08313.1997.
Tamura, M. *et al.* (2016) 'Developmental Inhibition of Gsk3 Rescues Behavioral and Neurophysiological Deficits in a Mouse Model of Schizophrenia Predisposition', *Neuron*, 89(5), pp. 1100–1109. doi: 10.1016/j.neuron.2016.01.025.
Tanaka, D. H. *et al.* (2010) 'CXCR4 is required for proper regional and laminar distribution of cortical somatostatin-, calretinin-, and neuropeptide Y-expressing gabaergic interneurons', *Cerebral Cortex*, 20(12), pp. 2810–2817. doi: 10.1093/cercor/bhq027.
Tanaka, T. *et al.* (2004) 'Lis1 and doublecortin function with dynein to mediate coupling of the nucleus to the centrosome in neuronal migration', *Journal of Cell Biology*, 165(5), pp. 709–721. doi: 10.1083/jcb.200309025.
Tavares, M. R. *et al.* (2015) 'The S6K protein family in health and disease', *Life Sciences*, 131, pp. 1–10. doi: 10.1016/j.lfs.2015.03.001.
Thorpe, L. M., Yuzugullu, H. and Zhao, J. J. (2015) 'PI3K in cancer: Divergent roles of isoforms, modes of activation and therapeutic targeting', *Nature Reviews Cancer*, 15(1), pp. 7–24. doi: 10.1038/nrc3860.
Tiveron, M. C. *et al.* (2006) 'Molecular interaction between projection neuron precursors and invading interneurons via stromal-derived factor 1 (CXCL12)/CXCR4 signaling in the cortical subventricular zone/intermediate zone', *Journal of Neuroscience*, 26(51), pp. 13273–13278. doi: 10.1523/JNEUROSCI.4162-06.2006.
Tokuda, S. *et al.* (2011) 'A novel Akt3 mutation associated with enhanced kinase activity and seizure susceptibility in mice', *Human Molecular Genetics*, 20(5), pp. 988–999. doi: 10.1093/hmg/ddq544.
Toma, K. *et al.* (2014) 'The timing of upper-layer neurogenesis is conferred by sequential derepression and negative feedback from deep-layer neurons', *Journal of Neuroscience*, 34(39), pp. 13259–13276. doi: 10.1523/JNEUROSCI.2334-14.2014.
Toma, K. and Hanashima, C. (2015) 'Switching modes in corticogenesis: Mechanisms of neuronal subtype transitions and integration in the cerebral cortex', *Frontiers in Neuroscience*, 9, p. 274. doi: 10.3389/fnins.2015.00274.
Tronche, F. *et al.* (1999) 'Disruption of the glucocorticoid receptor gene in the nervous system results in reduced anxiety', *Nature Genetics*, 23(1), pp. 99–103. doi: 10.1038/12703.
Tungadi, E. A. *et al.* (2017) 'Human microcephaly ASPM protein is a spindle pole-focusing factor that functions redundantly with CDK5RAP2', *Journal of Cell Science*, 130(21), pp. 3676–3684. doi: 10.1242/jcs.203703.

Tyagarajan, S. K. *et al.* (2011) 'Regulation of GABAergic synapse formation and plasticity by GSK3β-dependent phosphorylation of gephyrin', *Proceedings of the National Academy of Sciences of the United States of America*, 108(1), pp. 379–384. doi: 10.1073/pnas.1011824108.

U

Um, S. H., Frigerio, F. and Watanabe, M. (2004) 'Absence of S6K1 protects against age- and diet-induced obesity while enhancing insulin sensitivity', *Nature*, 431(7005), pp. 200–5. doi: 10.1038/nature02866.

V

Vanhaesebroeck, B. *et al.* (2010) 'The emerging mechanisms of isoform-specific PI3K signalling', *Nature Reviews Molecular Cell Biology*, 11(5), pp. 329–341. doi: 10.1038/nrm2882.

Vanhaesebroeck, B., Stephens, L. and Hawkins, P. (2012) 'PI3K signalling: The path to discovery and understanding', *Nature Reviews Molecular Cell Biology*. Nature Publishing Group, 13(3), pp. 195–203. doi: 10.1038/nrm3290.

Venigalla, R. K. C. *et al.* (2013) 'PDK1 regulates VDJ recombination, cell-cycle exit and survival during B-cell development', *EMBO Journal*, 32(7), pp. 1008–1022. doi: 10.1038/emboj.2013.40.

Vigneron, S. *et al.* (2010) 'RSK2 is a kinetochore-associated protein that participates in the spindle assembly checkpoint', *Oncogene*, 29(24), pp. 3566–3574. doi: 10.1038/onc.2010.105.

W

Wang, L. *et al.* (2007) 'PRAS40 regulates mTORC1 kinase activity by functioning as a direct inhibitor of substrate binding', *Journal of Biological Chemistry*, 282(27), pp. 20036–20044. doi: 10.1074/jbc.M702376200.

Wang, L. *et al.* (2017) 'Brain Development and Akt Signaling: the Crossroads of Signaling Pathway and Neurodevelopmental Diseases', *Journal of Molecular Neuroscience*, pp. 379–384. doi: 10.1007/s12031-016-0872-y.

Wang, Y. *et al.* (2011) 'CXCR4 and CXCR7 Have Distinct Functions in Regulating Interneuron Migration', *Neuron*, 69(1), pp. 61–76. doi: 10.1016/j.neuron.2010.12.005.

Watatani, K. *et al.* (2012) 'PDK1 regulates the generation of oligodendrocyte precursor cells at an early stage of mouse telencephalic development', *Genes to Cells*, 17(4), pp. 326–335. doi: 10.1111/j.1365-2443.2012.01591.x.

Wei, Y. *et al.* (1998) 'Phosphorylation of histone H3 at serine 10 is correlated with chromosome condensation during mitosis and meiosis in Tetrahymena', *Proceedings of the National Academy of Sciences of the United States of America*, 95(13), pp. 7480–7484. doi: 10.1073/pnas.95.13.7480.
Wichterle, H. *et al.* (2001) 'In utero fate mapping reveals distinct migratory pathways and fates of neurons born in the mammalian basal forebrain', *Development*, 128(19), pp. 3759–3771.
Wichterle, H. *et al.* (2003) 'Permissive corridor and diffusible gradients direct medial ganglionic eminence cell migration to the neocortex', *Proceedings of the National Academy of Sciences of the United States of America*, 100(2), pp. 727–732. doi: 10.1073/pnas.242721899.
Wiggin, G. R. *et al.* (2002) 'MSK1 and MSK2 Are Required for the Mitogen- and Stress-Induced Phosphorylation of CREB and ATF1 in Fibroblasts', *Molecular and Cellular Biology*, 22(8), pp. 2871–2881. doi: 10.1128/mcb.22.8.2871-2881.2002.
Williams, M. R. *et al.* (2000) 'The role of 3-phosphoinositide-dependent protein kinase 1 in activating AGC kinases defined in embryonic stem cells', *Current Biology*, 10(8), pp. 439–448. doi: 10.1016/S0960-9822(00)00441-3.
Wolfson, R. L. *et al.* (2016) 'Sestrin2 is a leucine sensor for the mTORC1 pathway', *Science*, 351(6268), pp. 43–48. doi: 10.1126/science.aab2674.
Wolfson, R. L. and Sabatini, D. M. (2017) 'The Dawn of the Age of Amino Acid Sensors for the mTORC1 Pathway', *Cell Metabolism*, 26(2), pp. 301–309. doi: 10.1016/j.cmet.2017.07.001.
Wong, F. K. *et al.* (2018) 'Pyramidal cell regulation of interneuron survival sculpts cortical networks', *Nature*, 557(7707), pp. 668–673. doi: 10.1038/s41586-018-0139-6.
Woodworth, M. B. *et al.* (2012) 'SnapShot: Cortical Development', *Cell*, 151(4), pp. 181–204. doi: 10.1038/nature13314.A.
Wullschleger, S. *et al.* (2011) 'How moderate changes in Akt T-loop phosphorylation impact on tumorigenesis and insulin resistance', *DMM Disease Models and Mechanisms*, 4(1), pp. 95–103. doi: 10.1242/dmm.005603.
Wyant, G. A. *et al.* (2017) 'mTORC1 Activator SLC38A9 Is Required to Efflux Essential Amino Acids from Lysosomes and Use Protein as a Nutrient', *Cell*, 171(3), pp. 642-654.e12. doi: 10.1016/j.cell.2017.09.046.

X

Xu, C. *et al.* (2017) 'Conditional deletion of PDK1 in the forebrain causes neuron loss and increased apoptosis during cortical development', *Frontiers in Cellular Neuroscience*, 11, p. 330. doi: 10.3389/fncel.2017.00330.
Xu, X. *et al.* (2019) 'The chemical diversity and structure-based discovery of allosteric modulators for the PIF-pocket of protein kinase PDK1', *Journal of Enzyme Inhibition and Medicinal Chemistry*, 34(1), pp. 361–374. doi:

10.1080/14756366.2018.1553167.

Y

Yang, H.-S. *et al.* (2003) 'The Transformation Suppressor Pdcd4 Is a Novel Eukaryotic Translation Initiation Factor 4A Binding Protein That Inhibits Translation', *Molecular and Cellular Biology*, 23(1), pp. 26–37. doi: 10.1128/mcb.23.1.26-37.2003.
Yang, S. *et al.* (2018) 'Reducing the levels of akt activation by PDK1 knock-in mutation protects neuronal cultures against synthetic amyloid-beta peptides', *Frontiers in Aging Neuroscience*, 9(1), p. 435. doi: 10.3389/fnagi.2017.00435.
Yuan, H. X. and Guan, K. L. (2015) 'The SIN1-PH domain connects mTORC2 to PI3K', *Cancer Discovery*, 5(11), pp. 1127–1129. doi: 10.1158/2159-8290.CD-15-1125.

Z

Zhang, J., Gao, Z. and Ye, J. (2013) 'Phosphorylation and degradation of S6K1 (p70S6K1) in response to persistent JNK1 Activation.', *Biochimica et biophysica acta*, 1832(12), pp. 1980–1988. doi: 10.1016/j.bbadis.2013.06.013.
Zhang, K. *et al.* (2016) 'Baicalin promotes hippocampal neurogenesis via SGK1- and FKBP5-mediated glucocorticoid receptor phosphorylation in a neuroendocrine mouse model of anxiety / depression', *Scientific Reports*, 6, p. 30951. doi: 10.1038/srep30951.
Zhao, Y., Bjørbæk, C. and Moller, D. E. (1996) 'Regulation and interaction of pp90(rsk) isoforms with mitogen-activated protein kinases', *Journal of Biological Chemistry*, 271(47), pp. 29773–29779. doi: 10.1074/jbc.271.47.29773.
Zhou, X. *et al.* (2014) 'Fine-tuning the intensity of the PKB/Akt signal enables diverse physiological responses', *Cell Cycle*, pp. 3164–3168. doi: 10.4161/15384101.2014.962954.
Zimmer, C. *et al.* (2004) 'Dynamics of Cux2 expression suggests that an early pool of SVZ precursors is fated to become upper cortical layer neurons', *Cerebral Cortex*, 14(12), pp. 1408–1420. doi: 10.1093/cercor/bhh102.
Zurashvili, T. *et al.* (2013) 'Interaction of PDK1 with Phosphoinositides Is Essential for Neuronal Differentiation but Dispensable for Neuronal Survival', *Molecular and Cellular Biology*, 33(5), pp. 1027–1040. doi: 10.1128/mcb.01052-12.

AGRAÏMENTS

Doncs res, em toca escriure uns agraïments en un moment horrible de la meva vida, així que disculpeu si acaben resultant més formals que alegres.
Primerament, un agraïment a Jose. Sense la seva confiança i tots els moments que m'ha tirat endavant, no estaria presentant la tesi, així de clar.
Un record especial per a en Shaobin. Semblava que no hi era, però sí.
A totes les estudiants de Màster que han passat i m'han aguantat: les dues Annes, la Carlota i la Rebeca.
Al Víctor, per recomanar-me per a fer el doctorat, i per ensenyar-me durant el Màster i fer-me venir ganes de fer un doctorat en primer lloc. A tots els Yustes, que no són pocs, més aviat infinits! Als de la meva època i als posteriors. Quin flotador d'emergència han estat! Als Lizcano, mare meva, si quasi semblaven els meus segons tutors, quan no era un dubte era un anticòs, quan no un equip un kit de Midi. Gràcies de cor. Al Jose Manuel López Blanco, per les competents quan les meves no sortien. I si he de nombrar grups no puc oblidar-ne dos: els Saures, que m'han salvat moltíssimes vegades de la misèria, com els Pepe's, que sense els vostres enzims no tindria el nou construct acabat.
A la Cristina, sobretot, perquè aquells cultius primaris són èpics, mítics, una historieta que em quedarà per contar als néts. I també per tot el consell continu que m'ha aportat sempre. A la Mar, que em va despertar interès en un camp que desconeixia del tot, va ser molt xulo filetejar cervells, i no m'ho hagués pensat mai! A la Núria, que va ser-hi en els meus primers contactes amb el microscopi, que bàsicament és la meitat de la tesi. A la Susana, persona a qui acudir en cas d'emergència.
A la gent amb la que dinava o he dinat en diferents moments de la vida: Paola, Meri, Elena, Montse i les demés, quines *rises*. També a la Sally, en Yussef (espero escriure-ho bé), thanks a lot for the conversations and the caring, they really cared for me. També a la Neus.
A les companyes que van fer pràctiques amb mi, passant d'un laboratori a l'altre, "això com els ho demanes?". No sé com ho hagués passat d'estar fent-les sola. A l'Elisabet, que ens les preparava.
A la Roser, que em va proposar i va gestionar moltes iniciatives didàctiques i de divulgació on vaig participar i em van encantar. A Cristina, que ens vam apuntar a una juntes i a la segona que va venir, també, perquè la primera havia estat molt bé. A Lydia i la resta de professionals amb qui vaig compartir el programa Inspira, tant enorme però sí, tan inspirador.
Al Lluís, per deixar la porta oberta a la meva tesi amb els resultats de la seva. I a ell i al seu laboratori, el del Dr Nguyen, pels plàsmids que necessitàvem per fer la electroporació *in utero*.

Als membres del comitè de seguiment, que també han hagut de patir veient-me discutir resultats negatius. Al personal d'administració del Departament i l'Institut, que m'han fet la vida burocràtica molt fàcil.
Al Dr Wieland Huttner. Finalment no va poder ser, però acceptar-me al seu laboratori va ser un moment molt alegre per mi. Tan de bo s'hagués pogut materialitzar. Al Dr Joaquim Egea, que ens hagués ajudat amb els experiments d'electroporació *in utero* si els haguéssim pogut fer.
Als meus amics, que mai han entès de què treballo (crec) però no ha importat.
Finalment, gràcies a la meva família, com sempre. A la Leia i l'Otto que han evitat que plorés la meitat dels dies. A l'Álvaro que s'ho mereix tot. Als meus pares i ma germana, no tinc paraules, com sempre us ho dec tot.
Doncs res, salut i força!

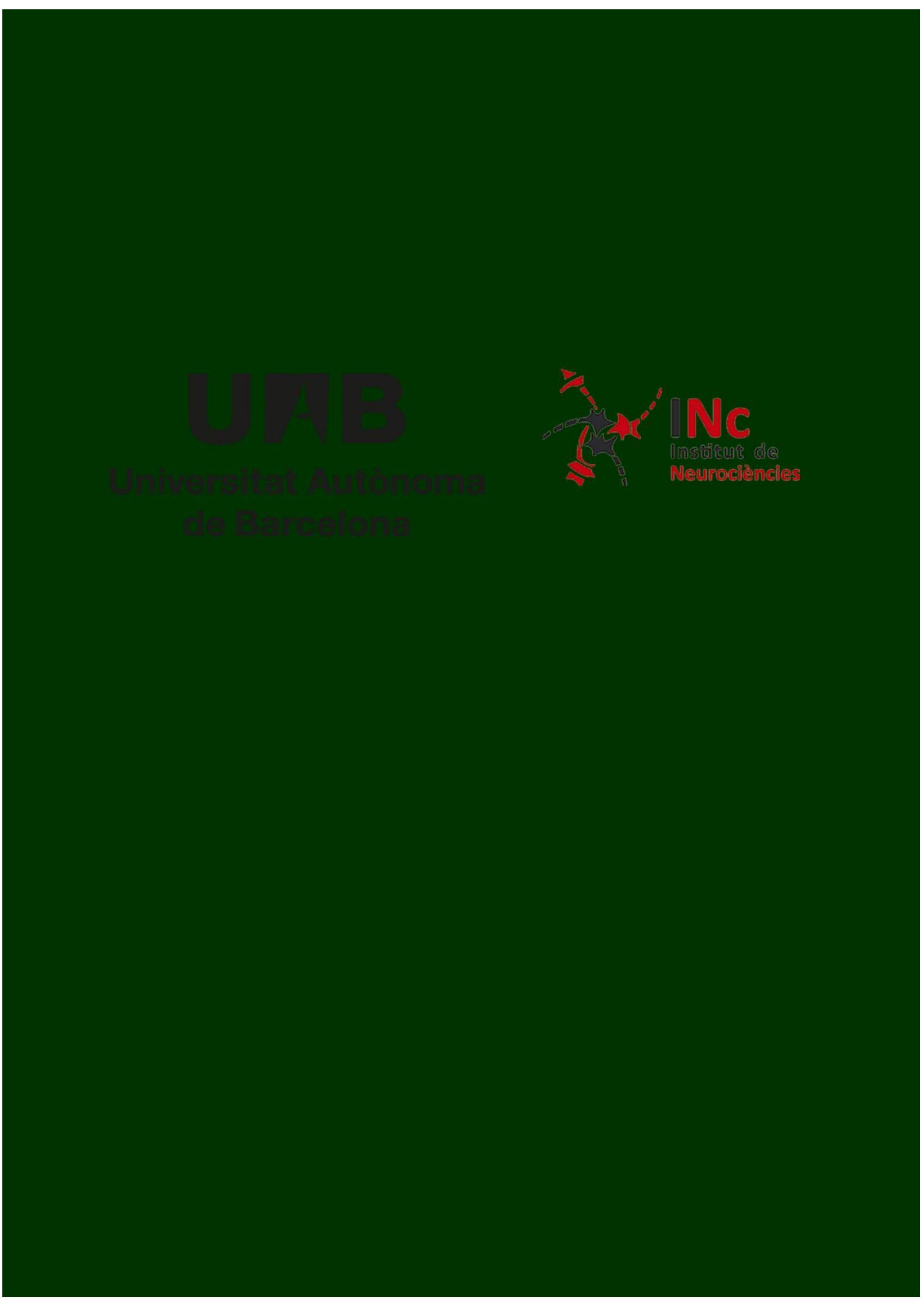
UAB
Universitat Autònoma
de Barcelona
INc
Institut de
Neurociències